University of Southampton

Faculty of Environmental and Life Sciences

Ocean and Earth Science

New insights into submarine geohazard and sediment transport revealed by repeat seafloor surveys

by

Muhamad Zaki Bin Zulkifli

ORCID ID 0009-0000-8587-0539

Thesis for the degree of Doctor of Philosophy

July 2024

University of Southampton

Abstract

Faculty of Environmental and Life Sciences

Ocean and Earth Science

Doctor of Philosophy

New insights into submarine geohazard and sediment transport revealed by repeat seafloor surveys

by

Muhamad Zaki Bin Zulkifli

The prevalence of submarine geohazards poses significant threats to coastal communities and global economies. This thesis investigates three main types of submarine geohazards: submarine landslides, submarine channel evolution, and volcaniclastic density currents triggered by volcanic eruptions. Utilizing innovative repeat seafloor surveys, the research aims to elucidate the processes behind these hazards and their implications for hazard assessment, sediment transport pathways, and depositional fate. The survey compare seafloor changes as long as between 13 years (Knight inlet) as well as daily changes (Squamish prodelta). The study examines various settings prone to different submarine geohazards, including a submarine prodelta linked to a seasonally active meltwater-fed river (Squamish Prodelta), a confined fjord's submarine channel system (Knight Inlet), and a remote volcanic island affected by a massive eruption (Hunga Tonga Volcano). The research seeks to enhance understanding of seafloor evolution, its effects on coastal infrastructure, and the interpretation of past sediment transport events from seafloor and depositional archives. Each chapter addresses a specific aspect of submarine geohazards, highlighting the central role of sediment dynamics. For instance, in the submarine channels of Knight Inlet, it is demonstrated for the first time that channel curvature significantly influences dominant processes and the rate of channel migration, with a threshold normalized radius of curvature of 1.54. The investigation of delta slope failures in Squamish Prodelta reveals that sediment loading and slope geometry are critical factors affecting the occurrence and magnitude of these failures. The study of seafloor changes following the Hunga Tonga volcanic eruption underscores the diverse scales of bedforms shaped on the seafloor and their impact on density flow pathways, ranging from zero to forty kilometres from the caldera. The identified hazards span a wide spatial and temporal spectrum, from events recurring over centuries (Hunga Tonga eruption) to daily occurrences (upstream-migrating bedforms in Squamish Prodelta). This thesis offers a nuanced understanding of the processes leading to submarine geohazards, emphasizing sediment dynamics' pivotal role. It advocates for continuous reassessment based on new empirical evidence. The implications extend beyond the specific geological phenomena studied, offering valuable insights for geological studies, environmental management, and risk assessment in submarine environments. The thesis concludes with a call for further exploration, emphasizing the need for ongoing monitoring, data acquisition, and interdisciplinary studies. This approach is essential to enhance understanding of submarine geohazards, contributing to the development of resilient infrastructure and improved hazard mitigation strategies.

Table of Contents

Table of Tables

Table of Figures

Table of Figures

Table of Figures

List of Accompanying Materials

1. Video 1: Squamish Prodelta difference map (JD118-JD236)
2. Video 2: Bedform migration before major failure (JD181)

Research Thesis: Declaration of Authorship

Print name: Muhamad Zaki Bin Zulkifli

Title of thesis: New insights into submarine geohazard and sediment transport revealed by repeat seafloor surveys

I declare that this thesis and the work presented in it are my own and has been generated by me as the result of my own original research.

I confirm that:

1. This work was done wholly or mainly while in candidature for a research degree at this University;
2. Where any part of this thesis has previously been submitted for a degree or any other qualification at this University or any other institution, this has been clearly stated;
3. Where I have consulted the published work of others, this is always clearly attributed;
4. Where I have quoted from the work of others, the source is always given. With the exception of such quotations, this thesis is entirely my own work;
5. I have acknowledged all main sources of help;
6. Where the thesis is based on work done by myself jointly with others, I have made clear exactly what was done by others and what I have contributed myself;
7. None of this work has been published before submission

Signature: ..... Date:.....

Acknowledgements

Embarking on this doctoral journey has been a profound and enriching experience, and I am deeply aware that this thesis is not solely the result of my individual efforts. I extend my heartfelt gratitude to the individuals who have been instrumental in guiding, supporting, and inspiring me throughout this four-year endeavour.

First and foremost, I would like to express my sincere appreciation to my primary supervisor, Mike Clare. Thank you for providing me with the opportunity to embark on this PhD project and for your unwavering guidance and support. Your open-door policy and encouragement have been invaluable, motivating me to persist in the face of challenges.

I extend my gratitude to my co-supervisors, Timothy Minshull and Hector Marin Moreno. Your scientific insights, constructive comments, and engaging discussions have significantly enriched the development of this thesis. I am thankful for your ongoing support and encouragement that have propelled me forward.

A special thank you to the Universiti Malaysia Terengganu for sponsoring my studies in the UK. Your support has been crucial in enabling me to pursue this academic endeavour.

I would also like to acknowledge the contributions of the panel chair, Esther Sumner. Thank you for ensuring the progression of my PhD and for your guidance that has contributed to my academic growth.

To my family back home in Malaysia, I am immensely grateful for your unwavering support and constant check-ins on my well-being. Despite the distance, your encouragement has been a source of strength throughout this journey.

Finally, heartfelt thanks to my peers, Lewis Bailey, Maarten Heijnen, and Daniela Vendettuoli. Your camaraderie, shared experiences, and collaborative spirit have added a meaningful dimension to my doctoral experience.

In this collective effort, each of you has played a vital role, and I am sincerely thankful for the positive impact you have had on my academic and personal growth.

With heartfelt gratitude,

Muhamad Zaki Bin Zulkif

Chapter 1 Introduction

1.1 Thesis overview

The occurrence of various geological phenomena under the sea can pose serious threats to coastal communities and global economies (DeVore and Sawyer, 2016). So-called 'submarine geohazards' may include large magnitude earthquakes that create strong ground motions, underwater landslides that can be orders of magnitude larger than their terrestrial equivalents, powerful seafloor flows of sediment known as turbidity currents that travel for hundreds of kilometres, and submerged volcanic eruptions (Clare et al., 2021; Lotteri et al., 2021; Paull et al., 2018; Synolakis et al., 2002; Talling et al., 2022). These often-large magnitude events can trigger tsunamis, remobilise vast areas of seafloor, and damage critical seafloor infrastructure, such as seafloor cables and pipelines that underpin global communications and energy security (Kvenvolden, 1999). In addition to posing a hazard, some of this these underwater processes are also responsible for the transfer of globally-important quantities of sediment and other particulate material into the deep-sea, representing some of the largest sediment transport events on the planet ((Cantero et al., 2014; Cartigny and Postma, 2017; Hage et al., 2019; Pohl et al., 2020). This thesis focuses on three main types of submarine geohazard, providing new insights into their behaviour to better understand the implications for hazards assessment, and the transport pathways and depositional fate of the sediment that they move. The research in this thesis focuses specifically on:

i) Submarine landslides.

ii) Sediment density flows in submarine channels.

iii) Volcaniclastic density currents triggered by volcanic eruptions,

and uses novel repeat seafloor surveys that capture changes in seafloor relief and elevation to understand the causative processes.

This thesis analyses data that have been acquired from different settings, which represent remote and dynamic environments that are susceptible to different types of submarine geohazard. These include a submarine prodelta that is connected to a seasonally active meltwater-fed river that experience high sediment fluxes during the Spring and Summer, a submarine channel system within a confined fjord that extends to deep water, and a remote and partially submerged volcanic island that was subject to even larger particulate fluxes delivered during one of the largest volcanic eruptions ever recorded. The study sites provide a range of different settings to study

different geohazards, but share the fact that they are extremely dynamic due to the large sediment fluxes involved, and that they host remote coastal communities that are vulnerable to the impacts of tsunamis and are also presently underserved by seafloor infrastructure, particularly telecommunications cables. Better understanding hazards in these locations will ensure the design of more resilient infrastructure and help to protect coastal communities.

1.2 Overarching aims

This thesis aims to understand:

i) How the seafloor evolves in different submarine environments; Submarine channels in fjord, Pro-delta slope, and areas surrounding a subaerial volcano.

ii) The implications for seafloor and coastal infrastructure (submarine geohazard);

iii) Implications for interpreting past sediment transport events from the seafloor and depositional archives.

The core of the observational study in these different areas is the same, which is an emphasis on the role of sediment transport and the associated submarine geohazards. For instance, in a submarine channel environment, it is important to understand the erosional and depositional processes, because they control the pathways, timescales, and fate of shallow-to-deep-sea transport of sediment, organic carbon, nutrients, and pollutants (Fernandes et al., 2020; Georgiopoulou and Cartwright, 2013; Mountjoy et al., 2018; Peakall et al., 2000; Straub et al., 2008). Sediment transport also plays a significant role in the initiation, propagation, and consequences of submarine landslides (Masson et al, 2006). The studies that make up this thesis highlight the importance of sediment dynamics, including the role of turbidity currents, sediment failures, and sediment deposition, in triggering and shaping submarine slopes (Hampton et al., 1996; Kurnio et al., 2023; Martínez-Doñate et al., 2021; Maslin et al., 2004; Masson et al., 2006; Roland et al., 2020; Stagna et al., 2023; Vanneste et al., 2014; X. Zhang et al., 2019). Observing submarine sediment transport after volcanic eruptions is crucial for understanding the complex processes that occur during and after these events. Several studies provide valuable insights into these processes and their implications. For example, White et al. (2006) discuss the long-term volumetric eruption rates, which provide insights into the overall scale and magnitude of volcanic eruptions. Understanding the volume of erupted material is crucial for estimating the amount of sediment that can be transported and deposited in the surrounding areas. Another study by (Paris, 2014; Paris et al., 2015) highlights the influence of parameters such as volume flux of mass flows, explosion energy, and duration of caldera collapse on tsunami generation.

1.3 Thesis rationale

This section now introduces the main geohazards that are investigated in this thesis, why it is important to study them, what is currently known about their nature, and some of the open questions that exist concerning their behaviour.

1.3.1 Submarine landslides and a need to understand the triggers and preconditioning factors that control slope instability

Submarine landslides occur on all the world's submerged continental margins and can involve the mobilization of large volumes of sediment; sometimes thousands of cubic kilometres in volume (e.g. Masson et al., 2006). The movement of such large volumes of sediment can displace the overlying seawater, generating a tsunami (Dai et al., 2023; Urgeles and Camerlenghi, 2013). Unlike tsunamis triggered by earthquakes, whose triggers can be readily detected using seismic monitoring networks, most submarine landslides go un-recognised by offshore monitoring; hence, tsunamis generated by submarine landslides can strike with little to no notice (Tappin, 2021). Submarine landslides can be far larger volume and can occur on much lower angles slopes than those on land, sometimes moving on slopes of less than two degrees (Masson et al., 2006; Urgeles and Camerlenghi, 2013). Submarine landslides can also attain high speeds (e.g. up to tens of metres per second; Piper et al., 1999) resulting in damage to expensive and important seabed infrastructure, such as oil platforms, pipelines, and submarine cables, and disrupt essential services, such as energy supply and communication networks (Fan et al., 2020; Masson et al., 2006).

Multiple causative factors have been proposed for the triggering of submarine landslides, including large external events such as ground shaking from large earthquakes, volcanic activity, destabilisation of slope sediments by wave action during large storms, and dissociation of gas hydrates e.g. (Clare et al., 2015; Fan et al., 2020; Hunt et al., 2018; Kvenvolden, 1993; Schulten et al., 2019; Urlaub et al., 2013); however, there is growing evidence that preconditioning factors that prime a slope to failure over prolonged time periods (potentially from days to thousands of years) may be more important than the effects of external events for slope instability (Casalbore et al., 2020; Zhang and Puzrin, 2022).

The Grand Banks incident (November 18, 1929) serves as a stark example of the destructive potential of a major landslide. Triggered by a seismic event with a magnitude of 7.2, this massive landslide, estimated at around 560 km^3 of sediment, wreaked havoc by creating substantial scour and erosion features (Schulten et al., 2019; Shor et al., 1990). The resulting high-magnitude tsunami added to the devastation, amplifying the destructive force unleashed by the event

(Løvholt et al., 2019). Furthermore, the earthquake-induced turbidity currents were of such intensity that they inflicted considerable damage on the region's submarine cable infrastructure, underscoring the profound and far-reaching impact of this disastrous occurrence (Stevenson et al., 2018).

A scarcity of studies that monitor the development of submarine slope failures mean that there are many open questions, about why only some submarine slopes are prone to failure and others are not, and which combinations of factors result in slope failure and why. Therefore, submarine landslides need to be studied using integrated, multi-disciplinary approaches that include monitoring of the conditions prior to, during and after slope failure (Vanneste et al., 2014). This thesis includes a focus on slope failures, specifically at a submerged river delta.

1.3.1.1 Slope failure at submerged river deltas

Delta slope failure is a significant process that can occur in river deltas. It refers to the collapse or failure of the delta slope, leading to the redistribution of sediment and potentially impacting the overall shape and stability of the delta (Syvitski and Saito, 2007). This process can be influenced by various factors, including river input, tidal processes, and delta progradation. River input is an important factor that affects delta slope failure. The stability of the delta slope depends on the amount and characteristics of sediment delivered by the river. High river discharge can lead to increased sediment accumulation and deposition, which can increase the weight and stress on the delta slope and potentially increase the risk of slope failure (Syvitski & Saito, 2007). Moreover, the grain size of the sediment can also affect the stability of the slope. Finer sediments are generally less stable and more prone to failure compared to coarser sediments (Edmonds and Slingerland, 2007).

Tidal processes, such as tidal currents and tidal fluctuations, can also affect delta slope failure. Tidal currents can erode and transport sediment, potentially leading to the removal of sediment from the delta slope and increasing the risk of slope failure (Sassi et al., 2012). Tidal fluctuations, especially during high tides, can also exert additional pressure on the delta slope, potentially contributing to slope failure (Sassi et al., 2011). The increased water level during tidal high can increase the hydrostatic pressure on the delta slope, which can affect the stability of the sediment and potentially trigger slope failure (Rossi et al., 2016). The cyclic nature of tidal fluctuations can lead to repeated loading and unloading of the delta slope, which can further contribute to slope instability over time (Ragno et al., 2020). However, the influence of tidal high on delta slope failure can be modulated by other factors such as river input and delta progradation. River input, including the amount and characteristics of sediment delivered by the river, can interact with tidal processes and influence the stability of the delta slope (Hoitink et al., 2017). Delta progradation, which refers to the outward growth of the delta, can also affect the

weight and stress on the delta slope, potentially contributing to slope failure (Edmonds et al., 2010).

Delta progradation, which refers to the outward growth of the delta, can also affect delta slope failure. The weight of the sediment can increase as the delta progrades, potentially leading to increased stress on the delta slope and increasing the risk of slope failure (Jorissen et al., 2018). The accumulation of sediment on the delta slope can contribute to slope instability and increase the risk of slope failure (Kim et al., 2009). Moreover, the sediment input from the river during delta progradation can contribute to the buildup of sediment on the delta slope, potentially increasing the risk of slope failure (Angamuthu et al., 2018). Moving forward, another factor that could influence delta slope failure would be sea-level fluctuations (Porebski and Steel 2005).

Exemplifying the hazardous repercussions of river delta slope failure, the fjords of British Columbia have been subject to the disastrous impacts of tsunamis, often triggered by submarine slope failures and landslides, posing formidable threats to coastal communities and waterways in the area (Bornhold et al., 2007). The profound impact of the 1975 underwater landslide in Kitimat Arm stands as a vivid illustration of the staggering destructiveness inherent in these occurrences, with tsunami waves surging to a towering height of over 8 metres (Nemati et al., 2023). The event's intensity was exacerbated by the exceptionally shallow conditions of Minette Bay at the head of Kitimat Arm, where the landslide coincided with an unusually low tide, as documented by (Skvortsov and Bornhold, 2007). The convergence of these factors magnified the dire nature of the event, underscoring the profound and devastating consequences unleashed upon the region (flooded all facilities in the upper delta of Kitimat Arm and generated wave amplitude of around 8.2 m) .

Delta slope failure is influenced by various factors, including river input, tidal processes, and delta progradation. The stability of the delta slope depends on the amount and characteristics of sediment delivered by the river. Tidal processes, such as tidal currents and tidal fluctuations, can also affect slope stability. Furthermore, the outward growth of the delta during progradation can increase the weight and stress on the delta slope, potentially contributing to slope failure. Understanding these factors is crucial for assessing the stability and potential risks associated with delta slope failure

1.3.2 Sediment density flows and a need for direct monitoring of seabed change

Sediment density flows can be initiated when submarine landslides start to mix with the ambient seawater and disintegrate, forming a flow that is driven downslope by its excess density (Kuenen and Migliorini, 1950; Talling et al., 2012). Such sediment density flows, that include flows such as debris flows (high sediment concentration flow) and turbidity currents (dilute flow), may also

initiate as sediment-laden river flood water plunges into the ocean or due to suspension of seafloor sediments by storms or waves (e.g. Inman et al., 1976; Bailey et al., 2021). Instances of damage to seafloor cables have revealed that sediment density flows such as turbidity currents can travel at speeds of up to 20 m/s across vast distances, sometimes in excess of 1000 km, where they are funnelled along submarine canyons and channels (e.g. Piper et al., 1999; Talling et al., 2022). Sediment density flows are also important because they are the dominant mechanism for the transfer of sediment and other particulate matter, including organic carbon and pollutants, from shallow to deep water (Bouma et al., 2012; Azpiroz-Zabala et al., 2017; Talling et al., 2023).

Over time sediment density flows can construct submarine canyons and channels, depositing large volumes of sediment at their termini in the deep sea, forming submarine fans; the largest accumulations of sediment on Earth (Bouma et al., 2012; Talling et al., 2007). The repeated influence of sediment density currents shapes the morphology of submarine channels over time, which can create an often-complex stratigraphic architecture from which it may be possible to reconstruct past flow behaviour, sediment fluxes and geohazards (Paull et al., 2010). However, precisely what controls why different channel morphological features develop and evolve in certain reaches of submarine channels, such as the growth of meander bends, the upstream migration of bedforms and steep steps known as knickpoints, remains unclear at field-scale due to limited direct observations that limit a conclusive link to their causative processes (Hage et al., 2018; Masson et al., 2006; Paull et al., 2010; Peakall et al., 2007; Pohl et al., 2020).

Illustrating the potentially devastating consequences of turbidity currents, consider the instance of the submarine cable break in Congo Canyon with the latest reported event being on the 6/8/2023. Historical data gleaned from prior cable breaks in the Congo Canyon indicates a higher occurrence of such events during periods of elevated river discharge (Talling et al., 2022). The relationship between river discharge and the activity of present-day turbidity currents has also been established, with more potent and prolonged turbidity currents posing a risk of damaging or severing cables, albeit infrequently (Talling et al., 2021). Given the rarity and impact of such events, comprehending the dynamics of turbidity currents in the Congo Canyon is imperative for designing resilient cable systems and mitigating potential environmental hazards (Howe et al., 2022). The significance of the Congo Canyon lies in its status as a vital site hosting one of the largest channels and turbidity current systems that discharge into the deep ocean worldwide. It receives substantial terrestrial sediments from nearby drainage basins. Additionally, the Congo Fan's turbidity current deposits serve as an archive, offering insights into past environmental and climate changes, and documenting the pathways sediment-laden currents follow through submarine channels (Azpiroz-Zabala et al., 2017) .

Direct measurements of sediment density currents within submarine channels have been difficult to obtain due to the remote and challenging locations where they occur (Clare et al., 2020; Inman et al., 1976; Khripounoff et al., 2003; Prior et al., 1987; Puig et al., 2014; Sumner and Paull, 2014). Recent technological advances in seafloor surveying have enabled the mapping of submarine channel systems and provided insights into their hydrodynamics and sediment transport (Mountjoy et al., 2018; Liu et al., 2012) . It has been found that turbidity currents in submarine canyons can transport volumes of sediment comparable to terrestrial river systems (~1.1 to 3.8 Mt (million metric tons)) (Azpiroz-Zabala et al., 2017). Morphological features in submarine channels have been shown to migrate far faster than in rivers, with hundreds of metres of migration for some knickpoints being recorded in less than a year in some very active channels (e.g. Guiastrennec- Faugas et al., 2021; Heijnen et al., 2020). Furthermore, repeat-bathymetric surveys have been used to examine the stratigraphic evolution of cyclic steps within submarine channels and lobes (Englert et al., 2021). However, repeat seafloor mapping studies of submarine channels, which show how these systems evolve, remain relatively scarce. This thesis utilizes repeat seafloor mapping to understand the process of sediment transport, its influence on submarine geohazards and how channels evolve. The following provides some more detail on some of the theorised processes that may be responsible.

1.3.2.1 Crescentic bedform migration

Crescentic bedform migration appears to be an important process in the evolution of submarine channels. These bedforms are formed by supercritical turbidity currents and have been observed to migrate upstream in proximal, sandy submarine channels (Hage et al., 2018). The bedform has also been observed to migrate downstream (Mountjoy et al., 2018; Xu et al., 2007). The migration of crescentic bedforms plays a key role in shaping the morphology and architecture of submarine channels (Peakall et al., 2000). It has been suggested that submarine channel flows are highly stratified and form broad overbank bodies of low-concentration fluid moving along the entire channel length (Peakall et al., 2000).

1.3.2.1 Knickpoint migration

The interaction between crescentic bedforms and knickpoints is also a significant aspect of submarine channel evolution. Knickpoints are upslope-migrating erosional features that can cause channel-wide erosion and asymmetry in channel geometry (Chen et al., 2021). The migration of knickpoints and their interaction with crescentic bedforms can influence the longer-term evolution of submarine channels and the resulting sedimentary record (Chen et al., 2021; Tek et al., 2021). Various factors, such as changes in base level, sediment supply, and channel geometry, affect the migration of knickpoints in submarine channels (Loget and Van Den

Driessche, 2009). The mechanics and dynamics of knickpoint migration in submarine channels have been studied using various methods. The helical flow orientation in curved channels has been investigated to understand the knickpoint behavior and migration patterns (Corney et al., 2006). Numerical models have also been used to analyze the flow mean velocities through submarine channel bends and assess the impact on knickpoint migration (Wynn et al., 2007). Knickpoint migration is an important process in submarine channel evolution. Knickpoints can form and migrate within the channel, affecting either the whole channel or only the axis of a channel, depending on the context (Guiastrennec-Faugas et al., 2020; Tek et al, 2021). The migration of knickpoints can result in cut-and-fill processes within the channel (Guiastrennec-Faugas et al., 2020).

1.3.2.2 Meander bend migration

Submarine channel meandering is a significant process in the evolution and morphology of these underwater channels. Meandering submarine channels show similar planform patterns to subaerial fluvial bends, suggesting similarities in fluid dynamics between the two channel types (Corney et al., 2006; Peakall et al., 2000). The development of channel sinuosity is often related to feedback between erosion and channel curvature (Peakall et al., 2000; Wells and Cossu, 2013). The lateral location of the velocity maximum within the channel is also a key flow feature that influences the evolution of submarine channel systems (Keevil et al., 2006; Peakall et al., 2000). The mechanics of fluvial meandering have been extensively studied, and some of the principles can be applied to submarine channels as well. However, a more recent study shows that the fluvial and submarine systems are quite different, thus making the correlation between the systems harder (Fukuda et al., 2023; Jobe et al., 2020). Alternate-bar instability in straight channels has long been recognized as the cause of fluvial meandering (Ikeda et al., 1981). The mechanics of meandering in both subaerial and submarine channels involve the interaction between flow dynamics, sediment transport, and channel morphology (Seminara, 2006).

1.3.3 Volcanism poses major hazards to submarine environments

More than three quarters of the world's volcanoes lie partially or fully submerged beneath the ocean (de Ronde et al., 2003). These volcanoes can pose a wide range of hazards when they erupt but also due to the steep slopes that lie on their flanks. The seafloor can undergo various changes and processes in the build-up to and after a volcanic island eruption. One major effect may arise from seafloor sediment failures around volcanic islands (e.g. Le Friant et al., 2015). These failures are caused by the landslides on the flanks or sector collapse of a volcanic island, which displace large amounts of material into the surrounding seafloor (Le Friant et al., 2015; Paris, 2015; Brunet et al., 2016; Tappin, 2022). The resultant sediment deposition can affect the surrounding marine

ecosystem, as it can cover existing habitats and disrupt the ecosystem balance (Herrera et al., 2023), and can impact coastal communities due to the large tsunamis that can be generated. A recent example is the flank collapse of Anak Krakatau offshore Indonesia in 2018, where half the island collapsed into the ocean, generating a tsunami that took many lives (Hunt et al., 2021). Such volcanic island collapses can be enormous in scale, representing some of the largest mass movements on the planet (Watt et al., 2014). The triggering of slope failure in such settings is thought to be closely related to volcanic activity and related seismicity (Hunt & Jarvis, 2017). The rheology of the volcanic material and the timing of failure and eruption are also important factors in determining the occurrence of slope failure (Cabaniss et al., 2020). This indicates that different types of volcanoes may produce different magnitudes of the eruptions. For example, subduction zone volcanoes may produce high magnitude hazards such as large-scale earthquakes and the release of hazardous gases and ash (Desonie et al., 1993). On the other hand, hotspot volcanoes, such as those found in the Hawaiian Islands, are known for their relatively steady and less explosive eruptions with hazards such as lava flows, gas emissions, and potential flank collapses (Xu et al., 2023). The timing and frequency of large flank collapses of volcanic islands have been extensively studied due to the hazards they pose (e.g. Boudon et al., 2013; Hunt et al., 2014; Barrett et al., 2020). Submarine landslides can generate a range of cascading hazards, one of which is volcaniclastic density currents. These dense flows of sediment, which are similar to turbidity currents, may also be triggered by other means, as recently recognised when the eruption column of Hunga volcano collapsed into the ocean, triggering fast-moving (up to 122 km/hour) and long run out density currents that wiped out seafloor biology and damaged telecommunications cables over distance of >100 km (Clare et al., 2023; Seabrook et al., 2023).

The 2018 lateral collapse of Indonesia's Anak Krakatau volcano vividly illustrates the devastating impact of eruption hazards. This catastrophic event, marked by a major volcanically-generated tsunami—the first in over a century—resulted in widespread loss of life and significant damage(Grilli et al., 2019). The collapse triggered a complex hazard cascade, emphasising the destructiveness of the triggered tsunami (Walter et al., 2019). Aerial photography, remote sensing, and advanced imaging techniques have provided crucial insights into the morphological changes, while photogrammetric methods revealed the dynamic eruption process(Banggur et al., 2023; Hochfeld et al., 2022). This tragic episode underscores the urgent need for effective detection, early warnings, and comprehensive disaster preparedness. Ongoing research highlights the importance of monitoring and preparedness for volcanic hazards, emphasising the challenges in detecting precursors and the critical role of improved warning systems(Grilli et al., 2021). The 2018 Anak Krakatau event serves as a stark example of the devastating consequences of eruption hazards, urging continued research, monitoring, and preparedness to mitigate risks and protect vulnerable communities.

1.3.4 Fingerprinting past hazardous events using their seafloor signature

Studying the seafloor morphology surrounding submarine volcanoes deposition is one of the primary methods used to assess the potential hazards associated with future eruptions. By analyzing sediment cores and studying the characteristics of deposited sediments, scientists can gain insights into the frequency, magnitude, and impacts of past volcanic events (Van Daele et al., 2014). However, few studies have been performed that fingerprint the signature of a major volcanic eruption leaving many uncertainties in the robustness of those interpretations (Te.g. rofimovs et al., 2012; Casalbore et al., 2023). Fields of bedforms on the flanks of submerged volcanoes have been proposed to be indicative of very large magnitude eruptions (e.g. Pope et al., 2018; Casalbore et al., 2021); however, the lack of field studies to provide a categorical link means that this has remained a hypothesis. This thesis analyses data from before and after the 2022 eruption of Hunga volcano to investigate what seafloor changes, particularly bedform migration, can tell us about the volcanic eruption, associated hazards and interpretation of seafloor characteristics at other volcanoes.

1.4 Structure of the thesis

This present chapter provides the rationale and context for the three specific research questions listed below and addressed in Chapters 2, 3 and 4. The science chapters are presented in this thesis in a publication journal format. The thesis aims to understand the processes that control submarine geohazards and sediment transport and assess which processes dominate in different systems and at different locations within those systems. All three of the study areas make use of observational study of submarine environments via repeat multibeam mapping. The difference between them is the location and hazard involved. In Chapter 2, the location involved is a deep-water submarine channel in Knight Inlet, British Columbia, and the focus is on the controls that drive erosional patterns within submarine channels and its subsequent morphological evolution. Chapter 3 focuses on a submerged prodelta offshore from the Squamish River (also in British Columbia), and aims to understand the drivers on repeated instances of submarine slope failure. Chapter 4 focuses on the seafloor impacts of a major volcanic eruption, specifically the 2022 eruption of the Hunga Tonga–Hunga Haʻapai volcano offshore Tonga in the South Pacific. Figure 1.1 shows the bathymetric map of the 3 study area. Finally, Chapter 5 brings together the thesis providing answers to the research questions, addresses the overarching aim and lays out future research arising from this PhD study.

1.4.1 Main research questions addressed by this thesis

This thesis addresses three main research questions, which correspond to the main science chapters 2, 3 and 4, and are as follows:

1.4.2 Chapter 2: Which are the processes that control the erosion and morphological evolution of submarine channels and why do they vary along their course?

A number of factors have been proposed to influence the evolution of submarine channels. One of these is meandering, which is the development of sinuous channel bends over time (Royden and Taylor Perron, 2013). However, other morphodynamic processes have been implicated in driving the evolution of channels, including dune-scale crescentic bedforms and steep steps in the channel called knickpoints, both of which migrate upstream (e.g. Bouchakour et al., 2023; Hage et al., 2018; Royden and Taylor Perron, 2013).

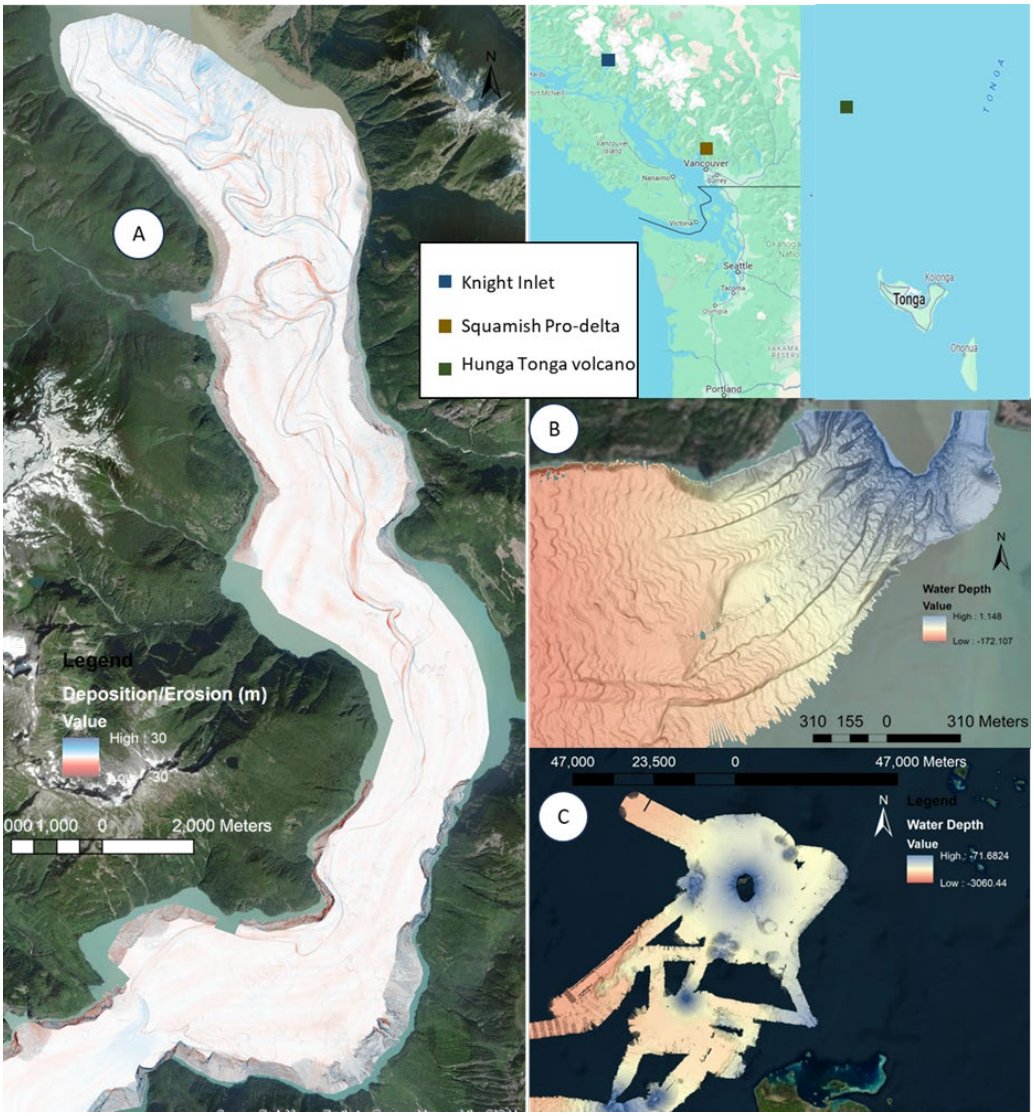

Figure 1.1: the bathymetry maps of the 3 study area, A) Knight Inlet, B) Squamish Prodelta, C) Hunga Tonga volcano.

The movement of these features influences the evolution of submarine channels in different ways. Knickpoints are sudden changes in channel slope that can move upstream or downstream, altering the channel shape(Gallen et al., 2011; Haviv et al., 2010). The knickpoints can cause changes in channel gradient, which affects how sediment is transported and deposited in the channel (Gallen et al., 2011). Likewise, the movement of crescentic bedforms, which are crescent-shaped sedimentary structures, can also impact the evolution of submarine channels (Hage et al., 2018). These bedforms can change the flow and sediment transport in the channel, resulting in changes in channel shape and sediment distribution (Hage et al., 2018). It is important to understand the factors that influence the evolution of submarine channels to predict and interpret their stratigraphic patterns (Sylvester et al., 2011). By examining the effects of meandering and the movement of seabed features, researchers can learn about the processes that form submarine channels and their associated sedimentary deposits (Royden & Perron, 2013; Hage et al., 2018; Bouchakour et al., 2023). This knowledge has various applications, such as exploring for deposits that host hydrocarbons and understanding Earth's geological history (Sylvester et al., 2011). However, which of these processes dominates submarine channel evolution remains unclear. Recent time-lapse surveys have suggested that crescentic bedforms are the ‘building blocks’ of submarine channels (Covault et al., 2017), while others indicate that knickpoint migration dominantly accounts for the erosion that occurs over decades within submarine channels (Heijnen et al., 2020). However, this is in stark contrast to the many studies of ancient systems based on outcrops or subsurface seismic data that indicate that meander bend migration is the dominant mechanism that drives submarine channel evolution, with sparse evidence for features such as knickpoints in the depositional record (e.g. Deptuck et al., 2007; Babboneau et al., 2010; Peakall et al., 2007; Tek et al., 2021; McArthur et al., 2022). Therefore, there are apparently contradictory hypotheses, and it remains unclear as to which process truly dominates, and also why this may vary spatially along the length of a submarine channel system.

To address this apparent contradiction, Chapter 2 presents a comparative analyse of two seafloor surveys, performed thirteen years apart, that cover the full extent of a submarine channel system in Knight Inlet, a fjord in British Columbia, Canada.

1.4.3 Chapter 3: Which processes control the collapse of submarine delta slopes?

Submarine slope failures pose a range of hazards, which can be particularly relevant at submarine deltas given that deltas are important hubs for human population and hence are vulnerable to landslide-tsunami and damage to the seafloor infrastructure that connects them (Tessler et al., 2015; Nienhuis et al., 2020). Several factors have been proposed as possible causes of submerged delta slope failure, such as river input, low tide, delta progradation (slope increase). Rivers can bring a high sediment load to a submerged prodelta top and slope, which

may initiate failure events (Normandeau et al., 2016; Winsemann et al., 2018; Hizzett et al., 2018; Kostic, 2018). Delta progradation, which is the outward expansion of the delta, can also affect slope failure. As the delta progrades and the slope increases, the increased sediment accumulation can cause the build-up of excess pore pressure within the fine-grained layer on the delta slope. This excess pore pressure reduces shear strength and can eventually result in catastrophic failure of the delta slope (Hilbe and Anselmetti, 2014).

Low tide conditions can also lead to delta slope failure. During low tide, the water level drops, causing a decrease in hydrostatic pressure on the delta slope. This pressure reduction can destabilize sediment, particularly where interstitial gas is present, and increase the probability of slope failure (e.g. Clare et al., 2017). It is also possible that erosional processes, such as the upstream migration of bedforms on, or at the base of, a prodelta slope may contribute to delta slope failure. These bedforms can change flow dynamics and sediment transport, resulting in changes in channel shape and sediment distribution. However, testing which different processes or combination of processes is responsible remains unclear due to a paucity of monitoring datasets. There exist few repeat seafloor surveys that have been performed at sufficient temporal resolution to: i) constrain the build up to, and timing of submarine slope failures; and ii) record multiple slope failures to explore differing controlling factors.

Chapter 3 addresses these issues through the analysis of 93 repeated multibeam bathymetric surveys performed on successive weekdays in 2011 at the Squamish prodelta in Howe Sound, a fjord in British Columbia. The findings reveal that slope failures are the result of a combination of modified slope geometry due to delta lip progradation and pore pressure fluctuations related to progressive and rapid sediment loading and tidal effects.

1.4.4 Chapter 4: What does bedform migration reveal about large volcanic eruptions?

The seafloor can undergo several changes after a volcanic island eruption. One of the observed changes is the creation of giant scours near the caldera (Haymon et al., 1993). The eruption can cause the collapse of the volcanic structure, creating a caldera. The collapse can also create a large depression on the seafloor, called a giant scour. This scour is caused by the removal of material during the eruption and can affect the seafloor topography. Moreover, volcanic island eruptions can cause submarine landslides and turbidity currents (Clare et al., 2018; Hunt and Jarvis, 2017). The eruption can destabilize the slopes of the volcanic island, causing the failure of material into the surrounding water. This can result in the production of turbidity currents, which are dense flows of sediment-rich water that can move downslope. These currents can transport sediment over long distances and affect the seafloor morphology. Another change that can occur after a volcanic island eruption is the development of various sizes of bedforms on the seafloor

(Normandeau et al., 2016). Bedforms are sedimentary structures that form due to the interaction between fluid flow and sediment transport. The eruption can release a large amount of sediment into the water, which can settle on the seafloor and form different bedforms. These bedforms can vary in size and shape depending on the characteristics of the eruption and the sediment properties. This chapter uses two multibeam bathymetric surveys, from pre- (2017) and post-eruption (April-June 2022). Based on the surveys, we found that multiple scales bedforms and scours can be found around the seafloor of the volcano. In summary, the aftermath of a volcanic island eruption induces profound transformations in the seafloor landscape, evidenced by the formation of expansive scours near the caldera, the occurrence of submarine landslides and turbidity currents, and the development of diverse bedforms of varying sizes. The comprehensive analysis, employing two multibeam bathymetric surveys conducted before (2017) and after the eruption (April-June 2022), reveals a nuanced tapestry of multiple-scale bedforms and scours across the volcanic seafloor.

1.5 Methods to study marine geohazards

Various methodologies are employed in the examination of marine geohazards, with one approach being laboratory-scale testing. This involves the use of physical models within flume tanks, enabling researchers to conduct experiments on a smaller scale. Such tests yield valuable insights into the behaviour of marine structures and phenomena (Mycek et al., 2013; Tang et al., 2022). Flume tank testing is particularly praised for its cost-effectiveness and its role in the initial evaluation of new concepts in marine engineering research (Gaurier et al., 2013). Another laboratory-based method involves the utilisation of core samples and geotechnical analysis. This method is crucial for understanding the processes, triggers, and prediction of submarine landslides, thereby assessing the associated risks (Masson et al., 2006). Nevertheless, laboratory-scale experiments encounter challenges related to scaling issues and the focus on small samples (de Leeuw et al., 2018; Keevil et al., 2007; Lai et al., 2022). Lai et al. (2022) also underscore the complexities inherent in such studies. The real word comparison especially in submarine setting may produce a varying results in terms of size and magnitude.

Numerical modelling represents a significant advancement in the study of submarine geohazards. Numerical models provide valuable insights into various phenomena and processes, aiding in the evaluation of seafloor changes and behaviour (Chen et al., 2022; S. Zhang et al., 2019). For example, a slope failure modelling may utilised several parameters in the model such as slope angle, grain size , permeability to create a potential failure model. This method is very useful as its gives you controls over the parameters. However, the effectiveness of numerical

models often relies on calibration with real-world observations, and gaps in the understanding of underlying physics persist (Bolla Pittaluga and Imran, 2014; Kameda and Yohei, 2021),

Field-scale studies offer an alternative avenue for investigating submarine geohazards, encompassing outcrop studies and subsurface geophysics (Hampton et al., 1996; Masson et al., 2006; Stevenson et al., 2015). These methods provide valuable insights into the geological and hydrological characteristics of the seafloor. They enable non-invasive subsurface characterization, facilitating the mapping of structures, faults, and voids critical for understanding geohazard potential (Arisona et al., 2020; Bakhshipour et al., 2013). In-situ geotechnical testing, such as the cone penetration test (CPT), constitutes a field-based method with reliability for assessing the liquefaction resistance of potentially liquefiable soils (Moss et al., 2006). Unlike laboratory-based methods, field-based approaches avoid scaling issues. While offering insights into past events, they may not always provide a comprehensive understanding of underlying processes (Englert et al., 2021; Masson et al., 2006).

Recent technological progress has brought about a transformative shift in the direct monitoring of marine geohazards, fostering a more nuanced comprehension of these phenomena. Clare et al. (2017) have made significant contributions by employing direct observations to monitor active flows, showcasing advancements in the direct monitoring of subaqueous sediment density flows and their triggers. These strides have notably bolstered the capacity to observe and decipher the intricacies of processes associated with marine geohazards (Talling et al., 2013).

The utilisation of Acoustic Doppler Current Profilers (ADCPs) for monitoring turbidity currents has garnered considerable attention in recent research. High-resolution ADCP measurements, as demonstrated by Heerema et al. (2022), Normandeau et al. (2019), and Sassi et al. (2012), enable the monitoring of turbidity currents. ADCPs, typically, are utilized for monitoring turbidity currents by suspending them at a specific elevation above the bed of a submarine canyon or river channel and ADCPs emit acoustic sound pulses into the water column and capture sound scattered back towards the instrument from particles suspended in the water. These devices compute flow velocity at various vertical intervals (bins) above the bed by analyzing the Doppler shift of the received signal along the four beams' axis. Through the integration of velocities from multiple beams, along with heading and tilt data, ADCPs ascertain Earth-referenced three-dimensional velocity components throughout a vertical profile, enabelling it to monitor turbidity currents (Simmons et al. 2020) .This approach facilitates the capture of dynamics within sediment-laden flows and the monitoring of suspended particles. Passive ocean seismometers play a vital role in discerning ground motions resulting from earthquakes and landslides. These instruments, as evidenced by Lai et al. (2018), Coltelli et al. (2016), and Clare et al. (2021), have been instrumental in capturing seismic data and monitoring various aspects in marine environments, including

debris flows, seismic activities, acoustic emissions, and ground movements originating from terrestrial landslides.

Conducting repeated seafloor surveys using multibeam echosounders proves instrumental in monitoring seafloor changes. This method enables the detection of alterations in bathymetry, sediment distribution, and seafloor morphology. The versatility of this approach is evident in its application to study diverse marine environments, such as volcanic regions, seamounts, and hydrothermal vent fields (Tontini et al., 2016; Fujiwara, 2021; Fundis et al., 2010; Thal et al., 2016). Data acquired from these surveys contributes to assessing the impact of geological events, such as volcanic eruptions and earthquakes, on seafloor morphology and elucidating the associated geohazard potential (Chiocci et al., 2011; Fujiwara, 2021; Fundis et al., 2010). Moreover, the repeated use of multibeam echosounders for seafloor surveys emerges as a powerful tool for studying changes in elevation and morphology. This method, highlighted in this thesis, stands out as the primary dataset for comprehensive examination and understanding.

1.5.1 The use of Multibeam bathymetric surveys to identify and characterise seafloor changes

The following text provides an overview of multibeam echosounders to provide context for those science chapters.

Multibeam echosounders are a type of active sonar system used for mapping the seafloor and collecting spatial information on its characteristics (Lecours et al., 2015). They belong to a group of active sonars that also includes sidescan sonars and singlebeam echosounders (Lecours et al., 2016). Multibeam echosounders operate by transmitting a controlled signal towards the seafloor and measuring the time it takes for the signal to return to the sensor (Lecours et al., 2016). By analysing the return signal, multibeam echosounders can determine the depth of the seafloor and create bathymetric maps (Gaida et al., 2020). In addition to bathymetry, multibeam echosounders can also provide information on backscatter, which is the amount of acoustic energy reflected back to the sensor (Lamarche and Lurton, 2018). Backscatter data can be used to infer information about the composition and roughness of the seafloor (Feldens et al., 2018).

How actually is the survey conducted? A multibeam echosounder comprises a transducer array and a receiver array. The transducer utilizes beamforming and beam steering to create a sound wave consisting of multiple beams. These beams are directed to form a swath perpendicular to the ship's track. Upon reaching the seafloor, the sound is reflected and captured by the receiver array, which consists of individual receivers oriented to detect sounds from specific directions. By measuring the two-way travel time of the beams, the water depth can be determined. The

configuration of multibeam echosounders allows for continuous depth measurements over an area as the vessel is in motion. Figure 1.2 shows the principal of multibeam echosounders.

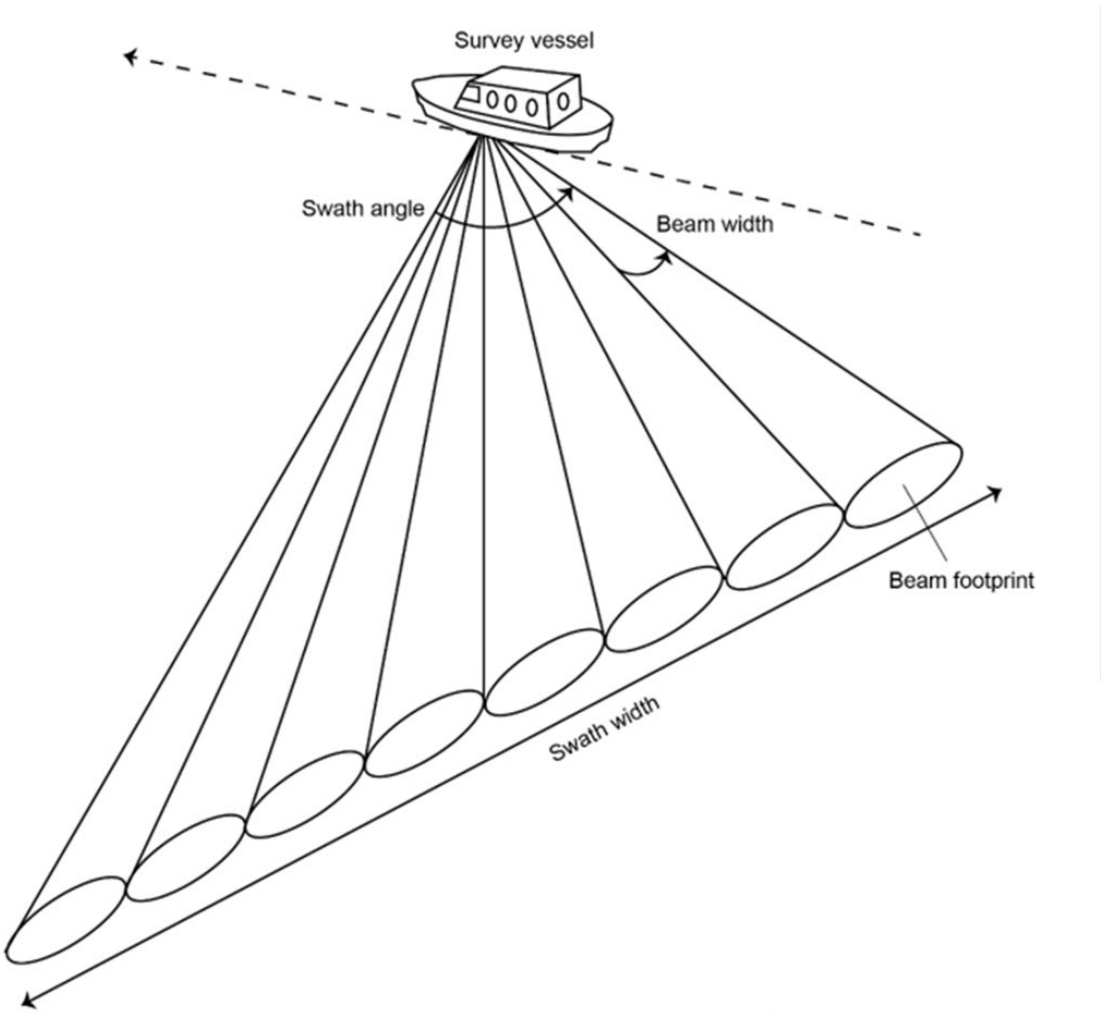

Figure 1.2: Principles of multibeam echosounders and surface vessel motions. Consist of a schematic overview of some of the parametres of a multibeam survey. Note how swath width and beam footprint will increase with water depth (after Seabeam, 2000)

When designing a multibeam survey, various factors must be considered. Firstly, the frequency range of the multibeam echosounder is crucial. Higher frequencies provide greater vertical accuracy in resolving seafloor elevation. However, higher frequency sounds are more easily attenuated in water and are not suitable for deeper waters. Therefore, the water depth determines the appropriate frequency for multibeam echosounders, the range can be around 500 kHz in coastal waters and 12 kHz in the deepest oceans. Next is the number of beams, often termed the amount of sounding, produced per swath is an important consideration. More beams per swath result in higher data quality. Another key property of multibeam echosounders is the angle of the beams generated by the transducer. The angle of individual beams determines the footprint of each sounding on the seafloor. A smaller footprint allows for the resolution of smaller-scale

features. Lastly, the maximum width of the swath must be established, the swath width can be adjusted based on preferences. Larger swath widths are preferred for maximizing coverage, while smaller swath widths are desirable when the survey's primary objective is the highest resolution. The data used in this thesis is of higher resolution.

So how do this high resolution data acquired? The horizontal resolution of multibeam bathymetry results from the combination of sounding density and the footprints of individual beam width. Sounding density, indicating the number of soundings per unit area, plays a crucial role in determining resolution. A higher sounding density generally leads to higher resolution. Yet, when sounding density surpasses a specific threshold, the resolution is constrained by the footprint of individual beams, hindering the detection of features smaller than that particular size. But, employing a grid size finer than the beam footprint can be advantageous, particularly in situations of high sounding density, as it allows for a more detailed depiction of the overall shape of larger features. With the increase of depth, the footprint of individual beams expands and sounding density decreases. This indicates that horizontal accuracy experiences a rapid decline as water depth increases. The resolution is important, but data obtained need to be precise in order to be usable.

The vertical precision of multibeam bathymetry is influenced by various factors. The accuracy of multibeam echosounders varies with water depth, typically falling within the range of 0.2% to 0.5% of the water depth, contingent on the particular device in use. Vertical precision may encounter additional obstacles arising from alterations in the water column structure. The stratification of the water column can lead to beam refraction, with outer beams characterized by higher angles of incidence being particularly vulnerable to fluctuations in the water column structure.

Finally, inaccuracies related to the motion of the ship can impact vertical accuracy. Even though the motion of the ship is corrected during the acquisition of multibeam data, the motion sensors may introduce their own errors leading to a reduction in vertical precision. The effect of motion can be reduced by slowing the speed of motion. Another ways would be to integrating the data with other remote sensing methods (Lubczonek et al., 2021). Another way is the use of advanced navigation and positioning systems. Integrating advanced navigation and positioning systems has the potential to alleviate the influence of ship motion on survey precision, consequently minimizing inaccuracies in multibeam echosounder surveys (Nakanishi & Hashimoto, 2011).

Multibeam echosounders have a wide range of applications. They are commonly used in fisheries and benthic habitat mapping to study the distribution and abundance of marine organisms and their habitats (Lecours et al., 2015). They can provide detailed information on the shape and structure of the seafloor, allowing researchers to study processes such as seafloor spreading and

sediment transport (Feldens et al., 2018). Multibeam echosounders are also used in environmental monitoring, such as monitoring suspended sediment concentrations and detecting mass movements (Hariyanto et al., 2021). Additionally, multibeam echosounders can be used to map the water column above the seafloor, providing information on the distribution of organisms and physical properties of the water column (Porskamp et al., 2022).

The use of multibeam echosounders for submarine geohazard analysis has proven to be a valuable tool in understanding and assessing potential risks and hazards in underwater environments. Multibeam echosounders provide high-resolution bathymetric data, allowing researchers to map and analyse the seafloor morphology and identify potential geohazards such as submarine landslides, fault lines, and underwater volcanoes (Diesing et al., 2014).

By combining multibeam bathymetry data with other data sources, such as backscatter and seismic data, researchers can gain a comprehensive understanding of the geological features and processes that contribute to submarine geohazards (Micallef et al., 2012). Backscatter data obtained from multibeam echosounders can provide information on the composition and roughness of the seafloor, aiding in the identification of potentially unstable or hazardous areas (Lamarche & Lurton, 2017). Seismic data can help detect subsurface structures and identify potential fault lines or areas of tectonic activity (Micallef et al., 2012).

Multibeam echosounders are also used to assess sediment dynamics and identify sediment transport pathways. By analysing the bathymetric data obtained from multibeam echosounders, researchers can identify features such as submarine channels, canyons, and others that indicate sediment transport processes and potential sediment-related geohazards (Janowski et al., 2018).

The information obtained from multibeam echosounders is crucial for geohazard assessment and management in underwater environments. Table 1.1 shows examples of the previous mapped area of submarine geohazard. It helps in identifying and characterizing potential risks, understanding the processes that contribute to geohazards, and informing decision-making for coastal development, resource management, and conservation efforts (Summers et al., 2021).

When working with multibeam echosounder data, there are potential sources of noise and errors that need to be considered. These factors can impact the accuracy and reliability of the data and may require additional processing or filtering techniques. Random noise is generated as a result of the overall accuracy of the multibeam echosounder and survey set-up (Hughes Clarke, 2018). The noise can be from physical factors (e.g. turbulence, acoustic scattering and absorption by seawater, bathymetry artifacts, bathymetry and tidal differences), sensor factors (e.g. fish activity, transducer performance, sound velocity variations, rough sea conditions), and human

factors (e.g. errors in system configuration and set-up, errors in data processing, inadequate data quality control and assurance) thus effecting the survey precision and accuracy.

Table 1.1: Example of the previous mapped area of submarine geohazard.

Location	**Repeated bathymetric survey**	**Processed observed**	**reference**
Squamish submarine delta, British Columbia, Canada	Survey every 6-24 months (from 2004 to 2009); survey every weekday (during Spring and Summer 2011 and 2012); single survey for 6 days (June 2013); 1 x annual survey (2015)	Delta-lip collapses, turbidity currents and bedform migration	Hughes Clarke et al. (2012, 2014), Clare et al. (2016), Hughes Clarke (2016), Hizzett et al. (2018), Hage et al. (2018),
Knight, Bute and Toba Inlets, British Columbia, Canada	2 x annual surveys (2005 and 2008); 1 x annual survey (2010)	Slope failure, turbidity currents	Conway et al. (2012
Fraser River Delta, Western Canada	1 x annual survey (1994, 2001, 2003, 2005); 2 x surveys (May 2006 and September 2006	Turbidity currents, slope failure	Hill et al. (2008); Lintern et al. (2018)
Monterey Canyon, California, USA	2 x annual surveys (September 2002 and February 2005); 2 x surveys (March 25, 2003 and March 26, 2006); 1 x annual survey (September 2003); 2 x surveys (September 2004 and November 2004)	Submarine landslide, bedforms migration	Smith et al. (2007); Xu et al. (2008); Paull et al. (2010)
Kaikoura Canyon, New Zealand	2 x surveys (2016)	Canyon flushing	Mountjoy et al. (2018)
Begawan Solo submarine delta, East Java	2 x annual survey (in 2009 and 2004)	Turbidity currents	Syahnur and Java (2016
Lake Geneva, Western Europe	1 x annual surveys (1891); 1 x annual survey (between December 2012 and November 2013); 4 x surveys (1986, 2000, 2008, 2012)	Turbidity currents, mass transport events	Silva et al. (2018); Corella et al. (2016)
Congo Canyon, offshore West Africa	1 x annual survey (2005, 2019)	Landslide, Knickpoint migration	Pope et al. (2022)
West Mata seamount, NE Lau basin	1 x annual survey (1996, 2008, 2009, 2011, 2012); 2 x surveys (May 2010 and December 2010)	Volcanic activities	Embley et al. (2014)
Monowai submarine volcano, Kermadec arc	1 x annual survey (1998, 2004)	Volcanic activities, landslide	Wright et al. (2008)
Hunga Volcano, Tonga	1 x annual survey (2015, 2016, 2017, 2022)	Volcanic activities, Bedform migration	Seabrook et al (2023)

Another common error pattern in difference mapping is differences aligned with the survey track lines. These errors express themselves as errors along the edges of a survey, if the track lines were orientated along the edge of one of the survey. This error can be due to a systematic error in the correction of the roll of the ship, or uncaptured variations in sound velocity structure of the water column, with a little uncertainty towards the data credibility. To avoid this, An error analysis was conducted by comparing the profile of the difference map at the area of little to no change, such as the overbank of the submarine channel. Some overbank have been found to be quite an active and dynamic environment (Tek et al., 2022). However, these locations sound to be inactive because of the lack of geomorphological changes in the area in between surveys. Figure 1.3 shows the error analysis conducted at the study location of chapters 2 and 3. The results show an error margin of around 1.4 m in the shallower region and 2m in the deeper region for Chapter 2, 0.35 m in the shallower reason and 0.5 m in the deeper region for Chapter 3. For Chapter 4, it is difficult to find an area with no changes due to the massive collapse of the volcano.

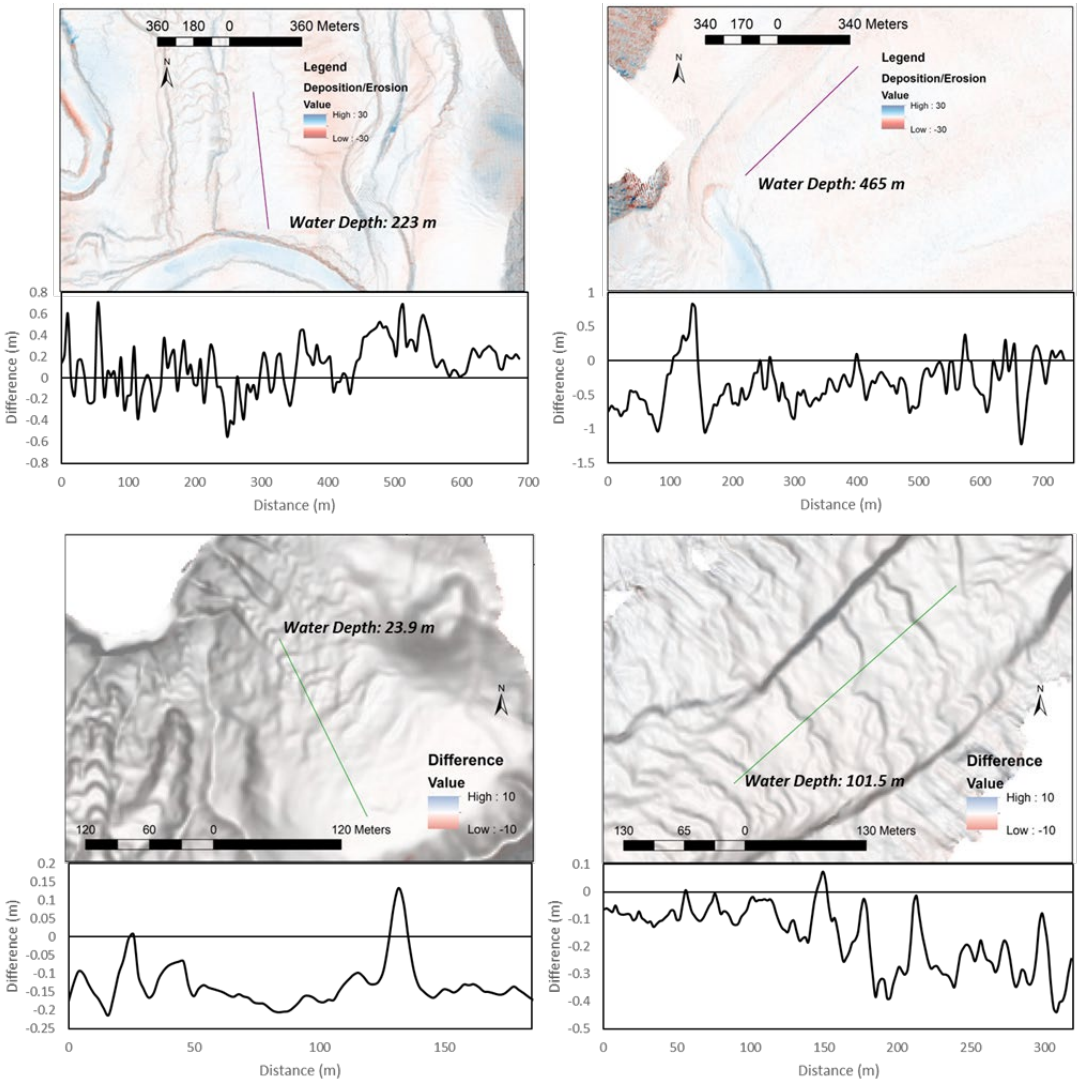

Figure 1.3: Error analysis conducted at study location of chapter 2 and 3.

1.6 Introduction to study areas

The following text provides an introduction to the three study sites that are the geographic focus of research in this thesis and provides justification for their selection.

1.6.1 Knight Inlet, British Columbia

Situated in the southern expanse of British Columbia, Canada, the Knight Inlet unfolds as a compelling fjord nestled within the Pacific Ranges of the Coast Mountains, boasting elevations exceeding 3000 meters (Holland, 1976). This locale, adorned with diminutive ice caps and valley glaciers sustained by intricately interconnected drainage basins, is imbued with profound geological significance. It is distinguished by a myriad of fjords, widely regarded as vestiges of the Quaternary glaciation era, contributing to the region's complex and storied geological history.(Wheeler et al., 1991). Predominantly composed of plutonic bedrock (Bornhold et al., 1994), the fjord landscape sets the stage for a comprehensive exploration of its unique features and evolutionary processes.

The rationale behind selecting the fjord as our study area lies in its distinctive attributes, primarily driven by the presence of submarine channels within a fjord environment. The steep valley walls and rapid expansion of deltas into deep waters make this locale an ideal setting for the examination of river flood plains and associated deltaic systems (Prior et al., 1987; Syvitski and Farrow, 1983). The choice of Knight Inlet specifically stems from its well-developed nature (Gales et al., 2019), distinguished by a total length of 102 km, an average width of 3 km, and notable depth metrics, including a mid-inlet depth of 420 m and a maximum depth of 550 m. Additionally, the inlet features two sills located at 74 and 110 km from its head (Gales et al., 2019).

The Klinaklini and Franklin rivers emerge as the primary contributors to the fjord’s hydrological dynamics, with the former accounting for over 80% of the freshwater input (Ren, 1992; Syvitski and Farrow, 1983). The Klinaklin River, depositing fine to coarse sands into the fjord, gives rise to transverse bedforms interpreted as channel-fill turbidites, generated by turbidity currents resulting from sediment failure on or near the delta front (Prior et al., 1986; Ren, 1992; Zeng et al., 1991).

The Klinaklini River flows into the fjord from the northwest, while the Franklin river enters from the east. Additionally, the Sim and Wolkesh rivers contribute to smaller deltas on the west and east sides of the fjord, respectively (Conway et al., 2012). This fjord experiences a periodic, seasonal influx of meltwater during the spring and summer, originating from the melting snowpack and

glaciers. This phenomenon significantly influences the flow dynamics of the river systems that supply water and sediment to the fjords, with daily discharge maxima often surpassing 1000 m^3/s (Bornhold et al., 1994).

The inflow of meltwater leads to the interaction of buoyant freshwater outflows on the surface and denser saline water inflows beneath, creating density differences. This interaction, occurring where freshwater plumes enter the heads of inlets, may result in turbid underflows, known as hyperpycnal flows (Bornhold et al., 1994; Ren et al., 1996). The density or turbidity area generated by this process becomes a pivotal factor influencing our study. Turbidity currents, occurring predominantly during the summer and early fall months (June to October) in Knight Inlets (Bornhold et al., 1994), are considered the primary geomorphic agents responsible for creating and continuously modifying the deep sinuous channels within these inlets (Bornhold et al., 1994; Prior et al., 1987; Ren et al., 1996). This dynamic setting makes Knight Inlets an active and compelling location for investigating turbidity currents and their impact on the seafloor.

The Knight Inlet serves as a compelling focus for our study on submarine channel evolution, offering a unique combination of geological features and well-defined hydrological characteristics that make it an exemplary site for understanding the intricate processes shaping its underwater topography.

1.6.2 Squamish Prodelta, British Columbia

River deltas, such as the Squamish prodelta, play a pivotal role in the world's sedimentary and carbon dynamics, as the majority of them contribute to the annual 20 Gt flow of fluvial sediments either find storage within deltas or undergo redistribution in the seas, according to the insights of (Milliman and Farnsworth, 2011). Nestled within the fjord-head system of Howe Sound, the Squamish Delta exhibits distinctive features that make it a compelling subject for scientific inquiry. One of the geological characteristics of this prodelta is It's rapid offshore depth increases to 100 m within 1 km from the coastline (Clarke et al., 2014). The delta front comprises three discrete channel-lobe systems with bed form fields generated by turbidity currents, revealing the dynamic nature of this environment (Hughes Clarke et al., 2012)

The Squamish River, a key contributor to the delta's sedimentary influx, annually transports over one million cubic metres of sediment to its delta and ultimately flows into Howe Sound (Hickin, 1989). Notably, the river's discharge, dominated by sediment transport, exceeds 350-500 $m^3\ s^{-1}$ during the May-October freshet, occasionally surging to flood peaks surpassing 1,000 $m^3\ s^{-1}$ (Clare et al., 2016; Clarke et al., 2014). The consequential bed load from the gravelly riverbed washes over the delta lip, resulting in a remarkable progradation of more than 10 metres in a single day, (Hizzett et al., 2018).

Examining slope failure involves a comprehensive consideration of various factors, and amidst this complexity, the Squamish Delta emerges as a standout location. The distinctive attributes of the Squamish Delta elevate its significance within the realm of slope failure studies. What sets this delta apart is not only its annual occurrence of massive discharge but also the interplay of tidal activities that exert a profound influence on morphological changes, leading to sediment accumulation and subsequent slope failure (Hickin, 1989; Hughes Clarke, 2016; Hughes Clarke et al., 2012).

Previous investigations shed light on the rapid occurrence of delta lip failure within a few hours following flood peak (Clare et al., 2016). Adding to the intricacy, Squamish Prodelta sediments are identified as gas-saturated, introducing complexity to determining factors governing slope failure in this region (Clarke et al., 2012).

Another noteworthy feature characterising the delta environment is the presence of bedforms, believed to result from turbidity current activities that locally erode and deposit sediment (Hughes Clarke, 2016). Bedform migration, attributed to turbidity currents generating cyclic steps, is inferred from various studies (Hughes Clarke, 2016; Hughes Clarke et al., 2012; Symons et al., 2016). Direct monitoring has revealed the occurrence of more than 100 turbidity currents during the spring and summer freshet each year, when seasonal meltwater amplifies river discharge from approximately 100 m3/s in winter to over 500 m3/s, reaching maximum heights of1000 m3/s (Hughes Clarke et al., 2012).

This dynamic scenario prompts an intriguing avenue of exploration—the active process of bedform migration during the freshet—and raises the question of whether these bedforms play a role in destabilising the delta slope. Thus, this research aims to delve into the complexities of the Squamish Delta environment, investigating the various factors contributing to slope failure, specifically focusing on the role of bedforms in delta slope destabilisation

1.6.3 Hunga volcano, Kingdom of Tonga

The Hunga Tonga volcano has become a focal point of scientific investigation, driven by a profound interest in understanding the impact of major volcanic eruptions on the seafloor. Situated approximately 70 km north-northwest of Tonga's capital, Nukualofa, the Hunga Tonga volcano is an underwater caldera volcano that drew particular attention due to its eruption on January 15, 2022.

This eruption, hailed as one of the largest in more than a century and described as a once-in-a-millennium event (Cassidy and Mani, 2022; Klein, 2022), provided an unprecedented opportunity for a comprehensive study. The magnitude of the eruption was high, manifesting in massive

eruption plumes, volcanic deposits, intense pyroclastic currents, far-reaching tsunamis, and widespread damage to infrastructure. Tragically, the event resulted in human fatalities and substantial destruction (Heidarzadeh et al., 2022; Lynett et al., 2022; Proud et al., 2022; Wright et al., 2022).

The evident risk to human livelihoods underscored the urgency of studying such eruptions, especially considering that most submerged volcanoes remain poorly documented. Comprehensive assessments of pre- and post-event seabed conditions are rare, particularly for eruptions of the magnitude witnessed at the Hunga Tonga volcano (Caress et al., 2012; Chadwick et al., 2019; Le Friant et al., 2015).

Beyond the immediate consequences, the novelty of the Hunga Tonga eruption presents a unique advantage for scientific inquiry. As a recent event, the traces and changes on the seafloor can predominantly be attributed to the eruption itself, minimising the uncertainties associated with potential reworking by other activities. This aspect enhances the reliability of observations and insights into the dynamic changes occurring in the aftermath of such a monumental volcanic event. Thus, the study of the Hunga Tonga volcano holds immense promise for advancing our understanding of the impact of major volcanic eruptions on the seafloor and informing strategies for mitigating associated risks to coastal communities and infrastructure

Chapter 2 A threshold in submarine channel curvature explains erosion rate and type

This chapter is currently under review for a publication in the Earth and Planetary Science Letters.

Zaki Zulkifli, Michael A. Clare, Maarten Heijnen, D. Gwyn Lintern, Cooper Stacey, Peter J. Talling, Matthieu J.B. Cartigny, Timothy A. Minshull, Hector Marin Moreno, Jeffrey Peakall, Stephen Darby

Author contributions: I am responsible for the analysis and the main author of this manuscript. M.H., D.G.L., C.S contribute in data aquisition. M.A.C., P.J.T., J.P and S.D. provided the main editorial support on the manuscript. Other authors provided access all the authors commented on the final version of this manuscript

Abstract:

Submarine channels are conduits for sediment-laden flows called turbidity currents, which play a globally significant role in the offshore transport of sediment and organic carbon and pose a hazard to critical seafloor infrastructure. Time-lapse repeat surveys of active submarine channels have recently shown that upstream-migrating knickpoints can dominate channel evolution. This contrasts with many studies of ancient outcrops and subsurface geophysical data that inferred channel bends migrate laterally, as occurs in meandering rivers. Here, we aim to test these two contrasting views by analysing two high-resolution repeat seafloor surveys acquired thirteen years apart across the entirety of an active submarine channel in Knight Inlet, British Columbia (2005-2018). We find that two main mechanisms control channel evolution, normalised channel radius of curvature (specifically, R^* - channel radius of curvature normalised to channel width) explains which of these mechanisms dominate. Pronounced outer bend migration only occurs at tight bends ($R^*<1.5$). In contrast, at broader bends and straighter sections ($R^*>1.5$), erosion is focused within the channel axis, where upstream-migrating knickpoints dominate. High centrifugal accelerations at tight bends promote super-elevation of flows on the outer channel flank, thus, enhancing outer bend erosion. At $R^*>1.5$, flow is focused within the channel axis, promoting knickpoints that migrate upstream at an order of magnitude faster than the rate of outer bend erosion at tight bends. Despite the dominance of knickpoints in eroding the channel axis, their stratigraphic preservation is very low. In contrast, the lateral migration of channel bends results in much higher preservation via lateral accretion of deposits on the inner bend. We conclude that multiple mechanisms can control evolution at different channel reaches and that

the role of knickpoints has been underestimated from past studies that focused on deposits due to their low preservation potential.

2.1 Introduction

Submarine channels are the primary conduit for the transfer of sediment from shallow to deep water and occur on most continental slopes worldwide (Mulder, 2011). Globally-important quantities of sediment and organic carbon are transported through these channels by density flows called turbidity currents (Azpiroz-Zabala et al., 2017; Rabouille et al., 2019; Talling et al., 2024). Submarine channel deposits form some of the most significant sediment accumulations on our planet, creating substantial hydrocarbon reserves, stratigraphic archives of climate change, and carbon burial (Babonneau et al., 2010; Clift and Gaedicke, 2002; Covault et al., 2014; Sylvester and Covault, 2016). Other than being a significant contributor to deep-sea sediment transport (e.g., Paull et al., 2018), turbidity currents also pose a threat to seafloor infrastructure, including hydrocarbon pipelines and the global network of seafloor cables that provide critical energy and communications (Carter et al., 2014; Sequeiros et al., 2019). Therefore, it is vital to understand which processes control sediment transport and storage in submarine channels and over which timescales, as this governs the hazard posed to seafloor structures, the efficiency of organic carbon burial, and the nature of sediment transfer to the deep sea.

Despite many studies over the past decades, there remains disagreement about which mechanism is the dominant control on submarine channel evolution. First, upstream-migrating crescentic bedforms have been proposed to play a dominant role in channel evolution on steep slopes such as the continental slope where high Froude numbers are favoured. They act as a building block of such depositional systems, from the proximal channel axis, levee-overbanks, down to the channel-lobe transition zone (Covault et al., 2014, 2017; Hamilton et al., 2015; Vendettuoli et al., 2019). Such bedforms have been linked to fast-moving turbidity currents that undergo a switch (hydraulic jump) from Froude super- to sub-critical conditions as they pass over the bedform (Spinewine et al., 2009; Hughes Clarke, 2016; Covault et al., 2017; Hage et al., 2018), and are common, particularly within the proximal reaches of many submarine channels worldwide, (e.g., Symons et al., 2016; Covault et al., 2017; Hage et al., 2018). Depending on the aggradation rate of the system, the resultant deposits are preserved either as low-angle, backstepping beds (high aggradation) or lenticular bodies (low aggradation), typically comprising massive sands (Hage et al., 2019).

Second, the upstream migration of steep steps in channel gradient, known as knickpoints (that can be tens of metres high), has recently been suggested to play an even more critical role in channel evolution (e.g. Guiastrennec-Faugas et al., 2020, 2021; Heijnen et al., 2020). Submarine

knickpoints may form as a result of erosion by a turbidity current undergoing a large hydraulic jump, due to retrogressive collapse of a steep downstream slope, or due to sediment build-up at tight bends, or some combination of these processes (Heijnen et al., 2020; Guiastrennec-Faugas et al., 2021). The rate of knickpoint migration (100-450 m/year) in submarine channels may exceed that of equivalent features in rivers by 2-6 orders of magnitude, depending on substrate strength and discharge (Heijnen et al., 2020). Knickpoint migration results in localised but pronounced (tens of metres) down-cutting into previously emplaced channel axis deposits and forms tabular channel-wide deposits, which are also focused within the channel axis (Mitchell, 2006; Heijnen et al., 2020). Despite these recent studies demonstrating the important role of knickpoints in shaping modern active systems, the identification of knickpoints in ancient systems remains sparse, with few studies providing clear evidence of their deposits (e.g. Heiniö and Davies, 2007; Stright et al., 2017; Tek et al., 2021; Allen et al., 2022).

Finally, the lateral migration of channel bends has also been inferred to play a key role in submarine channel evolution (e.g. Peakall et al., 2000, 2007; Babonneau et al., 2010; Kolla et al., 2012; Jobe et al., 2016; Palm et al., 2021). Channel bends have been observed from seafloor and subsurface seismic surveys, particularly on large deep-sea fans and in many of the lower reaches of deep-sea submarine channels (e.g. Peakall et al., 2007; Babonneau et al., 2010). While submarine channel bends may share many morphological similarities with rivers, the nature of flow within submarine channels and the morphology of expansion of bends can vary from that observed in rivers (e.g. Peakall et al., 2000; Peakall and Sumner, 2015; Covault et al., 2021). However, the overall pattern of erosion in submarine channels is focused on the outer bend, while deposition occurs on (or just downstream of) the inner bend, forming laterally accreted packages of sediment and/or oblique accretion deposits (Peakall and Sumner, 2015). Abundant evidence of lateral accretion packages that indicate channel bend migration has been found in many ancient submarine channel systems worldwide (e.g. Abreu et al., 2003; Dykstra and Kneller, 2009; Babonneau et al., 2010; Jobe et al., 2016).

There are thus many different potential mechanisms that may control submarine channel evolution; however, the limited number of examples of direct monitoring of modern active submarine channel systems and the resultant geomorphic evolution, means that the factor (or factors) that are most dominant remain unclear (e.g. Talling et al., 2015). Past studies have focused mainly on depositional archives (subsurface geophysical imaging, sediment coring, and ancient outcrops), (e.g. Zeng et al., 1991; Babonneau et al., 2010; Covault et al., 2016), supplemented by scaled-down analogue laboratory experiments (e.g. Keevil et al., 2006), and numerical modelling (e.g. Giorgio Serchi et al., 2011; Sylvester et al., 2011; Tian et al., 2023)). Therefore, most observational studies analyse the resultant deposits, which are highly incomplete due to punctuated erosion caused by successive flows (e.g. Silva et al., 2019;

Vendettuoli et al., 2019). Laboratory and numerical models (e.g. Keevil et al., 2006; Sylvester and Covault, 2016) provide useful insights into channel evolution, but whilst flow fields have been examined at field-scale (Parsons et al., 2010; Wei et al., 2013; Sumner et al., 2014; Azpiroz-Zabala et al., 2024) there remain few studies that have examined flow processes and channel evolution in natural channels, particularly ones that cover the entirety of a channel system (e.g. Hughes Clarke, 2016; Paull et al., 2018; Gales et al., 2019). As a result, there is a compelling need for a field-scale study that focuses on flow processes in channel evolution.

Recent advances in repeat seafloor mapping now enable field-scale monitoring of submarine channel evolution at high temporal (minutes to years) resolution and provide the opportunity to test deposit-based models and hypotheses. While such monitoring campaigns face many challenges (e.g. accessibility, high cost, and infrequency of events; Talling et al., 2015), a growing number of active submarine channels have now been repeatedly mapped over the past decade to better understand the nature of the processes that shape them (e.g. Conway et al., 2012; Hughes Clarke, 2016; Paull et al., 2018; Silva et al., 2019; Vendettuoli et al., 2019; Heijnen et al., 2020). Most of these channel systems that have been time-lapse surveyed are in relatively shallow (<600 m) water on steep slopes and remain only partially surveyed (i.e. not from source to sink). However, insights gained from repeat bathymetric surveys allow us to address key questions about how and why channels evolve.

2.2 Aims

In this paper, we analyse repeat seafloor surveys acquired 13 years apart that cover the entirety of a modern, active submarine channel system (from river source to termination at a deep-sea lobe) in Knight Inlet, British Columbia, Canada. Such extensive surveys are rare; we know of only one published study that has repeatedly surveyed from source to deep-sea sink (Heijnen et al., 2020). We aim to answer the following questions: First, which processes dominate the evolution of the submarine channel in Knight Inlet? Previous studies have identified crescentic bedforms, channel bends and knickpoints in Knight Inlet and other submarine channels in similar fjord settings (Conway et al., 2012; Gales et al., 2019). New repeat seafloor mapping data allow us to quantify the amount of net erosion and net deposition attributed to these different processes and understand how they shape the channel. We see that different reaches of the channel are affected to a different extent by these various processes. This motivates our second question. Why does the influence of these processes (bedform migration, outer bend erosion, and knickpoint migration) vary spatially along the channel? We investigate whether channel morphology and its influence on flow behaviour explain the nature and rate of erosion and migration. The curvature of the river and tidal channel systems has been shown to play a vital role

in controlling meander bend growth rate (e.g., Hickin and Nanson, 1975; Finotello et al., 2018; Sylvester et al., 2019), so we ask whether a similar control exists in submarine channels. Finally, what is the likely preservation of stratigraphic evidence for the different mechanisms that influence channel evolution? We compare the depositional signature of the different processes and discuss if their variable preservation potential may bias the interpretation of processes that operated and dominated in ancient submarine channel systems.

2.3 Data and Methods

We analyse two bathymetric surveys acquired in 2005 and 2018 in Knight Inlet, British Columbia, Canada. The surveys cover the full extent of a 41 km-long submarine channel system, which extends from two prodeltas fed by the Klinaklini (responsible for 80% of the sediment supply; Bornhold et al., 1994) and Franklin Rivers to a terminal lobe at approximately 450 m water depth (Figure 2.2A). Sediment supply from these two rivers is seasonally variable, mainly supplied during the spring and summer freshet due to snowmelt. Previous measurements using seafloor current meters have shown that many (at least 25-30) turbidity currents occur each year within the submarine channel and are most likely during windows of heightened river discharge (Bornhold et al., 1994); as observed in other submarine channels in the region (e.g. Howe Sound – Hughes Clarke, 2016). River discharges in the winter are typically below 100 m^3/s but can reach peaks of 1200 m^3/s in the spring and summer (Bornhold et al., 1994). Sediments in the submarine channel are typically fine to coarse sands, with silt and clay deposits dominating the areas outside the channel (Ren et al., 1996).

Bathymetric data were obtained using a Kongsberg Maritime EM710 (70-100 kHz) multibeam echosounder deployed from the RV Vector operated by the Canadian Coastguard Service. Data were gridded into 5 m x 5 m bins for the 2005 survey and 2 m x 2 m for the 2018 survey. The vertical resolution of the data is <0.5% of the water depth (Conway et al., 2012; Hughes Clarke et al., 2014). Hence in the deepest water (~450 m) surveyed here, this vertical resolution is 2.25 m.

The bathymetric data were analysed using ESRI ArcGIS software. Greyscale slope maps were generated to visualise channel morphology, and a raster calculator was used to generate differences in elevation between the two surveys. As part of this process, the 2018 2 x 2 m bin-size survey was re-sampled to match the coarser 5 x 5 m gridding of the 2005 survey. In the bathymetric difference maps, red colours indicate areas of net erosion (negative values), while blue colours indicate areas of net deposition (positive values). Confidence in the calculated elevation differences is reduced at the edges of the survey area (i.e. well outside the channel limits) and where elevation differences were equal to or below the vertical resolution of the bathymetric data. Seabed elevation changes and eroded volumes were calculated using the

raster calculator tools in ArcGIS software. Channel width was calculated by measuring the horizontal distance orthogonal to the channel axis between breaks in slope on the channel flanks (Fig 2.1). We measure the channel width at the apex of each bend. This measurement was completed manually, and each flank was selected manually as the point where flows could overflow outside the channel. The mean channel width is 236 m. Sinuosity, defined as the ratio between the length along the channel and the straight-line distance between the endpoints, was calculated using the RiverMetric package in QGIS software. Sinuosity was calculated every 10 m down the channel over a length scale of 1000 m. The mean channel sinuosity is 1.76. The location for the measurement of the radius of curvature was decided purely by visual fitting at the arc of the channel bend, which was measured in ArcGIS for each of the channel bends (Fig 2.2). The measurement of the radius of curvature is achieved through a circle that most nearly fits the curve of a given channel bend (Weihaupt, 1989). In order to compare observations at Knight Inlet with other systems, we present a normalised radius of curvature R^*, where for each bend, we divide the radius of curvature, R, by the local channel apex width (B), following a widely-adopted approach for terrestrial rivers first applied by Hickin and Nanson (1975). Radius of curvature is the inverse of the channel curvature ($1/R$). Figure 2.1 shows how the measurements are made in this study.

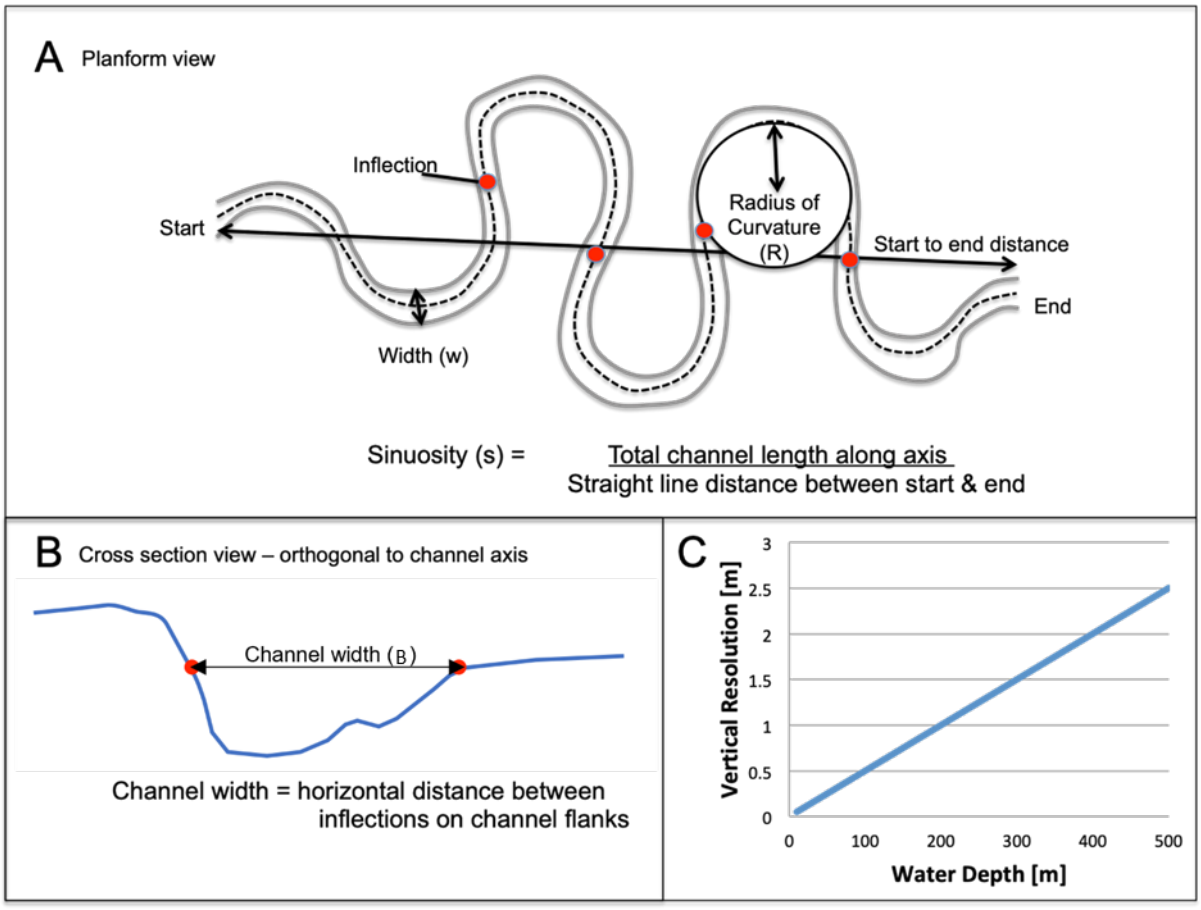

Figure 2.1: Illustration of measurements made in this study. A) Planform view of the channel to illustrate sinuosity, radius of curvature and channel width. B) Cross-section view to

illustrate the measurement of channel width, which was taken orthogonal to the channel axis. C) Plot showing how the vertical resolution of the multibeam bathymetric data changes as a function of water depth.

2.4 Results

Differences in elevation above the vertical resolution of the bathymetric data are observed at several locations along the full length of the channel, from the prodelta that forms the start of the submarine channel to the lobe at the channel's deep-water terminus (Fig 2.2). Three different types of seafloor change are observed over the thirteen-year interval: i) crescentic bedform migration and associated local channel incision; ii) upstream-migration of knickpoints; and iii) lateral migration of channel bends. We now discuss where these seafloor changes occur within the submarine channel at Knight Inlet.

2.4.1 Processes responsible for seafloor change

2.4.1.1 Crescentic bedforms on the prodelta slope

The steep (~5°) submarine prodelta front at the channel head is dominated by crescentic bedforms, which have typical wavelengths of 10 m and amplitudes of 5 m. Bedforms are observed across the entire prodelta front, but discernible elevation changes (i.e. above the vertical resolution of the data, which is <0.5 m here) are only seen down-stream of the Klinaklini and Franklin Rivers (herein termed the 'active delta'; a locus for sediment accumulation of up to 9 m vertically). This area is not solely net aggradational, as a new channel has been locally incised (up to 5 m depth), cutting a new pathway that is covered with crescentic bedforms (Fig 2.3A). As bathymetric resolution reduces in greater water depths, it is possible that such features may occur farther down the channel but cannot be imaged reliably.

2.4.1.2 Upstream-migration of knickpoints

Farther downslope from the prodelta, where a single channel is established on an average slope of 1.4°, the upstream-migration of up to 5-10 m-high knickpoints, with steep headwalls (~40°) dominates several reaches of the channel (Fig 2.3B and 2.3D). Knickpoints occur at multiple points along the channel (Fig 2.2), including distinct 10 m-high isolated knickpoints at 270 m, 280 and 300 m water depth, a series of three 5 m-high knickpoints that migrate upstream up to 1 km around a large channel bend between 260 m and 300 m water depth (Fig 2.3B), and several small (5 m-high) knickpoint at 425 m water depth ((Fig 2.3D). The elevation change for this latter smallest knickpoint is close to the vertical resolution of the multibeam data at this depth. Hence, we cannot be fully confident in its migration. However, the changes for the other larger and

shallower water knickpoints far exceed the vertical resolution at their equivalent water depths, and those larger knickpoints clearly migrate upstream. Erosion created by the migration of knickpoints results in up to 10 m of elevation change, which is almost exclusively focused within the axis of the channel. Occasionally there is some minor erosion focused towards the outer bend of the channel where a series of three knickpoints occur in the large channel bend (Fig 2.3B).

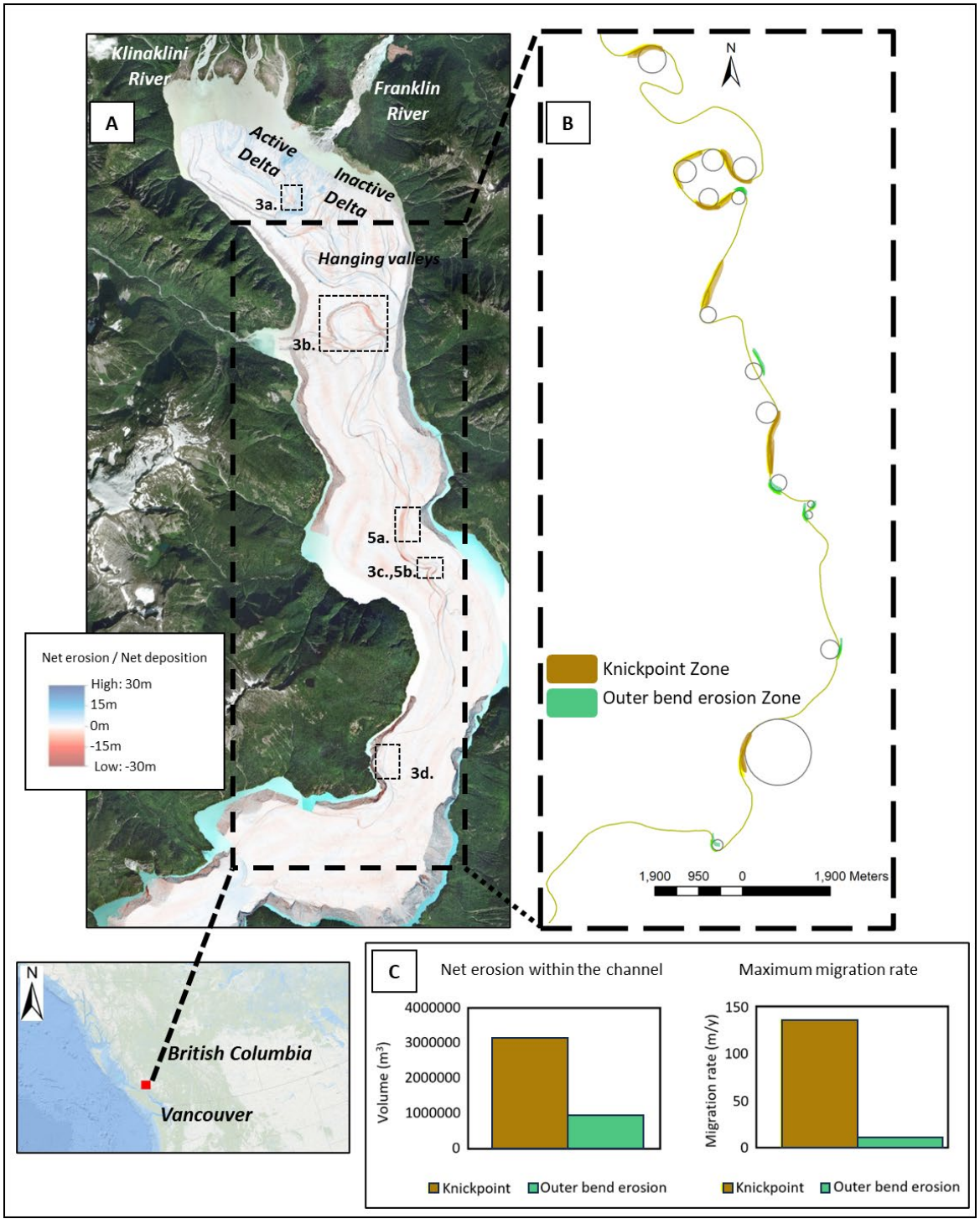

Figure 2.2: A) An overview of the elevation change and satellite data between 2005 and 2018 for the study area, illustrating locations that are detailed in Figure 2.3, B) Curvature of

radius annotated for the channel beds along the submarine channel, annotated with the locations where erosion related to knickpoints or outer bend migration was identified, C) Total eroded volumes over 13 years, differentiating that relating to knickpoints and outer bend erosion, D) Maximum migration rate measured for knickpoints (distance upstream) and at channel bends (distance orthogonal to the channel axis) over 13 years.

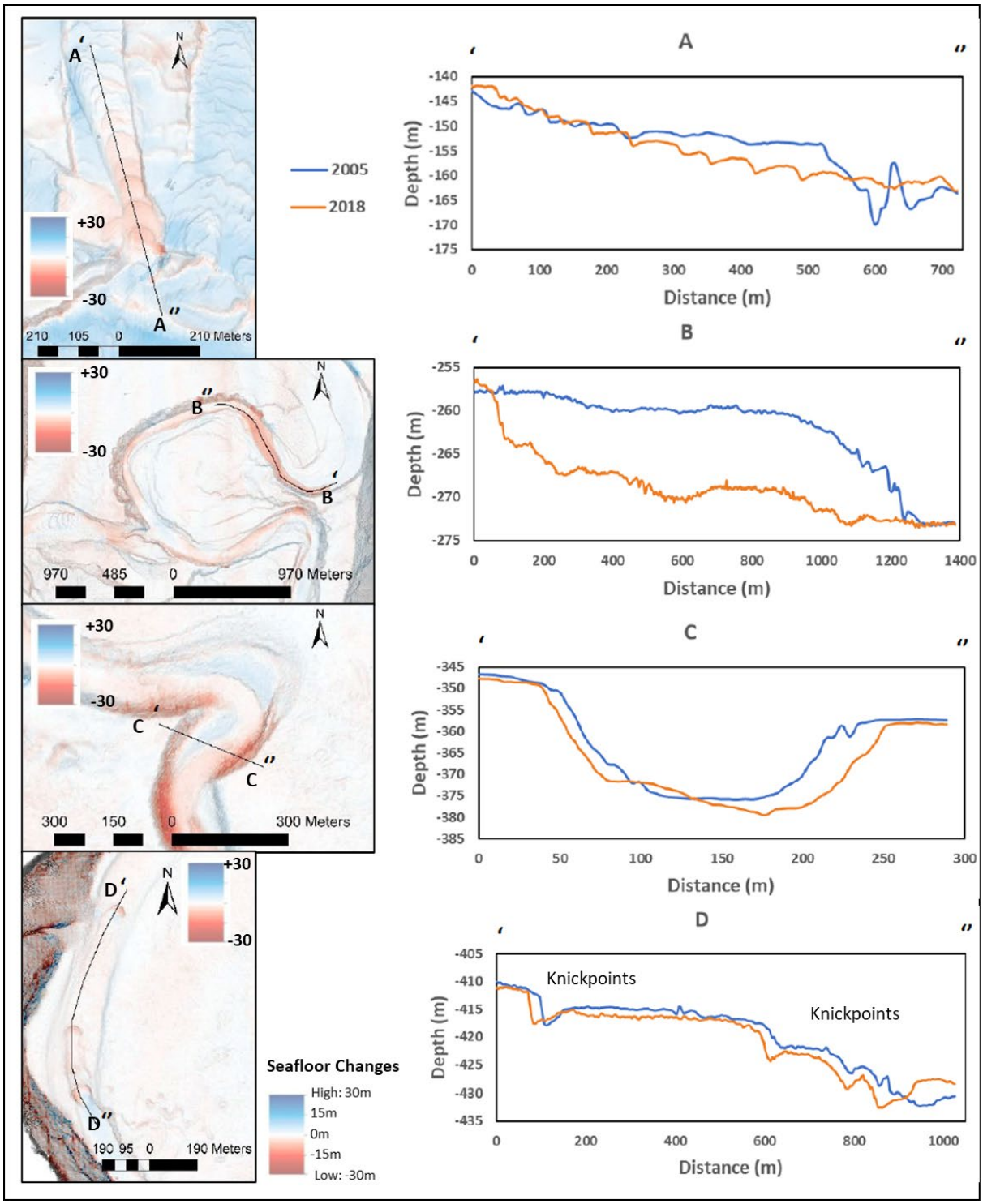

Figure 2.3: Examples of changes in seabed elevation in planform maps and cross sections, A) Example of migrating bedforms in the proximal prodelta channel, B) Up-channel

migration of a major knickpoint, C) An example of outer bend erosion, D) Changes due to migration of a minor knickpoint. See Figure 2.Aa for locations.

2.4.1.3 Lateral migration of outer bends

We observe localised erosion focused on the outer flank of some, but not all, bends throughout the channel system. The most prominent erosion of this type is observed at the tightest (R^*<1.54) channel bend, which is located about 23 km down the channel at 375 m water depth (Fig 2.3C). The outer flank of the channel shifted 30 m laterally, resulting in up to 20 m vertical erosion. Up to 6 m sediment thickness accumulated on the inner bend, forming a point bar that accreted 10 m laterally (Fig 2.3C).

2.4.2 Migration rates and eroded volumes

It is not possible to determine an upflow migration rate for the crescentic bedforms that dominate the relatively steep prodelta slope, as the same bedform crest cannot be reliably identified in multiple surveys. Those crescentic bedforms likely migrated many times during the 13-year period between surveys (e.g. Vendettuoli et al., 2019). We thus observe a time-averaged pattern of net sediment accumulation on the prodelta, with local incision by minor channels. Knickpoints show the fastest channel migration rates of all the observed bedform features, with a maximum measured upstream movement of 1625 m (Fig 2.4), which equates to an average-migration rate of 136 m/year. In contrast, the lateral channel migration observed at outer bends is much lower, with a maximum observed lateral shift in the channel flank of only 67 m, which equates to an average migration rate of 5.6 m/year. The minimum total volume of sediment eroded by knickpoint migration is 3.18 x 10^6 m^3, compared to the 9.34 x 10^5 m^3 attributed to outer bend erosion. Thus, it seems that knickpoints dominate the erosion (accounting for ~77% of the total) observed in this channel system, but their influence is not equal along the full length of the channel and is highly spatially variable.

2.4.3 Channel curvature explains whether knickpoints or outer bend erosion dominate

Alternations between reaches characterised by knickpoint migration or outer bend erosion occur along the channel length and show no clear relationship with distance from the active delta (Fig 2.2). Downslope of the prodelta, overall channel gradient remains constant (1.4°) and is not a major control of channel evolution. Instead, we find that outer bend erosion only dominates at the tightest bends in the system (Fig. 4A), where the normalised radius of curvature of the channel is below a threshold value of R^* = 1.54 (Fig. 2.4B). In contrast, when R^* > 1.54 (i.e. the straightest

sections of the channel), erosion is dominated by knickpoints that migrate at a faster rate, upstream and around the bend, rather than orthogonal to the bend (Fig. 2.4B). Where R^* slightly exceeds 1.54 (i.e. around the broad looped bend; Fig. 2.3C), knickpoints tend to swing towards the outer edges of the channel, which leads to some, albeit minor, erosion on the outer bend. However, where $R^* >> 1.54$ (i.e. the straightest channel sections), erosion is exclusively focused within the channel axis (Fig. 2.5A). The normalised radius of curvature of the channel appears to correspond to locations where erosion is either dominated by outer bend ($R^*<1.54$) or knickpoint migration ($R^*>1.54$).

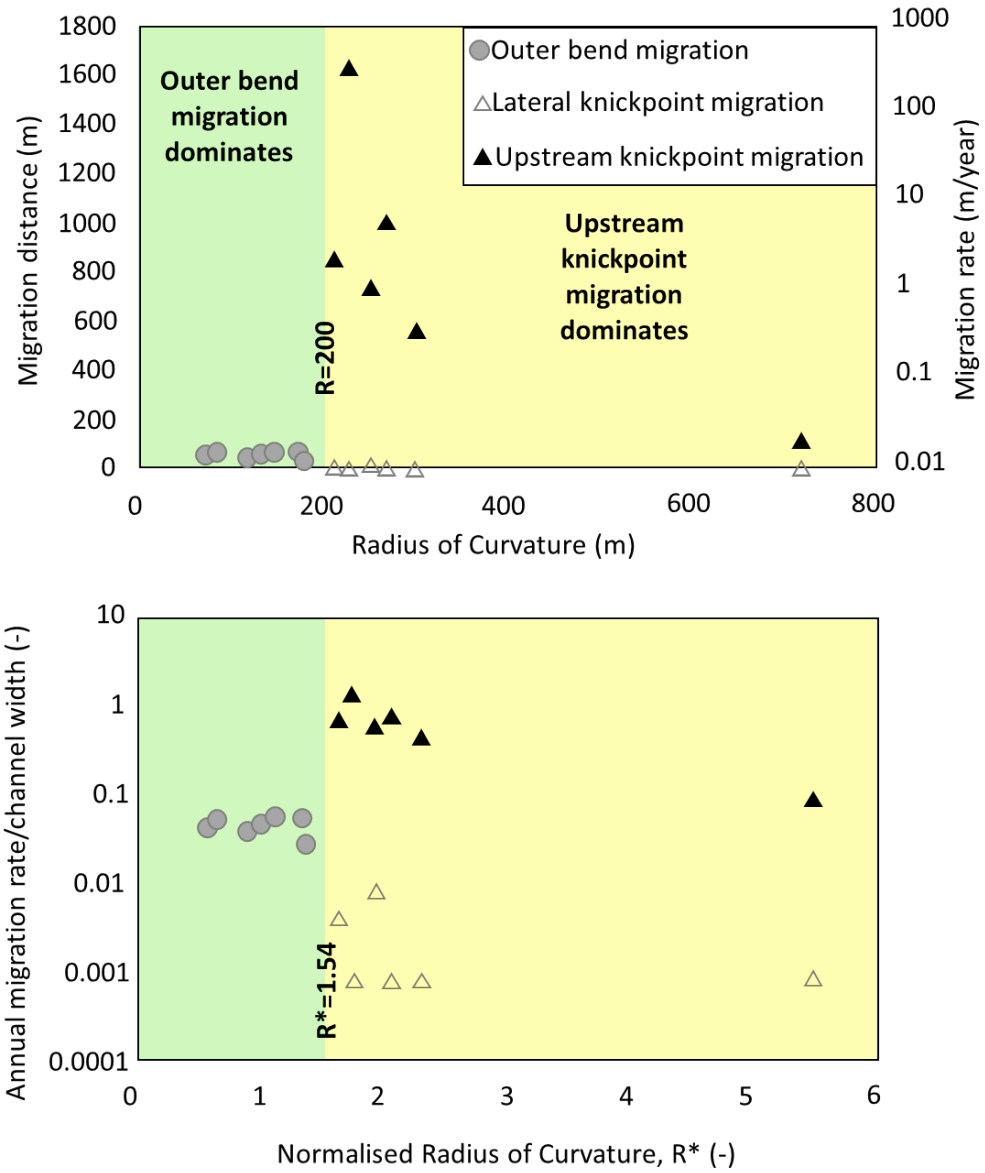

Figure 2.4: A) A threshold in the radius of curvature (R=200 m) is observed, above which rapid upstream migration of knickpoints occurs with only limited outer bend erosion, while outward bend erosion dominates below the threshold, B) Migration rates and radii of curvature are normalised to channel width, showing that R* ~ 1.5 threshold for the

normalised radius of curvature appears to control the rate and nature of erosion – dictating whether knickpoints or outer bend erosion will dominate.

2.5 Discussion

We now first discuss the processes that dominate erosion in the submarine channel in Knight Inlet and how and why channel normalised radius of curvature may correlate with the type and rate of erosion observed. We compare our findings to observations from fluvial and tidal channels and discuss their implications for reconstructing past flow behaviour from ancient submarine channel deposits. Small features such as crescentic bedforms are not discussed due to resolution limitation.

2.5.1 Knickpoints dominate submarine channel erosion

We show that net erosion in the submarine channel at Knight Inlet is dominated (77%) by upstream-migration of knickpoints rather than outer bend erosion (23%). This study thus contributes to a growing recognition that knickpoints play a key role in channel evolution, as in the nearby Bute Inlet (Heijnen et al., 2020) and Capbreton Canyon in the Bay of Biscay (Guiastrennec-Faugas et al., 2020, 2021). Even in the case of the most prominent channel bend in Knight Inlet, a series of three knickpoints was observed to migrate almost 1 km upstream around the bend rather than undergoing lateral migrating across the bend and enlarging the channel. This focus on erosion within the channel axis likely explains the long-term preservation of this channel bend, which was first observed in low-resolution seafloor surveys acquired in the late 1980s and has not experienced any cut-off in that time (Bornhold et al., 1994; Ren et al., 1996; Conway et al., 2012).

2.5.2 Why does channel curvature dictate the mode of erosion?

Outer bend erosion does play a significant role, however, in some bends. We found that some sections of the channel (where bends are tightest; R^*<1.54) are dominated by outer bend erosion, and the traces of knickpoints cannot be identified. Therefore, we now explore why the nature and rate of erosion differ so markedly depending on normalised radius of curvature. Frequent turbidity currents are known to occur within Knight Inlet (Bornhold et al., 1994), and given the similarities in their source-type, triggering, channel morphology and seafloor substrate, it is reasonable to assume that their nature is similar to flows (of up to 4 m/s) that have been measured in detail in other nearby fjord-head submarine channel systems (Bornhold et al., 1994; Hughes Clarke, 2016; Hage et al., 2019; Chen et al., 2021). Flows that travel around a bend experience centrifugal acceleration, which is defined by:

$$F = U^2/R$$

where F is centrifugal acceleration, U is the velocity of the flow, and R is the radius of curvature. Thus, centrifugal acceleration will be higher at tighter (i.e., lower radius) channel bends, and if we assume turbidity currents in this system have a nominal velocity of 4 m/s, a threshold for outer bend erosion occurs when the centrifugal component of flow, $F > 0.08$ m/s^2. Higher centrifugal accelerations around channel bends create super-elevation of the flow on the outer bend of the channel, setting up a helical secondary (i.e. cross-channel) flow that directs the primary downstream flow towards the outer bank resulting in enhanced erosion (Dorrell et al., 2013; Sylvester et al., 2019). In straighter (i.e. higher radius of curvature) sections of the channel, the influence of centrifugal acceleration is diminished, and flows will show much less super-elevation, limiting the potential for outer bend erosion. Enhanced flow super-elevation, and enhanced secondary flow, are thus inferred to explain why outer bend erosion only occurs at the tightest (lowest radius of curvature) channel bends (Fig. 2.5).

In fluvial systems, the primary forcing of this curvature-induced outer bank erosion has been debated, driven either by deposition at the inner bend (bar push), or by erosion at the outer bank (bank pull), which then drives inner bend deposition (Eke et al., 2014). However, in submarine channels, outer bend erosion (bank pull) has been argued for, creating space for the inner bend deposits (Peakall and Sumner, 2015; Palm et al., 2021). Consequently, it is probable that this curvature-induced outer bend erosion is driving the evolution of these channel bends (Fig. 2.5).

Recent studies in modern systems have suggested that knickpoint erosion is associated with high Froude number flows, with erosion enhanced on the steep downstream step as the over-riding flows undergo a hydraulic jump (Guiastrennec-Faugas et al., 2020, 2021; Heijnen et al., 2020; Chen et al., 2021). In moderate amplitude bends, approaching the transition point of $R^* = 1.54$, a combined effect of helical flow fields resulting from centrifugal acceleration and Froude-supercritical flow may occur wherein upstream-migration of knickpoints dominates. However, the focus of erosion may swing towards the outer bend (as seen in Bute Inlet and the Capbreton Canyon) (Heijnen et al., 2020; Guiastrennec-Faugas et al., 2020, 2021) due to the influence of centrifugal acceleration on the flow field (Fig 2.6). Therefore, we address previous contradictions concerning which process dominates channel evolution, showing that different processes can dominate different reaches of the same submarine channel (i.e. no one process fully dominates). This variation is argued herein to dominantly be the result of localised variations in the curvature of the channel and its relative influence on the primary and secondary flow of turbidity currents. Channel curvature plays an important role in not only controlling the rate of erosion but also the nature of erosion. Once a knickpoint is formed, its migration dominantly up the channel, rather than orthogonal to it, may itself lead to a straighter section of the channel forming between

knickpoints. Hence, we infer that there is likely a positive feedback loop between channel morphology and the mechanism of erosion.

Herein we have focused on the centrifugal force and the role of curvature, as reflected in the observations, but it is instructive to examine the role of the centrifugal force in more detail. The centrifugal force that deflects the primary downstream flow laterally is a function of both radius of curvature and velocity, and therefore changes in velocity would also be expected to alter the transition point. Given this, it is perhaps surprising that the transition between curvature and processes — outer bend erosion and knickpoints — is as clear and sharp as it is. For individual bends, the answer to this apparent paradox likely lies in the observations that most geomorphic work is associated with bankfull flows (Wolman and Miller, 1960) and that sinuous submarine channels act to filter the maximum size and thus the velocity of the flows that traverse them through flow stripping at bends (Amos et al., 2010). As a consequence, the variation in velocity, at a given bend, for channel forming flows may not be a key parameter and thus radius of curvature is the controlling characteristic. Nonetheless, flows will progressively decelerate downstream, albeit the rate at which this occurs in Knight Inlet is unknown. Such deceleration will lead to a progressive decrease in the angle of secondary current deflection towards the outer bank relative to the primary (downstream) flow, so it might be expected to alter the value of R^* at which this transition occurs. The present study has too few bends to examine whether such a spatial variation in distance occurs, and as noted, it also lacks the velocity data to test this idea. Longitudinal variations in velocity will similarly affect knickpoint processes, but again the influence of such changes is unknown.

2.5.3 Channel curvature influences migration rate and its direction relative to the channel axis

Channel curvature is also an important control of meander bend migration rate in terrestrial rivers and shallow water channel systems. Normalising radius of curvature, R, to channel width, B, to give R^*, enables migration rates to be compared between rivers and tidal channels. Previous studies have found that bend migration is highest at a normalised radius of curvature of $R^* \approx 3$, wherein rates of migration drop off rapidly on either side of that value (Hickin and Nanson, 1975; Finotello et al., 2018). Note that curvature can also be analysed continuously around a bend, and in that case it has been argued that there is no decrease in migration rates in the very tightest bends, when allowing for the observed spatial lag between maximum curvature and maximum migration (Sylvester et al., 2019, 2021). Herein, however, we use a single measure of normalised radius of curvature, R^*, for a bend following the approach of Hickin and Nanson (1975) in order to enable comparison with the aforementioned fluvial and tidal datasets.

In comparison, annual migration rates (0.021-0.043 m/year/channel width) for channel bends below our observed normalised radius of curvature threshold (equivalent to R^*<1.54) are broadly comparable to mean values reported for rivers and tidal channels worldwide (~0.03 m/year/width; Finotello et al., 2018). Whilst using the continuous curvature approach, Covault et al. (2020, 2021) also showed a strong relationship between migration rate and channel curvature for submarine channels. In the present study, for values of R^* > 1.54, however, there is a significant departure. Specifically, the observed rates of outer bend erosion at Knight Inlet are at least an order of magnitude lower than those in rivers and tidal channels at R^*>1.54. At Knight Inlet, we see a dominance of upstream-focused knickpoint migration, which themselves migrate at least an order of magnitude faster than those in rivers. Physical experiments of submarine channel systems have suggested that the migration rate will reduce as the radius of curvature decreases (Dorrell et al., 2018), in keeping with the eventual near cessation of movement of high sinuosity bends in many systems (Peakall et al., 2000). However, these experiments did not feature an erodible bed, so knickpoints could not form, and these experiments may lack key features of Knight Inlet (Dorrell et al., 2018). What is common, however, is that these observations indicate that the relationships that exist for fluvial and tidal channels do not extend to submarine channels shaped by turbidity currents. Specifically, in the present case we show a marked break in migration rates as a function of normalised radius of curvature, and show that knickpoint dominated bends have much lower migration rates than equivalent fluvial and tidal bends. This study of Knight Inlet thus adds to a growing body of research that concludes that turbidity currents can have a distinct behaviour from rivers, due to the reduced density contrast between the flow and the ambient surrounding medium, their propensity to super-elevate and run up slopes due to momentum, their often-variable density stratification, and the nature of secondary circulation as they travel around channel bends (e.g. Peakall and Sumner, 2015; Jobe et al., 2016; Shumaker et al., 2018). We also recognise that other factors that could not be tested in this study may play a contributory role, such as contrasts in density, cohesion or mechanical strength between the substrate outside the channel compared to that within the axis (Schumm, 1963). Future studies should aim to provide constraints to these physical properties.

As knickpoint incision develops, the vertical incision may start to entrench the axis of the channel, further inhibiting the development of bends and lateral migration of the channel, creating a positive feedback. This raises the question of how tight bends initiate in such channel systems. However, the present dataset does not allow this question to be explicitly answered. We postulate that perhaps some other perturbation to the morphology is required, as could be created by channel wall collapse (resulting from lateral flank-steepening during knickpoint incision) that asymmetrically widens the channel locally, or due to collapse of material into the axis that creates a new topographic barrier that reroutes turbidity currents. More temporally

closely spaced timelapse surveys are required to document any such events, and enable processes to be examined in more detail.

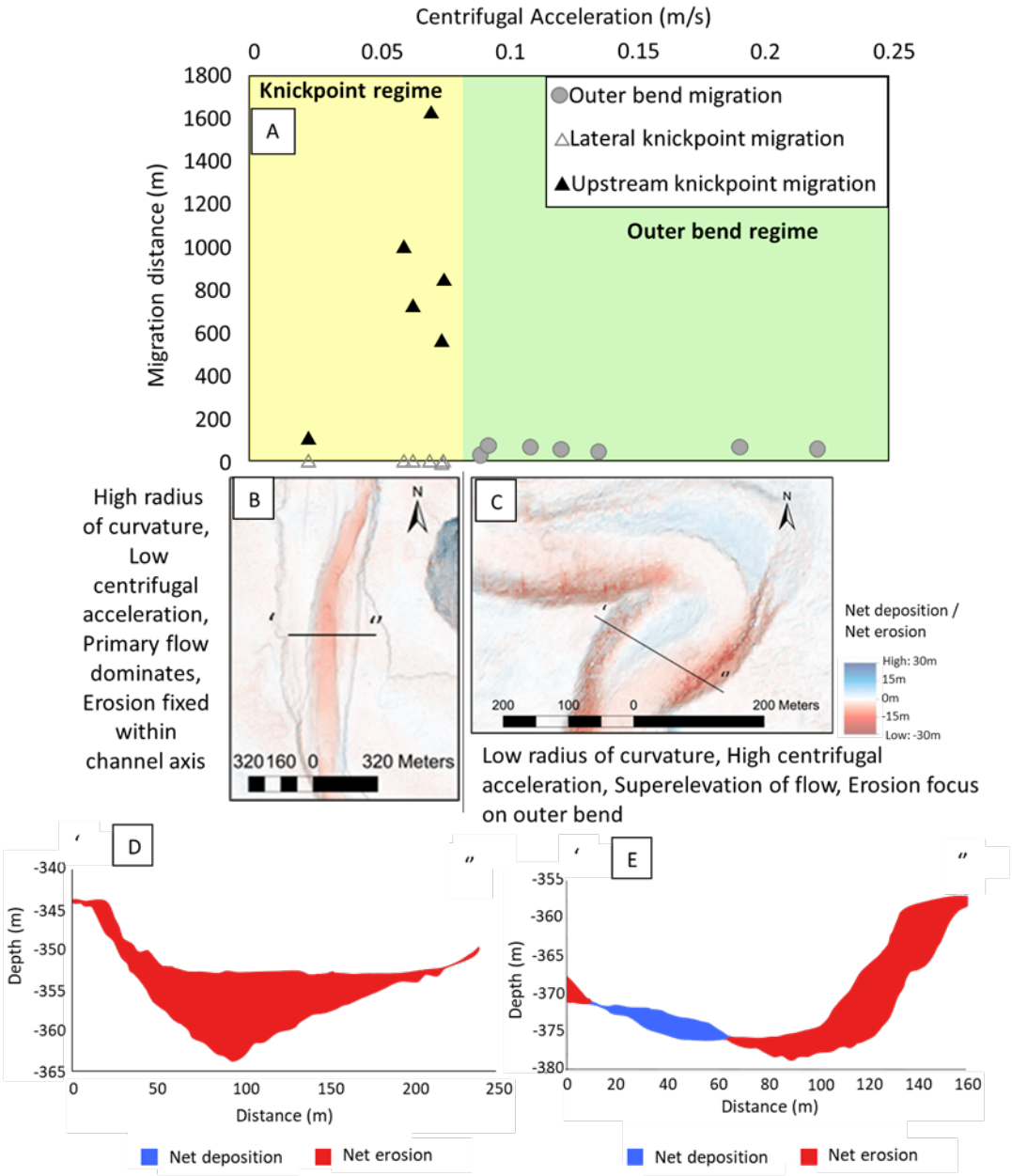

Figure 2.5: A)Centrifugal accelerations derived at erosion locations based on flows with an assumed primary velocity of 4 m/s compared with the normalised radius of curvature (R*). Erosion is focused within the channel axis at low centrifugal accelerations (B,D), prompting a knickpoint incision. In contrast, secondary circulation plays a more important role at high centrifugal accelerations, deflecting the primary downstream velocity towards the outer bank and consequently focusing erosion on the outer bend (C,E).

2.5.4 How widely applicable is this model to other submarine channels?

We consider it broadly reasonable that other similarly active submarine channel systems may behave according to our model; however, we recognise that there may be other controls on erosion rate and style that may cause some deviation.

The nature of sediment that is transported will control the substrate that accumulates, which will erode differently depending on whether it comprises dominantly granular or cohesive sediment (e.g. Mastbergen and van den Berg, 2003; Winterwerp et al., 2012). Subsurface and tectonic features and processes can steer flows, and preferentially focus or deflect the locus of erosion or deposition. Shallow sub-cropping or outcropping bedrock, mobile subsurface salt or mud, active or relict fault scarps, and active neotectonics can all play a role in controlling the course and steepness of submarine channels that may lead to deviations from our model (Heinio and Davies, 2007; Mitchell, 2014; Micallef et al., 2014; Covault et al., 2021; Mitchell et al, 2021). Morphologic disturbances such as flank collapses may also fundamentally modify or reset the channel morphology, switching the nature and rate of erosion. For example, flank collapses in the Congo Canyon and Hikurangi Channel have been documented to reach volumes of up to 19 km^3, which change the channel base level and drive the vertical incision of knickpoints or prompt channel avulsions (Pope et al., 2022; McArthur et al., 2024). Biological effects are increasingly-recognised to play a role in affecting the morphology of submarine channels, which can modify the rate at which erosion occurs, but are not included in our current model (e.g. Azpiroz-Zabala et al., 2024). Biological effects can be extremely varied and may increase or decrease the erosion rate relative to the same bed shear stress and can also modulate the nature of erosion (e.g. where biostabilisation occurs, erosion may be inhibited until en-masse excavation occurs; Peakall et al., 2020). Furthermore, thermohaline-driven bottom currents have been shown to influence the morphologic evolution of submarine channels, often creating strong cross-sectional asymmetry and long-term unidirectional migration of the axis (e.g. Miramontes et al., 2020; Fuhrmann et al., 2020).

Our model most likely relates to highly active (i.e. high sediment supply) submarine channels, that occur on relatively low gradient, passive margin slopes, with a mixed grain size distribution, and likely precludes those in tectonically-active regions and which are significantly-affected by bottom currents. In the present-day sea level highstand, this likely relates to other similarly-scaled fjord-head channel systems such as those elsewhere in British Columbia, Norway, New Zealand, Greenland and Patagonia, and to river-fed submarine channels that represent some of the largest systems on our planet such as the Indus, Bengal and Congo channels. We hope that the model we present provides the basis for testing, and sees the acquisition of future repeat surveys to characterise and quantify erosion rates in these and other systems worldwide,

preferably allied to three-dimensional flow field data to improve understanding of the flow dynamics.

2.5.5 Why does the depositional record under-represent knickpoints?

Repeat seafloor surveys in Knight Inlet and other systems now show that knickpoints can dominate erosion in active, deep-sea submarine channels, and knickpoints are increasingly being recognised from new high-resolution seafloor surveys of submarine channels around the world (e.g. Ceramicola et al., 2014; Gales et al., 2019; Guiastrennec-Faugas et al., 2020, 2021; Heijnen et al., 2020; Chen et al., 2021). Despite this apparent importance of knickpoints, evidence of knickpoints remains sparse from studies of ancient systems, in contrast to abundant examples of outer bend erosion and development of meandering channels (e.g. Dykstra and Kneller, 2009; Babonneau et al., 2010; Sylvester et al., 2011; Maier et al., 2012; Jobe et al., 2016). While the migration rates associated with knickpoints are up to an order of magnitude higher than that for outer bend erosion in Knight Inlet, Bute Inlet and Capbreton Canyon, knickpoints remain focused within the channel/canyon axis. Successive reworking by crescentic bedform migration has been shown to result in very low stratigraphic preservation potential on prodeltas and proximal areas of the submarine channel. For example, less than 11% of the deposits that accumulated in the axis of submarine channels on the submerged Squamish Delta over one year remained in place, as they were subsequently reworked and redeposited further downstream (Vendettuoli et al., 2019); only lenticular sand bodies were preserved that represent the infill of scours at the base of bedforms with their uppermost parts stripped and reworked (Hage et al., 2019; Englert et al., 2021). As successive knickpoints can migrate upstream through the same section of the channel over time (Heijnen et al., 2020), they also likely rework or remove much of the evidence of the preceding knickpoint or any crescentic bedforms. Therefore, the diagnosis of knickpoints from ancient outcrop-based depositional records may be especially challenging, relying upon the identification of erosion surfaces, relatively thin, tabular channel fill packages, or rapid changes from lag deposits to fine-grained sediments on preserved terraces (Tek et al., 2021; Allen et al., 2022).

In contrast, the lateral migration of the channel axis at tight bends means that depositional packages form on the inner bend of the channel, as well as erosion on the outer bend. These laterally-accreting inner bend deposits thus have a much higher preservation potential than either crescentic bedforms or knickpoints. Timelapse surveys performed by Guiastrennec-Faugas et al. (2021) and Heijnen et al. (2022) reveal that the presence of knickpoints within the depositional record may not be preserved beyond annual timescales. We, therefore, conclude that this contrast in preservation potential explains the apparent under-recognition of knickpoints compared to outer bend erosion from ancient depositional archives and that previous models

based on such records may have similarly under-represented the role of knickpoints in the life cycle of submarine channels. However, improvements in the acquisition and processing of seismic data, coupled with a greater process-based understanding has meant that the diagnostic signature of knickpoints is starting to become better recognised (e.g. Sylvester and Covault, 2016; Hansen et al., 2017; Tek et al., 2021). This present study contributes to a growing body of literature that reveal the diagnostic criteria for knickpoint identification, including their morphology, scale and now the reaches of a channel that may be more prone to knickpoint migration. Future studies should aim to look for pronounced erosion surfaces, tabular, channel-confined fills, and rapid vertical grain-size transitions on terraces to investigate the significance of knickpoints.

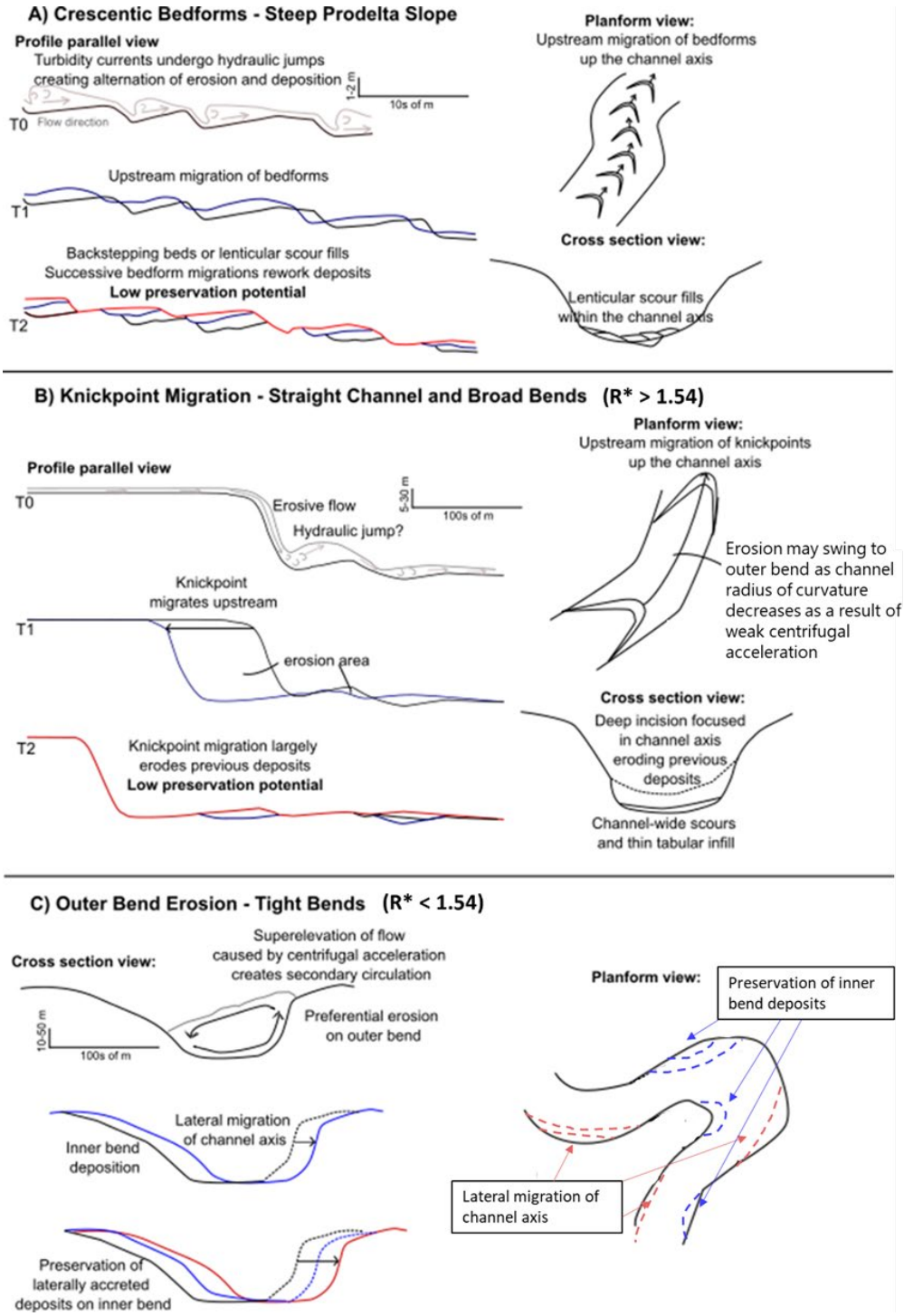

Figure 2.6: Illustration of how different process influence channel evolution. A) The process of crescentic bedforms that dominated the steep prodelta slope. B)The process of knickpoint migration that dominates straight channels and broad bends. C) The process of outer bend erosion that dominates the tight bend.

2.5.6 Potential Hazard and Mitigation

In addition to providing insights into sediment transport, hydrodynamics and geomorphic evolution, the findings of this study have wider relevance for the understanding of hazards in submarine channels and fjord environments. Such settings are often the location of economically important seafloor infrastructure, such as seafloor cables and pipelines, and in the case of fjords often provide critical connections for remote high-latitude communities to digital communications and energy security. Specific lessons learned concern how and where the channel relief will change and how the nature of flows interact with that morphology as this can inform strategies for designing resilient infrastructure routes where it is necessary to cross submarine canyons or channels. The results indicate that while significantly large lateral movement of the channel was not observed, fast rates of knickpoint migration can occur at bends with large radii of curvature. These migrations can initiate cut-and-fill cycles, resulting in substantial changes in seafloor morphology and potentially impacting sediment transport and deposition processes (Guiastrennec-Faugas et al., 2020). Such alterations pose significant risks to the stability of the seabed and any infrastructure laid upon it, and can undermine structures such as cables and pipelines, leaving them in a vulnerable suspended position.

Knickpoint migration can involve the vertical removal of tens of metres of sediment almost instantaneously, and the upslope migration can be over 100s of metres in a single year (as seen in other systems Heijnen et al., 2020; Pope et al., 2022). The topographic effect of knickpoints, which create a cliff-like feature in the channel axis, can result in rapid acceleration of turbidity currents, leading to greater impacts on any infrastructure immediately downstream (Chen et al., 2021; Hsu et al., 2008). It is thus preferable to make sure that any infrastructure is: i) routed suifficiently far upstream of any knickpoint faces such that it does not end up in suspension due to migration of the knickpoint; and ii) sufficiently far downstream such that the fastest flow does not interact within it. Therefore sections of channel that feature tighter bends and that are prone to slower rates of outer bend erosion may be preferable for cable or pipeline crossings to those that experience knickpoint-related erosion, but it is also important to assess other hazards such as local slope failures of the channel flanks that may occur in such locations. Other areas of the channel experience less erosion, particularly further down the system into deeper water, where it is likely that fewer flows occur (as most are restricted to the upper reaches of the channel (Bailey et al., 2023; Heijnen et al., 2022). This study reveals changes that can occur over 13 years,

which is highly relevant for the typical engineering design life of structures like pipelines and cables (typically 10-30 years); however, it is possible that some more extreme events, such as canyon-flushing flows that run down the full length of a canyon-channel system and which can create profound erosion, have not been captured (e.g. Talling et al., 2022). There is thus a need for more studies to acquire more repeat seafloor surveys to determine whether the same controls operate in different settings, and to determine the temporal and spatial variations in hazards to seafloor infrastructure.

2.6 Conclusions

Based on repeat seafloor surveys across the entirety of a submarine channel in Knight Inlet, British Columbia, we document changes in elevation between 2 surveys conducted 13 years apart. These time lapse surveys are used to investigate the controls on channel evolution. Upstream-migration of crescentic bedforms dominates the steep (5^0) prodelta slope, while upstream-migration of knickpoints accounts for 77% of the observed erosion in the rest of the channel system, dwarfing that attributed to outer bend erosion. Different reaches of the channel are affected to different degrees by these contrasting processes. However, we show for the first time that channel curvature exerts a strong influence on which process will dominate and the overall rate of migration. Tight channel bends (R < 200 m; R^* < 1.54) are dominated by outer bend erosion, which we relate to enhanced centrifugal acceleration that drives super-elevation of turbidity currents and focuses erosion on the outer bend. In contrast, broader channel bends and straighter sections of the channel (R>200 m; R^*>1.54) are locations where knickpoints cut deep (up to 20 m) into the channel axis, migrating much faster (up to 136 m/year upstream) compared to the rate of outer bend erosion (up to 6 m/year orthogonal to the channel axis). Despite the apparent dominance of knickpoints in sculpting the channel, we suggest that their depositional signature is likely to leave a much less well preserved trace in the rock record, compared to that of laterally-accreting channel bend deposits. We, therefore, conclude that previous studies may have under-appreciated the role of knickpoints in channel cut, maintenance and fill.

Chapter 3 What are the controls for delta front slope failure? Insights from detailed monitoring at Squamish Delta, British Columbia

Muhamad Z. Zulkifli, Michael A. Clare, Timothy A. Minshull, Hector Marin Moreno, John Hughes Clarke, Peter J. Talling

Author contributions: I am responsible for the analysis and the main author of this manuscript. J.H.C., P.J.T contribute in data acquisition . M.A.C., T.A.M. and H.M.M. provided the main editorial support and comments on the manuscript.

Abstract:

Submarine slope failures pose a hazard to seafloor infrastructure and coastal communities. Given the high population densities, slope failures can have a particularly significant impact around river deltas, generating damaging tsunamis and breaking critical telecommunications connections. Despite the risks they pose, a lack of detailed monitoring means that the factors that lead to slope collapse remain poorly constrained. Numerical modelling is typically used to assess future slope stability; however, sparse observational data ensure that we cannot yet determine how submerged delta slopes evolve and progress to failure at the field scale. Here, we aim to close this gap by analysing repeat seafloor surveys of the submerged Squamish Prodelta, British Columbia, to determine the physical controls on slope instability. Multibeam bathymetric surveys were performed on 93 consecutive weekdays in 2011, during which time at least five large (>50,000 m^3) delta slope collapses occurred, as well as numerous smaller slope failures. These surveys allow us to determine how the delta slope and geometry changes on an unusually detailed timeframe (i.e. daily) in the build-up to slope collapse and how it relates to variable sediment supply from the feeding river and tidal fluctuations. Analysis of the five largest collapses reveals that a single mechanism is not responsible for every failure. Different parts of the delta encounter major failure at different times and locations as revealed by measuring and mapping out the delta head and quantifying the sediment accumulation delivered by the river and the tidal elevation. Slope failure appears to relate to a combination of modified slope geometry due to delta lip progradation and pore pressure fluctuations related to progressive sediment loading and tidal effects. Small-scale features such as the migration of crescentic bedforms can also play an important role in destabilising delta slopes. This study provides new insights into how multiple individual and compounding processes can contribute to the failure of slopes on submerged

deltas with implications for determining the fate of particulate material that accumulates at submerged deltas and the hazards associated with underwater slope failures.

3.1 Introduction

Delta slope failure, a prevalent geological phenomenon in submarine environments, entails the collapse or instability of sedimentary deposits at the front of river deltas. This occurrence has far-reaching implications, posing hazards to coastal and underwater infrastructure and ecosystems (Clare et al., 2017; Hilbe & Anselmetti, 2014; Xue et al., 2019). Delta slope failure can have catastrophic consequences, generating tsunamis due to the displacement of water (e.g. Hansen et al., 2016; Lee et al., 2006; Lintern et al., 2019) and long-runout turbidity currents that extend beyond the toe of the landslide deposit, endangering underwater infrastructure and ecosystems (Hizzett et al., 2018). Moreover, variable scales of delta slope failures with apparently unknown triggers have been observed, underscoring the difficulties in understanding and predicting such events (Clare et al., 2016).

The impact of delta slope failures is not confined to coastal areas, as over-steepening of the upper slope can also trigger deep-seated failures, compromising the stability of the adjacent geological formations (Fielding, 2015). Furthermore, the collapse of delta slopes can produce debris flows, mudflows, and deep-seated creeps, aggravating the hazards associated with these events (Dixon et al., 2012). Seismically induced slope failures are perilous, as they can generate destructive tsunamis and additional hazards (Hilbe and Anselmetti, 2014). The risk of slope failure can escalate to intolerable levels, especially when the elements at risk change, highlighting the potential for widespread and severe impacts (Li et al., 2016).

Delta slope failure has been a subject of intensive research, employing various methods to comprehend the triggers, processes, and implications of these geological phenomena. Previous research has adopted a range of approaches that include using 3D seismic data to examine kinematic indicators from mass-transport complexes, revealing the structural characteristics of slope failures (Bull et al., 2009). Moreover, research has integrated high-resolution bathymetric, reflection seismic, and lithological data to document the sedimentary and morphological signatures of subaqueous mass movements, elucidating the triggers and consequences of delta slope failures (Hilbe and Anselmetti, 2014). Previous studies have encountered considerable challenges in documenting large-scale slope failures in the sedimentary record, reflecting the difficulty in identifying and studying such events (Wolinsky and Pratson, 2007). Furthermore, previous studies have also addressed the challenges in identifying and studying small-scale landslides and slope failures in submarine flanks, stressing the need for detailed mapping and analysis of these events (Casalbore et al., 2020; Fielding, 2015). Additionally, previous studies

have addressed the impact of different triggers, such as rapid sediment accumulation and aseismic events, on slope failures in deltaic systems (Casalbore et al., 2021, 2020; Hilbe and Anselmetti, 2014; Hizzett et al., 2018).

Many factors have been suggested as the trigger of delta slope instability. Figure 3.1 shows a chart of the factors that can contribute to delta slope instability. Previous studies have explored the interplay between sediment supply and slope stability, revealing the mechanisms through which sediment dynamics can induce slope failures. For example, research has investigated the role of sediment density flows in sculpting the morphological expression of bedforms on fjord-lake deltas, emphasising the influence of specific discharge and flow depth on sediment transport and deposition (Normandeau et al., 2016). Moreover, investigations have derived quantitative relationships between sediment supply and slope for clinoforms prograding at limiting equilibrium, imparting insights into the link between sediment supply and slope stability (Wolinsky and Pratson, 2007). Additionally, research has examined the effects of delta progradation and aggradation on slope failure, with elevated pore pressures and specific weak layers within stratified sequences identified as key factors influencing landslide occurrence (Fan et al., 2016).

Delta slope failure can be induced by external loading, such as storm activity and earthquakes, resulting in significant geological hazards. Studies have elucidated the role of storm waves in reworking the delta front, possibly leading to slope instability and failure (Kostaschuk and McCann, 1989). Moreover, the influence of earthquakes on slope failures has been evidenced by the identification of mass failure triggered by seismic events, underscoring the role of external seismic loading in slope instability (Kremer et al., 2015). Another external factor is sea level change, as the rise and fall can affect sediment supply and sediment starvation, impacting the depositional processes as well as changing the morphology in the delta (Buatois et al., 2012;Caldwell et al., 2019; Porębski & Steel, 2006). Delta slope failure can also be induced by geometrical changes to the delta slope and front, such as an increase in slope angle or undercutting of the slope. Studies have demonstrated that increasing slope angles can compromise slope stability and cause failure (Norris et al., 2008). Experiments have shown that geometrical transitions such as slope changes and height differences can affect the wave loading on slopes (Van Bergeijk et al., 2022). Additionally, research has revealed that the specific discharge and flow depth near the delta front rollover point can lead to the erosion of sediments and undercutting of the slope (Normandeau et al., 2016).

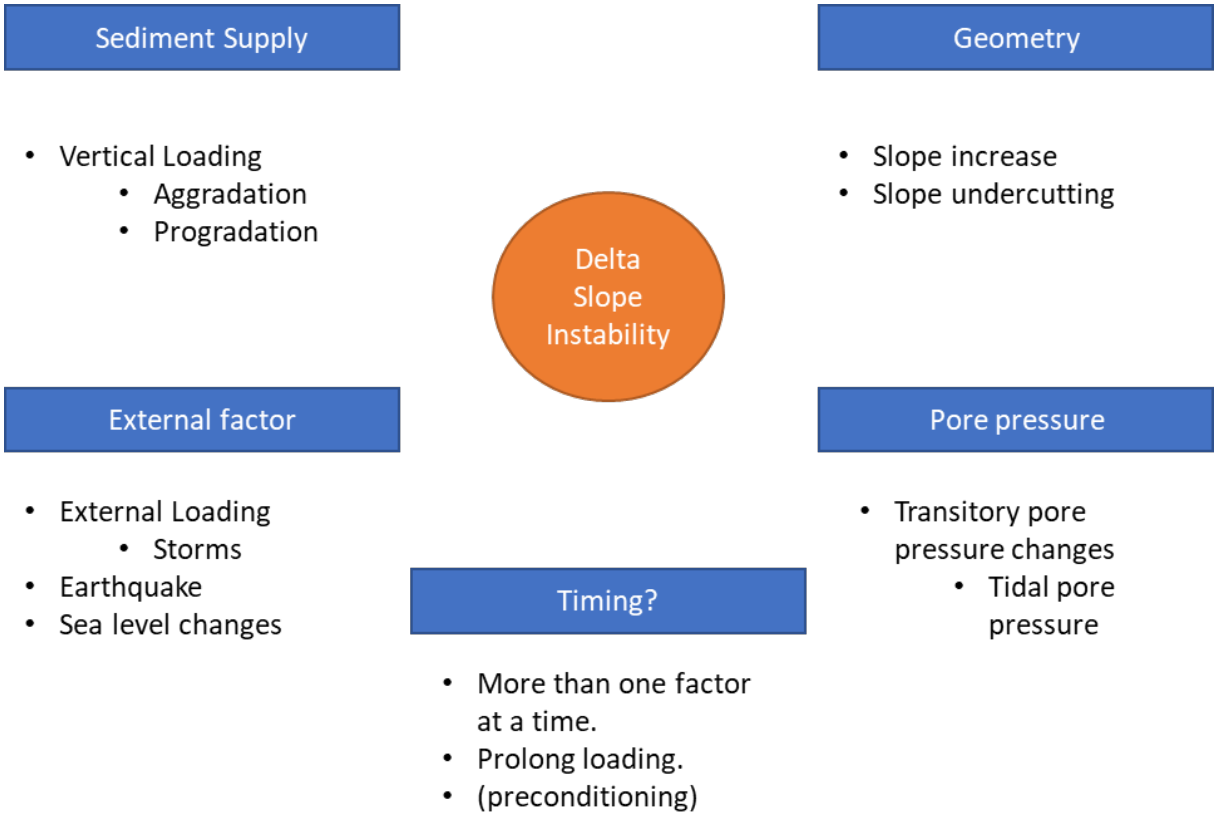

Figure 3.1: Chart of the factors that can contribute to delta slope instability, this includes sediment supply that influence the vertical loading on the slope, external factor such as storms that put external loading on the slope and earthquake, slope geometry as in the increase of the slope angle and slope undercutting, pore pressure changes such one incited via tide, timing, which is in terms of prolong loading as well as the combination of all this factor throughout a period of time.

Changes in subsurface pore pressure can have a significant impact on the stability of delta slopes, which can induce slope failure. Research has demonstrated that prolonged loading, such as through the accumulation of sediment, can elevate pore pressures within the deltaic sediments, possibly resulting in slope failure (e.g. Chillarige et al., 1997; Clare et al., 2016). Moreover, the occurrence of ground water seepages due to prolonged loading has been shown to increase the degree of saturation and pore water pressure, possibly causing slope failure (Khan et al., 2021). Additionally, the cyclic variations in pore water pressure due to tidal effects have been associated with changes in the effective stress within the slope, possibly compromising slope stability due to gas expansion (Chillarige et al., 1997; Rahardjo et al., 2005).

Another factor is timing, or rather the combination of multiple factors in the build-up to slope failure. This can also be termed as preconditioning. The preconditioning to delta slope failure can involve a complex interplay of geological, geotechnical, and environmental factors that increase the vulnerability of deltaic environments to slope instability. These factors include supercritical

sediment density flows, prolonged loading, gas outbursts and many others (e.g. Clare et al., 2016; Normandeau et al., 2016; Zhang et al., 2015).

Therefore, there are many proposed mechanisms that may explain slope failure; however, field studies that provide temporal constraint of multiple submerged failures and the evolution of environmental conditions are rare, limiting a field-scale explanation of where, why and how slope failure occurs at a submerged delta. This study takes advantage of unique daily timelapse seafloor surveys from the Squamish Prodelta, British Columbia, that reveal how the geometry of a submerged delta evolves in the build up to and following slope failures, to assess which conditions explain collapse.

3.2 Aim

The Squamish River carries more than 1 million cubic metres of sediment per year of sediment to its delta annually (Hughes Clarke, 2016). During the spring and summer freshet each year, seasonal meltwater increases the river discharge from ~100 m3/s in the winter to >500 m3/s, with peaks of up to 1000 m^3/s (Hughes Clarke et al., 2012). The Squamish Prodelta is a dynamic and active depositional environment that experiences frequent influx of sediment to the delta front, making it the location of frequent slope failure. Direct monitoring has revealed that >100 turbidity currents may occur annually; many of which are triggered by slope failures, the remainder being triggered from settling of a surface plume of sediment (Hage et al., 2019; Hizzett et al., 2018). These slope failures have important implications for the sediment transport, morphology, and ecology of the delta and its adjacent marine areas. However, the mechanisms and factors that control the slope instability of the delta front are not well understood. Therefore, the overarching aim of this study is to determine the controls of delta front slope failure in the Squamish delta based on analysis of repeat seafloor surveys.

The specific objectives of this study are as follows. First, to identify the main processes and triggers that contribute to slope failure initiation and propagation in the Squamish delta front, such as, river discharge, tidal currents, wave action, and sediment loading. Second, to examine the spatial and temporal variability of slope failure occurrence and magnitude in different parts of the delta front, and to understand the reasons for such variability. For example, why some parts of the delta are more prone to failure than others, and why some failures are larger and more destructive than others. Third, to analyse the role of slope geometry or sediment depositional geometry in influencing the stability and failure of the delta front, and to evaluate how these geometries change over time due to sediment accumulation and erosion.

By achieving these objectives, this study will provide new insights into the dynamics and evolution of the Squamish delta and its delta front, and will also contribute to the wider knowledge of delta slope failure mechanisms and their impacts.

3.3 Method

This study analyses previously-acquired multibeam bathymetric surveys to map and profile the Squamish Prodelta and measure the seafloor changes and characterise the resultant stratigraphic architecture. Seafloor surveys were performed for 93 consecutive weekdays in 2011 (from 17th April 2011 to 24th August 2011). In this study we refer to days by Julian Day (JD), with the first survey day being JD117. Multibeam bathymetric data were acquired from the RV Heron using an EM710 multibeam sonar with a vertical resolution of 0.2% of water depth and a horizontal resolution of 3% water depth (Hughes Clarke et al., 2012). Surveys could not be performed on weekends due to the intensity of water sports activity around the prodelta. Changes in the seafloor elevation were determined by generating daily difference maps between pairs of successive weekday surveys. These successive seafloor surveys were compared to identify any slope failure at the delta head based on the identification of obvious headscars from which sediment was evacuated. The volume of evacuated sediment is determined for each major slope failure to provide a relative magnitude. Changes were detected at the pixel scale, which has a horizontal resolution of 2 m × 2 m and vertical resolution of approximately 0.1 m (Hizzett et al., 2018; Hughes Clarke et al., 2012). This repeat mapping also enables the identification of other changes to the seafloor, including smaller features such as the upslope migration of crescentic bedforms created by turbidity currents that also affect the prodelta slope, and may play a role in slope instability.

By determining the change between the first and last seafloor surveys, the total amount of sediment deposited and eroded within the delta head is calculated across the entire survey duration. This enables an assessment of to what extent sediment accumulates on the delta and remains locked up, compared to how much sediment is transferred to deeper water.

To provide an assessment of the role of sediment supply on slope stability, the daily river discharge is used as a proxy, which was recorded in m^3/second at a gauging station 12 km upstream from the Squamish Prodelta at Brackendale, Environmental Canada station 08GA022. The minimum tidal elevation of each day was analysed to assess the potential effects of tidally modulated pore pressure variations based on measurements reported in Hughes Clarke et al. (2012). Finally, delta progradation and aggradation rates were quantified from the bathymetric difference mapping to ascertain how vertical loading and changes in delta slope affect slope stability. Prodelta aggradation is measured by mapping out the upward (deposition) and

downward (erosion) movement of the delta head from the northwest to the southeast of the prodelta. Prodelta progradation is measured by mapping out the outward (deposition) and inward (erosion) movement of the delta head from the northwest to the southeast of the prodelta. Each movement is measured based on its difference from the first survey (JD117). The purpose of this analysis is to have a quantification of how the prodelta moved and became reshaped throughout the survey duration and to what extent the geometry of the prodelta influences slope instability.

3.4 Results

3.4.1 Where and when does slope failure happen?

3.4.1.1 Observation

The repeat seafloor surveys reveal the occurrence of five major slope failures over the course of our survey timeline (as also previously noted by Clare et al., 2017 and Hizzett et al., 2018). Each slope failure exhibited distinct characteristics, occurring at different locations on the delta head, varying in size, shape, and magnitude as the survey progressed. This variation prompts critical questions: Why do certain parts of the delta head exhibit greater activity than others? What factors contribute to the differences in slope failure magnitudes? This study aims to unravel these complexities.

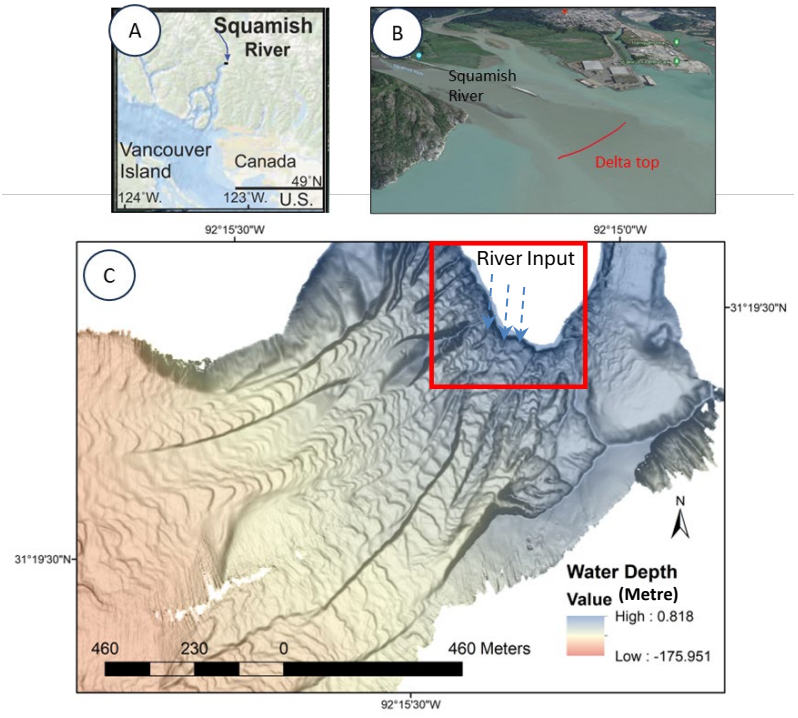

Figure 3.2: A) Location of the study area (Vendettuoli et al., 2019), B) image of the delta with the notation of the location of the delta head, C)bathymetric map of the study area, the red box is the delta top (the focus of the study.

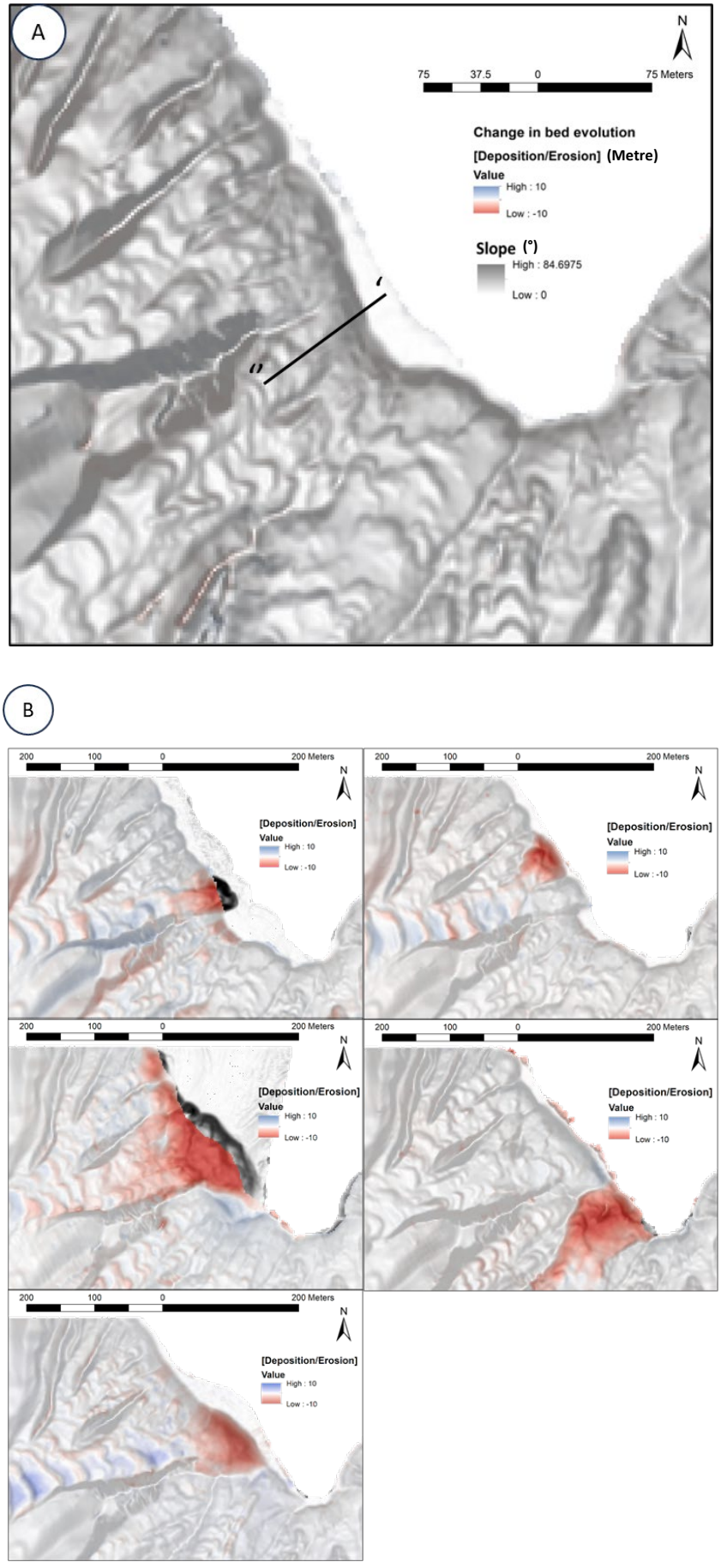

Figure 3.3: A) a slope map of the delta top with a box showing where the measurements in this study take place and the profile line for slope profile analysis (Fig 3.4B); B) difference

maps of a focused area of the delta showing changes associated with the five major delta slope failures.

Figure 3.2A depicts the location of the study area, with Figure 3.2B specifically highlighting the portion of the delta head that is the primary focus of our investigation. Figure3.2C is the bathymetric map of the study area. Figure 3.3A is a close up of the red box in figure 3.2C and it is slope map with a beck box that shows the area in which measurement such as sediment volume, areas, as well as delta progradation and aggradation is measured. Figure 3.3B provides a difference map detailing all five major failures, showcasing location, magnitude, and timing variations. This figure is a foundational reference for understanding the nuances of each slope failure.

The initial major failure (F1) was identified during the survey on Julian Day 138 (JD138) (Fig 3.3B), occurring in the middle part of the observed delta head. This event resulted in the evacuation of approximately 10,883 m^3 of sediment, affecting an area of 3,982 m^2 (Table 3.1). Subsequently, the second major failure (F2) occurred 14 days later (JD138), situated northwest of the first failure and encompassing 16,610 m^3 of evacuated material over an area of 10,579 m^2. The third major failure (F3), the largest in magnitude, occurred on JD181 (24 days after the second failure), situated in the middle part of the delta head and covering areas affected by the first two failures. This event led to the evacuation of a substantial 89,581 m^3 of materials, spanning an area of 12,562 m^2. The fourth major failure (F4), happening 8 days after the third (JD189), occurred on the eastern end of the delta head, evacuating 34,008 m^3 of materials over an area of 10,041 m^2. Notably, this failure exhibited a distinct location compared to the preceding failures, raising intriguing questions about spatial patterns. The fifth and final major failure (F5) recorded in the survey transpired on JD235, 46 days after the fourth failure, situated northwest of the previous failure and overlapping with the third failure. However, it did not extend towards the further northwest as the third failure did. This event resulted in the evacuation of approximately 39,642 m^3 of sediment, covering an area of 13,767 m^2. Table 3.1 details the measurements taken for each major failure.

Table 3.1: measurement taken for each major failure, this includes the day of the failure, eroded sediment volume, eroded area, the river input of the day, minimum tide of the day and progradation of the delta top leading to the failure.

No.	**F1**	**F2**	**F3**	**F4**	**F5**
Day	138	152	181	189	235

Eroded Volume (m^3)	10883	16610	89581	34008	39642
Eroded Area (m^2)	3982	10579	12562	10041	13767
River input (m^3/s)	342	454	922	775	973
Tide (m)	0.25	0.69	0.58	1.74	1.46
Progradation (m)	2.99	3.61	15.97	7	20.1

Contrary to initial expectations, the slope angle of the prodelta front did not undergo significant changes throughout the survey, indicating a continued progradation of the delta. The slope remains remarkably similar throughout, with a typical slope gradient of 12° to 14° (Fig 3.4B). Erosion slightly dominates the volumetric change on the prodelta slope during the survey period, with erosion accounting for approximately 318,943 m^3 of volumetric change, compared to the deposition of around 292,655 m^3 (Fig 3.4A).

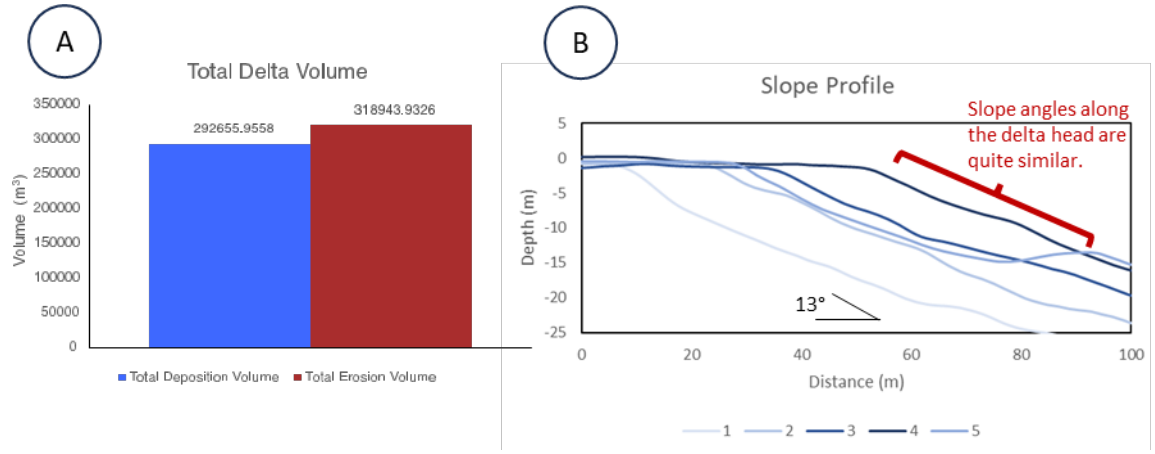

Figure 3.4: A) chart of the total delta volume showing that the delta is more prone to erosion process (53%), B) profile of the delta slope as the delta head progresses by comparing the slope at the same location at 5 different times and shows that the slope remains similar in terms of slope angle at around 13°.

To gain deeper insights into the controlling factors on the locations of slope failures, we considered several potentially influential factors related to slope failure: river input, tidal elevation, delta volume, and delta progradation (Fig 3.5). River input analysis showcases the maximum hourly discharge from the river throughout the day (Fig 3.5A). Notably, four of the major

failures coincide with a peak in river input, indicating a potential correlation between river discharge and slope instability.

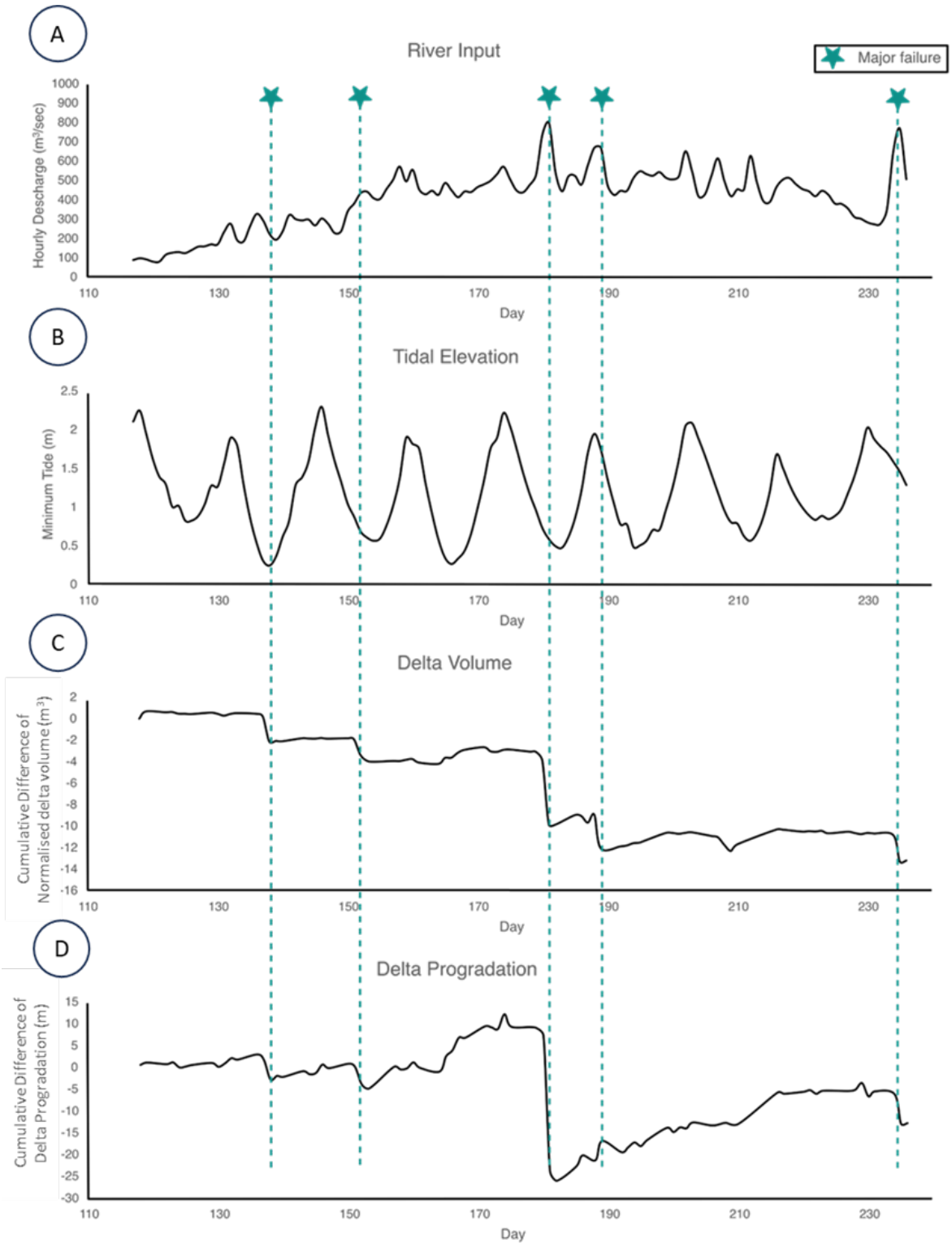

Figure 3.5: Plot of the potential factors to trigger slope failure, The star markers on the plot highlight the days of major slope failures: A) river input shows that major failure happened when there is a peak or after a peak in river discharge. B) tidal elevation indicating the major failure occurs with low minimum tide with the exception of failure 4, C) delta volume shows a step like features indicating that the slope under

steady deposition through a period of time before a major failure swept away the accumulated sediment, D) delta progradation indicating that towards the day of a major failure, the slope would undergo an increase in progradation.

However, not all peaks in discharge feature a matching slope failure. Failure 1 does not coincide with a peak in river discharge, instead lagging two days after such a peak. The magnitude of river input at the time of each slope failure appears to correspond to the magnitude of sediment evacuated.

The tidal elevation coincides with each slope failure (Fig 3.5B). Most failures occurred after a peak tide, except for Failure 4. The range between the highest and lowest minimum tide values, approximately 1 metre, indicates that low tide may contribute to slope failure, particularly after a peak tide.

Delta volume analysis illustrates the cumulative difference of the normalised delta volume daily (Fig 3.5C). The volume is normalised by dividing it by the area of the measured volume because, due to part of the delta area being in shallow water, not every survey can cover the whole study area. This plot exhibits a step feature in every failure, further emphasising the net erosional slope of the delta head.

The delta progradation analysis depicts the cumulative difference in delta progradation on each survey day (Fig 3.5D). The plot shows a step-like feature during major failures, indicating sharp changes as the delta moves backwards (negative values). Additionally, the plot illustrates the delta head steadily moving forward before reaching maximum values a couple of days before major failures. This trend, however, did not apply to Failure 4. The step-like feature suggests a cyclical pattern wherein the delta prograde steadily before retrograding during major failures. The magnitude of progradation and the time spent in this cycle increased throughout the survey.

Failure 4 did not exhibit stepped features in the plot, possibly due to its focus on the east end of the delta, contributing unsubstantial changes in delta movement once all other values were averaged out. The results strongly suggest that delta progradation significantly influences slope stability.

3.4.1.2 Interpretation

Based on the sediment volume analysis (Fig 3.4A), it is apparent that the prodelta is not solely a site of growth, nor a focus on long-term storage of sediment transported by the river. This is a highly dynamic environment, with most of the erosion being accounted for by slope failures. The factors influencing the variations in location, magnitude, and timing of slope failures were

investigated to explore the underlying mechanisms that drive the dynamics of this prodelta evolution over a sub-annual timescale.

The collective findings provide insights into the intricate dynamics leading to major slope failures in the delta head. The synchronous occurrence with peak river input, the nuanced influence of tide, the relationship between delta progradation and stability, and the erosional nature of the delta head all contribute to a more profound understanding of slope failure mechanisms. It is apparent that while sediment flux from the river, tidal elevation, and delta progradation and aggradation changes can be matched to each slope failure, they do not all change consistently, and there is no single explanation for the five different slope failures.

3.4.2 Changes in prodelta slope geometry

The investigation into delta slope failure reveals a complex interplay of factors, including river input, low tide, and delta progradation. However, the intriguing question of why failures occur at different locations on the delta head remains unanswered. To address this, we delved into the geometry of the delta head, specifically exploring how prodelta progradation and aggradation vary.

A detailed analysis of the progradation of the prodelta top, with specific emphasis on individual plots for each failure (F1 to F5), was conducted (Fig 3.6). Plot F1 illustrates limited areas of erosion and inward movement of the delta head, shaping the upcoming major erosion, while deposition occurs on another part of the delta head. Plot F2 depicts continued outward progradation after the first major failure, maintaining a smaller scale and conforming to the shape of the previous failure. Plot F3 showcases significant changes, with the delta head prograding approximately 10 metres from a distance of 0 to 200 metres, followed by erosion from the previous failure. The third failure eradicates the previous deposition, moving the prodelta top by around 50 metres inwards. Subsequent plots (F4 and F5) reveal that the prodelta continues to build outward, with the fourth failure affecting the slope at distances of 200 to 300 metres and the fifth failure occurring around the distance of 130 to 260 metres. The average prodelta progradation plot underscores the dominance of outward movement at distances 0 to 120 metres, while inward movement becomes more pronounced at distances 120 to 300 metres.

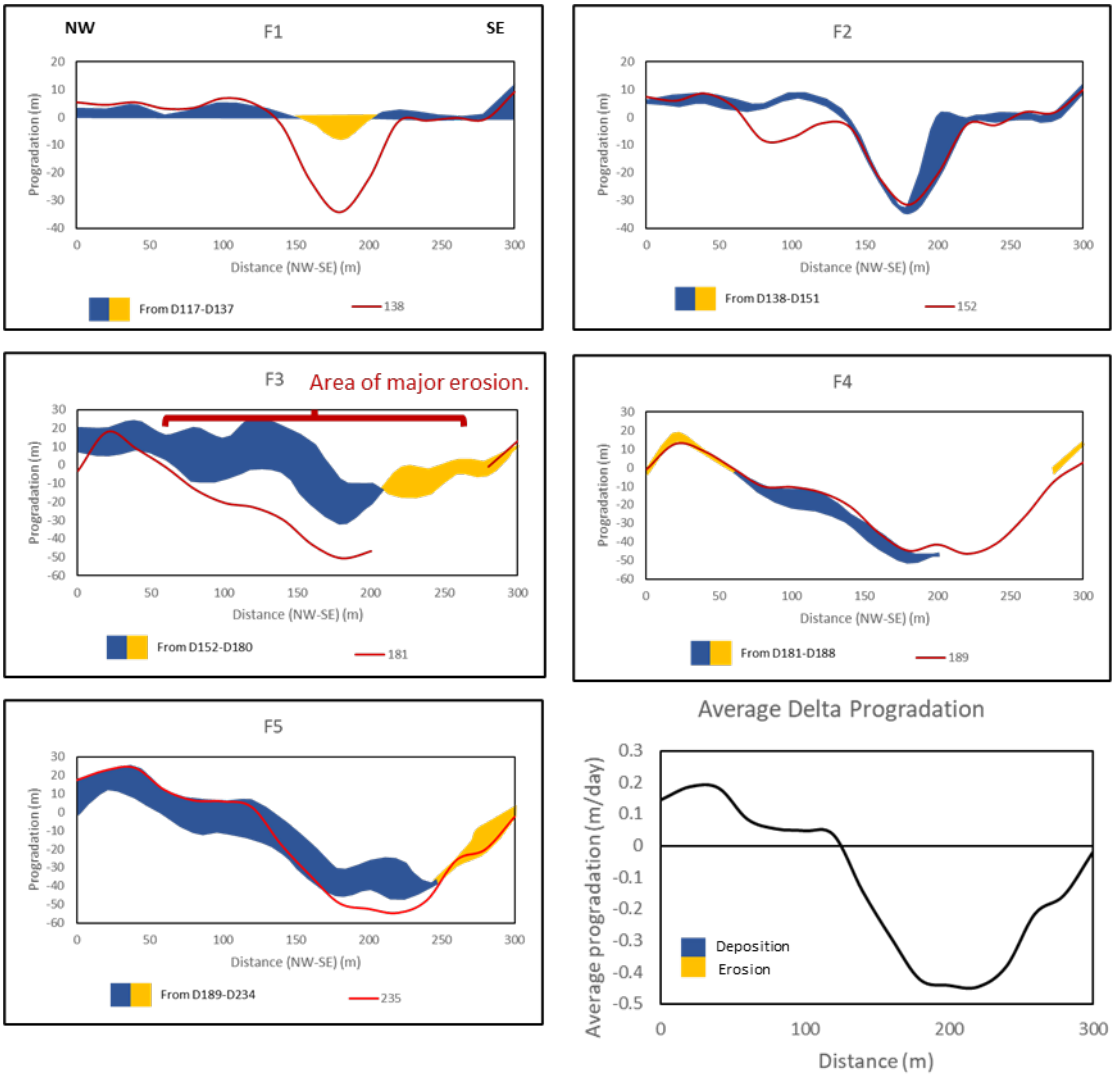

Figure 3.6: Plot of delta progradation for each major failure and the average delta progradation throughout the survey, the blue area represents deposition and the red area represents erosion, the measurement of the deposition and area was calculated from the next day of the previous major failure to the day before the next major failure with the exception of the first failure where the measurement was calculated from the first survey.

An overview of the aggradation of the delta head as a whole, measuring both upward (deposition) and downward (erosion) movement from the northwest to the southeast of the delta. Comparing the progradation and aggradation plots reveals similar patterns in terms of the location of erosion and deposition. As the delta head prograde outward, it would also move upward in terms of aggradation, reflecting deposition. Conversely, as the prodelta moves backwards, the prodelta would move downward in terms of aggradation, corresponding to erosion. The average delta aggradation plot further emphasises that distances from 50 to 120 m from the delta top are more prone to erosion, while distances from 120m onward are highly

erosion-dominated. The delta shows that it has undergone more inward and downward movement (erosion) than outward and upward movement (deposition) (Fig 3.8)

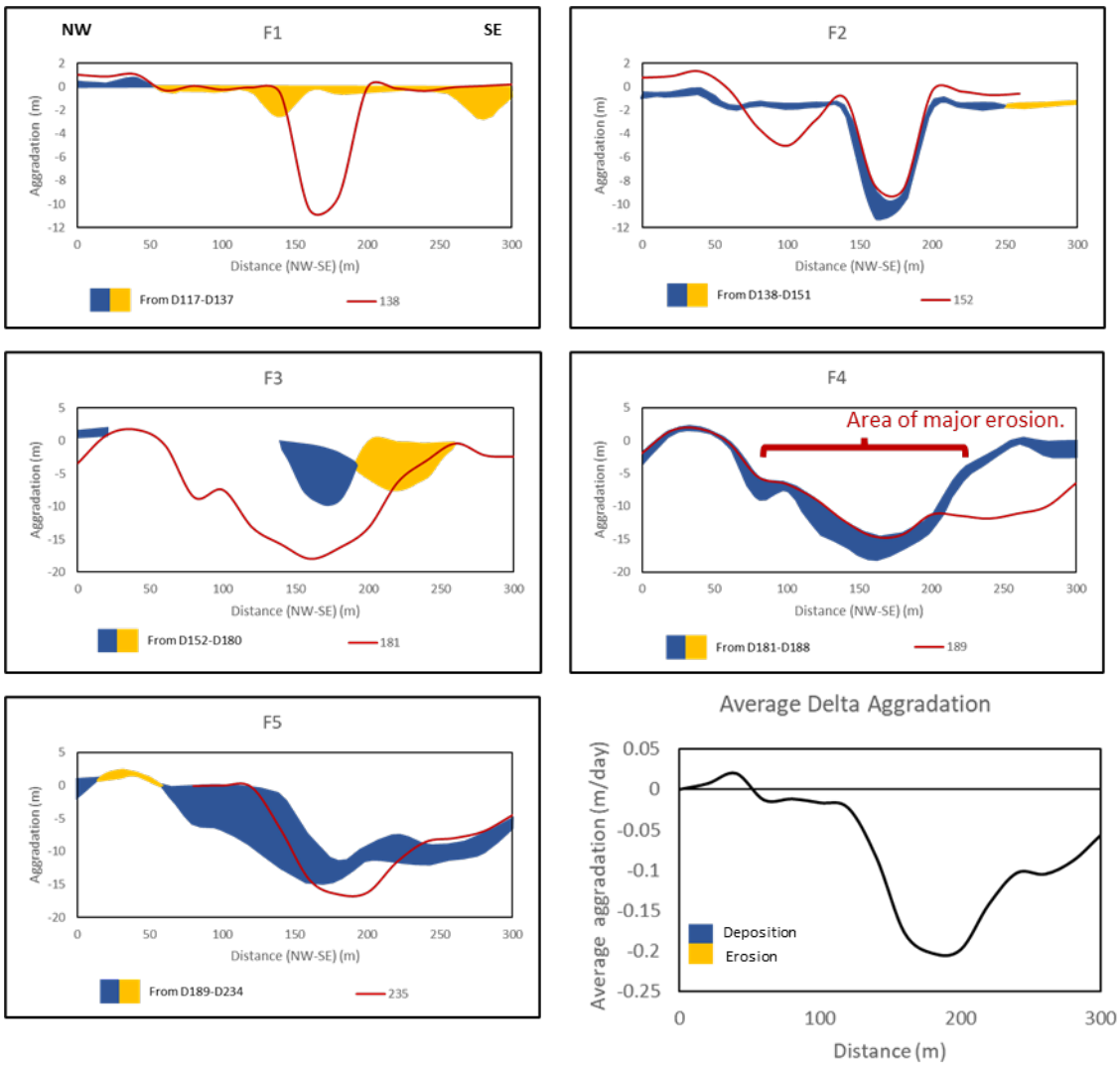

Figure 3.7: Plot of delta aggradation for each major failure and the average delta aggradation throughout the survey, the blue area represents deposition and the red area represents erosion, the measurement of the deposition and area was calculated from the next day of the previous major failure to the day before the next major failure with the exception of the first failure where the measurement was calculated from the first survey.

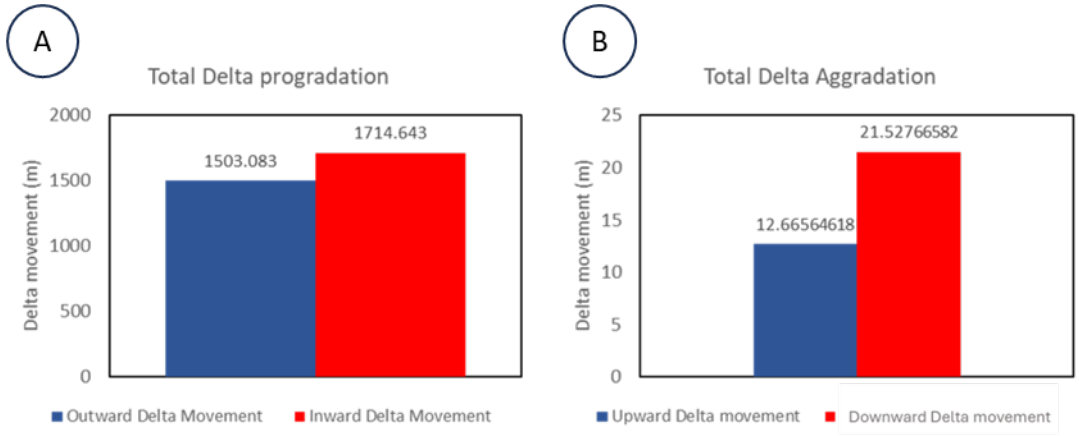

Figure 3.8: A) the chart of the total delta progradation (Delta moves inward more than outward), B) the chart of the total delta aggradation (Delta move downward more than upward).

Despite the overall similarity between the progradation and aggradation plots, slight differences in shape illustrate the influence of crescentic bedforms and small-scale features around the delta head. These features may influence slope failure dynamics, introducing additional complexity to the system.

The analysis of bedforms was conducted by observing the slope map and a profile that traverses the slope, offering insights into the dynamics of the observed landslides. The slope map highlights variations in slope at key points; specifically JD127, JD138, JD142, and JD153 (Fig 3.9). The profile corresponding to the slope map captures subtle changes post-failure, particularly in lines 1, 2, and 3. A comparative examination between the profiles of JD137 to JD138 and JD152 to JD153 reveals noteworthy alterations in slope topography. These changes indicate the impact of the observed failures on the overall slope morphology.

The analysis reveals a landslide characterised by a series of smaller failures progressing from the southeast to the northwest region of the slope. The initial failure occurred within the distance range of 140 to 180 m on JD138, followed by a subsequent failure spanning the distance of 60 to 120 m on JD152. The sequence culminated in a smaller failure within the distance range of 0 to 40 m on JD153. These delineated points on the slope map offer a spatial understanding of the landslide's progression. Analysis of the slope map further reveals that an active upstream migration of bedforms can encourage the process of delta slope destabilisation. Particularly, the bedforms exhibit activities akin to bedform migration as they traverse the slope. This observation underscores the potential role of bedform migration in contributing to slope instability. The results of this analysis highlight the importance of considering not only external factors such as river input and tide but also the intricate geometry of the prodelta top and slope. The observed patterns of progradation and aggradation provide valuable insights into the dynamics of slope

failure, with the influence of crescentic bedforms adding an additional layer of complexity to the understanding of deltaic systems.

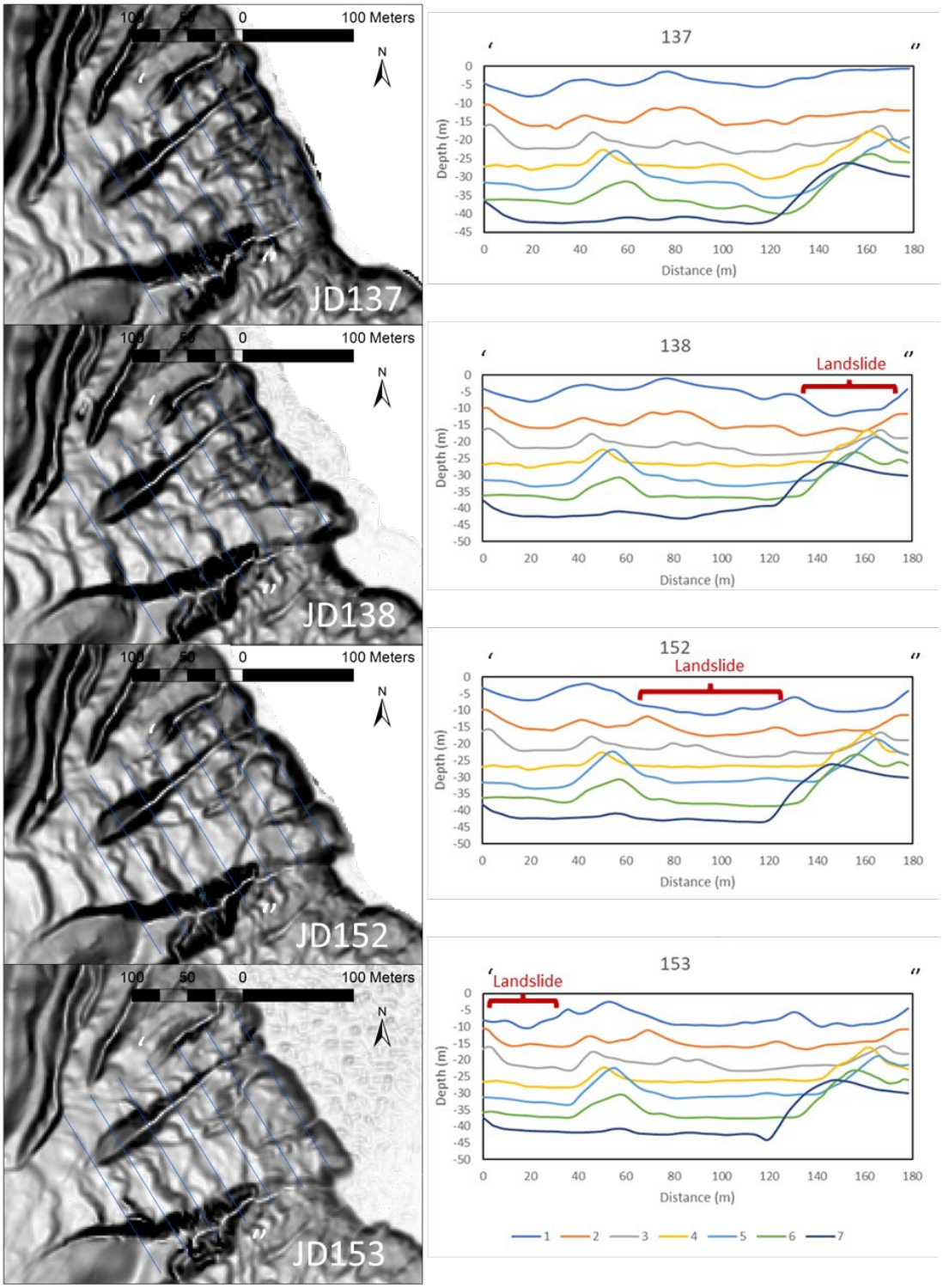

Figure 3.9The slope map and profile along the slope of JD137, JD138, JD152, and JD153 Show bedform migration influencing the failure on these days. The failure moves from the right side of the profile to the left side of the profile. The profile(lines 1 to 7) is based on the blue line on the slope map.

To assess the magnitude of the influence of bedform migration on slope failure, another bedform analysis was done on the slope map and profile captured on two days before the significant event, denoted as JD181 (Fig 3.10). the analysis highlights the noteworthy periods in upslope bedform migration, evident in the alterations observed in lines 2, 3, 4, and 5 between profiles JD179 and JD180 (Fig 3.10B) — just a day before the largest failure. This observation underscores the influence of bedforms in impacting slope stability, not only in the context of smaller failures but also in the occurrence of major ones.

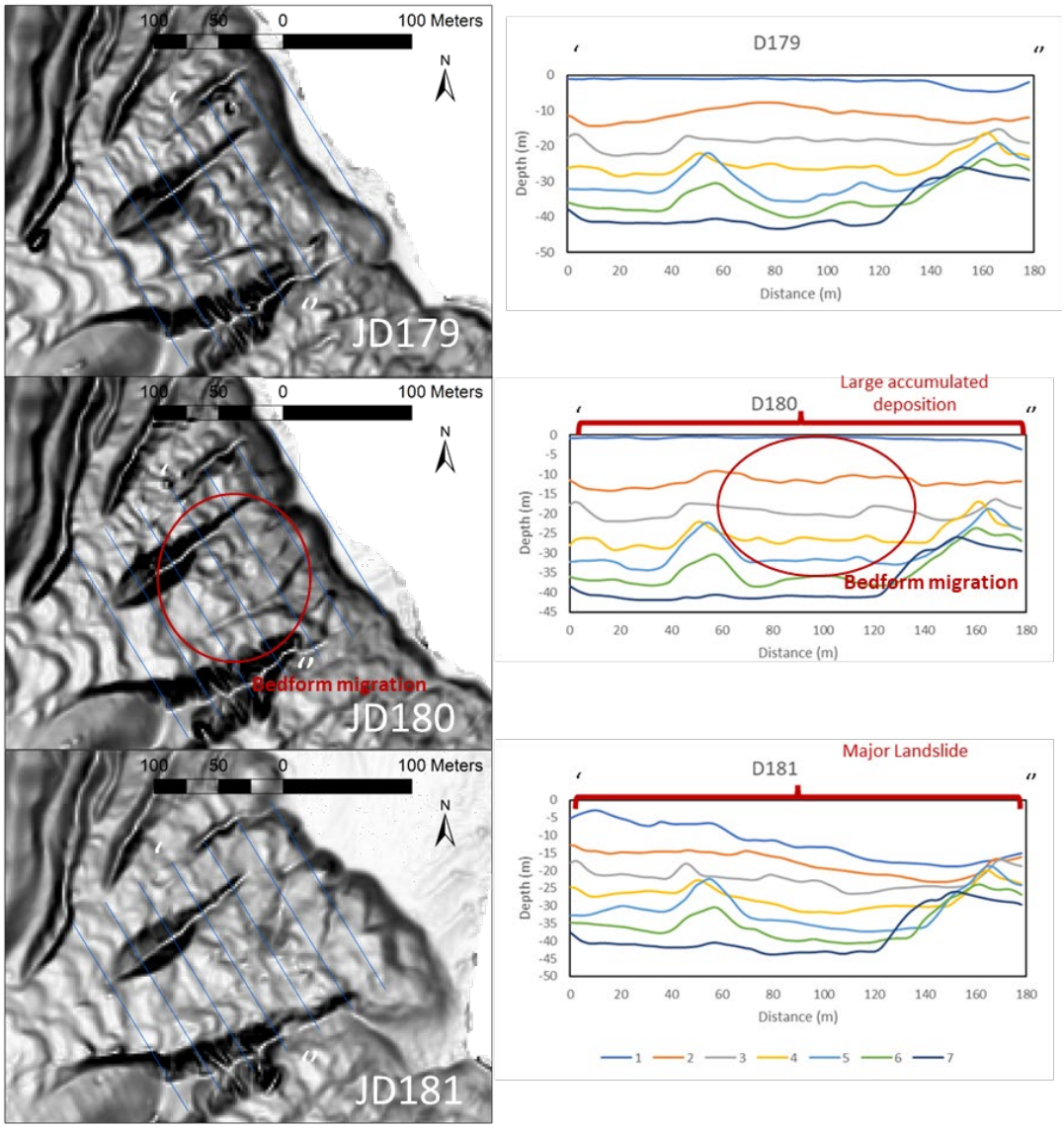

Figure 3.10: the slope map and profile along the slope of JD179, JD180, and JD181 showing upslope bedform migration activities the days before the major failure on the JD181.

The slope map offers a spatial visualisation of the impending event, allowing for the identification of critical points and changes in the slope's configuration. Simultaneously, the profile analysis pinpoints the activities of bedform migration, revealing their upslope movement. The observed alterations in lines 2, 3, 4, and 5 visually represent the bedform-induced changes. The correlation

between the activities of bedform migration and the impending major failure is evident from the identified changes in the slope profile. This temporal analysis, conducted over the two days preceding the event, establishes a connection between upslope bedform migration and slope stability.

3.5 Discussion

3.5.1 Which factors control slope failure at the Squamish Prodelta?

The findings of our study shed light on a myriad of factors contributing to delta head slope failure, underscoring the complexity of the processes involved. Our results align with previous research (Clare et al., 2016; Forel, 1887; Mulder, 2011; Piper and Normark, 2009), indicating that slope failure in deltaic environments is rarely attributable to a single factor but rather to a combination or multitude of contributors.

A prominent factor revealed by our data is the apparent link between delta head slope failure and spikes in river discharge. It is intuitive that elevated river input, accompanied by enhanced sediment flux, should be a key trigger for slope instability. The rapid settling of sediment on the delta head can induce heightened pore pressure with insufficient time for dissipation, as highlighted by the studies of (Parsons et al., 2001) and prior work by (Carter et al., 2014). The distance pathway and consolidation coefficient, influenced by sediment permeability (Terzaghi, 1943), play a pivotal role in the pore pressure decapitation process. However, not all peaks in river discharge correspond to a slope failure, and not all slope failures (i.e. F1) were coincident with a peak in river discharge. Therefore, this cannot be the sole explanation for slope failures.

The role of tide levels in slope failure cannot be overlooked, especially in the context of minimum tide levels acting as potential triggers, as observed in the instances of the first and second slope failures. The lower river discharge during these events suggests a possible correlation between minimum tide levels and slope failure. Tidal unloading can lead to instability, where reduced sea level reduces the hydrostatic pressure in action, and causes expansion of gas trapped in pores in the sediment that weakens the sediment, potentially leading to liquefaction (Kramer, 1988). We do not have any data that proves the presence of gas in the pore fluids, but given the fact that the Squamish River, and other similar rivers in the region, transport organic-rich material from the river, this is a plausible scenario (e.g. Hage et al., 2020). The presence of saturated gases within the delta could further complicate the stability dynamics, particularly when combined with the effects of river discharge and low tide (Clarke et al., 2012).

Progradation and aggradation emerge as additional factors influencing delta head slope failure (Bendixen and Kroon, 2017; Bourriquen et al., 2016; Clare et al., 2016). As the delta progresses, the accumulation of sediment at the delta front results in the development of steep slopes, thereby increasing the potential for instability and failure (Kim et al., 2009). Downstream migration associated with delta progradation shapes characteristic delta configurations, influencing slope morphology and stability as this process can increase pore pressure (Lee, 2009), as well as degrading the sediment stiffness and shear strength (Sultan et al., 2004). The aggradation resulting from rapid sediment loading exacerbates the challenges of pore pressure dissipation, contributing to slope destabilisation (Zoccarato et al., 2018). We do not see any obvious change in the slope of the delta, hence such a geometric change is not a candidate for explaining the slope failures. However, the progradation and aggradation rates are relatively high (0.4 m/ day for aggradation and 1.1 m/day for progradation). Previous work has suggested that it may take hours to weeks for pore pressures to dissipate following such accumulations; hence, this rate of prodelta build-up and build-out may result in conditions that are regularly close to or in excess of stability for much of the freshet when sediment is rapidly delivered by the river to the prodelta slope (Bailey et al., 2021). That we see net erosion on the prodelta appears to be a function of sediment supply being so high that the delta slope cannot solely continue to accumulate and regularly tips the balance to collapse. Another noteworthy factor potentially contributing to slope failure is the geometry of the slope. The findings reveal varying levels of activity along different parts of the slope concerning progradation and aggradation (within the distance range of 100 to 250 m) creating a hotspot for sediment deposits. This different in sediment depositional patterns can be linked to the proximity of these areas to the river mouth(Liu et al., 2009) and the quantity of sediment transported by river discharge. Notably, the initial two failures are more localised (150 m–200 m and 60 m–150 m), while the third failure impacts the slope over a distance of 40 m–250 m, reflecting an increase in sediment input over time. In addition to the localised deposition affecting slope stability, morphological changes along the slope itself may contribute to slope destabilization. The predominant morphological feature identified in the data is bedforms, predominantly found along the delta slope. Upslope bedform migration was also observed in the days leading up to the third major failure. This abrupt downslope alteration could potentially influence the delta top.

Our study highlights the intricate interplay of factors contributing to delta head slope failure. Both river input and tidal elevation likely play pivotal roles, as they can load and unload the sediment pile that accumulates on the prodelta slope. The combination of these factors puts sudden vertical loading on the slope, hindering and temporally modulating pore pressure dissipation, all of which can trigger slope failure. These findings contribute to a wider understanding of deltaic

slope dynamics and have implications for the management and mitigation of slope failure in similar environments.

3.5.2 Bedform migration influence on slope failure

Crescentic bedforms, a distinctive feature observed on the Squamish Prodelta, Canada, have garnered attention due to their similarities with those found in other modern submarine canyon and channel systems (Hage et al., 2018; Talling et al., 2013; Vendettuoli et al., 2019). Cyclic steps, characterized by turbidity currents that undergo a series of hydraulic jumps are thought to be integral to the formation of crescentic bedforms (Cartigny et al., 2011; Normandeau et al., 2016; Postma et al., 2014). The occurrence of hydraulic jumps on these cyclic steps is attributed to turbidity currents that switch between Froude super- and sub-critical flow states (Fildani et al., 2013; Kostic, 2011; Lamb et al., 2008; Turmel et al., 2015).

While such features have been shown to be important building blocks in submarine channels, and may affect the transport of particulate material to the deep sea (e.g. Covault et al., 2017; Slootman and Cartigny, 2020), their influence on the stability of submerged deltas has largely been ignored.

Bedform analysis through slope map and profile analysis offers a detailed depiction of the landslide event. The spatial distribution of smaller failures, coupled with identifying bedform activities and changes in the slope profile, contributes significantly to our understanding of the complex dynamics leading to slope instability in the Squamish Delta. As bedforms migrate upslope, they may induce failures at the slope toe, rendering the sediment upslope unstable and increasing the likelihood of failure (Farre et al., 1983). Analogous instances, such as offshore Pointe Odden, Gabon (Biscara et al., 2012), and La Jolla Submarine Canyon, California (Paull et al., 2013), show similar links between crescentic bedform migration suggesting that such a process may be more widespread in its contribution to small-scale slope instability and failures.

It emphasises that bedforms play a significant role not only in smaller-scale failures but also in influencing the occurrence of larger, more consequential slope failures. This internally generated process may also explain why it is so challenging to pinpoint a single priming or triggering mechanism to the slope failures at Squamish Prodelta, and perhaps elsewhere.

3.5.3 A multi-faceted model for explaining slope failures at submerged prodeltas

Based on the results, a model detailing a sequential process leading to slope failure on the Squamish Prodelta was produced (Fig 3.11). The different stages commence with the delivery of

sediment to the prodelta (3.11a), setting a cascade of events in motion. This sediment influx triggers the aggradation and progradation of the slope (3.11b).

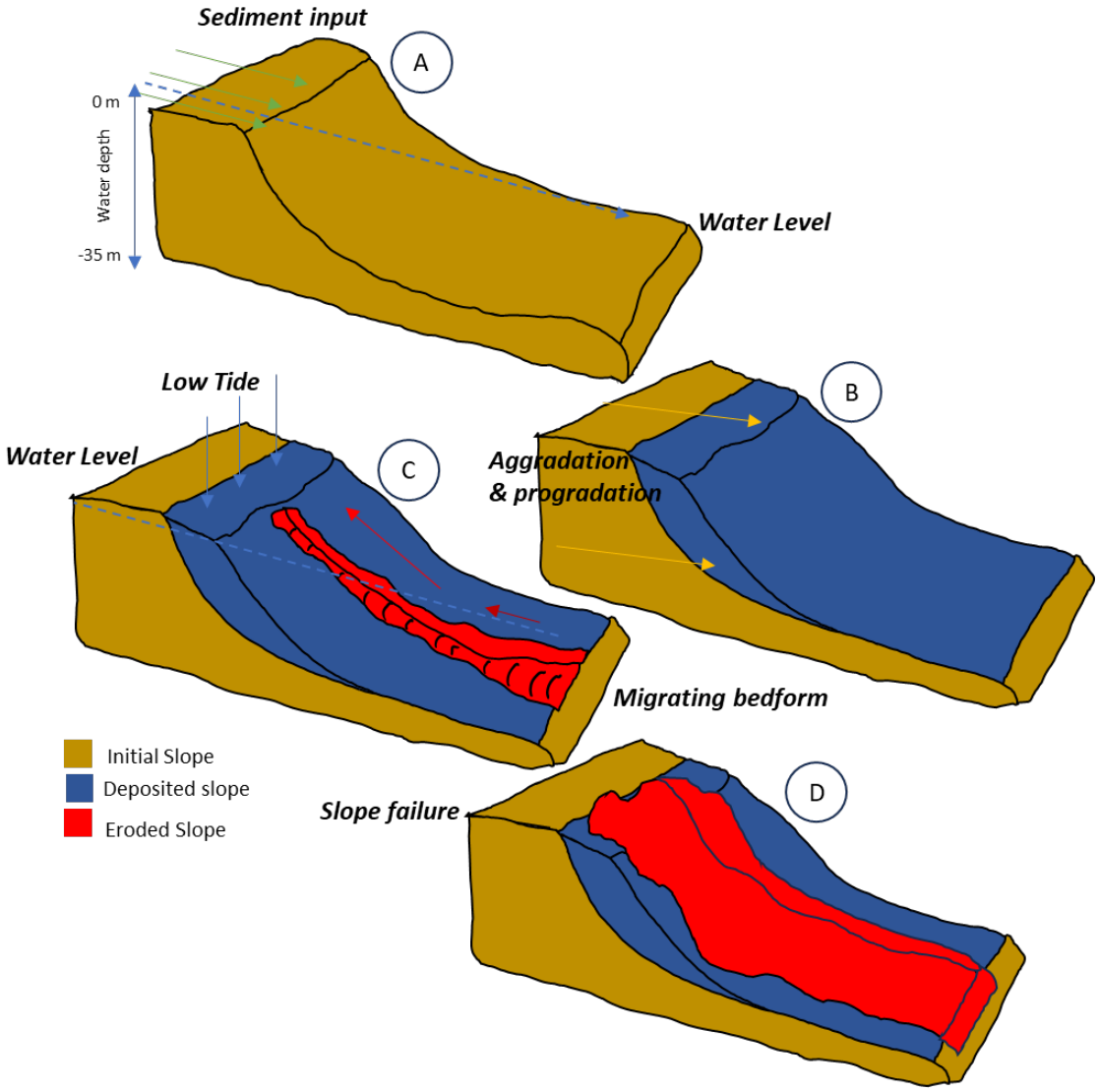

Figure 3.11: Illustration of how the slope evolves: A) slope received sediment input from river discharge, B) slope continue to receive sediment and continue with the process of progradation and aggradation thus accumulating more sediment at the delta top, a sudden loading of the deposited sediment may effect pore pressure of the slope incusing instability, C) slope effected by low tide effect triggering pore water pressure dissipation effecting the stability of the slope and upslope migration bedform are presence and making its wat to the delta top altering the morphology of the delta slope and effecting the stability of the delta top, D) the combination of the previous factor will trigger a slope failure.

The sediment influx induces significant alterations in slope geometry and simultaneously destabilising the slope due to the rapid loading of sediment and the resultant sudden pore pressure dissipation. The subsequent stage (3.11c) involves the added complication of low tide,

contributing to further instability through abrupt changes in pore water pressure. Additionally, the reworking of the toe of the slope as a result of localised undermining or oversteepening by upslope crescentic bedform migration exacerbates the destabilisation of sediment at the top of the slope. This multifaceted interplay of factors, including sediment loading, low tide effects, and bedform migration, collectively intensifies the slope's vulnerability to collapse. The culmination of these interacting elements unfolds in the final stage (3.11d), resulting in a slope failure.

The interconnected influence of sedimentation, changes in tide, and bedform activities contribute collectively to the complex dynamics leading to slope instability at the Squamish Delta. This gives an overview of the stepwise processes that culminate in slope failure. The initiation of sediment input, followed by aggradation and progradation, sets the stage for destabilisation. The additional impact of low tide and bedform migration further amplifies the destabilising factors, ultimately contributing to the observed slope failure in the Squamish Delta. It is worth commenting that this study is based solely upon changes that were observed in the prodelta during the active discharge season (i.e. the freshet). It is therefore unclear how conditions may change during the autumn and winter, when river discharge is lower.

The processes observed here at Squamish Prodelta are far from unique and are likely important processes at many other seasonally active, high sediment supply submerged deltas worldwide (Nienhuis et al., 2020). The study site is not affected by significant waves (due to the sheltering effect of the fjord); hence, to what extent these findings relate to wave-dominated deltas remains unclear, and other processes, such as large storms that can cyclically disturb delta sediments where not observed during the monitoring period. The cumulative effects of sediment delivery to the prodelta, bedform migration, and geometric modifications that drive slope failure mean that pro-deltas such as that observed here are not simply sites of net sediment storage (Hage et al., 2022). Instead, the effects of slope failure re-exhume previously buried sediments and transport them to deeper water. This re-exhumation has implications for the efficiency of burial of reactive organic carbon that can become mineralised (i.e. reducing burial efficiency) and also for the periodic release of previously buried pollutants such as microplastics, which may be suddenly dispersed to deeper water ecosystems. This repeated storage and release is only apparent due to the temporal resolution of the seafloor surveys that were performed. It is likely that many other submerged delta systems show similar behaviour, however, the timescale of any repeat seafloor surveys (or the general lack of such repeated surveys in general) means that we have not previously had the observational data to determine this. Future repeat surveys of submerged prodeltas will undoubtedly reveal new insights into their behaviour, the timings and fluxes involved in prodelta construction, and in loss of material due to slope failures. The combination of river sediment delivery and submerged slope failures play a crucial role in the construction, periodic destruction, and evolution of prodeltas.

3.5.4 Potential Hazard and Mitigation

Slope failure can result in significant sediment transport and reworking of large volumes of sediment that can damage seafloor and undersea infrastructure, as well as having potential to generate tsunami (Xue et al., 2019). The findings of this study highlight potential hazards associated with delta slope collapses on the submerged Squamish pro-delta in the Howe Sound, particularly during peak river discharge seasons. How Sounds is very similar to many other seasonally active river-head fjord settings, such as those found across British Columbia, as well as elsewhere (e.g. New Zealand, Canada, Chile etc). While slope failures are not uncommon, their occurrence did not lead to disastrous events (i.e. tsunamigenesis) during the survey period, due to their limited scale. The repeated collapse of the submerged slope may preclude the occurrence of much larger tsunamigenic failures, but could have implications for seafloor structure such as cables should they have been laid near to the prodelta, which experiences many (in some cases >100) turbidity currents every year (Clare et al., 2017). The outcomes of this study serve as a valuable guide for constructing hazard mitigation strategies, including slope failure prediction and selecting suitable locations for seafloor infrastructure around or near delta slopes, which may be related to many other submerged deltas worldwide. The study underscores the significance of sediment supply as a key controlling factor in slope failure, emphasising the need to consider this variable in slope failure assessments.

Furthermore, the role of slope geometry, such as aggradation, progradation, and the migration of bedforms along the delta slope, was identified as contributing factors to slope failure. This information enables the planning of infrastructure placement to avoid areas with high sediment supply that have prograded significantly and exhibit extensive bedform migration along the slopes. However, the lack of data extending to low sediment input seasons underscores the urgent need for future studies to investigate slope failure triggering factors during less active periods and compare the results with those obtained during peak discharge seasons. Such efforts will not only enhance the understanding of delta slope dynamics but also contribute to more effective hazard mitigation strategies in similar environments.

3.6 Conclusion

This investigation into the Squamish Prodelta's slope failures has revealed a complex interplay of processes, shedding light on when, where, and why these events occur. The prodelta top and slope witnessed five major slope failures, each presenting unique characteristics in terms of size, shape, and magnitude. Spatial analysis and temporal mapping revealed distinct locations and varied magnitudes for each failure, prompting a deeper exploration into the contributing factors. The spatial distribution of slope failures, as depicted in Figure 3.2, showcases the

intricate dynamics at play on the delta head. The sequential failures, varying in magnitude and location, instigated critical questions regarding the underlying mechanisms driving these events. Our study addressed these queries by examining factors such as river input, tidal elevation, delta progradation, and aggradation. River input (more likely sediment fluxes driven by river discharge) emerged as a prominent influence on slope failure, with four major failures coinciding with peaks in river discharge. A link between river input and the magnitude of slope failure underscores the role of sediment loading triggered by elevated river discharge. Contrary to prior expectations, the slope angle of the delta head remained relatively stable, suggesting a continuous progradation of the delta. Erosion outweighed deposition, emphasising its dominant role in shaping the delta during the study period. Intriguingly, minimum tidal elevations emerged as potential triggers for slope failure, especially in the first and second events. The cyclical pattern of prodelta progradation, as observed in Figure 3.6, provided insights into the interconnected dynamics of prodelta morphology and slope stability. Additionally, the erosional nature of the prodelta head, highlighted by Figure 3.4, showcased the stepwise processes leading to slope failure. Bedform migration, characterised by crescentic bedforms, added a layer of complexity to the slope failure dynamics. Figure 3.9 illustrates the spatial progression of bedform-induced failures, emphasising their influence on slope instability. The correlation between bedform migration and major failures, as evidenced in Figure 3.10, emphasised the role of these features in both small-scale and significant landslides. Figure 3.11 provides a comprehensive overview of the sequential processes leading to slope failure, elucidating the impact of sediment input, aggradation, progradation, low tide, and bedform migration. From here we can say that slope failures are likely the results of a combination of enhanced slope geometry due to prodelta lip progradation and pore pressure fluctuations relating to sediment loading and tidal effects and small scale features such as crescentic bedforms also play a role in slope failure. The interconnected nature of these factors culminated in the observed slope failure, emphasising the need for a holistic understanding of deltaic processes. Our study advances the understanding of prodelta head slope failure dynamics by unravelling the multifaceted interactions between river input, tide levels, prodelta morphology, and bedform migration. The findings contribute to an improvement in assessing slope instability in submerged deltaic environments, offering valuable insights for future research and mitigation strategies in similar geological settings. The complex interplay of factors underscores the need for a holistic approach to studying and managing slope failure in submerged deltaic systems

Chapter 4 Variable scales of bedforms created and shaped by the 2022 ocean-entering eruption of Hunga Volcano, Kingdom of Tonga

Muhamad Z. Zulkifli, Michael A. Clare, Isobel Yeo, Sally Watson, Richard Wysoczanski., Sarah Seabrook, Kevin Mackay, James. E. Hunt, Marta Ribó,

Author contributions I am responsible for the analysis and am the main author of this manuscript. I.Y., S.W., R.W., S.S., K.M., J.E.H., M.R. contributed to data acquisition and M.A.C. provided the main editorial support and comments on the manuscript..

Abstract:

The eruption of the Hunga Tonga-Hunga Ha'apai Volcano (now known as Hunga Volcano) in January 2022 represented a major event that had wide-reaching impacts for coastal communities, seafloor infrastructure and benthic ecosystems. The eruption's intensity resulted in the substantial alteration of the island's surface, but the transformations beneath the sea surface were even more profound. Here, to understand the impacts on the seafloor, this study analyses bathymetric data that encompass both pre- and post-eruption periods to elucidate seafloor changes induced by the volcanic activity. This study focuses on submarine bedforms that were observed within a distance of 100 km of the volcano, shaped by fast-moving density currents that were formed when the eruption column collapsed into the ocean and on to the seafloor. These bedforms can be classified into three distinct types based on their dimensions, specifically wavelength and wave height, each exhibiting unique characteristics which provide insights into the behaviour of the currents that shaped them as well as of how local seafloor topography can steer and modify flow behaviour that varies in different locations as a result of internal controls. For example, flows that decelerated away from the volcano, and that were in a net-depositional regime, locally appear to have re-accelerated and re-commenced erosion several tens of kilometres away from the volcano due to the influence of topographic confinement. This study shows how a single volcanic eruption can generate a spectrum of bedforms with regards to their wave height and wavelength, as a result of the evolution of the density currents away from their source. Similar scale bedforms are observed on the flanks of other partially and fully submerged volcanoes, which enables diagnosis of locations that may have experienced similarly-hazardous eruptions in the past; however, the bedforms observed in the most distal reaches surveyed are similar to those that have been linked to non-volcanic triggers. This study demonstrates that a broader context is likely required before hazardous

events can be diagnosed from individual bedform fields. The findings have particular relevance for the assessment of risks posed to seafloor infrastructure such as submarine telecommunications cables that can be inferred from the nature of bedforms and demonstrate the value of repeated bathymetric surveys for identifying the source and extent of seafloor density currents.

4.1 Introduction

The Hunga Tonga-Hunga Ha'apai (hereafter Hunga) Volcano eruption offshore from the Kingdom of Tonga on 15th January 2022 was the most explosive eruption this century, representing at least as large an eruption at Mount Pinatubo in 1991 (Seabrook et al., 2023). The eruption had widespread impacts that were felt worldwide (Borrero et al., 2023; Li et al., 2023; Pakoksung et al., 2022; Poli and Shapiro, 2022). The eruption resulted in the almost complete removal of the volcano's aerial portion and widespread deposition of ash and debris on the surrounding land masses (Lynett et al., 2022). This catastrophic event was characterized by the formation of a far-reaching volcanic plume that reached over 57 kilometres tall into the sub-mesosphere, the propagation of atmospheric Lamb waves that travelled more than three times around the world, and the generation of diverse tsunami waves (triggered by the Lamb Wave that reached the other side of the Pacific Ocean, and more locally that inundated islands in Tonga and Fiji), (Amores et al., 2022; Proud et al., 2022; Sun et al., 2022). These observations underscore the wide-ranging consequences of major volcanic eruptions, highlighting the critical need for a comprehensive understanding of their severity, extent, and varied effects through the collection of extensive pre- and post-eruption data (Breard et al., 2016; Sovilla et al., 2008). Perhaps the most significant economic impact of the eruption was the damage to two seafloor cables that connected the island of Tongatapu (the main island of Tonga) to the global telecommunications network and domestically. Around one hour after the main eruption of Hunga Volcano, the international cable was damaged, resulting in Tonga being cut off from the rest of the world and unable to connect to the internet (Clare et al., 2023). It was five days before satellite communications were resumed, enabling <1% of the previous bandwidth, and five weeks before the international cable was repaired owing to the extensive damage and burial (Clare et al., 2023). The domestic cable was not repaired until 1.5 years later, as 125 km of new cable needed to be manufactured to replace the extensively damaged and buried cable. Benthic environmental surveys performed three months after the eruption revealed that all seafloor life was either stripped from the seafloor, or else buried, with the exception of a few locations where topography provided refuges for some organisms (Seabrook et al., 2023).

Hunga Volcano is situated along the Tonga–Tofua-Kermadec Ridge, a submarine mountain range positioned on the most seismically active subduction boundary on Earth (Schofield, 1967). The geological history of this volcano includes past eruptions, notably the Surtseyan eruptions in 2009 and 2014–2015, resulting in the formation of a subaerial tuff cone structure and the emergence of a new landmass between two existing islands (Smallhorn-West et al., 2019). Initially covering an area of 1.94 km^2, this newly formed landmass underwent an active phase starting in late 2021, marked by intermittent eruptions from December 29, 2021, to January 4, 2022 (Lynett et al., 2022). The emergent land area at Hunga Tonga expanded from approximately 3 km2 in early December to 5 km2 in January, thereby increasing the island's surface area by around 2 km^2 (Lynett et al., 2022). Following a period of reduced activity, the submarine volcano unleashed a series of intense, explosive eruptions commencing around 04:15 UTC (17:15 local time) on January 15, 2022 (Poli and Shapiro, 2022).

Precisely what caused the extensive damage to the cables and loss of benthic life was unclear until detailed seafloor surveys were performed after the eruption. Unusually for this part of the world, detailed seafloor surveys existed prior to the eruption, having been performed in 2015 and 2016. The availability of pre- and post-eruption surveys enabled the creation of elevation difference maps that identified a diversity of seafloor changes. Seabrook et al. (2023) showed how up to 800 m vertical change occurred within the centre of the volcano caldera, accounting for an erupted mass of >6 km3. Away from the volcano, other seafloor changes were observed including large scours and incision of gullies that are up to 120 m deep, which have been related to fast-moving (up to 122 km/hour) seafloor density currents laden with volcaniclastic material that were triggered when the eruption column collapsed into the ocean (Clare et al., 2023). Prior studies had suggested that the presence of such large bedforms or scours may be diagnostic of major explosive eruptions, particularly fields of sediment waves and bedforms around the submerged part of the submarine volcano that span several tens of kilometres and exhibiting wave heights and wavelengths of hundreds and thousands of metres respectively (Gardner, 2010; Leat et al., 2010; Pope et al., 2018; Silver et al., 2009; Wright et al., 2006). These bedforms may play a crucial role in understanding the geological processes and hazards associated with underwater volcanic activity, including those formed by eruption-fed density flows as well as those resulting from landslides (Pope et al., 2018); however, the absence of pre- and post-eruption surveys has meant that the attribution of such bedforms to major volcanic eruptions has remained speculative (Casalbore et al., 2021). The unique datasets acquired available before and after the 2022 Hunga Volcano eruption have enabled a categorical link between large scours and a major eruption for the first time (Clare et al., 2023). While recent studies examined the seafloor change following the eruption (Clare et al., 2023; Seabrook et al. 2023), they only addressed the large-scale bedforms and did not explore the full range of seafloor changes across the entire survey area (in particular

smaller dune-scale bedform fields, i.e. metres wave height, 10s-100s metres wavelength) nor the implications for understanding the nature and evolution of the volcaniclastic density currents along their course and into deeper waters.

Bedforms formed by eruption-fed density currents may be triggered by the collapse of eruption columns or the disintegration of active lava domes, while those formed by landslides can result from various factors such as volcanic shelf failure, edifice uplift, magma intrusion and extrusion, or the sudden accumulation of large volumes of pyroclasts during volcanic eruptions (Cas and Wright, 1991; Head and Wilson, 2003; Kokelaar and Busby, 1992; Watt et al., 2014). Distinguishing between these bedforms involves considering criteria such as symmetry, internal architecture, and wavelength, with a focus on the dimensions of the bedforms, particularly wavelength and wave height; as analysed by Symons et al. (2016) in a global review analysing the dimensions of bedforms through comparative wavelength and wave height log plots allows for distinguishing their origin based on their scale, relief, revealing insights into the nature of the flow that formed them (Karstens et al., 2023; Pope et al., 2018; Symons et al., 2016). This study focuses on a comparative morphological assessment of different scales of bedforms shaped by the 2022 Hunga Volcano eruption with a view to understand the nature of density currents created following such a major eruption.

4.2 Aims

The research aims to study the formation of multiple scales of bedforms around the volcanic edifice and surrounding areas to understand the magnitude of processes brought by the major volcanic eruption. Our first objective is to analyse the morphological changes of the seafloor, specifically focusing on the formation of bedforms in the submarine area surrounding the Hunga Tonga volcano, ranging from near the caldera to a distance of 40 kilometres away from the caldera. Additionally, we seek to compare our measurements of the bedform dimensions (wavelength and wave height log plots) with those presented in the studies by (Karstens et al., 2023; Pope et al., 2018) to address existing gaps in the datasets. Our third objective is to interpret the formation of the bedforms, including distinguishing the magnitude and pathways of the flow based on their remnants.

4.3 Data and Methods

This study analyses two bathymetric surveys of the (pre-eruption and post-eruption) areas surrounding the Hunga Tonga volcano. Those surveys cover 16 km around the caldera. The survey also extends 39 km northwest of the caldera and 560 km southwest of the caldera (in this study, the focus is only around 40 km from the caldera) (Fig 4.1A). Data were acquired during Expedition

FK160407 in May 2016 by the RV Falkor using a Kongsberg EM302 (DOI: 10.26022/IEDA/330859); a small boat survey in November 2015 using a WASSP multibeam echosounder; and the satellite-derived bathymetry in 2017 from Land Information New Zealand as part of the Pacific Regional Navigation Initiative (Purkis et al., 2023). Data were imported into QPS Qimera v2.3.1 for processing, then gridded and exported at 50 m resolution for consistent comparison. In all surveys, the sound velocity corrections were applied based on sound velocity probe measurements or calculated from (conductivity, temperature, depth, CTD) casts during acquisition.

The post-eruption surveys were performed on the TESMaP expedition TAN2206 of the R/V Tangaroa to the site in April and May 2022. These surveys consisted of ship-based multibeam bathymetric data collected using a Kongsberg EM302 multibeam echosounder operating at 30 kHz, with 288 beams (432 sounding per swath) and beam widths of 1° along- and 2° across the track. Kongsberg proprietary Seafloor Information System (SIS) acquisition software was used to collect the data. GPS was differentially corrected by the Fugro SeaStar XP Wide Area Differential GPS (WADGPS) to provide positioning for these surveys. Heave and attitude correction was applied using Applanix POS/MV 320 motion sensor (roll, pitch, and heading are accurate to 0.02° or better; heave is accurate to ±5% of the measured vertical displacement or ±5 cm, whichever is larger, for movements that have a measured period up to 20 s). The data were processed and cleaned using QPS Qimera v2.3.1, then gridded and exported at 50 m horizontally. Backscatter mosaics were created using Qimera v2.3.1, 3-sigma, to maximise contrast for the dataset and mosaics exported at the same horizontal resolution as the bathymetry (50 m). Backscatter data help to identify bedforms in deeper water areas where the scale of bedforms is close to or at the resolution of the multibeam bathymetric data.

The bathymetric data were analysed using ESRI ArcGIS software. Greyscale slope maps were generated to visualise seafloor morphology, and a raster calculator was used to generate differences in elevation between the two surveys. In the elevation difference maps, red colours indicate areas of erosion (negative values), while blue colours indicate areas of deposition (positive values). Confidence in the calculated elevation differences is reduced at the edges of the survey area and where elevation differences were equal to or below the vertical resolution of the bathymetric data. Seabed elevation changes and eroded volumes were calculated using the raster calculator tools in ArcGIS software. Both surveys do not perfectly overlap. Thus, not all areas can be compared using a different map. The focus area in this study consists of three areas labelled A, B, and C (Fig 4.1B).

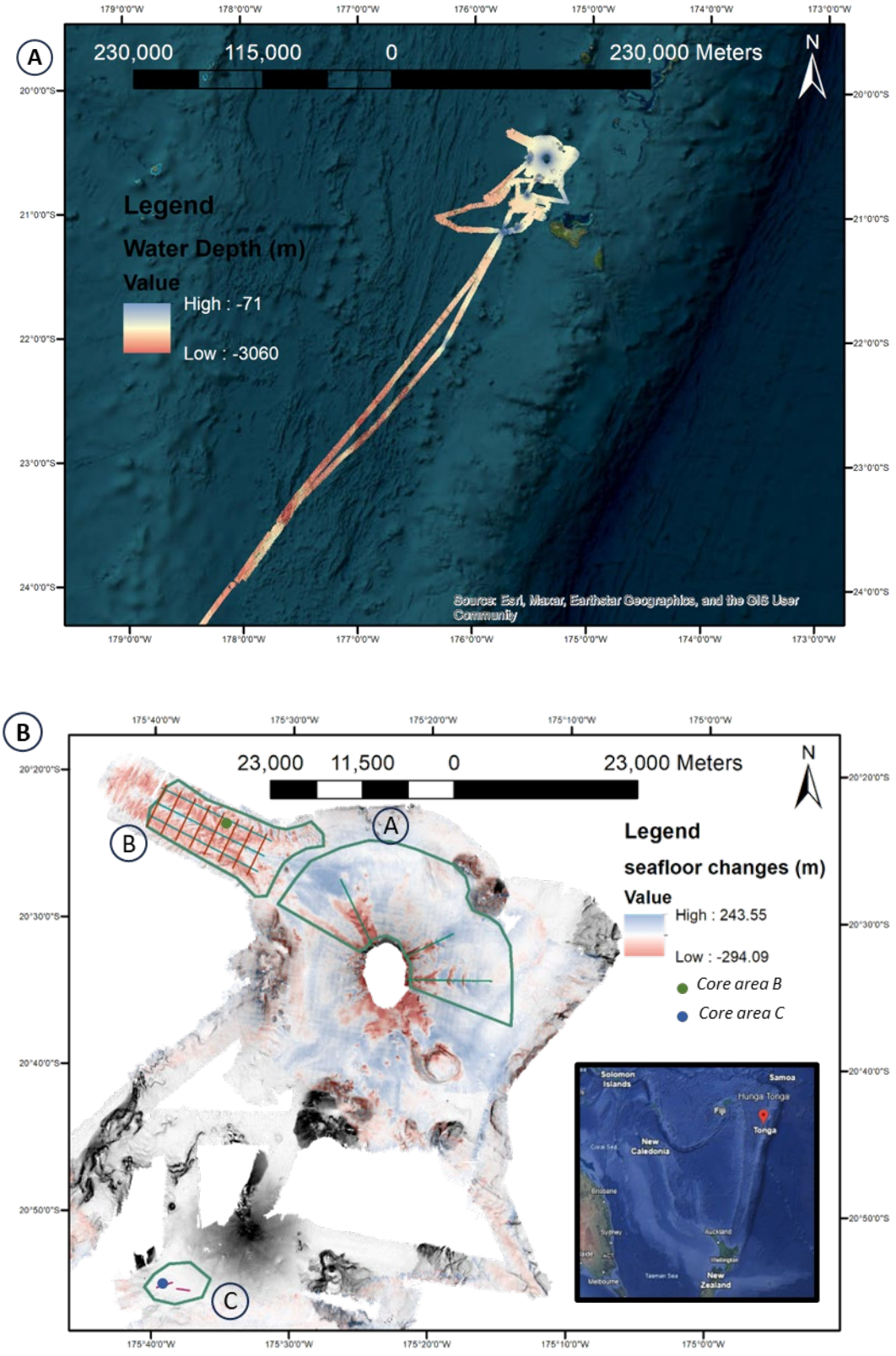

Figure 4.1: A) bathymetric map of the study area, B) Difference map of the study area and location of different bedform areas A, B, and C. location of bedform profile as well as the location of core samples.

However, for this study, both area A and area B overlap, with the exception of area C. The pre-eruption data also only extends for around 120 km southwest of the caldera compared to the

post-eruption data, extending to around 560 km. Area C only has the bathymetry data for the post-eruption survey. Even so, area C has backscatter data. The bathymetry's resolution (pre and post-eruption) and backscatter data is 50 m. The usual vertical uncertainties in contemporary multibeam echosounders are approximately 1% of the water depth. In the surveyed areas, this potential vertical uncertainty spans from 20 cm in shallow waters to 20 m in the deepest areas. However, in numerous surveyed regions, the measured difference between seemingly unaffected volcano regions was generally less than 2 m, making these morphological changes identifiable in the datasets.

4.4 Results

4.4.1 Overview of morphological changes after the eruption

Hunga Volcano, located between the uninhabited islands of Hunga Tonga and Hunga Ha'apai in the Kingdom of Tonga, underwent significant transformations during its recent eruption on the 15th of January 2022. This volcanic activity, distinct from its previous eruption in 2015, resulted in the creation of a 120-meter high and 2-kilometre wide near-circular tephra cone, merging with the volcanic island at the time (Garvin et al., 2018; Seabrook et al., 2023; Vaiomounga, 2017). However, the explosive events in 2022 led to the complete separation of the island, leaving only a small remnant at the surface (Gupta et al., 2022; Seabrook et al., 2023).

While surface changes are evident, this study focuses on the subsurface morphological alterations triggered by the eruption. More than 6 cubic kilometres of seafloor materials were evacuated during the eruption, with volcaniclastic density currents estimated to have runout for over 100 kilometres through the seafloor that transported much of that material (Seabrook et al., 2023). Major seafloor changes can be observed after the eruption. These include: i) Deeply incised gullies that radiate from the caldera on the outer volcano flanks. These gullies are locally up to 120 m deep; ii) Large crescentic scours on the eastern flank of the volcano that are up to 53 m deep and 2485 m wide; iii) Depositional lobes of material that accumulate downslope of the scours or gullies, which are up to tens of metres in thickness, forming where slopes reduce to less than ten degrees (Fig. 4.2A). These features have been the focus of recent studies (i.e. Clare et al,, 2023; Seabrook et al., 2023); however, we also observe other features with smaller dimensions, but that also appear to be important with regards to erosion, deposition and general reshaping of the seafloor. These other features include: iv) crescentic bedform fields in the northwest of the study area that extend beyond an area of lobate deposition (Fig 4.3A); and v) dune-scale bedforms (1-2 m wave hight) around 40 km from the volcano (Fig. 4.4A), that are only discernible from backscatter data due to the absence of pre-eruption bathymetric data and

would unlikely be discernible from the difference map due to the water depths in which they occur and the associated resolution of the multibeam bathymetric data. This study details these latter features, adding to previous preliminary high-level studies.

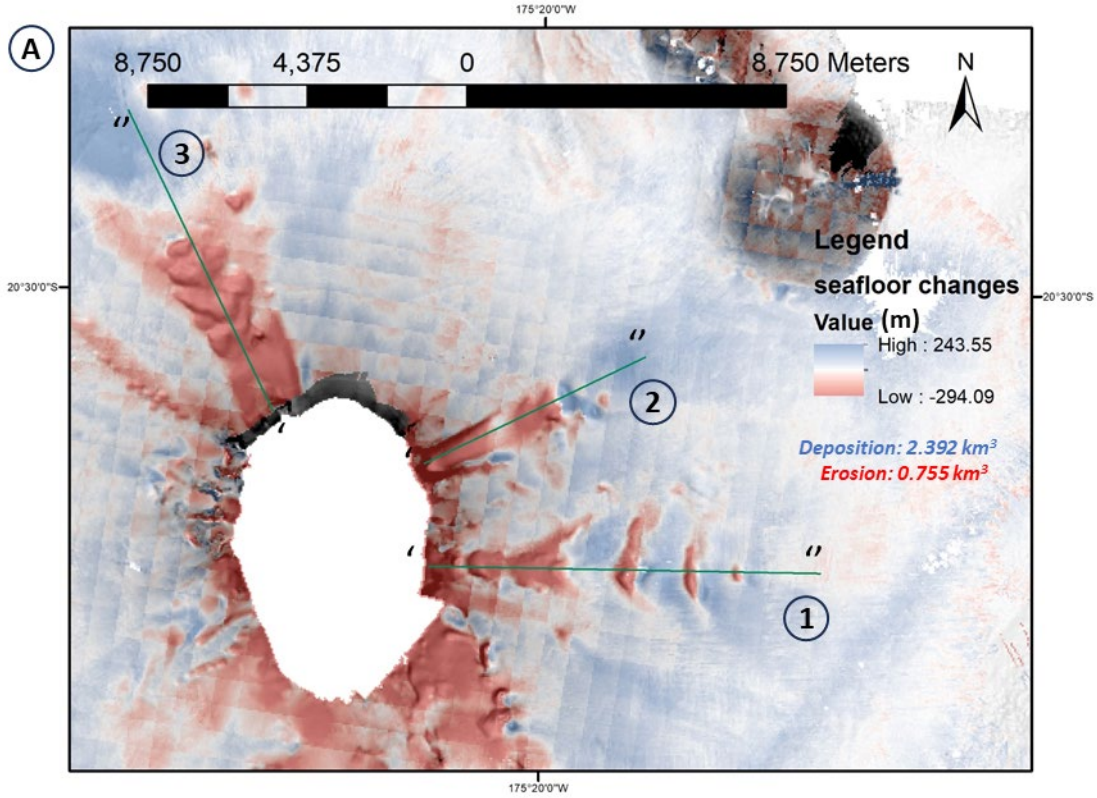

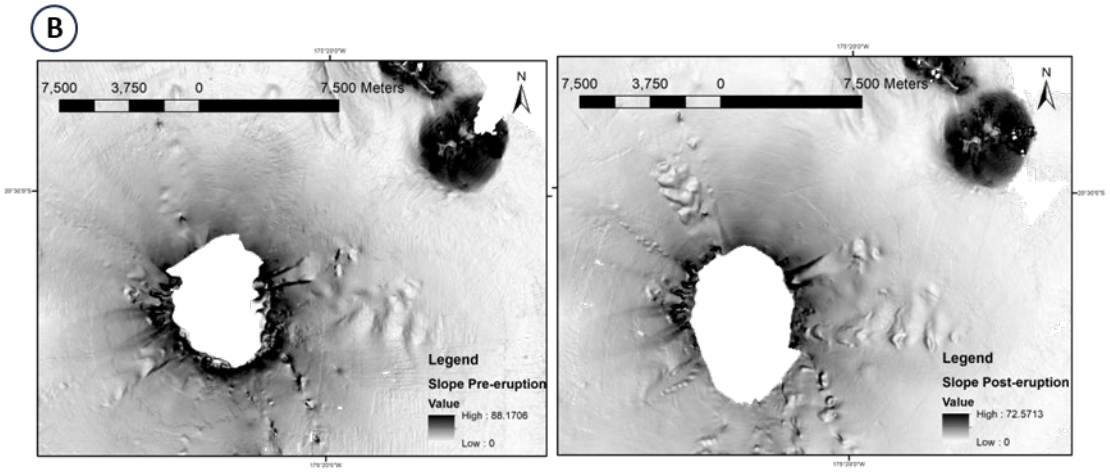

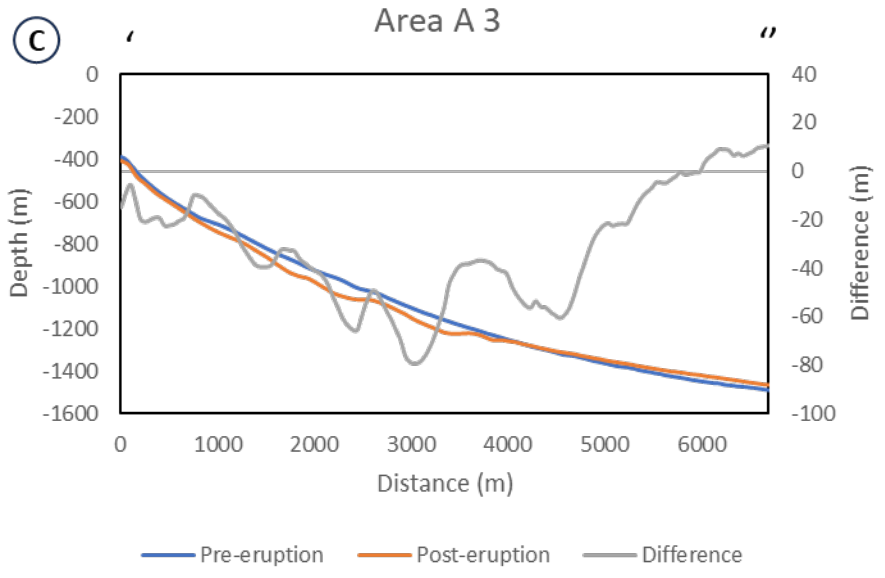
C
Area A 3
Depth (m)
Difference (m)
Distance (m)
Pre-eruption
Post-eruption
Difference

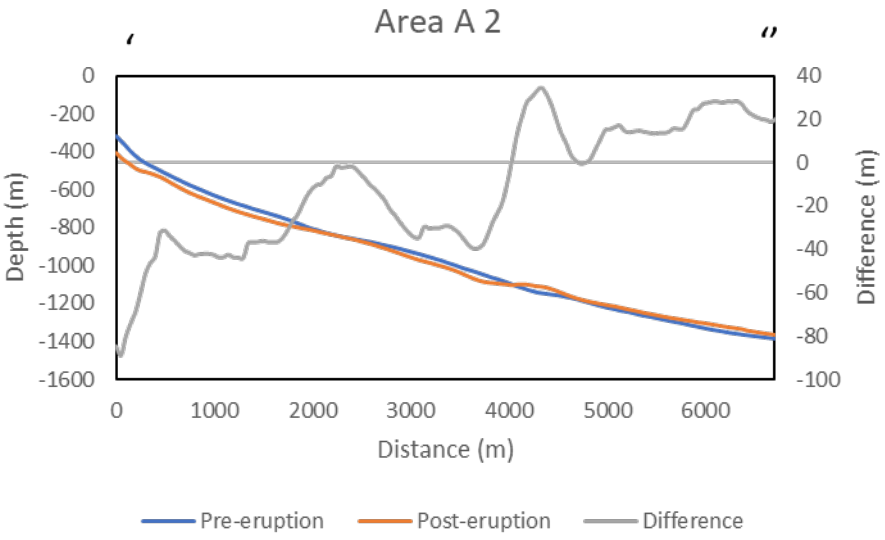
Area A 2
Depth (m)
Difference (m)
Distance (m)
Pre-eruption
Post-eruption
Difference

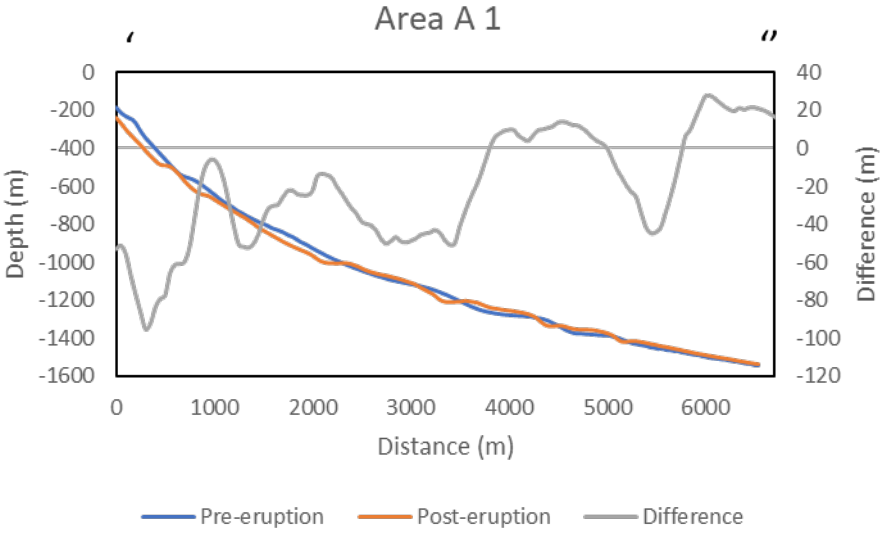
Area A 1
Depth (m)
Difference (m)
Distance (m)
Pre-eruption
Post-eruption
Difference

Figure 4.2: A) Difference map of area A, B) Slope map of pre and post-eruption of area A, C) Profile of large-scale scour on area A

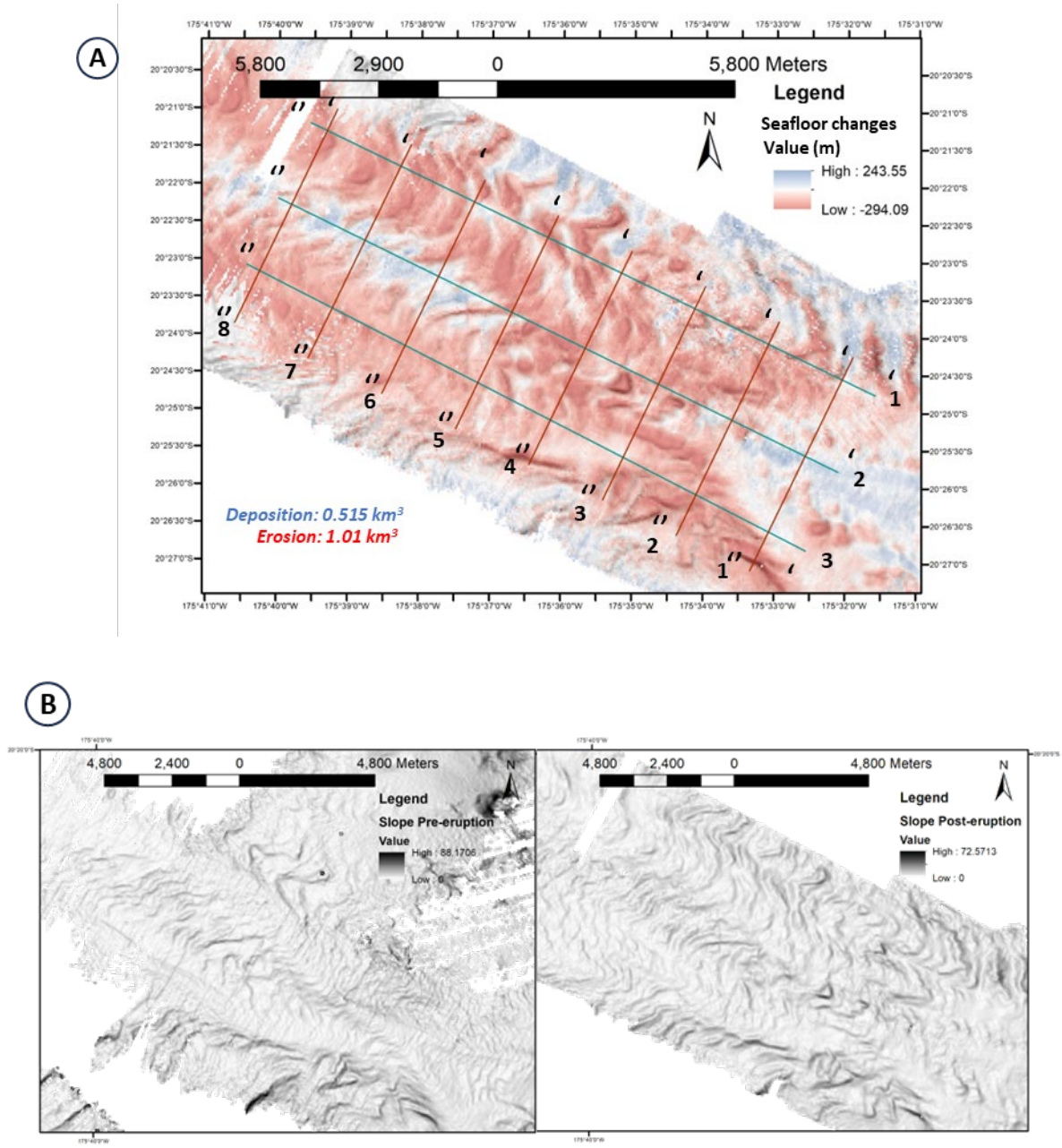

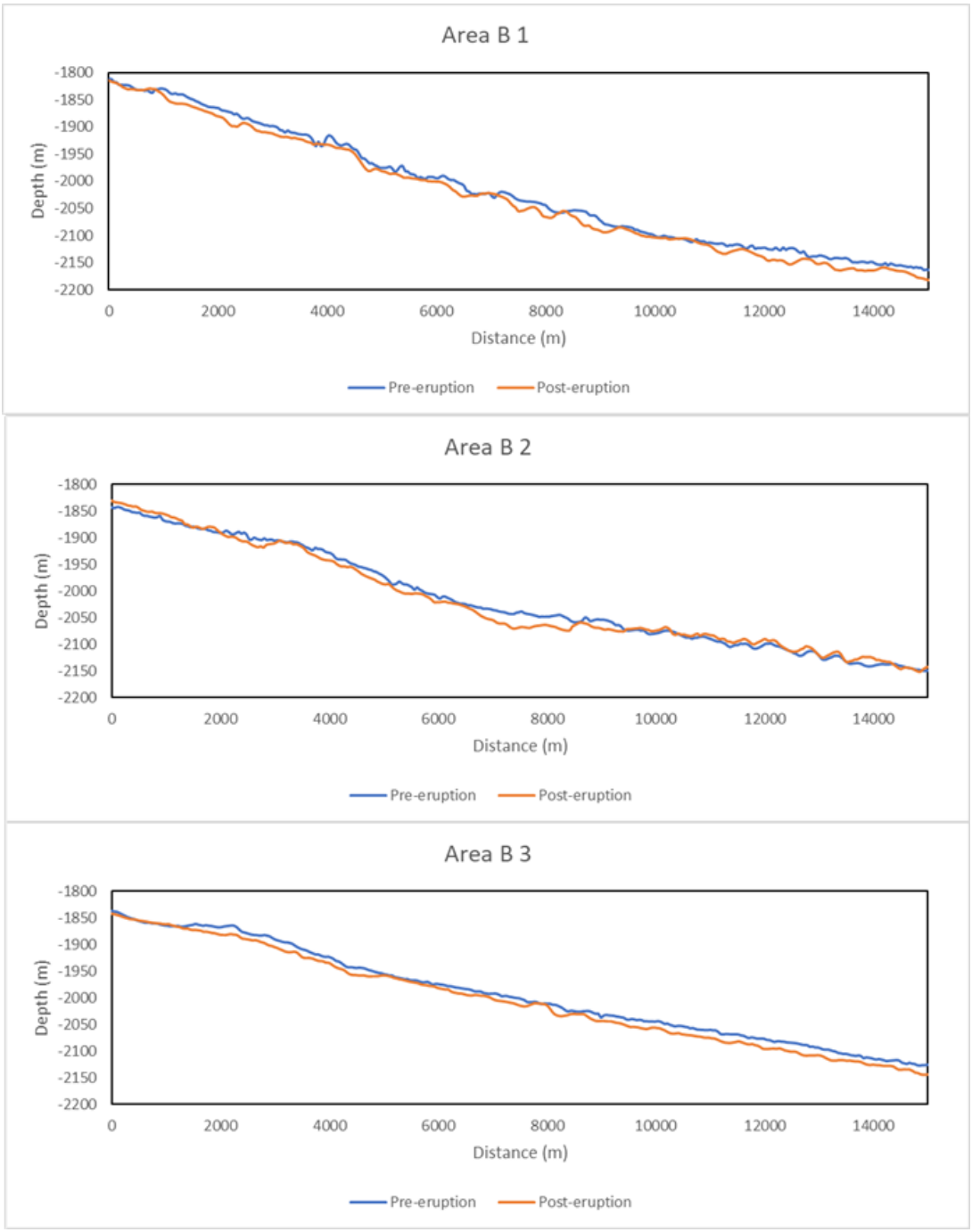

Figure 4.3: A) Difference map of area B, B) Slope map of pre and post-eruption of area b, c) Profile of large-scale scour on area B

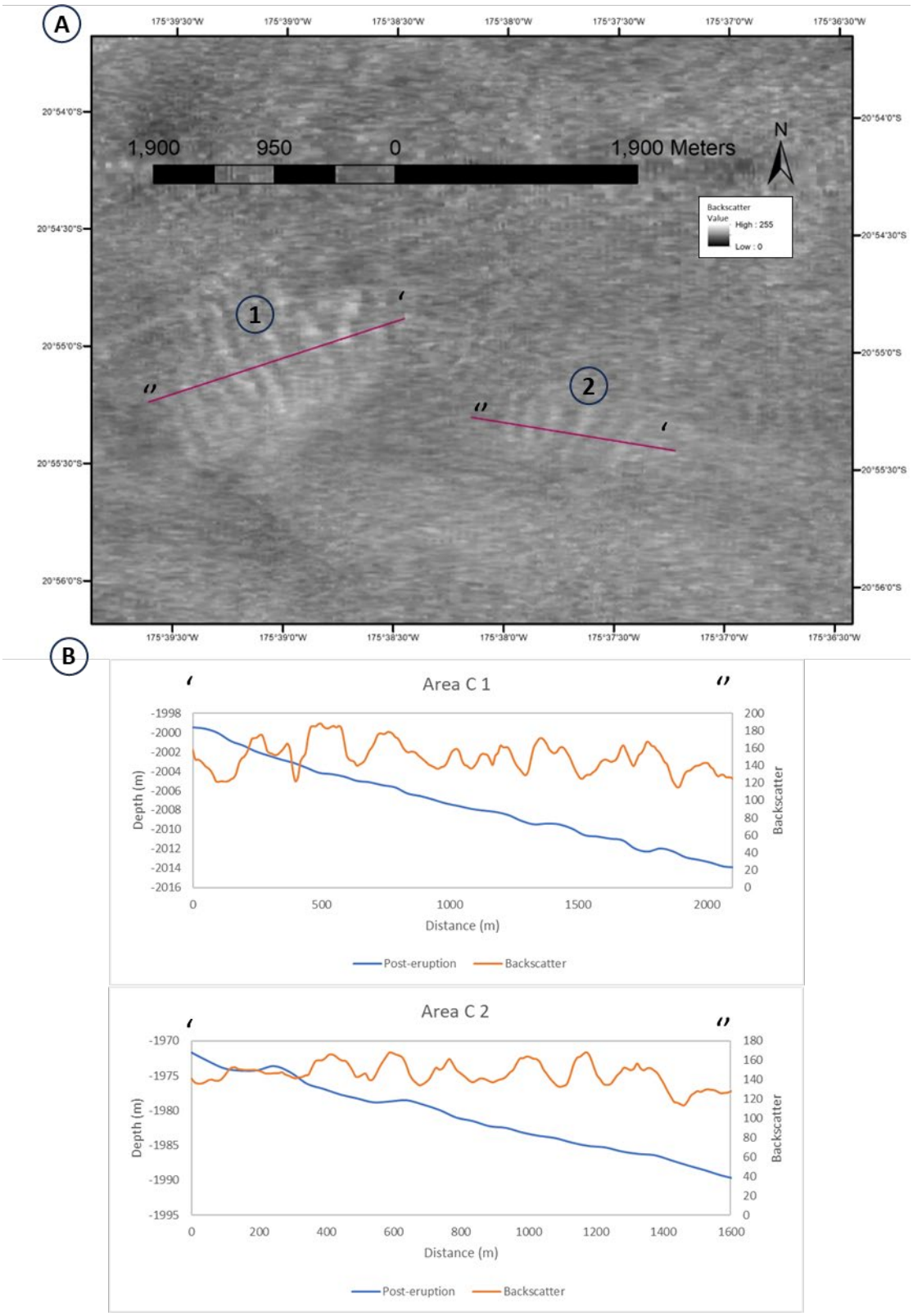

Figure 4.4: A) Backscatter image of area C, B) Profile of small-scale bedform of area C

Based on the different seafloor features and changes that are observed, the study area is divided into three distinct regions: A) a proximal zone that is characterised by linear gullies, large crescentic scours and depositional lobes on the steep volcano flanks; B) a medial zone that lies

16 km to the north-west of the volcano that includes the crescentic bedform fields; and C) a more distal zone that lies 40 km from the volcano that features the dune-scale bedforms (Fig.4.1B). The emphasis of this study lies in understanding the variations in bedforms between these areas.

4.4.2 Various scales of bedforms created around Hunga Volcano

In unravelling the genesis of bedforms surrounding the volcano, an analysis of the bedform dimensions becomes imperative. Drawing inspiration from a global study of submarine bedforms conducted by Symons et al. (2016) and updated to focus on those on volcanic flanks by Pope et al. (2018), the dimensions of bedforms on a wavelength and wave height log plot was plotted (Fig4.5A). Previous work by those authors indicated that bedforms typically fall into two distinct clusters. We observe three different types of bedforms.

Numerous profiles were selected in each designated area to ascertain the wavelength and wave height of the bedforms. The wavelength, measured from trough to trough, and the wave height, gauged from the maximum relief of the slope, were key metrics in this endeavour. The resultant wavelength and wave height log plot also incorporates data from Pope et al., 2018. and Karstens et al 2023. Data from these studies allow the measurement in this study to be compared with other bedforms in different volcanic systems.

Insights gleaned from this analysis facilitated the successful differentiation and categorisation of bedforms within three distinct areas, classifying them into three specific groups. Bedforms in Area A manifested as scours ranging from 19 to 56 metres in wave height and 628 to 2485 metres in wavelength. In contrast, bedforms in Area B exhibited a wavelength and wave height spanning 7 to 41 meters and 362 to 2577 metres, respectively. Notably, bedforms in Area C were characterised by smaller dimensions, featuring wavelengths between 0.2 to 1.9 metres and wave heights ranging from 109 to 522 metres. The data show that Area C predominantly housed diminutive bedforms, reaching just under 2 meters in wave height (Fig 4.5B), in stark contrast to the more substantial bedforms present in both Area A and Area B. Most bedforms in Area A exhibited higher wave heights than those in Area B, and both areas shared bedforms with relatively extensive wavelengths. Area A comprises several substantial scours along the slope, each reaching depths of tens of meters. In contrast, areas B and C assume undulating waveforms, with Area B's waves tens of meters in height, while those in Area C measure less than 2 meters in height (Fig 4.5B).

Building upon these findings and drawing parallels with Symons et al. 2016's plot, the classification of bedforms in each area emerges. Area A is identified as hosting large-scale scours, Area B as accommodating large-scale bedforms, and Area C as housing small-scale bedforms. The comparison with the earlier study reveals that the plot of small-scale bedforms in

our data appears comparatively diminutive in weight compared to other locales. This discrepancy may be attributed to the geographical distance of Area C from the volcano. Due to this distance, it is questionable if these bedforms were to be attributed to the major eruption. But one crucial detail linking this bedform with the major eruption is its close proximity to a damaged seafloor cable due to the volcanic eruption. With the classification of bedforms in each area accomplished, we can now extrapolate insights into the dimensions of these bedforms and decipher the processes shaping their formation.

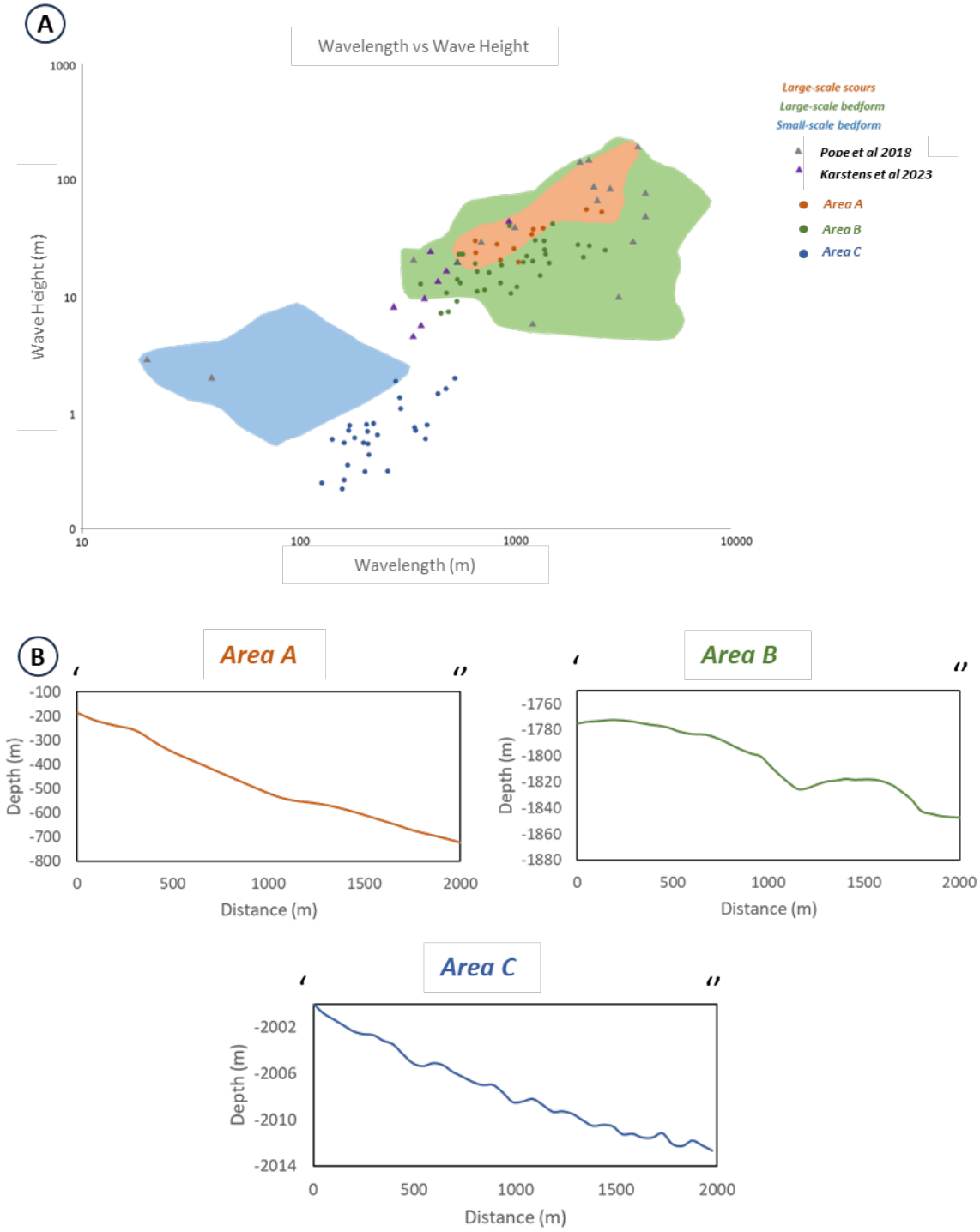

Figure 4.5: A) the bedform's wavelength and wave height log plot around the study area and other volcanos from similar plots of Pope et al. 2018 and Karstens et al. 2023 (Santorini). B) Profile of each bedform in areas A, B, and C

4.4.3 Volumetric change compared between proximal and medial zones

Beyond bedform identification, the maps reveal the extent of seafloor material erosion and deposition following the eruption. The study calculates the volume of eroded and deposited materials in areas A and B, while the lack of pre-eruption data precludes analysis in area C. Area A, chosen for its prominent bedform features in contrast to the opposites area of the caldera that is devoid of significant bedform features (Fig 4.2A), exhibited a deposited volume of 2.392 cubic kilometres and an eroded volume of 0.755 cubic kilometres. Area B demonstrated a deposited volume of 0.1151 cubic kilometres and an eroded volume of 1.01 cubic kilometres (Fig 4.3A). This reveals that the seafloor flows that emanated from the volcano began a phase of erosion after having been dominantly depositional as they travelled to the northwest limits of the study area on their way to deeper water in the Lau Basin. These findings underscore the dominance of depositional processes in Area A (76%) and the prevalence of erosion in Area B (87%).

4.4.4 Complex nature of seafloor change in Area B

4.4.4.1 What makes Area B complex?

Bedforms in Area A and Area C exhibit less complexity compared to those in Area B,. The large-scale scours in area A are easy to identify, and these scours are only located near the caldera. The processes in this area are also straightforward, where erosion dominates the slope near the caldera and gradually transitions to deposition (Fig 4.2C). Area C consists of relatively small bedforms, with their presence more discernible through the backscatter profile, and the pattern of these bedforms is rather simple (Fig 4.4A). Contrastingly, Area B appears more intricate than Areas A and C. The difference map depicts Area B's more chaotic bedform pattern (Fig 4.3A).

4.4.4.2 Reasons for Area B’s complexity

The complexity of Area B's bedforms is elucidated through a comprehensive profiling approach. Several profiles were plotted both longitudinally and transversely across the bedforms to decode their structure (Fig 4.3A). The analysis of three downslope profiles revealed an upslope migration pattern of the bedforms(Fig 4.3B). To further discern the post-eruption morphology, seven additional profiles that lie perpendicular to the downslope ones were examined for distinctive channelling features (Fig 4.6). This profile analysis was instrumental in tracing potential flow

paths, marked by alterations in the bedforms, sediment dynamics, and the impact of erosive flows. The data suggest that multiple flows may ingress at profile 1, bifurcating at profile 2, then converging and interweaving at profiles 3 and 4, only to diverge once more from profiles 5 to 8. Such flow dynamics are likely contributors to the pronounced erosion observed within this region (Fig 4.7). Another way to understand such flow dynamics would be by looking into samples of seafloor sediments by coring (Fig 4.8). Core samples from both areas B and C reveal that the pyroclastic materials deposited in Area B are much coarser (medium sand) than those in Area C (fine sand). Nevertheless, both cores exhibit complex stratigraphy, showing multiple pulses going through the bedforms. From this, it can be seen that areas B and C undergo similar multiple flows, but the difference is in the amount of density flow deposited in the area. This could also mean that the amount of pyroclastic materials going through area C is lesser than in B. The core sample analysis revealed a variance in the deposition of pyroclastic materials between Areas B and C, with Area B bearing the brunt of denser flows. This disparity in sediment deposition underscores the differential impact of eruptive activities across the landscape.

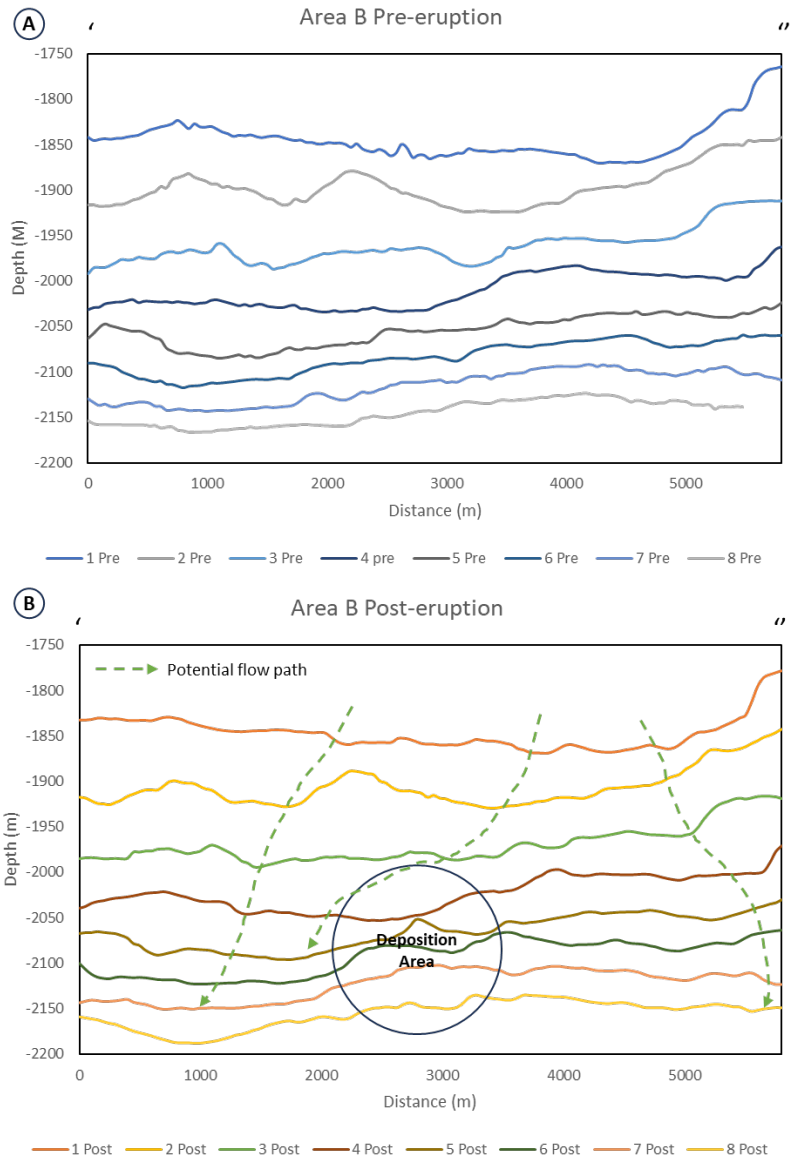

Figure 4.6: A) Pre-eruption profile along the bedform of area B, B) Post-eruption profile along the bedforms of area B

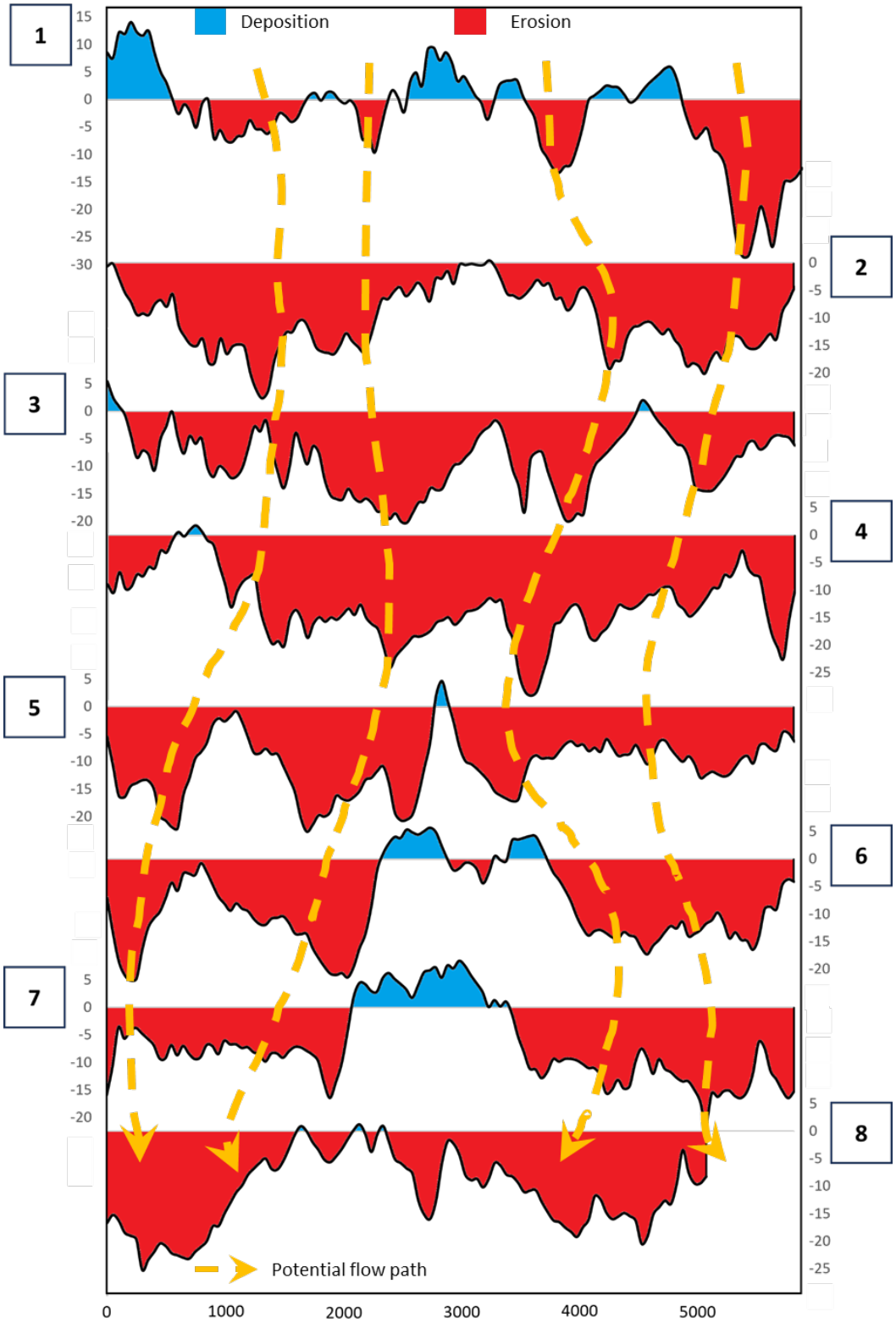

Figure 4.7: Potential flow path plot base on the deposition and erosion profile along the bedform of area B

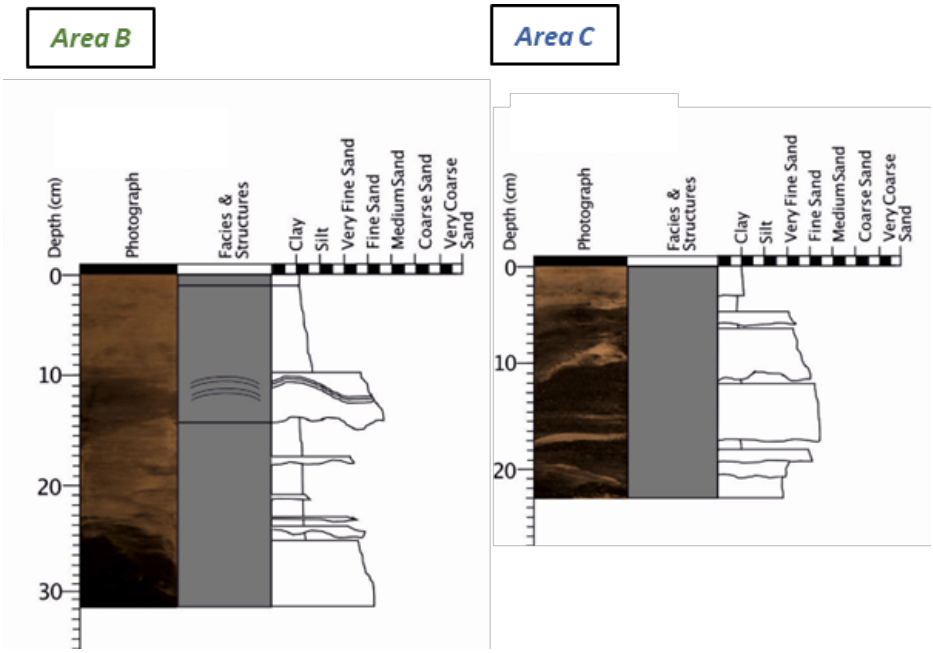

Figure 4.8: Core sample acquired in area B and C.

4.5 Discussion

4.5.1 Origin of submarine bedforms around Hunga Volcano

Having categorized the bedforms in three distinct areas based on their wavelength and wave height characteristics, we can now delve into the potential processes underlying their formation. Area A is identified as a large-scale scour, distinguished by its pronounced negative relief in comparison to other regions (Symons et al., 2016). This bedform originates at arcuate headwalls, displaying lateral confinement on the upper slope with significantly elevated values of wavelength and wave height (Leat et al., 2010). Widely observed, this bedform radiates from a caldera, showcasing distinct upper headscars that suggest a genesis linked to landslides (Pope et al., 2018). However, the absence of detailed seismic data poses a challenge in comprehending the formation process, exacerbated by the lack of internal layering (Lee et al., 2002). Massive deposition post-bedform termination further implicates a landslide origin in this area.

In Area B, the bedform is categorized as large sediment waves, and it is postulated that these bedforms arise from the interaction of turbidity currents with preexisting irregular topography, particularly the bedforms pre-eruption, thus amplifying the existing terrain (Cattaneo et al., 2004; Ercilla et al., 2002). These large sediment waves are also interpreted as supercritical flow bedforms (Cartigny et al., 2014; Kostic, 2014; Zhong et al., 2015). The interplay of erosion and deposition over a cyclic step in supercritical flow with sufficiently high shear stresses is posited as the mechanism behind the formation of this bedform (Symons et al., 2016).

Another potential cause for this bedform could be active bottom currents (Fuhrmann et al, 2020). When these currents run into obstructions, they can remodel the seabed sediments, producing drifts, moats, and sediment waves (Pandolpho, 2023). Very large subaqueous sediment waves with substantial dimensions, such as wavelengths of 1.4-2 km and wave heights of 30-50 m, have been found to be produced by the interaction between internal solitary waves and along-slope bottom currents (Chen et al., 2017). Furthermore, when strong, continuous currents meet with huge, long-period waves, the depth of bed reworking and sediment transport rates are most noticeable (Wilberg et al., 1996). However, the datasets did not provide any clear indications of the presence of active bottom current around the volcano. Due to the major eruption that triggers strong density flow, this is thought to be the most likely cause.

In contrast, bedforms in Area C are classified as small-scale, and their origin is attributed to the migration of cyclic steps from a supercritical flow (Symons et al., 2016). Density Flow being the driving factor for its formation, its location further away from the caldera decreases bedform wavelength and wave height (Leat et al., 2010). From this classification, it is evident that the bedform in Area A finds its genesis in the collapse of the caldera, while those in Areas B and C are influenced by eruption-fed density flow. This nuanced understanding sheds light on the diverse processes shaping these bedforms in different areas surrounding the volcano.

The extensive scouring observed near the eruption source is likely a result of the rapid collapse of the eruption column, leading to the expulsion of substantial eroded materials from the steep caldera sides(Clare et al., 2023). This process results in the significant deposition of sediment as the slope angle decreases downstream of the bedform suggesting that the flow generated from the collapse is a dense granular flow with high basal friction (Clare et al., 2023; Iverson, 1997; Major, 1997).

The powerful, high-density flow, with its pronounced erosive effect, is probably attributed to the steep slope of the collapsed volcanic column (Clare et al., 2023). This formidable flow continues its course towards areas B and C. In the case of area B, the upstream migration of bedforms indicates the presence of supercritical flow undergoing a series of hydraulic jumps (Cartigny et al., 2014; Clare et al., 2023; Symons et al., 2016). While the bedform in area C cannot be conclusively identified as an upslope migrating bedform due to the absence of pre-eruption data, it likely results from cyclic-step migration caused by density flows (Symons et al., 2016).

Bedforms in Area A manifest as slopes ranging from 3 to 16 degrees, with a water depth of 0.6 to 1.5 kilometres, extending approximately 0 to 10 kilometres around the caldera. Area B exhibits slopes between 0.6 to 6 degrees, a water depth of 1.7 to 2.2 kilometres, and is situated around 16 to 38 kilometres from the caldera. Area C features slopes between 0.4 to 2 degrees, a water depth exceeding 1.8 kilometres, and is located at a distance greater than 40 kilometres from the caldera

(Fig 4.9). The flow going through areas B and C may not be the same continuous flow due to the location and orientation differences. The flow still needs to travel further and at different slope angles.

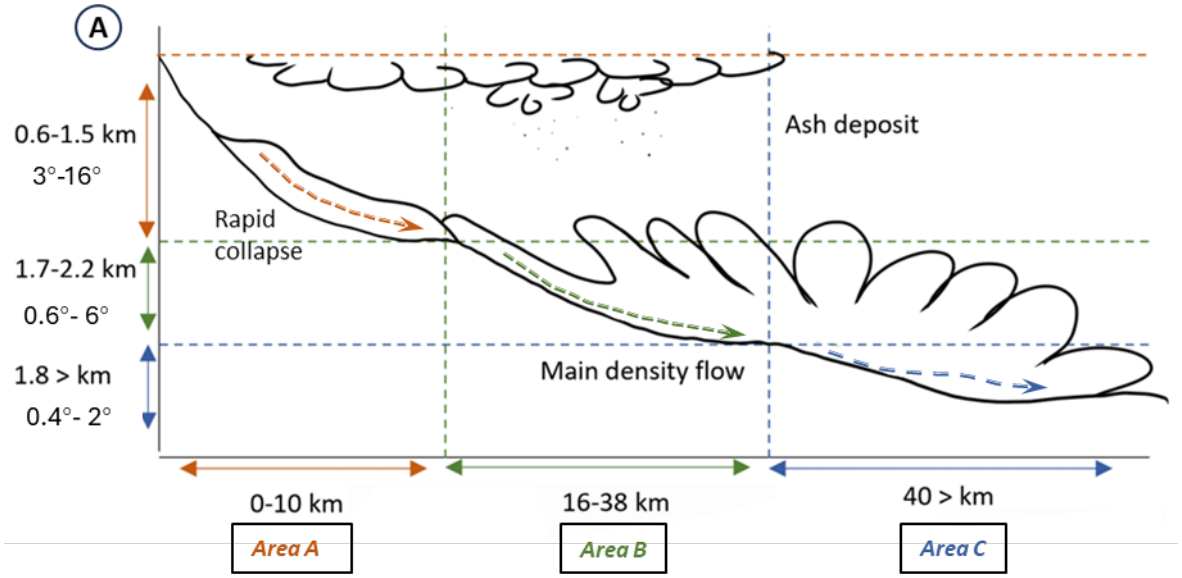

Figure 4.9: Illustration of how volcanic activity moves with depth and distance

4.5.2 Flow pathway and evolution of density currents resulting from Hunga Volcano eruption.

The density flow significantly shaped the seafloor morphology in both bedform areas B and C, which must traverse distinct paths due to their geographical locations. Area C, situated in the southwest part of the caldera, requires a flow moving in a different direction than Area B, located in the northwest. Figure 4.10A shows maps of the study area, illustrating potential flow pathways towards areas B and C. Additionally, 3D imagery showcases the topography around these areas facing the caldera (Fig 4.10B).

Upon closer examination of the surrounding topography, it becomes apparent that Area B is positioned between two seamounts, forming a natural funnel for the flow passing through the area, and the caldera exhibits a distinctive erosion scour directed towards Area B, suggesting that this region experienced a more potent or larger magnitude of density flow (Seabrook et al., 2023). In contrast, Area C not only resides at a greater distance from the caldera but also has a mountain obstructing its path. This obstruction diminishes the channelling effect of the flow, resulting in a significantly reduced flow magnitude. While flow redirection might occur, it will likely lead to a reduction in power or the termination of flow altogether. Another aspect to consider when stating that the flow may have undergone redirection, is that the two bedforms in Area c have a slight difference in orientation while having similar wavelength and wave height. Although it is not certain, it is possible that the two bedforms are the result of flow that comes in at different

detections or the results of a combination of flows with a similar magnitude but from different directions.

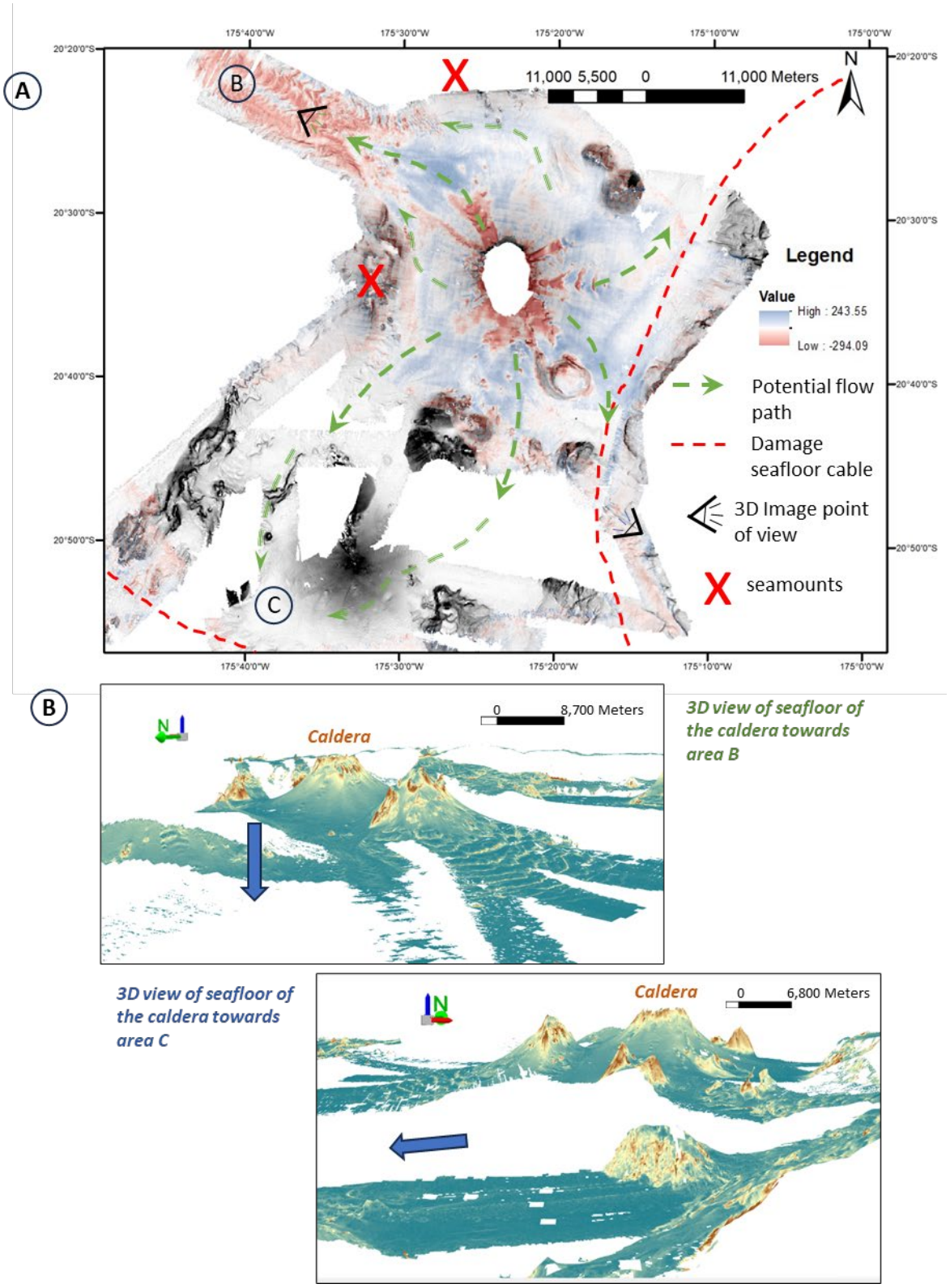

Figure 4.10: A) Illustration of flow movement throughout the seafloor topography; B) 3D view of the seafloor surrounding the caldera.

Another aspect to consider would be the complexity of the bedform in area B. As stated before, area B is dominated by the erosion process compared to the others. As analysed before, the

cross-cutting of the channel and the merging and separating of the flow path in area B could be one of the reasons for this to happen. Consequently, seafloor morphology is crucial in comprehending flow pathways and magnitudes. Other studies have also looked into the potential flow pathways from this eruption (Clare et al., 2023; Seabrook et al., 2023). However, this study not only considers the role of topography as a guide for the flow direction but also includes an analysis of bedform morphology (shape, size, and orientation) to give a more detailed prediction.

4.5.3 Potential Hazard and Mitigation

The eruption under investigation unleashed a multitude of hazards, both immediate and indirect, with global implications. The transoceanic tsunami it triggered, as documented by Carvajal et al. (2022), has had far-reaching consequences beyond the Pacific basin. The event also gave rise to destructive planetary meteotsunami waves, as highlighted by Denamiel et al. (2023), emphasising its catastrophic nature. While the bedforms on the seafloor studied here may not obviously pose a major hazard, the processes involved in their formation, particularly density flows, can have a significant impact. This was evident in the breaking of a seafloor cable near Area C, which featured small-scale bedforms, a clear indication of the formidable force exerted by density flows during the eruption. This was the only international telecommunications cable to connect to the Kingdom of Tonga. When it was damaged, Tonga lost internet connections at a critical time for disaster response and were only re-connected 5 weeks afterwards (Clare et al., 2023).

A holistic approach to hazard mitigation is imperative to prevent losses from submarine cable breaks, which should include an understanding of seafloor change, the drivers and controls on the different hazards, and developing backup strategies if damage occurs. The initial step entails surveying the surrounding area to identify an appropriate route corridor. This study highlights the value of repeated seafloor surveys to monitor volcanic activity and growth, as proposed by Caress et al. (2012). By intensifying seafloor mapping through repeat surveys, a comprehensive understanding of the volcanic arc can be garnered to inform cable routing decisions. Moreover, attention should be directed towards avoiding regions with prominent bedforms, as they may indicate potential density flow pathways during major eruptions. Additionally, establishing robust eruption warning systems for civilian populations is paramount to safeguarding lives and minimising the impact of future events. Regional seismo-acoustic monitoring of volcanic activity and associated hazards, such as seismicity and slope failure, holds promise in providing advanced warning of eruptions, akin to the 2022 event, and delineating safe zones for post-eruption resettlement efforts. These crucial mitigation measures, when implemented, offer a comprehensive framework for mitigating the risks posed by submarine volcanic eruptions and their aftermath. In terms of providing resilience in the instance of any damage to cables, it is

important to recognise that the extent of damage can be vast (10s-100s of km). Therefore, holding sufficiently long spare sections of cable in stock will assist in ensuring repairs can be done quickly. Access to backup communications, such as low level satellites or microwave connections will ensure that communications cam continue if a break happens, albeit at a lower capacity. The main recommendation is to ensure that any island has diverse connections, such that if one is damaged then others may survive to keep communications traffic running.

4.6 Conclusions

Conducting a seafloor survey of the Hunga Volcano revealed three distinctive bedform features in the surrounding environment, each uniquely classified by their dimensions—specifically, wavelength and wave height. These bedforms include large-scale scour characterised by high wave height and wavelength (19-56 meters, 628-2485 meters), large-scale bedform with a high wavelength and somewhat lower wave height (ranging from 362 to 2577 meters and 7 to 41 meters, respectively), and small-scale bedform with a wavelength of 109 to 522 meters and a wave height of 0.2 to 1.9 meters.

These bedforms are distributed across different parts of the seafloor, suggesting distinct processes influencing their origin. Bedform type A, located in close proximity to the caldera, was largely influenced by the collapse of the erupted column. In contrast, bedforms B and C undergo significant reshaping due to the impact of supercritical flow and cyclic steps as the highly dense flow travels from the caldera to the bedform area. This study emphasises the important role of bedform morphology (size, shape, and orientation) in understanding how a major eruption operates and provides new insights that may inform the assessment of volcanic flow pathways that can help in hazards assessment and mitigation.

The study further emphasises the role of seafloor topography in influencing density flow movement and magnitude. Notably, despite both areas B and C experiencing flows generated by the same eruption, differences in seafloor topography result in variations in flow power between the two areas.

Additionally, the research reveals that a single eruption can produce diverse magnitudes of collapse (landslides) and density flows, contributing to a more varied seafloor morphology, particularly in forming bedforms around the volcano. The study also tries to show that small-scale bedforms are worth studying when looking into the activity of a major eruption. The lack of datasets that look into such bedforms, particularly in the case of volcanic environments, is very prevalent. Although the study faces limitations due to data gaps, a more comprehensive investigation with robust datasets, including the addition of seismic imagery, can provide

deeper insights into how massive eruptions reshape the seafloor within a specific environment, such as the Hunga Volcano

Chapter 5 Conclusion

This thesis has focused on understanding the drivers and rate of change to the seafloor that resulted from three distinct phenomena, which also pose a potential hazard to coastal communities and/or seafloor infrastructure: i) submarine channel evolution through knickpoint migration and meander bend growth at Knight Inlet; ii) delta slope failure at Squamish Prodelta; and iii) volcaniclastic density currents created by the collapse of the eruption column into the ocean at Hunga Volcano.

The central theme of this thesis has revolved around understanding the role of sediment transport and the hazards associated with these processes by assessing their magnitude, geometry, rate, and timing. To achieve this overarching objective, the three study areas were examined utilising repeated multibeam bathymetry datasets, with a comparative analysis between pre- and post-hazard conditions. While such datasets have been rare in the past, there has been a marked growth in the acquisition of such data, providing new insights into a wide range of processes. The hazards identified in this these span a wide spatial and temporal spectrum, ranging from events that recur on the order of centuries, such as major explosive volcanic eruptions that enter the ocean (Hunga Volcano), to those forming within decadal scales as exemplified by knickpoint migration and channel meandering that would alter seafloor morphology resulting in potential seafloor infrastructure being damaged (Knight Inlet), to delta slope failure (Squamish Pro Delta) that can recur on an approximately monthly basis (during summer), and upstream-migrating bedforms (Squamish Prodelta) that can migrate on daily or more frequent basis. Clearly, assessing the timescales of recurrence (and hence associated seafloor change) requires appropriately timed repeat seafloor surveys. More frequent surveys often reveal previously unrecognised seafloor change, demonstrating the value of such datasets. The diversity of the processes leading to hazards and their occurrences are schematically illustrated in Figure 5.1, each of which has markedly different impacts on the seafloor and poses differing magnitudes of hazard. Throughout the thesis, specific attention has been given to different environments, creating a nuanced and varied perspective on submarine geohazards. It is recognised that this does not represent a truly comprehensive view of all submarine environments; however, the processes observed at the study sites are seen in many other sites across varying scales and settings, from lakes to fjords, open ocean continental slopes and volcanic islands worldwide.

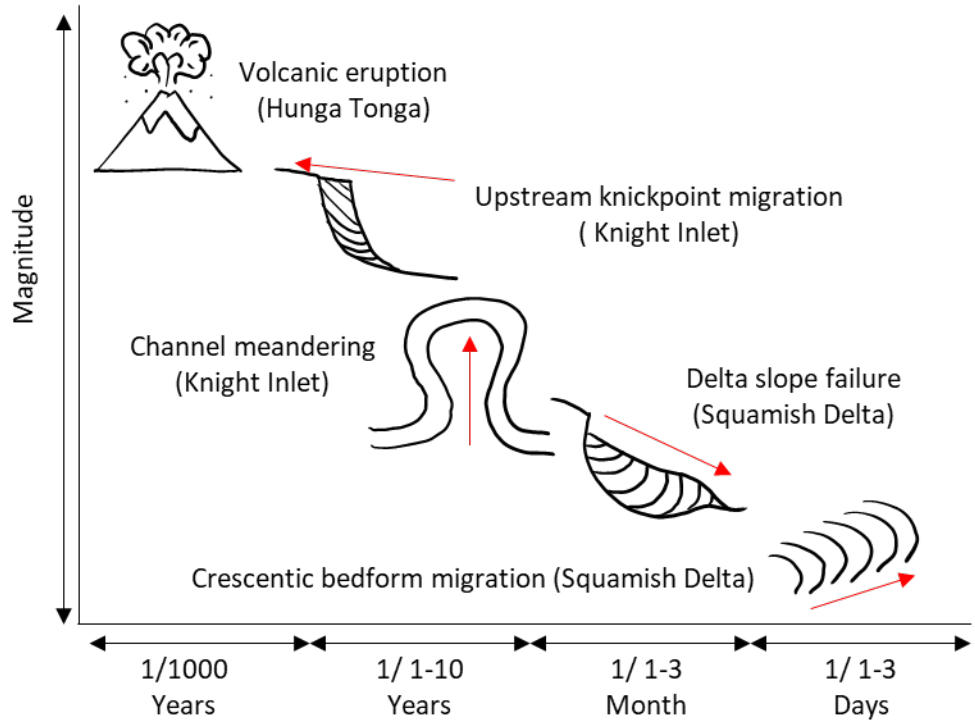

Figure 5.1: Plot of relative magnitude of seafloor change vs time of different process of submarine geohazards addressed in this thesis.

Each chapter of this thesis has delved into a specific aspect of these processes. In Chapter 2, the role of channel morphology in influencing submarine channel evolution was identified. Chapter 3 explored the triggering factors of delta slope failure, elucidating multiple conditions leading to failures of varying magnitudes and locations. Finally, Chapter 4 examined seafloor changes following a massive volcanic eruption, focusing on diverse sediment waves surrounding the volcano and their implications for volcanic activities. A common thread across these studies is the pivotal role of sediment displacement and its controlling factors. Chapter 2 highlighted how channel sinuosity is the dominant control of erosion modes within the channel. Chapter 3 revealed the influence of river input on sediment deposition and other processes that modify subsurface pore pressure on delta slope failure. Chapter 4 analysed the effects of volcaniclastic density flows resulting from a massive eruption on the surrounding seafloor, leading to large eroded scour and the formation of diverse bedforms across varying scales that are a function of the initial flow, but also affected by local seafloor relief. This thesis contributes to a wider understanding of the process leading to submarine geohazards, emphasising the importance of sediment dynamics as revealed by seafloor changes under the influence of various geological phenomena.

5.1 Answering the initial science questions

This section revisits the initial science questions posed in Chapter 1 and suggests future directions for research based on each of the related science chapters. These sections also touch on the aim of the thesis, which is to understand how the seafloor evolves in different submarine environments in the cases of Knight Inlet, Squamish Pro-delta, and Honga Volcano. This section also touches on the Implications of interpreting past sediment transport events from the seafloor and depositional archives. The other thesis's aim, which is to understand the implications for seafloor and coastal infrastructure, will be discussed in the next section.

5.1.1 Which are the processes that control the erosion and morphological evolution of submarine channels and why do they vary along their course?

Chapter 2 examined changes in elevation within a submarine channel in Knight Inlet, British Columbia, over a 13-year period through repeat seafloor surveys. These surveys provided valuable insights into the dynamic nature of the channel's morphological evolution. Upstream migrating crescentic bedforms play a significant role on the steep prodelta slope, indicating their importance in the evolution of this specific region. Upstream-migrating knickpoints account for a substantial (77%) of observed erosion in the rest of the channel system and appear to be the dominant agent for erosion, surpassing the effects of outer bend erosion that is more commonly observed in subaerial fluvial channels. However, different reaches of the channel are affected to varying degrees by these different processes, with upstream-migrating knickpoints that focus erosion within the channel axis dominating in some locations and outer bend erosion more prevalent in others. Tight channel bends are the locations that tend to experience outer bend erosion and meander expansion, while broader bends and straighter sections are characterised by knickpoint migration that is focused on the channel axis. This leads to a novel finding, which is the strong influence of channel curvature on process dominance and migration rates. Tight bends are dominated by outer bend erosion, which is attributed to enhanced centrifugal acceleration. In contrast, broader bends and straighter sections, where knickpoints cutting deep into the channel axis, migrate at a much faster rate compared to outer bend erosion. Despite the apparent dominance of knickpoints in sculpting the channel over decadal timescales, Chapter 2 suggests that their depositional signature is likely to be less well preserved in the rock record compared to outer bend erosion. This insight indicates that previous studies may have underestimated the role of knickpoints in channel cut, maintenance, and fill. This calls for a re-evaluation of the role of knickpoints in shaping submarine channels. There is a need to reconsider the impact of knickpoints on channel morphology and to re-examine the rock record to look for features diagnostic of their influence. Local channel morphology can play an important role in dictating

which process dominates erosion and can influence the evolution of differing reaches of the same system. Future studies: Future research is required to deepen the understanding of submarine channel dynamics, specifically focusing on the role of channel curvature in different geological and environmental contexts, as Chapter 2 focused on one setting only – a seasonally active river-fed channel system in a fjord. There is value in conducting comparative studies, extending the investigation to diverse submarine channels worldwide and incorporating sediment record analysis for a comprehensive examination of the underlying processes (Jobe et al., 2020). By examining the interplay between channel curvature, dominant processes, and migration rates, there is an opportunity to gain valuable insights into the variability of these dynamics. This approach facilitates the exploration of how channel curvature influences processes, offering a nuanced perspective on the extent of its impact. The comparative analysis can be expanded beyond similar fjord channel systems to encompass more open and deeper systems. Such an example could be the Indus Fan channel system, which represents one of the largest deep-sea fans on the planet and that has abundant meandering channels (Salmanidou et al., 2019). Figure 5.2 shows a bathymetry map of a meandering channel in the Indus Fan.

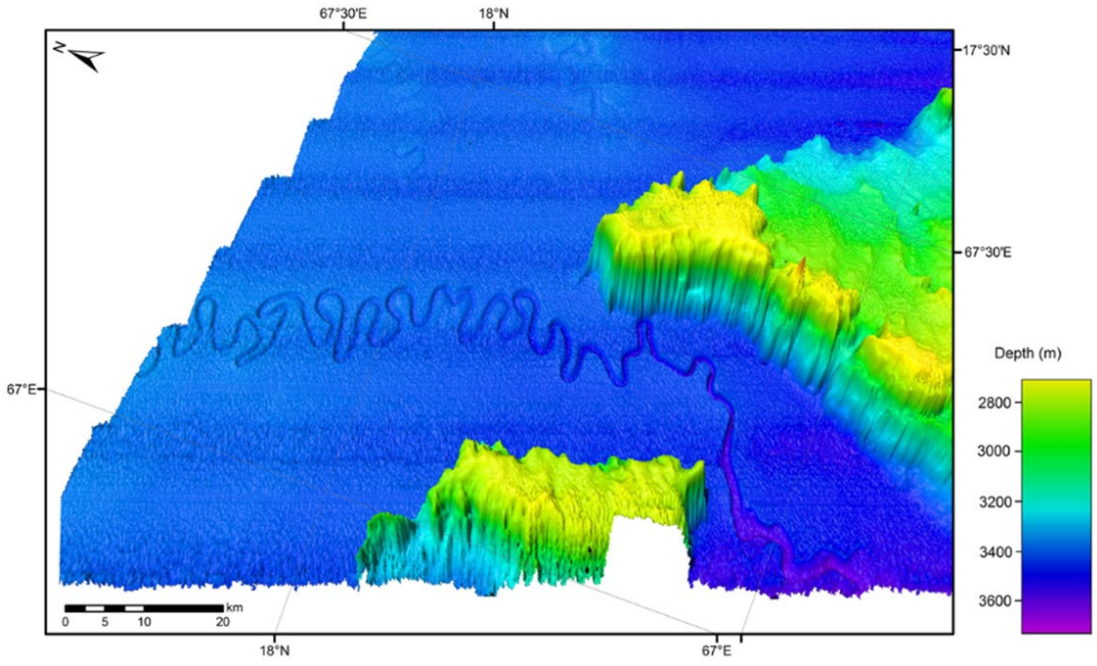

Figure 5.2: bathymetry map of one of the channel in the Indus Fan from (Mishra et al., 2016) showing highly developed meandering submarine channel at high depth, making this area verry different then knight inlet, thus an analysis of channel curvature and its effect of the dominating process might produce an interesting comparison with Knight inlet.

An intriguing aspect of future research involves examining the influence of channel curvature on processes around bends. This exploration seeks to determine the extent to which channel

curvature affects the dynamics of submarine channels—whether it exerts a substantial impact or has negligible consequences. This investigation promises valuable insights into the nuanced relationship between channel curvature and channel evolution. To enhance the understanding of processes within the channel, future research should consider incorporating sediment record analysis, such as through analysis of high-resolution, subsurface geophysical data. This approach would enable a detailed examination of the channel stratigraphic geometries, providing a longer-term perspective on the evolution of these submarine systems. Sediment record analysis will add a further layer of depth to the study, offering crucial information on the processes that shape the channel over time (Covault et al., 2016; Jobe et al., 2016). The proposed future research directions aim to advance The comprehension of submarine channel dynamics by exploring the role of channel curvature in diverse settings. Conducting comparative studies and incorporating sediment record analysis will contribute to a more holistic understanding of the factors influencing submarine channel evolution, with potential implications for geological and environmental research.

5.1.2 Which processes control the collapse of submarine delta slopes?

The investigation into slope failures in the Squamish Prodelta, as detailed in Chapter 3, has yielded new insights into the timing, locations, and underlying causes of these events based on 93 repeat seafloor surveys on the frequency of every weekday. The dynamic nature of the delta was pronounced by the occurrence of five notable slope failures, each characterised by distinct features and behaviours. Chapter 3 specifically delved into key factors, such as river flow, tide levels, delta growth, and slope stability, aiming to unravel the complexities behind these failures. One key finding was that peak river discharge generally coincided with major slope failures, suggesting that sediment loading during high river flow played a crucial role. Low tide levels, especially during the earlier failure, were identified as potential triggers for slope failure but did not fully explain all failures. The cyclical pattern of delta progradation also provided insights into the interconnected dynamics of delta morphology and slope stability. The study also highlighted the role of crescentic bedforms in these failures, emphasising their impact on both small-scale and large-scale landslides. From these observations, we conclude that slope failures in the Squamish Delta seem to result from a mix of factors, including enhanced slope growth due to delta progradation, changes in pore pressure from sediment loading and tides, and the influence of small-scale features like crescentic bedforms. Understanding these interconnected factors is crucial for managing and studying slope failures in deltaic environments. These findings contribute to a broader framework for assessing and addressing slope instability, providing valuable insights for future research and mitigation strategies in similar areas.

Future studies: Future research aimed at advancing the understanding of slope failure dynamics in deltaic systems. The proposed investigations involve conducting comparative studies with diverse deltaic environments and employing dynamic computational modelling to simulate bedform migration and its impact on slope stability.

To gain insights into the commonalities and differences in slope failure dynamics across various deltaic environments, an extension of the study to other deltaic systems with distinct geological settings and environmental conditions would be useful. Such surveys will need to be performed at an appropriate frequency to capture the dynamic seafloor changes. This entails more comprehensive daily surveys in different river delta systems, providing a comparative basis for understanding the nuanced factors influencing slope failure dynamics. As such surveys may need to be acquired at highly rapid (e.g. daily intervals), there may be a benefit in applying autonomous technologies, such as Autonomous Underwater Vehicles (AUVs) that can be programmed for regular repeat surveys (Zheng et al., 2017).

Developing dynamic models to simulate the migration of bedforms and assess their influence on slope stability is also crucial for advancing the understanding of deltaic slope failures. Such models should involve numerical simulations incorporating key parameters such as bedform shape, migration rate, and sediment characteristics. By using dynamic modelling, researchers can explore the intricate relationships between migrating bedforms and slope failure, unveiling how small changes within the slope contribute to larger-scale failures. Building upon the current study's findings, future research should delve into the influence of different dimensions of migrating bedforms on the magnitude and geometry of delta slope failures. This entails investigating how variations in bedform size and shape contribute to the overall stability or vulnerability of the delta slope. Such an exploration promises to uncover critical insights into the specific factors that drive slope failure dynamics in deltaic environments. The proposed future research directions aim to enhance the understanding of slope failure dynamics in deltaic systems through comparative studies and dynamic modelling. By expanding the scope of the study to diverse deltaic environments and exploring the influence of bedform dimensions, researchers can contribute valuable knowledge to the field of geomorphology and slope stability in deltaic settings.

The role of subsurface pore pressure is increasingly recognised as a dominant control on slope stability, yet this is rarely monitored in the field (e.g. Sultan et al., 2020). Advances in field-scale monitoring would provide helpful calibration of numerical models and constraints on hypotheses based on repeat surveys.

5.1.3 What does bedform migration reveal about large volcanic eruptions?

Chapter 4 represents a study that focuses on seafloor change around the edifice of Hunga Volcano, Tonga, and further afield following the 2022 eruption. The results provide valuable insights into how a major volcanic eruption can have profound, yet locally variable, impacts on the seafloor environment, damaging seafloor infrastructure such as telecommunications cables and blanketing benthic communities. The research, conducted through analysis of bathymetric data from both pre-and post-eruption periods, reveals the diverse scales of bedforms that were shaped on the seafloor following the runout of fast-moving volcaniclastic density currents that travelled >100 km. The remarkable morphological changes observed after the eruption, which would not normally be observed due to a lack of repeat seafloor surveys that constrain a major ocean-entering eruption, underscore the magnitude of the volcanic event and the value of such repeat surveys. The focus of this study is specifically on sediment waves and bedforms that were categorised into three distinct types based on their dimensions: wavelength and wave height. The analysis of bedform dimensions in three designated areas around the volcano revealed the presence of large-scale scours, large sediment waves, and small-scale bedforms. The classification and comparison of these bedforms contribute to a deeper understanding of the underlying mechanisms shaping the seafloor environment. Furthermore, the study emphasises the significant role played by seafloor topography in influencing the movement and magnitude of density flows, even originating from the same eruption event. The origin of these bedforms is explored, with the large-scale scours likely resulting from vertical collapse of the eruption column onto steep slopes. In contrast, the large sediment waves are attributed to the interaction of turbidity currents with pre-existing irregular topography, while the small-scale bedforms likely represent the distal part of the flow as it decelerated. The chapter goes on to highlight the influence of seafloor topography on density flow pathways and magnitudes. The geographical locations of large sediment waves and small-scale bedforms, their proximity to the caldera, and the presence of natural obstacles shape distinct flow pathways, resulting in variations in flow power between the two areas. Chapter 4 contributes to the understanding of the impacts of the Hunga Volcano eruption on the seafloor environment, a uniquely documented eruption. By combining bathymetric data, classification of bedforms, and consideration of seafloor topography, the chapter provides a new perspective on the intricate processes governing the underwater landscape in the aftermath of a major volcanic event. While the study faces limitations due to data gaps in some locations, it lays the foundation for future investigations with more robust datasets, including seismic imagery, to further unravel the complexities of seafloor morphology following massive volcanic eruptions.

Future studies: The scope of this investigation can be extended through a more comprehensive comparative analysis with other submarine volcanoes, taking into account variations in

geological settings and eruption dynamics. The comparative methodology will likely reveal both commonalities and disparities in bedform development and seafloor reshaping processes, thereby providing a more expansive understanding of the repercussions of volcanic activities on underwater topography. It is important that the observational extent of the compared volcano mirrors the 40-kilometre radius of the caldera observed in the study. Investigation of sediment transport patterns shifts the focus of the comparative analysis beyond the identification of different bedform types to encompass a detailed examination of sediment transport patterns associated with the compared volcano. A meticulous exploration of sediment movement and deposition in response to volcanic activities holds the potential to yield valuable insights into broader geological processes, contributing substantively to a more holistic model of seafloor evolution within volcanic environments. Address the existing data gaps by incorporating high-resolution seismic imaging techniques in forthcoming surveys. The integration of subsurface seismic imagery is pivotal, as it affords a presently-missing view of subsurface structures, enabling researchers to visualise and interpret the internal architecture of the Subsurface (Laake et al., 2011; Metwalli et al., 2019). This augmentation promises not only to enhance overall data quality but also to significantly contribute to a more precise understanding of the geological processes governing the morphology of the submarine landscape.

5.2 Hazard and Mitigation

Each of the three scientific chapters delves into the potential hazards inherent in the processes occurring within distinct study areas. These hazards encompass a broad spectrum, ranging from the devastating coastal destruction caused by tsunamis resulting from major volcanic eruptions to the intricate and costly destruction of seafloor cables due to powerful density flows. Chapter 4, in particular, sheds light on the substantial impact of these hazards, contrasting with the comparatively less impactful or benign events observed in chapters 2 and 3. This discrepancy can be partially attributed to the relative absence of substantial seafloor infrastructure in the latter areas, which diminishes the immediate impact of the processes at play.

However, despite the varying degrees of impact, the findings from all three chapters hold significant value in the realm of hazard mitigation strategies. For instance, Chapter 2 presents a compelling argument for choosing loose bends as more suitable locations for seafloor infrastructure compared to tight bends, which are more susceptible to hazards. Furthermore, Chapter 3 gives a strong emphasis on the critical analysis of sediment supply to deltas, as this can serve as a crucial indicator of potential destabilisation and subsequent hazards. Additionally, an understanding of slope geometry, encompassing factors like delta slope progradation and the migration of bedforms, emerges as pivotal in evaluating and mitigating slope destabilisation risks.

Chapter 4 offers a deeper dive into the formidable power of density currents triggered by major volcanic eruptions, showcasing their potential to wreak havoc on seafloor features and infrastructure. Moreover, the chapter highlights how bedforms can act as essential indicators, delineating pathways for these powerful flows and aiding in hazard prediction and mitigation efforts.

While these scientific chapters contribute significantly to hazard mitigation knowledge, there remain areas that warrant further exploration and study. Continued research efforts, including repeated seafloor surveys, are essential to deepen the understanding of seafloor dynamics, refine hazard assessment methodologies, and develop more robust hazard mitigation strategies for the future.

5.3 Broader implications

The broader implications of the study extend beyond the specific geological phenomena investigated at Knight Inlet, Squamish Prodelta, and Hunga Volcano. The findings presented in each chapter contribute to a multifaceted understanding of submarine geohazards, particularly emphasising the crucial role of sediment dynamics in shaping the seafloor under the influence of various geological processes. The thesis provides an improved understanding of submarine geohazards by exploring three distinct phenomena: submarine channel evolution, delta slope failure, and volcanic eruption. This emphasis on sediment processes contributes to a more holistic comprehension of underwater geological hazards, as Allin et al. (2018), Jobe et al. (2018), and Urlaub et al. (2015) have shown the importance of understanding sedimentary processes when studying submarine geohazards, especially slope instability and density currents, as well as for the purpose of assessing seafloor hazards for seafloor infrastructure.

The study challenges and calls for a revaluation of previous assumptions in the field of submarine geology. For instance, in the context of submarine channel evolution (Chapter 2), the significance of knickpoints in channel cut, maintenance, and fill is highlighted, challenging previous studies that may have underestimated their role. This underscores the importance of continuously reassessing existing paradigms based on new empirical evidence. Recent studies also provide similar perspectives on the important knickpoint of submarine channel evolution (Allen et al., 2022; Chen et al., 2021; Heijnen et al., 2020). The findings have implications for geological studies, environmental management, and risk assessment in submarine environments, emphasising the need for an integrated and dynamic approach to studying and mitigating the impacts of geohazards on the seafloor.

This thesis has revealed the following key points:

- Local changes in seafloor morphology can fundamentally dictate the nature and style of erosion, for example, controlling whether erosion is focused within the channel (through knickpoint migration) or on the outer bends (e.g. meander bend growth). The controls can vary along the length of a single system, which has various implications for the routing of seafloor infrastructure such as cables.

- Slope failure of submerged slopes is dominantly controlled by sediment delivery; however, this can be complicated by many factors, such as tidally-modulated subsurface pore pressures and localised erosion that modifies the slope geometry. A detailed understanding of slope stability requires time-series observations of both the controls and the resultant seafloor morphology.

- A major ocean-entering volcanic eruption can result in diverse scales of seafloor change, some of which are very large and provide diagnostic links to the massive fluxes of sediment involved, while others are small and would not be obviously related to a large event if observed on their own without sufficient contextual data. Local seafloor relief can strongly steer and modify the nature of flows that can vary significantly as they move away from their point of origin.

- Repeat seafloor surveys performed in new settings at a frequency appropriate for the processes that are to be observed. In many parts of the world (e.g. the South Pacific Ocean), detailed maps of the seafloor are currently missing, so an important first step is acquiring these fundamental first of their kind data.

To address questions that have arisen through this thesis study, it is suggested that the following is undertaken:

- Acquisition of sub-surface geophysical data to better link the depositional architectures observed in ancient rock records with the changes observed from repeat seafloor surveys. Linking these datasets may be difficult, but proper planning on the survey may provide a good solution for both surveys that can be confidently linked together. For example, conducting a high-resolution shallow subsurface survey on a location that is known to have been passed by upstream knickpoint migration (Before reworking) can increase the likelihood of the process being recorded in the subsurface.

- Analysis of depositional records acquired from sediment coring that provide a longer term understanding of the drivers on seafloor evolution and the stratigraphic preservation of the influence of different events.

- Morphological analysis of repeated surveys across different scales and types of settings is used to determine to what extent the controls identified in this thesis are universal and whether

other complicating factors also play a role. Sites could include, for example, major submarine channel systems offshore from rivers (e.g. Bengal or Indus Fan), deep-sea submarine canyons (e.g. Congo Canyon, West Africa), and other submerged volcanic systems in other locations (e.g. Caribbean). Other parts of the seafloor that were not studied in this thesis would be beneficial to explore, such as the channel levee, tectonically active area and mud volcanos. With the expectation of an increased number of datasets in the future, The development of tools such as artificial intelligence (AI) would be very beneficial. The reliability of AI is still questionable at the moment, but further development and good human intervention may produce great results in Hazard prediction and mitigation in the future

Appendix A

Additional figures and tables:

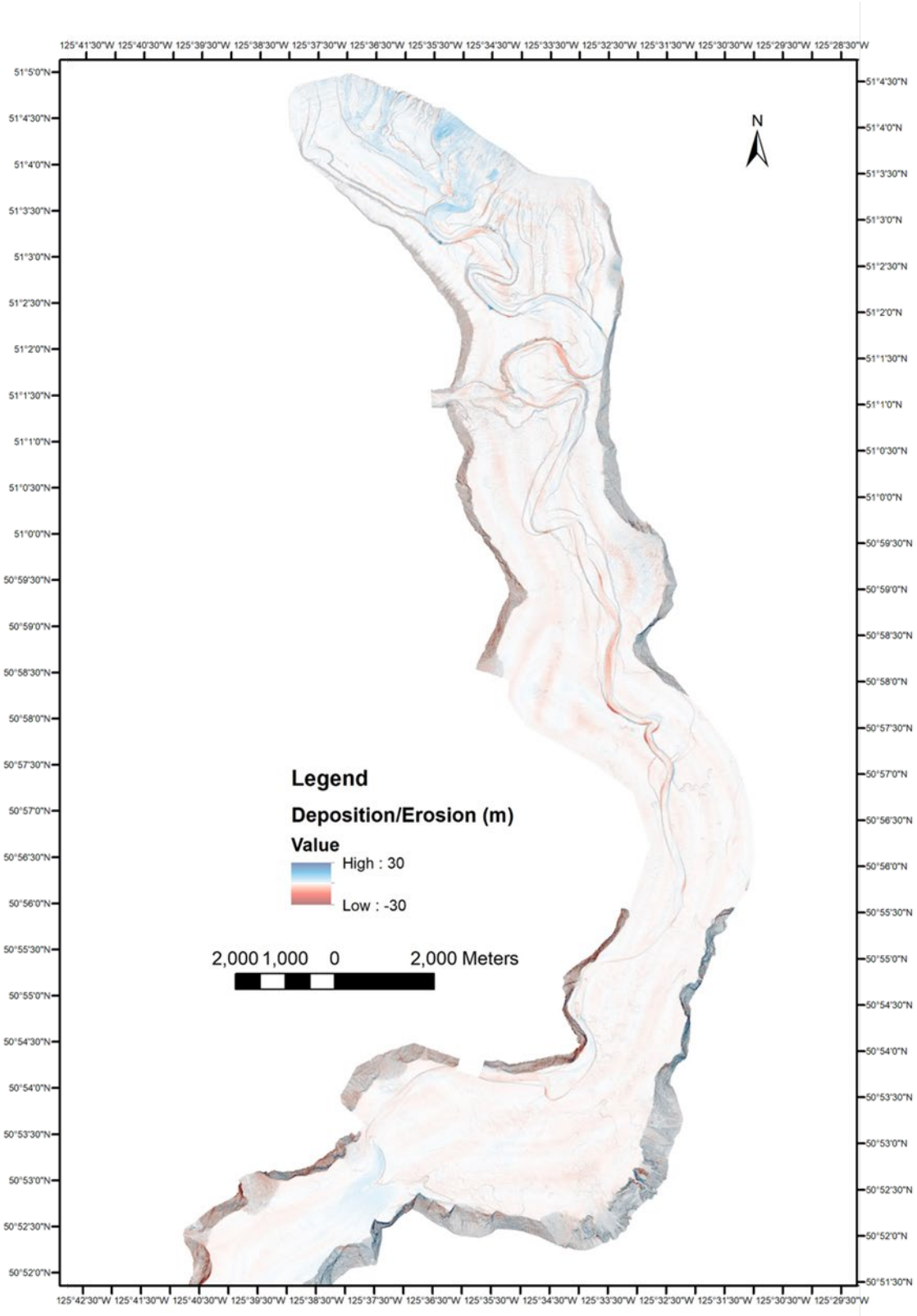

Figure A.3: Difference map of Knight inlet.

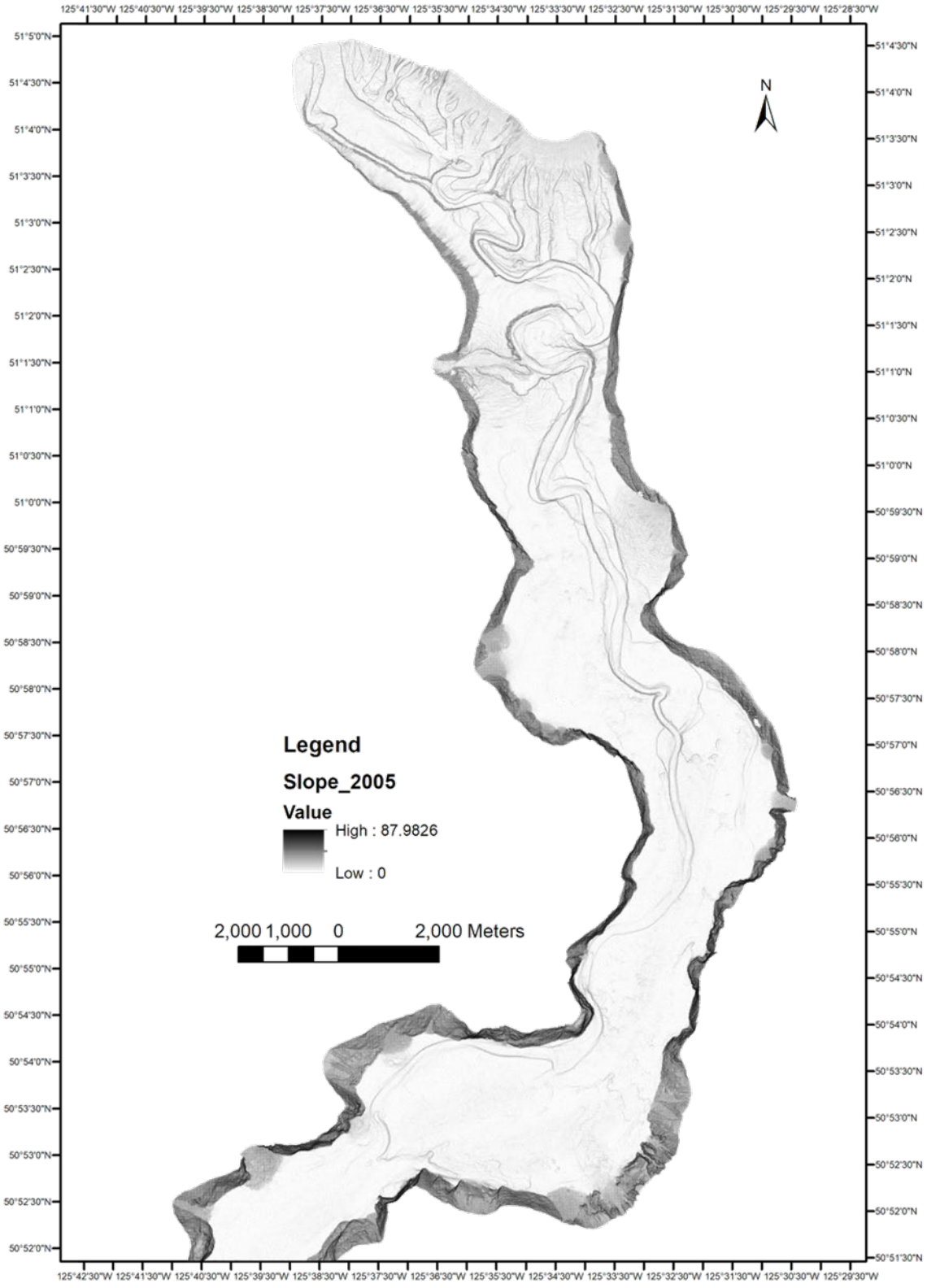

Figure A.4: 2005 slope map of Knight inlet.

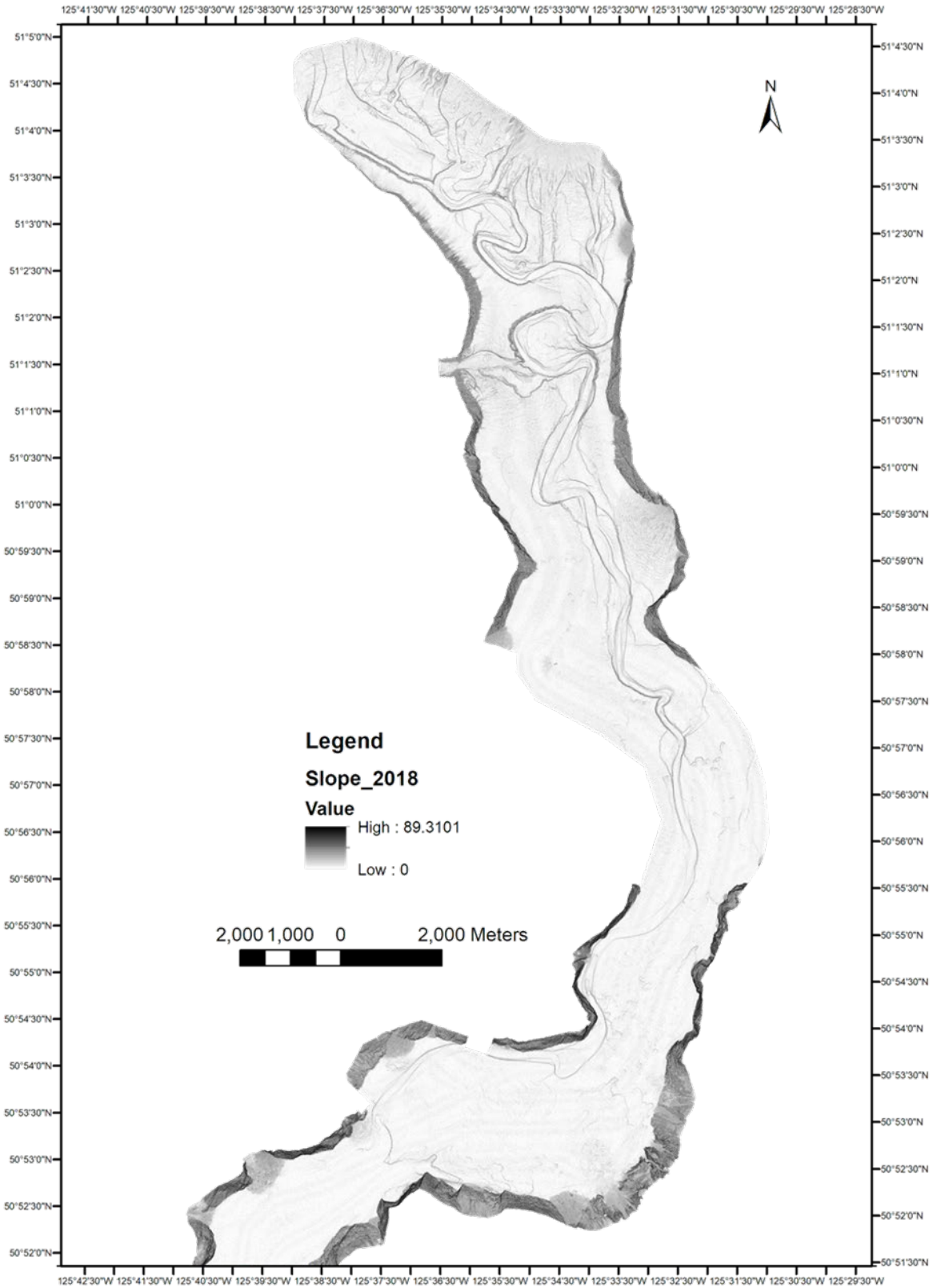

Figure A.5: 2018 slope map of Knight inlet.

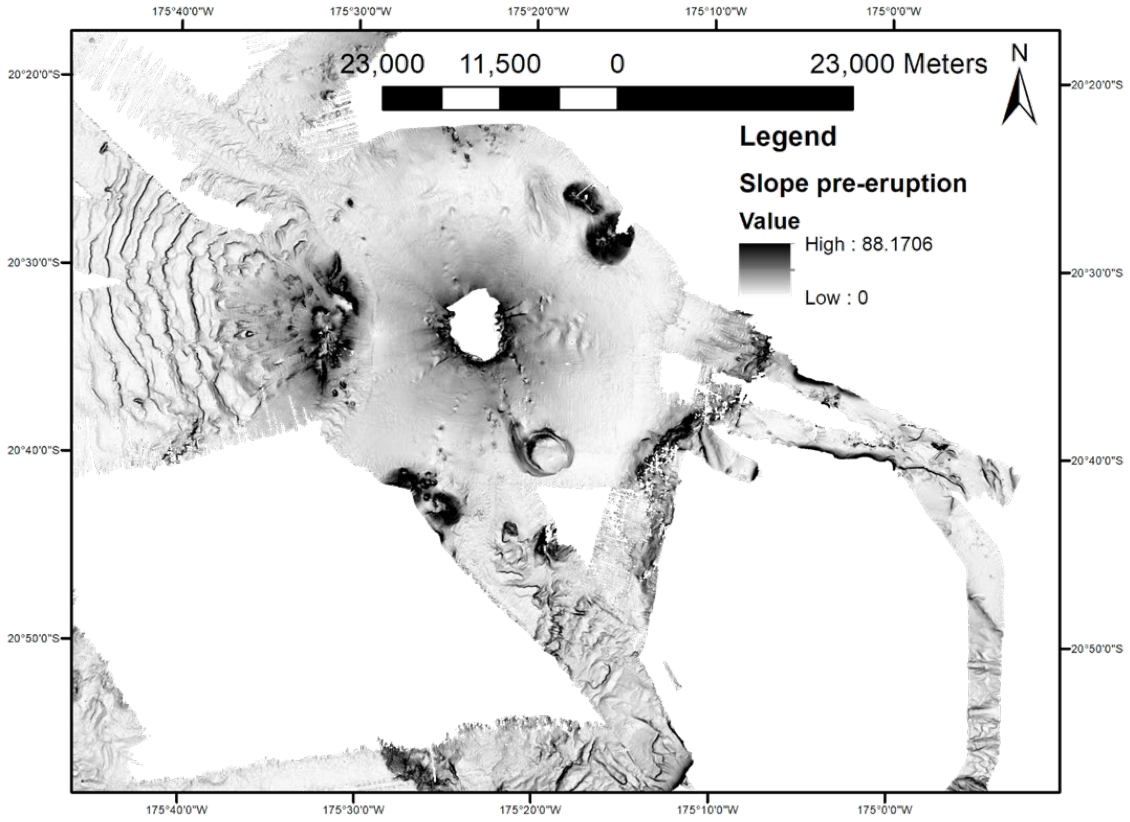

Figure A.6: Pre-eruption slope map of Hunga volcano.

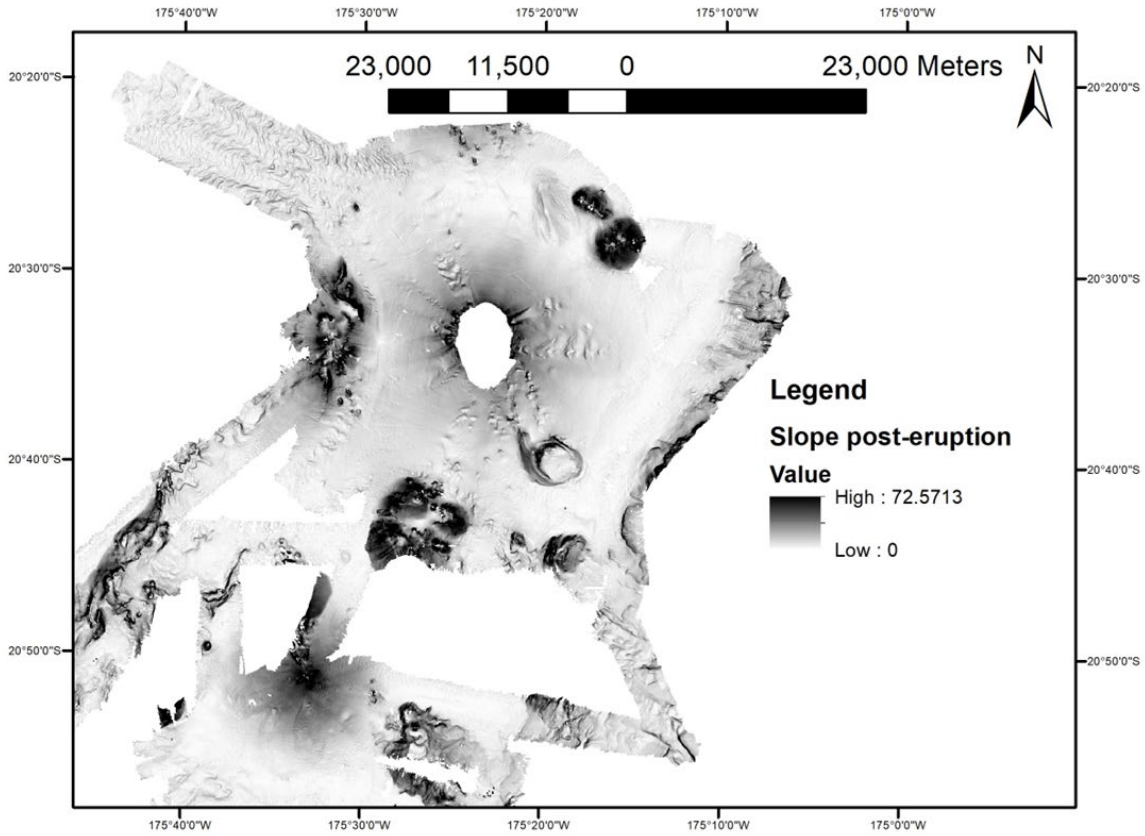

Figure A.7: Post-eruption slope map of Hunga volcano.

Table A.1: Details of curvature that undergone knickpoints migration in Knight inlet.

Radius of curvature (m)	Migration (m)	centrifugal acceleration	Normalised radius of curvature
146.5266	67.54	0.10919519	1.308273214
178.37345	32.019	0.089699448	1.372103462
173.8156	62.209	0.092051576	1.3905248
72.51255	51.00995	0.22065146	0.500086552
83.8937	63.683	0.190717539	0.621434815
132.22	58.22	0.121010437	1.612439024
117.6426	45.412	0.136005155	0.980355

Table A.2: Details of curvature that undergone outer bend erosion in Knight inlet.

Radius of curvature (m)	Migration (m)	centrifugal acceleration	Normalised radius of curvature
146.5266	67.54	0.10919519	1.308273214
178.37345	32.019	0.089699448	1.372103462
173.8156	62.209	0.092051576	1.3905248
72.51255	51.00995	0.22065146	0.500086552
83.8937	63.683	0.190717539	0.621434815
132.22	58.22	0.121010437	1.612439024
117.6426	45.412	0.136005155	0.980355

Table A.3: Detail on river discharge and tidal elevation in Squamish pro-delta.

J Day	Hourly discharge [m3/sec]	Tidal Elevation (m)
117	95.86	2.11
118	107.96	2.25
119	104.18	1.95
120	97.94	1.63
121	95.99	1.4
122	122.7	1.3
123	129	1.01
124	133.2	1.02
125	137.85	0.83
126	151.19	0.83
127	162.58	0.89
128	164.28	1.04
129	178.34	1.28
130	174.02	1.27
131	314.36	1.57
132	319.42	1.9
133	217.82	1.8
134	202.28	1.29
135	319.86	0.86

136	342.03	0.54
137	318.54	0.31
138	254.34	0.25
139	207.56	0.37
140	270.09	0.62
141	345.48	0.83
142	310.62	1.29
143	308.2	1.39
144	327.78	1.6
145	281.43	2.03
146	331.45	2.3
147	308.64	1.93
148	244.89	1.6
149	275.55	1.33
150	369.72	1.05
151	401.56	0.88
152	454.355	0.69
153	447.2	0.61
154	443.755	0.57
155	428.12	0.6
156	476.35	0.77
157	551.36	1.02
158	618.7	1.37
159	523.64	1.9
160	609.4	1.82
161	488.99	1.76
162	451.44	1.31
163	471.845	0.92
164	453.825	0.58
165	516.36	0.35
166	484.67	0.27
167	433.95	0.34
168	469.195	0.44
169	475.29	0.66
170	486.56	0.99
171	497.09	1.35
172	512.72	1.76
173	561.44	1.9
174	596.8	2.22
175	555.28	2.05
176	462.57	1.76
177	460.185	1.45
178	495.74	1.18
179	554.72	0.96
180	916.44	0.73
181	922.1	0.59
182	631.24	0.5

183	479.81	0.48
184	585.4	0.62
185	588.1	0.86
186	506.84	1.22
187	625.96	1.71
188	758.985	1.95
189	775.32	1.74
190	542.12	1.37
191	444.285	1.05
192	471.315	0.78
193	471.315	0.78
194	538.76	0.49
195	570.1	0.51
196	550.24	0.57
197	567.1	0.71
198	570.1	0.71
199	538.76	0.97
200	531.48	1.25
201	534	1.62
202	714.455	2.05
203	645.1	2.09
204	454.09	1.89
205	471.58	1.67
206	568.3	1.43
207	680.9	1.19
208	565	0.96
209	441.9	0.81
210	474.76	0.79
211	488.45	0.63
212	729.055	0.57
213	569.8	0.67
214	426.265	0.88
215	440.31	1.21
216	484.4	1.68
217	535.68	1.51
218	547.16	1.3
219	518.6	1.13
220	486.02	1
221	476.615	0.9
222	428.915	0.84
223	465.75	0.89
224	459.39	0.85
225	402.86	0.89
226	387	0.98
227	380	1.18
228	321.4	1.4
229	314.14	1.69

230	302.22	2.03
231	291.72	1.89
232	303.48	1.79
233	384.5	1.71
234	973.76	1.59
235	973.35	1.46
236	589.3	1.29

Table A.4: Detail on Cumulative Difference of Normalised delta volume in Squamish pro-delta.

J Day	Cumulative Difference of Normalised delta volume (m3)
118	0.037368799
119	0.698666648
122	0.629398536
123	0.654468579
124	0.497346726
125	0.484156925
126	0.456561132
129	0.589079301
130	0.487711097
131	0.315606
132	0.465774557
133	0.543955092
136	0.480659076
137	0.222945878
138	-2.102989746
139	-2.050601492
140	-2.072527437
143	-1.796094792
144	-1.814447387
145	-1.828765392
146	-1.774646465
147	-1.830628585
150	-1.793737978
151	-1.873061013
152	-3.320023598
153	-3.884155047
154	-3.982018989
157	-3.911956682
158	-3.923383073
159	-3.803690755
160	-3.727938205
161	-4.051631879
164	-4.178441291
165	-3.63178478
166	-3.602113101
167	-3.150971616

168	-2.876328285
171	-2.626874213
172	-2.999722315
173	-3.06072286
174	-2.876497184
175	-2.84226658
178	-3.031627113
179	-3.056648977
180	-3.881852844
181	-9.827508651
182	-9.838198495
185	-8.9520973
186	-9.033874966
187	-9.646880121
188	-8.915698675
189	-12.0492585
192	-11.86752367
193	-11.77567144
194	-11.56523117
195	-11.50518616
196	-11.27166085
199	-10.610363
200	-10.60941076
201	-10.68582928
202	-10.60224738
203	-10.55297132
206	-10.88988942
207	-11.0061327
208	-11.72222515
209	-12.29273856
210	-11.67381319
216	-10.29563067
217	-10.30505611
220	-10.4880897
221	-10.4423539
222	-10.47759861
223	-10.42015959
224	-10.64367914
227	-10.49838415
228	-10.61110557
229	-10.71611429
230	-10.6136685
231	-10.65950527
234	-10.81525116
235	-13.28127137
236	-13.18124193

Table A.5: Detail on Cumulative Difference of Delta Progradation in Squamish pro-delta.

J Day	Cumulative Difference of Delta Progradation (m)
118	0.61625
119	1.126875
122	0.770625
123	1.184375
124	0.0275
125	0.244625
126	0.599375
129	1.0375
130	0.1675
131	0.955625
132	2.14125
133	1.845
136	2.995625
137	1.696875
138	-2.74625
139	-1.91875
140	-2.125625
143	-0.850625
144	-1.52
145	-1.235625
146	0.690625
147	-0.12625
150	0.8575
151	0.15875
152	-3.7675
153	-4.8519375
154	-3.877125
157	0.158125
158	-0.426875
159	-0.176875
160	1.174375
161	-0.07125
164	-0.9275
165	2.5325
166	3.95875
167	6.89
168	6.8595
171	9.461875
172	9.21875
173	8.864375
174	12.22625
175	9.40125
178	9.279375
179	8.991875
180	7.255625

181	-23.696875
182	-25.99456731
185	-22.75633654
186	-20.18149038
188	-21.266875
189	-16.864375
192	-19.416875
193	-18.338125
194	-17.20625
195	-18.013125
196	-16.58625
199	-13.835625
200	-14.805
201	-13.733125
202	-13.939375
203	-12.62125
206	-13.290625
208	-12.69625
210	-12.916875
216	-5.748125
217	-6.021875
220	-5.561875
221	-5.1925
222	-6.03
223	-5.33625
227	-5.383125
228	-5.065
229	-3.57125
230	-6.610625
231	-5.47125
234	-6.09625
235	-12.8875
236	-12.766875

Table A.6: Detail on the wavelength and wave height of bedforms around Hunga volcano.

Area A	Wavelength (m)	Wave Height (m)
1	686.2944162	56.61016949
2	1095.431472	97.30538922
3	604.0540541	39.7706422
4	765.1474531	67.27828746
5	992.3224568	252.0833333
6	571.0172745	121.3541667
7	2252.45098	320.5128205
8	1983.660131	200.6644518
9	940.9448819	49.27536232
10	1140.419948	71.01449275

11	888.4514436	55.31400966
Area B		
1	1713.14741	64.35897436
2	1341.22807	28.67052023
3	909.7560976	19.32432432
4	800.304878	23.37837838
5	584.592145	28.775
6	554.5243619	29.13513514
7	500.3984064	33.22580645
8	2091.883614	54.41767068
9	485.8823529	19.5508982
10	341.8478261	20.92672414
11	1289.371981	42.13235294
12	384.6003899	22.01048951
13	1050.569476	63.34975369
14	530.1960784	22.45318352
15	1108.924485	30.76687117
16	727.3195876	22.85060976
17	640.2061856	16.45901639
18	1030.385488	36.01092896
19	535.7630979	22.09259259
20	480.8196721	9.562962963
21	948.5148515	24.90875912
22	607.8767123	42.57246377
23	411.9834711	28.6097561
24	498.4790875	57.55474453
25	890.8127208	78.49462366
26	1408.55615	71.8134715
27	2391.136802	93.47826087
28	1177.294686	49.11660777
29	606.1643836	27.75
30	1155.821918	58.15
31	1217.808219	34.49101796
32	537.6712329	25.98802395
33	1711.594203	41.53571429
34	1272.463768	34.78571429
35	871.0144928	20.85714286
Area C		
1	145.4402516	0.962732919
2	145.1795841	0.629139073
3	184.4990548	0.678807947
4	208.3333333	0.880184332
5	194.8717949	1.064516129
6	204.8076923	1.087557604
7	169.2307692	1
8	376.6917293	3.77826087
9	261.6984402	2.481099656

10	124.7833622	1.037800687
11	100.5199307	0.845360825
12	311.6117851	1.546391753
13	340.5	2.428057554
14	305.3968254	1.646090535
15	307.3015873	1.769547325
16	143.4920635	1.481481481
17	186.031746	1.061728395
18	189.8412698	1.135802469
19	146.031746	0.806584362
20	140.952381	1.004115226
21	158.7301587	0.864197531
22	143.877551	1.517647059
23	152.5510204	2.670588235
24	136.2244898	0.941176471
25	238.2653061	4.082352941
26	243.3673469	3.976470588
27	493.3673469	4.070588235
28	431.0043668	5.242105263

Bibliography

Abreu, V., Sullivan, M., Pirmez, C., and Mohrig, D., 2003, Lateral accretion packages (LAPs): an important reservoir element in deep water sinuous channels: Marine and Petroleum Geology, v. 20, p. 631–648, doi:10.1016/j.marpetgeo.2003.08.003.

Allen, C., Gomis Cartesio, L.E., Hodgson, D.M., Peakall, J., Milana, J-P., 2022. Channel incision into a submarine landslide on a Carboniferous basin margin, San Juan, Argentina: Evidence for the role of knickpoints. The Depositional Record, 8, 628-655. doi: 10.1002/dep2.178 3.

Allin, J.R., Hunt, J.E., Clare, M.A., Talling, P.J., 2018. Eustatic sea level controls on the flushing of a shelf-incising submarine canyon. Geol. Soc. Am. Bull. 130, 222–237. https://doi.org/10.1130/B31658.1

Amores, A., Monserrat, S., Marcos, M., Argüeso, D., Villalonga, J., Jordà, G., Gomis, D., 2022. Numerical simulation of atmospheric Lamb waves generated by the 2022 Hunga-Tonga volcanic eruption.

Amos, K.J., Peakall, J., Bradbury, P.W., Roberts, M., Keevil, G. and Gupta, S., 2010. The influence of bend amplitude and planform morphology on flow and sedimentation in submarine channels. Marine and Petroleum Geology, 27, 1431-1447. doi:10.1016/j.mapetgeo.2010.05.004

Angamuthu, B., Darby, S.E., Nicholls, R.J., 2018. Impacts of natural and human drivers on the multi-decadal morphological evolution of tidally-influenced deltas. Proc. R. Soc. Math. Phys. Eng. Sci. 474, 20180396. https://doi.org/10.1098/rspa.2018.0396

Arisona, A., Ishola, K.S., Nawawi, M.N.M., 2020. Subsurface void mapping using geophysical and geotechnical techniques with uncertainties estimation: case study of Kinta Valley, Perak, Malaysia. SN Appl. Sci. 2, 1171. https://doi.org/10.1007/s42452-020-2967-x

Azpiroz-Zabala, M., Cartigny, M.J.B., Talling, P.J., Parsons, D.R., Sumner, E.J., Clare, M. A., Simmons, S.M., Cooper, C., Pope, E.L., 2017. Newly recognized turbidity current structure can explain prolonged flushing of submarine canyons. Sci. Adv. 3, e170020 https://doi.org/10.1126/sciadv.1700200.

Azpiroz-Zabala, M., Sumner, E.J., Cartigny, M.J.B., Peakall, J., Clare, M.A., Darby, S.E., Parsons, D.R., Dorrell, R.M., Özsoy, E., Tezcan, D., Wynn, R.B., Johnson, J., 2024. Benthic biology influences sedimentation in submarine channel bends: Coupling of biology, sedimentation and flow. The Depositional Record, 10, 159-175. doi: 10.1002/dep2.265

Babonneau, N., Savoye, B., Cremer, M., and Bez, M., 2010, Sedimentary Architecture in Meanders of a Submarine Channel: Detailed Study of the Present Congo Turbidite Channel (Zaiango Project): Journal of Sedimentary Research, v. 80, p. 852–866, doi:10.2110/jsr.2010.078.

Bailey, L.P., Clare, M.A., Rosenberger, K.J., Cartigny, M.J., Talling, P.J., Paull, C.K., Gwiazda, R., Parsons, D.R., Simmons, S.M., Xu, J. and Haigh, I.D., 2021. Preconditioning by sediment accumulation can produce powerful turbidity currents without major external triggers. Earth and Planetary Science Letters, 562, p.116845.

Bailey, L., Clare, M., Pope, E., Haigh, I. D., Cartigny, M., Talling, P. J., ... & Heijnen, M. (2023). Predicting turbidity current activity offshore from meltwater-fed river deltas. Earth and Planetary Science Letters, 604, 117977. https://doi.org/10.1016/j.epsl.2022.117977

Bakhshipour, Z., Huat, B.B.K., Ibrahim, S., Asadi, A., Kura, N.U., 2013. Application of Geophysical Techniques for 3D Geohazard Mapping to Delineate Cavities and Potential Sinkholes in the Northern Part of Kuala Lumpur, Malaysia. Sci. World J. 2013, e629476. https://doi.org/10.1155/2013/629476

Banggur, W.F.S., Pratama, A., Ismail, T., Nurfiani, D., Prayoga, A.S., Kartadinata, M.N., Syahbana, D.K., Mardiono, D., Bani, P., 2023. Review of morphological changes of Anak Krakatau before and after 2018 eruption using Aerial photogrammetry. IOP Conf. Ser. Earth Environ. Sci. 1245, 012028. https://doi.org/10.1088/1755-1315/1245/1/012028

Barrett, R., Lebas, E., Ramalho, R., Klaucke, I., Kutterolf, S., Klügel, A., Lindhorst, K., Gross, F. and Krastel, S., 2020. Revisiting the tsunamigenic volcanic flank collapse of Fogo Island in the Cape Verdes, offshore West Africa. Geological Society, London, Special Publications, 500(1), pp.13-26.

Bendixen, M., Kroon, A., 2017. Conceptualizing delta forms and processes in Arctic coastal environments. Earth Surf. Process. Landf. 42, 1227–1237. https://doi.org/10.1002/esp.4097

Biscara, L., Hanquiez, V., Leynaud, D., Marieu, V., Mulder, T., Gallissaires, J.-M., Crespin, J.-P., Braccini, E., Garlan, T., 2012. Submarine slide initiation and evolution offshore Pointe Odden, Gabon — Analysis from annual bathymetric data (2004–2009). Mar. Geol. 299–302, 43–50. https://doi.org/10.1016/j.margeo.2011.11.008

Bolla Pittaluga, M., Imran, J., 2014. A simple model for vertical profiles of velocity and suspended sediment concentration in straight and curved submarine channels. J. Geophys. Res. Earth Surf. 119, 483–503. https://doi.org/10.1002/2013JF002812

Bornhold, B.D., Harper, J.R., McLaren, D., Thomson, R.E., 2007. Destruction of the first nations village of Kwalate by a rock avalanche-generated tsunami. Atmosphere-Ocean 45, 123–128. https://doi.org/10.3137/ao.450205

Bornhold, B.D., Ren, P., and Prior, D.B., 1994, High-frequency turbidity currents in British Columbia fjords: Geo-Marine Letters, v. 14, p. 238–243, doi:10.1007/BF01274059.

Borrero, J.C., Cronin, S.J., Latu'ila, F.H., Tukuafu, P., Heni, N., Tupou, A.M., Kula, T., Fa'anunu, O., Bosserelle, C., Lane, E., Lynett, P., Kong, L., 2023. Tsunami Runup and Inundation in Tonga from the January 2022 Eruption of Hunga Volcano. Pure Appl. Geophys. 180, 1–22. https://doi.org/10.1007/s00024-022-03215-5

Bouchakour, M., Zhao, X., Miclăuș, C., Yang, B., 2023. Lateral migration and channel bend morphology around growing folds (Niger Delta continental slope). Basin Res. 35, 1154–1192. https://doi.org/10.1111/bre.12750

Boudon, G., Villemant, B., Le Friant, A., Paterne, M. and Cortijo, E., 2013. Role of large flank-collapse events on magma evolution of volcanoes. Insights from the Lesser Antilles Arc. Journal of volcanology and geothermal research, 263, pp.224-237.

Bouma, A. H., Normark, W. R., Barnes, N. E., Submarine Fans and Related Turbidite Systems (Springer-Verlag, 2012).

Bourriquen, M., Baltzer, A., Mercier, D., Fournier, J., Pérez, L., Haquin, S., Bernard, E., Jensen, M., 2016. Coastal evolution and sedimentary mobility of Brøgger Peninsula, northwest Spitsbergen. Polar Biol. 39, 1689–1698. https://doi.org/10.1007/s00300-016-1930-1

Breard, E.C.P., Lube, G., Jones, J.R., Dufek, J., Cronin, S.J., Valentine, G.A., Moebis, A., 2016. Coupling of turbulent and non-turbulent flow regimes within pyroclastic density currents. Nat. Geosci. 9, 767–771. https://doi.org/10.1038/ngeo2794

Buatois, L. A., Santiago, N., Herrera, M. L., Plink-Björklund, P., Steel, R. J., Espin, M., ... & Parra, K. (2012). Sedimentological and ichnological signatures of changes in wave, river and tidal influence along a neogene tropical deltaic shoreline. Sedimentology, 59(5), 1568-1612. https://doi.org/10.1111/j.1365-3091.2011.01317.x

Bull, S., Cartwright, J., Huuse, M., 2009. A review of kinematic indicators from mass-transport complexes using 3D seismic data. Mar. Pet. Geol. 26, 1132–1151. https://doi.org/10.1016/j.marpetgeo.2008.09.011

Cabaniss, H.E., Gregg, P.M., Nooner, S.L., Chadwick, W.W., 2020. Triggering of eruptions at Axial Seamount, Juan de Fuca Ridge. Sci. Rep. 10, 10219. https://doi.org/10.1038/s41598-020-67043-0

Caldwell, R. L., Edmonds, D. A., Baumgardner, S., Paola, C., Roy, S., & Nienhuis, J. H. (2019). A global delta dataset and the environmental variables that predict delta formation on marine coastlines. Earth Surface Dynamics, 7(3), 773-787. https://doi.org/10.5194/esurf-7-773-2019

Cantero, M.I., Balachandar, S., Cantelli, A., Parker, G., 2014. A simplified approach to address turbulence modulation in turbidity currents as a response to slope breaks and loss of lateral confinement. Environ. Fluid Mech. 14, 371–385. https://doi.org/10.1007/s10652-013-9302-7

Caratori Tontini, F., Crone, T.J., de Ronde, C.E.J., Fornari, D.J., Kinsey, J.C., Mittelstaedt, E., Tivey, M., 2016. Crustal magnetization and the subseafloor structure of the ASHES vent field, Axial Seamount, Juan de Fuca Ridge: Implications for the investigation of hydrothermal sites. Geophys. Res. Lett. 43, 6205–6211. https://doi.org/10.1002/2016GL069430

Caress, D.W., Clague, D.A., Paduan, J.B., Martin, J.F., Dreyer, B.M., Chadwick, W.W., Denny, A., Kelley, D.S., 2012. Repeat bathymetric surveys at 1-metre resolution of lava flows erupted at Axial Seamount in April 2011. Nat. Geosci. 5, 483–488. https://doi.org/10.1038/ngeo1496

Carter, L., Gavey, R., Talling, P., and Liu, J., 2014, Insights into Submarine Geohazards from Breaks in Subsea Telecommunication Cables: Oceanography, v. 27, p. 58–67, doi:10.5670/oceanog.2014.40.

Cartigny, M.J.B., Postma, G., 2017. Turbidity Current Bedforms, in: Guillén, J., Acosta, J., Chiocci, F.L., Palanques, A. (Eds.), Atlas of Bedforms in the Western Mediterranean. Springer International Publishing, Cham, pp. 29–33. https://doi.org/10.1007/978-3-319-33940-5_6

Cartigny, M.J.B., Postma, G., van den Berg, J.H., Mastbergen, D.R., 2011. A comparative study of sediment waves and cyclic steps based on geometries, internal structures and numerical modeling. Mar. Geol. 280, 40–56. https://doi.org/10.1016/j.margeo.2010.11.006

Cartigny, M.J.B., Ventra, D., Postma, G., van Den Berg, J.H., 2014. Morphodynamics and sedimentary structures of bedforms under supercritical-flow conditions: New insights from flume experiments. Sedimentology 61, 712–748. https://doi.org/10.1111/sed.12076

Cas, R.A., Wright, J.V., 1991. Subaqueous pyroclastic flows and ignimbrites: an assessment. Bull. Volcanol. 53, 357–380. https://doi.org/10.1007/BF00280227

Casalbore, D., Clare, M.A., Pope, E.L., Quartau, R., Bosman, A., Chiocci, F.L., Romagnoli, C., Santos, R., 2021. Bedforms on the submarine flanks of insular volcanoes: New insights

gained from high resolution seafloor surveys. Sedimentology 68, 1400–1438. https://doi.org/10.1111/sed.12725

Casalbore, D., Passeri, F., Tommasi, P., Verrucci, L., Bosman, A., Romagnoli, C., Chiocci, F.L., 2020. Small-scale slope instability on the submarine flanks of insular volcanoes: the case-study of the Sciara del Fuoco slope (Stromboli). Int. J. Earth Sci. 109, 2643–2658. https://doi.org/10.1007/s00531-020-01853-5

Cassidy, M., Mani, L., 2022. Huge volcanic eruptions: time to prepare. Nature 608, 469–471. https://doi.org/10.1038/d41586-022-02177-x

Cattaneo, A., Correggiari, A., Marsset, T., Thomas, Y., Marsset, B., Trincardi, F., 2004. Seafloor undulation pattern on the Adriatic shelf and comparison to deep-water sediment waves. Mar. Geol., COSTA - Continental Slope Stability 213, 121–148. https://doi.org/10.1016/j.margeo.2004.10.004

Ceramicola, S., Praeg, D., Coste, M., Forlin, E., Cova, A., Colizza, E., and Critelli, S., 2014, Submarine Mass-Movements Along the Slopes of the Active Ionian Continental Margins and Their Consequences for Marine Geohazards (Mediterranean Sea), in Krastel, S., Behrmann, J.-H., Völker, D., Stipp, M., Berndt, C., Urgeles, R., Chaytor, J., Huhn, K., Strasser, M., and Harbitz, C.B. eds., Submarine Mass Movements and Their Consequences: 6th International Symposium, Cham, Springer International Publishing, Advances in Natural and Technological Hazards Research, p. 295–306, doi:10.1007/978-3-319-00972-8_26.

Carvajal, M., Sepúlveda, I., Gubler, A., & Garreaud, R. (2022). Worldwide signature of the 2022 Tonga volcanic tsunami. Geophysical Research Letters, 49(6). https://doi.org/10.1029/2022gl098153

Chadwick, W.W., Rubin, K.H., Merle, S.G., Bobbitt, A.M., Kwasnitschka, T., Embley, R.W., 2019. Recent Eruptions Between 2012 and 2018 Discovered at West Mata Submarine Volcano (NE Lau Basin, SW Pacific) and Characterized by New Ship, AUV, and ROV Data. Front. Mar. Sci. 6.

Chen, H., Wang, Z., Li, L., & Wen, M. (2017). Occurrence of submarine canyons, sediment waves and mass movements along the northern continental slope of the south china sea. Journal of Earth System Science, 126(5). https://doi.org/10.1007/s12040-017-0844-9

Chen, J., Lv, B., Peng, L., Huang, B., 2022. Study on resistance characteristics of submarine near water surface. MATEC Web Conf. 355, 01002. https://doi.org/10.1051/matecconf/202235501002

Chen, Y., Parsons, D.R., Simmons, S.M., Williams, R., Cartigny, M.J.B., Hughes Clarke, J.E., Stacey, C.D., Hage, S., Talling, P.J., Azpiroz-Zabala, M., Clare, M.A., Hizzett, J.L., Heijnen, M.S., Hunt, J.E., Lintern, D.G., Sumner, E.J., Vellinga, A.J., Vendettuoli, D., 2021. Knickpoints and crescentic bedform interactions in submarine channels. Sedimentology 68, 1358–1377. https://doi.org/10.1111/sed.12886

Chillarige, A.V., Morgenstern, N.R., Robertson, P.K. and Christian, H.A., 1997. Seabed instability due to flow liquefaction in the Fraser River delta. Canadian Geotechnical Journal, 34(4), pp.520-533

Chiocci, F.L., Cattaneo, A., Urgeles, R., 2011. Seafloor mapping for geohazard assessment: state of the art. Mar. Geophys. Res. 32, 1–11. https://doi.org/10.1007/s11001-011-9139-8

Clare, M., Lintern, D.G., Pope, E., Baker, M., Ruffell, S., Zulkifli, M., Simmons, S., Urlaub, M., Belal, M., Talling, P., 2021. Seismic and Acoustic Monitoring of Submarine Landslides:

Ongoing Challenges, Recent Successes and Future Opportunities. EarthArXiv. https://doi.org/10.31223/X5703Q

Clare, M., Lintern, D.G., Rosenberger, K., Hughes Clarke, J.E., Paull, C., Gwiazda, R., Cartigny, M.J.B., Talling, P.J., Perara, D., Xu, J., Parsons, D., Jacinto, R.S., Apprioual, R., 2020. Lessons learned from the monitoring of turbidity currents and guidance for future platform designs. Geol. Soc. Lond. Spec. Publ. 500, 605–634. https://doi.org/10.1144/SP500-2019-173

Clare, M.A., Hughes Clarke, J.E., Talling, P.J., Cartigny, M.J.B., Pratomo, D.G., 2016. Preconditioning and triggering of offshore slope failures and turbidity currents revealed by most detailed monitoring yet at a fjord-head delta. Earth Planet. Sci. Lett. 450, 208–220. https://doi.org/10.1016/j.epsl.2016.06.021

Clare, M.A., Le Bas, T., Price, D.M., Hunt, J.E., Sear, D., Cartigny, M.J.B., Vellinga, A., Symons, W., Firth, C., Cronin, S., 2018. Complex and Cascading Triggering of Submarine Landslides and Turbidity Currents at Volcanic Islands Revealed From Integration of High-Resolution Onshore and Offshore Surveys. Front. Earth Sci. 6.

Clare, M.A., Talling, P.J., Hunt, J.E., 2015. Implications of reduced turbidity current and landslide activity for the Initial Eocene Thermal Maximum – evidence from two distal, deep-water sites. Earth Planet. Sci. Lett. 420, 102–115. https://doi.org/10.1016/j.epsl.2015.03.022

Clare, M.A., Vardy, M.E., Cartigny, M.J.B., Talling, P.J., Himsworth, M.D., Dix, J.K., Harris, J.M., Whitehouse, R.J.S., Belal, M., 2017. Direct monitoring of active geohazards: emerging geophysical tools for deep-water assessments. Surf. Geophys. 15, 427–444. https://doi.org/10.3997/1873-0604.2017033

Clare, M.A., Yeo, I.A., Watson, S., Wysoczanski, R., Seabrook, S., Mackay, K., Hunt, J.E., Lane, E., Talling, P.J., Pope, E., Cronin, S., Ribó, M., Kula, T., Tappin, D., Henrys, S., de Ronde, C., Urlaub, M., Kutterolf, S., Fonua, S., Panuve, S., Veverka, D., Rapp, R., Kamalov, V., Williams, M., 2023. Fast and destructive density currents created by ocean-entering volcanic eruptions. Science 381, 1085–1092. https://doi.org/10.1126/science.adi3038

Clarke, J.E.H., Marques, C.R.V., Pratomo, D., 2014. Imaging Active Mass-Wasting and Sediment Flows on a Fjord Delta, Squamish, British Columbia, in: Krastel, S., Behrmann, J.-H., Völker, D., Stipp, M., Berndt, C., Urgeles, R., Chaytor, J., Huhn, K., Strasser, M., Harbitz, C.B. (Eds.), Submarine Mass Movements and Their Consequences: 6th International Symposium, Advances in Natural and Technological Hazards Research. Springer International Publishing, Cham, pp. 249–260. https://doi.org/10.1007/978-3-319-00972-8_22

Clarke, J.H., Brucker, S., Muggah, J., Church, I., Cartwright, D., Kuus, P., Hamilton, T., Pratomo, D., Eisan, B., 2012. The Squamish ProDelta: monitoring active landslides and turbidity currents, in: Canadian Hydrographic Conference. pp. 1–15.

Clift, P., Gaedicke, C., 2002. Accelerated mass flux to the Arabian Sea during the middle to late Miocene. Geology 30, 207–210. https://doi.org/10.1130/0091-7613(2002)030<0207:AMFTTA>2.0.CO;2

Coltelli, M., Cavallaro, D., Carlino, M.F., Cocchi, L., Muccini, F., D'Alessandro, A., Claude, M.E., Monaco, C., Ibáñez, J.M., Zgur, F., Patanè, D., Carmisciano, C., D'Anna, G., Gonzales, M.T.P., Teixidò, T., D'Anna, R., Fertitta, G., Passafiume, G., Speciale, S., Grassa, F., Karageorgis, A.P., Sormani, L., Facchin, L., Visnovic, G., Cotterle, D., Blanos, R., Mansutti, P., Sulli, A., Cultrera, F., Carrión, F., Rapisarda, S., 2016. The marine activities performed within the TOMO-ETNA experiment. Ann. Geophys. 59, S0428–S0428. https://doi.org/10.4401/ag-7081

Conway, K.W., Barrie, J.V., Picard, K., and Bornhold, B.D., 2012, Submarine channel evolution: active channels in fjords, British Columbia, Canada: Geo-Marine Letters, v. 32, p. 301–312, doi:10.1007/s00367-012-0280-4.

Corney, R.K.T., Peakall, J., Parsons, D.R., Elliott, L., Amos, K.J., Best, J.L., Keevil, G.M., Ingham, D.B., 2006. The orientation of helical flow in curved channels. Sedimentology 53, 249–257. https://doi.org/10.1111/j.1365-3091.2006.00771.x

Covault, J., Sylvester, Z., Hubbard, S., Jobe, Z., and Sech, R., 2016, The stratigraphic record of submarine-channel evolution: The Sedimentary Record, v. 14, p. 4–11, doi:10.2110/sedred.2016.3.

Covault, J.A., Kostic, S., Paull, C.K., Ryan, H.F., and Fildani, A., 2014, Submarine channel initiation, filling and maintenance from seafloor geomorphology and morphodynamic modelling of cyclic steps: Sedimentology, v. 61, p. 1031–1054, doi:10.1111/sed.12084.

Covault, J.A., Kostic, S., Paull, C.K., Sylvester, Z., and Fildani, A., 2017, Cyclic steps and related supercritical bedforms: Building blocks of deep-water depositional systems, western North America: Marine Geology, v. 393, p. 4–20, doi:10.1016/j.margeo.2016.12.009. 15.18.

Covault, J.A., Sylvester, Z., Hudec, M.R., Ceyhan, C. and Dunlap, D., 2020, Submarine channels 'swept' downstream after bend cutoff in salt basins. The Depositional Record, 6, 259-272.

Covault, J.A., Sylvester, Z., Ceyhan, C. and Dunlap, D.B., 2021. Giant meandering channel evolution, Campos deep-water salt basin, Brazil. Geosphere, 17(6), pp.1869-1889.

Dai, Z., Li, X., Lan, B., 2023. Three-Dimensional Modeling of Tsunami Waves Triggered by Submarine Landslides Based on the Smoothed Particle Hydrodynamics Method. J. Mar. Sci. Eng. 11, 2015. https://doi.org/10.3390/jmse11102015

de Leeuw, J., Eggenhuisen, J.T., Cartigny, M.J.B., 2018. Linking submarine channel–levee facies and architecture to flow structure of turbidity currents: insights from flume tank experiments. Sedimentology 65, 931–951. https://doi.org/10.1111/sed.12411

Denamiel, C., Vasylkevych, S., Žagar, N., Zemunik, P., & Vilibić, I. (2023). Destructive potential of planetary meteotsunami waves beyond the hunga tonga–hunga ha'apai volcano eruption. Bulletin of the American Meteorological Society, 104(1), E178-E191. https://doi.org/10.1175/bams-d-22-0164.1

Deptuck, M.E., Sylvester, Z., Pirmez, C. and O'Byrne, C., 2007. Migration–aggradation history and 3-D seismic geomorphology of submarine channels in the Pleistocene Benin-major Canyon, western Niger Delta slope. Marine and Petroleum Geology, 24(6-9), pp.406-433.DeVore, J.R., Sawyer, D.E., 2016. Shear Strength of Siliciclastic Sediments from Passive and Active Margins (0–100 m Below Seafloor): Insights into Seismic Strengthening, in: Lamarche, G., Mountjoy, J., Bull, S., Hubble, T., Krastel, S., Lane, E., Micallef, A., Moscardelli, L., Mueller, C., Pecher, I., Woelz, S. (Eds.), Submarine Mass Movements and Their Consequences: 7th International Symposium, Advances in Natural and Technological Hazards Research. Springer International Publishing, Cham, pp. 173–180. https://doi.org/10.1007/978-3-319-20979-1_17

de Ronde, C.E.J., Massoth, G.J., Baker, E.T. & Lupton, J.E., 2003, Submarine hydrothermal venting related to volcanic arcs, In, Giggenbach Memorial volume, S.F. Simmons and I.G Graham (eds.). Society of Economic Geology and Geochemical Society Special Publication 10, 91-109.

Desonie, D., Duncan, R., & Natland, J. (1993). Temporal and geochemical variability of volcanic products of the marquesas hotspot. Journal of Geophysical Research Atmospheres, 98(B10), 17649-17665. https://doi.org/10.1029/93jb01562

Di Traglia, F., Fornaciai, A., Casalbore, D., Favalli, M., Manzella, I., Romagnoli, C., Chiocci, F.L., Cole, P., Nolesini, T. and Casagli, N., 2022. Subaerial-submarine morphological changes at Stromboli volcano (Italy) induced by the 2019–2020 eruptive activity. Geomorphology, 400, p.108093.

Diesing, M., Green, S.L., Stephens, D., Lark, R.M., Stewart, H.A., Dove, D., 2014. Mapping seabed sediments: Comparison of manual, geostatistical, object-based image analysis and machine learning approaches. Cont. Shelf Res. 84, 107–119. https://doi.org/10.1016/j.csr.2014.05.004

Dixon, J.F., Steel, R.J., Olariu, C., 2012. River-dominated, shelf-edge deltas: delivery of sand across the shelf break in the absence of slope incision. Sedimentology 59, 1133–1157. https://doi.org/10.1111/j.1365-3091.2011.01298.x

Dorrell, R.M., Darby, S.E., Peakall, J., Sumner, E.J., Parsons, D.R., and Wynn, R.B., 2013, Super-elevation and overspill control secondary flow dynamics in submarine channels: Journal of Geophysical Research: Oceans, v. 118, p. 3895–3915, doi:10.1002/jgrc.20277.

Dorrell, R.M., Peakall, J., Burns, C., and Keevil, G.M., 2018, A novel mixing mechanism in sinuous seafloor channels: Implications for submarine channel evolution: Geomorphology, v. 303, p. 1–12, doi:10.1016/j.geomorph.2017.11.008.

Dykstra, M., and Kneller, B., 2009, Lateral accretion in a deep-marine channel complex: implications for channellized flow processes in turbidity currents: Sedimentology, v. 56, p. 1411–1432, doi:10.1111/j.1365-3091.2008.01040.x.

Edmonds, D., Slingerland, R., Best, J., Parsons, D., Smith, N., 2010. Response of river-dominated delta channel networks to permanent changes in river discharge. Geophys. Res. Lett. 37. https://doi.org/10.1029/2010GL043269

Edmonds, D.A., Slingerland, R.L., 2007. Mechanics of river mouth bar formation: Implications for the morphodynamics of delta distributary networks. J. Geophys. Res. Earth Surf. 112. https://doi.org/10.1029/2006JF000574

Eke, E., Czapiga, M.J., Viparelli, E., Shimizu, Y., Imran, J., Sun, T., Parker, G., 2014. Coevolution of width and sinuosity in meandering rivers. J. Fluid Mech. 760, 127–174. https://doi.org/10.1017/jfm.2014.556.

Englert, R.G., Hubbard, S.M., Cartigny, M.J.B., Clare, M.A., Coutts, D.S., Hage, S., Hughes Clarke, J., Jobe, Z., Lintern, D.G., Stacey, C., Vendettuoli, D., 2021. Quantifying the three-dimensional stratigraphic expression of cyclic steps by integrating seafloor and deep-water outcrop observations. Sedimentology 68, 1465–1501. https://doi.org/10.1111/sed.12772Ercilla, G., Alonso, B., Wynn, R.B., Baraza, J., 2002. Turbidity current sediment waves on irregular slopes: observations from the Orinoco sediment–wave field. Mar. Geol. 192, 171–187. https://doi.org/10.1016/S0025-3227(02)00554-6

Fan, G., Zhang, J., Wu, J., Yan, K., 2016. Dynamic Response and Dynamic Failure Mode of a Weak Intercalated Rock Slope Using a Shaking Table. Rock Mech. Rock Eng. 49, 3243–3256. https://doi.org/10.1007/s00603-016-0971-7

Fan, W., McGuire, J.J., Shearer, P.M., 2020. Abundant Spontaneous and Dynamically Triggered Submarine Landslides in the Gulf of Mexico. Geophys. Res. Lett. 47, e2020GL087213. https://doi.org/10.1029/2020GL087213

Farre, J.A., McGregor, B.A., Ryan, W.B.F., Robb, J.M., 1983. Breaching the Shelfbreak: Passage from Youthful to Mature Phase in Submarine Canyon Evolution, in: Stanley, D.J., Moore, G.T. (Eds.), The Shelfbreak: Critical Interface on Continental Margins. SEPM Society for Sedimentary Geology, p. 0. https://doi.org/10.2110/pec.83.06.0025

Feldens, P., Schulze, I., Papenmeier, S., Schönke, M., Schneider von Deimling, J., 2018. Improved Interpretation of Marine Sedimentary Environments Using Multi-Frequency Multibeam Backscatter Data. Geosciences 8, 214. https://doi.org/10.3390/geosciences8060214

Fernandes, A.M., Buttles, J., Mohrig, D., 2020. Flow substrate interactions in aggrading and degrading submarine channels. J. Sediment. Res. 90, 573–583. https://doi.org/10.2110/jsr.2020.31

Fielding, C.R., 2015. Anatomy of falling-stage deltas in the Turonian Ferron Sandstone of the western Henry Mountains Syncline, Utah: Growth faults, slope failures and mass transport complexes. Sedimentology 62, 1–26. https://doi.org/10.1111/sed.12136

Fildani, A., Hubbard, S.M., Covault, J.A., Maier, K.L., Romans, B.W., Traer, M., Rowland, J.C., 2013. Erosion at inception of deep-sea channels. Mar. Pet. Geol., Special Issue: Internal architecture, bedforms and geometry of turbidite channels 41, 48–61. https://doi.org/10.1016/j.marpetgeo.2012.03.006

Finotello, A., Lanzoni, S., Ghinassi, M., Marani, M., Rinaldo, A., and D'Alpaos, A., 2018, Field migration rates of tidal meanders recapitulate fluvial morphodynamics: Proceedings of the National Academy of Sciences, v. 115, p. 1463–1468, doi:10.1073/pnas.1711330115.

Forel, F.A., 1887. Le ravin sous-lacustre du du Rhône dans le lac Léman. Verlag nicht ermittelbar.

Freundt, A., 2003. Entrance of hot pyroclastic flows into the sea: experimental observations. Bull. Volcanol. 65, 144–164. https://doi.org/10.1007/s00445-002-0250-1

Fuhrmann, A., Kane, I. A., Clare, M., Ferguson, R. A., Schomacker, E., Bonamini, E., ... & Contreras, F. (2020). Hybrid turbidite-drift channel complexes: an integrated multiscale model. Geology, 48(6), 562-568. https://doi.org/10.1130/g47179.1

Fujiwara, T., 2021. Seafloor Geodesy From Repeated Multibeam Bathymetric Surveys: Application to Seafloor Displacement Caused by the 2011 Tohoku-Oki Earthquake. Front. Earth Sci. 9.

Fukuda, S., Vet, M. d., Skevington, E. W. G., Bastianon, E., Fernández, R., Wu, X., ... & Dorrell, R. M. (2023). Inadequacy of fluvial energetics for describing gravity current autosuspension. Nature Communications, 14(1). https://doi.org/10.1038/s41467-023-37724-1

Fundis, A.T., Soule, S.A., Fornari, D.J., Perfit, M.R., 2010. Paving the seafloor: Volcanic emplacement processes during the 2005–2006 eruptions at the fast spreading East Pacific Rise, 9°50'N. Geochem. Geophys. Geosystems 11. https://doi.org/10.1029/2010GC003058

Gaida, T.C., Mohammadloo, T.H., Snellen, M., Simons, D.G., 2020. Mapping the Seabed and Shallow Subsurface with Multi-Frequency Multibeam Echosounders. Remote Sens. 12, 52. https://doi.org/10.3390/rs12010052

Gales, J.A., Talling, P.J., Cartigny, M.J.B., Hughes Clarke, J., Lintern, G., Stacey, C., and Clare, M.A., 2019, What controls submarine channel development and the morphology of

deltas entering deep-water fjords? Earth Surface Processes and Landforms, v. 44, p. 535–551, doi:10.1002/esp.4515.

Gallen, S.F., Wegmann, K.W., Frankel, K.L., Hughes, S., Lewis, R.Q., Lyons, N., Paris, P., Ross, K., Bauer, J.B., Witt, A.C., 2011. Hillslope response to knickpoint migration in the Southern Appalachians: implications for the evolution of post-orogenic landscapes. Earth Surf. Process. Landf. 36, 1254–1267. https://doi.org/10.1002/esp.2150

Gardner, J.V., 2010. The West Mariana Ridge, western Pacific Ocean: Geomorphology and processes from new multibeam data. GSA Bull. 122, 1378–1388. https://doi.org/10.1130/B30149.1

Garvin, J.B., Slayback, D.A., Ferrini, V., Frawley, J., Giguere, C., Asrar, G.R., Andersen, K., 2018. Monitoring and Modeling the Rapid Evolution of Earth's Newest Volcanic Island: Hunga Tonga Hunga Ha'apai (Tonga) Using High Spatial Resolution Satellite Observations. Geophys. Res. Lett. 45, 3445–3452. https://doi.org/10.1002/2017GL076621

Gaurier, B., Davies, P., Deuff, A., Germain, G., 2013. Flume tank characterization of marine current turbine blade behaviour under current and wave loading. Renew. Energy 59, 1–12. https://doi.org/10.1016/j.renene.2013.02.026

Georgiopoulou, A., Cartwright, J.A., 2013. A critical test of the concept of submarine equilibrium profile. Mar. Pet. Geol., Special Issue: Internal architecture, bedforms and geometry of turbidite channels 41, 35–47. https://doi.org/10.1016/j.marpetgeo.2012.03.003

Giorgio Serchi, F., Peakall, J., Ingham, D.B., and Burns, A.D., 2011, A unifying computational fluid dynamics investigation on the river-like to river-reversed secondary circulation in submarine channel bends. Journal of Geophysical Research – Oceans, v. 116, C06012. doi:10.1029/2010JC006361

Grilli, S.T., Tappin, D.R., Carey, S., Watt, S.F.L., Ward, S.N., Grilli, A.R., Engwell, S.L., Zhang, C., Kirby, J.T., Schambach, L., Muin, M., 2019. Modelling of the tsunami from the December 22, 2018 lateral collapse of Anak Krakatau volcano in the Sunda Straits, Indonesia. Sci. Rep. 9, 11946. https://doi.org/10.1038/s41598-019-48327-6

Grilli, S.T., Zhang, C., Kirby, J.T., Grilli, A.R., Tappin, D.R., Watt, S.F.L., Hunt, J.E., Novellino, A., Engwell, S., Nurshal, M.E.M., Abdurrachman, M., Cassidy, M., Madden-Nadeau, A.L., Day, S., 2021. Modeling of the Dec. 22nd 2018 Anak Krakatau volcano lateral collapse and tsunami based on recent field surveys: Comparison with observed tsunami impact. Mar. Geol. 440, 106566. https://doi.org/10.1016/j.margeo.2021.106566

Guiastrennec-Faugas, L., Gillet, H., Peakall, J., Dennielou, B., Gaillot, A., and Jacinto, R.S., 2021, Initiation and evolution of knickpoints and their role in cut-and-fill processes in active submarine channels: Geology, v. 49, p. 314–319, doi:10.1130/G48369.1.

Guiastrennec-Faugas, L., Gillet, H., Silva Jacinto, R., Dennielou, B., Hanquiez, V., Schmidt, S., Simplet, L., and Rousset, A., 2020, Upstream migrating knickpoints and related sedimentary processes in a submarine canyon from a rare 20-year morphobathymetric time-lapse (Capbreton submarine canyon, Bay of Biscay, France): Marine Geology, v. 423, p. 106143, doi:10.1016/j.margeo.2020.106143.

Gupta, A.K., Bennartz, R., Fauria, K.E., Mittal, T., 2022. Eruption chronology of the December 2021 to January 2022 Hunga Tonga-Hunga Ha'apai eruption sequence. Commun. Earth Environ. 3, 1–10. https://doi.org/10.1038/s43247-022-00606-3

Hage, S., Cartigny, M., Clare, M., Sumner, E. J., Vendettuoli, D., Clarke, J. E. H., ... & Vellinga, A. (2018). How to recognize crescentic bedforms formed by supercritical turbidity currents

in the geologic record: insights from active submarine channels. Geology, 46(6), 563-566. https://doi.org/10.1130/g40095.1

Hage, S., Cartigny, M., Heerema, C., Heijnen, M., Açıkalın, S., Clare, M., ... & Talling, P. J. (2022). Turbidity currents can dictate organic carbon fluxes across river-fed fjords: an example from bute inlet (bc, canada). Journal of Geophysical Research: Biogeosciences, 127(6). https://doi.org/10.1029/2022jg006824

Hage, S., Cartigny, M.J., Sumner, E.J., Clare, M.A., Hughes Clarke, J.E., Talling, P.J., Lintern, D.G., Simmons, S.M., Silva Jacinto, R., Vellinga, A.J. and Allin, J.R., 2019. Direct monitoring reveals initiation of turbidity currents from extremely dilute river plumes. Geophysical Research Letters, 46(20), pp.11310-11320.

Hage, S., Galy, V.V., Cartigny, M.J.B., Acikalin, S., Clare, M.A., Gröcke, D.R., Hilton, R.G., Hunt, J.E., Lintern, D.G., McGhee, C.A. and Parsons, D.R., 2020. Efficient preservation of young terrestrial organic carbon in sandy turbidity-current deposits. Geology, 48(9), pp.882-887.

Hamilton, P.B., Strom, K.B., and Hoyal, D.C.J.D., 2015, Hydraulic and sediment transport properties of autogenic avulsion cycles on submarine fans with supercritical distributaries: Journal of Geophysical Research: Earth Surface, v. 120, p. 1369–1389, doi:10.1002/2014JF003414.

Hampton, M.A., Lee, H.J., Locat, J., 1996. Submarine landslides. Rev. Geophys. 34, 33–59. https://doi.org/10.1029/95RG03287

Hansen, L., Waldmann, N., Storms, J.E., Eilertsen, R.S., Ariztegui, D., Chapron, E. and Nesje, A., 2016. Morphological signatures of mass wasting and delta processes in a fjord-lake system: insights from Lovatnet, western Norway. Norwegian journal of geology, 96(3), pp.9-30. 29.33.

Hansen, L., Janocko, M., Kane, I., and Ben Kneller, B., 2017, Submarine channel evolution, terrace development, and preservation of intra-channel thin-bedded turbidites: Mahin and Avon channels, offshore Nigeria: Marine Geology, v. 383, p. 146-167, doi:10.1016/j.margeo.2016.11.011.

Hariyanto, I.H., Pratomo, D.G., Maulana, M.A., 2021. Determination of the relevant multibeam echosounder frequency to estimate the suspended sediment concentrations for environmental damage monitoring of mass movement. IOP Conf. Ser. Earth Environ. Sci. 936, 012007. https://doi.org/10.1088/1755-1315/936/1/012007

Haviv, I., Enzel, Y., Whipple, K.X., Zilberman, E., Matmon, A., Stone, J., Fifield, K.L., 2010. Evolution of vertical knickpoints (waterfalls) with resistant caprock: Insights from numerical modeling. J. Geophys. Res. Earth Surf. 115. https://doi.org/10.1029/2008JF001187

Haymon, R.M., Fornari, D.J., Von Damm, K.L., Lilley, M.D., Perfit, M.R., Edmond, J.M., Shanks, W.C., Lutz, R.A., Grebmeier, J.M., Carbotte, S., Wright, D., McLaughlin, E., Smith, M., Beedle, N., Olson, E., 1993. Volcanic eruption of the mid-ocean ridge along the East Pacific Rise crest at 9°45–52'N: Direct submersible observations of seafloor phenomena associated with an eruption event in April, 1991. Earth Planet. Sci. Lett. 119, 85–101. https://doi.org/10.1016/0012-821X(93)90008-W

Head, J.W., Wilson, L., 2003. Deep submarine pyroclastic eruptions: theory and predicted landforms and deposits. J. Volcanol. Geotherm. Res. 121, 155–193. https://doi.org/10.1016/S0377-0273(02)00425-0

Heerema, C.J., Cartigny, M.J.B., Jacinto, R.S., Simmons, S.M., Apprioual, R., Talling, P.J., 2022. How distinctive are flood-triggered turbidity currents? J. Sediment. Res. 92, 1–11. https://doi.org/10.2110/jsr.2020.168

Heidarzadeh, M., Gusman, A.R., Ishibe, T., Sabeti, R., Šepić, J., 2022. Estimating the eruption-induced water displacement source of the 15 January 2022 Tonga volcanic tsunami from tsunami spectra and numerical modelling. Ocean Eng. 261, 112165. https://doi.org/10.1016/j.oceaneng.2022.112165

Heijnen, M.S. et al., 2020, Rapidly-migrating and internally-generated knickpoints can control submarine channel evolution - Nature Communications: Nature Communications, v. 11, p. 3129, doi:10.1038/s41467-020-16861-x.

Heijnen, M.S., Clare, M.A., Cartigny, M.J., Talling, P.J., Hage, S., Pope, E.L., Bailey, L., Sumner, E., Lintern, D.G., Stacey, C. and Parsons, D.R., 2022. Fill, flush or shuffle: How is sediment carried through submarine channels to build lobes?. Earth and Planetary Science Letters, 584, p.117481.

Heiniö, P., Davies, R.J., 2007. Knickpoint migration in submarine channels in response to fold growth, western Niger Delta. Mar. Pet. Geol., 24, 434–449. https://doi.org/10.1016/j.marpetgeo.2006.09.002

Herrera, S., Chadwick, W.W., Jackson, M.G., Konter, J., McCartin, L., Pittoors, N., Bushta, E., Merle, S.G., 2023. From basalt to biosphere: Early non-vent community succession on the erupting Vailulu'u deep seamount. Front. Mar. Sci. 10.

Hickin, E.J., 1989. Contemporary Squamish River sediment flux to Howe Sound, British Columbia. Can. J. Earth Sci. 26, 1953–1963. https://doi.org/10.1139/e89-165

Hickin, E.J., and Nanson, G.C., 1975, The Character of Channel Migration on the Beatton River, Northeast British Columbia, Canada: GSA Bulletin, v. 86, p. 487–494, doi:10.1130/0016-7606(1975)86<487:TCOCMO>2.0.CO;2.

Hilbe, M., Anselmetti, F.S., 2014. Signatures of slope failures and river-delta collapses in a perialpine lake (Lake Lucerne, Switzerland). Sedimentology 61, 1883–1907. https://doi.org/10.1111/sed.12120

Hizzett, J.L., Hughes Clarke, J.E., Sumner, E.J., Cartigny, M.J.B., Talling, P.J., Clare, M.A., 2018. Which Triggers Produce the Most Erosive, Frequent, and Longest Runout Turbidity Currents on Deltas? Geophys. Res. Lett. 45, 855–863. https://doi.org/10.1002/2017GL075751

Hochfeld, I., Hort, M., Schwalbe, E., Dürig, T., 2022. Eruption dynamics of Anak Krakatau volcano (Indonesia) estimated using photogrammetric methods. Bull. Volcanol. 84, 73. https://doi.org/10.1007/s00445-022-01579-z

Hoitink, A.J.F., Wang, Z.B., Vermeulen, B., Huismans, Y., Kästner, K., 2017. Tidal controls on river delta morphology. Nat. Geosci. 10, 637–645. https://doi.org/10.1038/ngeo3000

Holland, S.S., 1976. Landforms of British Columbia: A Physiographic Outline. Department of Mines and Petroleum Resources.

Howe, B.M., Angove, M., Aucan, J., Barnes, C.R., Barros, J.S., Bayliff, N., Becker, N.C., Carrilho, F., Fouch, M.J., Fry, B., Jamelot, A., Janiszewski, H., Kong, L.S.L., Lentz, S., Luther, D.S., Marinaro, G., Matias, L.M., Rowe, C.A., Sakya, A.E., Salaree, A., Thiele, T., Tilmann, F.J., von Hillebrandt-Andrade, C., Wallace, L., Weinstein, S., Wilcock, W., 2022. SMART Subsea Cables for Observing the Earth and Ocean, Mitigating Environmental Hazards, and Supporting the Blue Economy. Front. Earth Sci. 9.

Hsu, S. K., Kuo, J., Lo, C., Tsai, C., Doo, W. B., Ku, C. Y., ... & Sibuet, J. (2008). Turbidity currents, submarine landslides and the 2006 pingtung earthquake off sw taiwan. Terrestrial, Atmospheric and Oceanic Sciences, 19(6), 767. https://doi.org/10.3319/tao.2008.19.6.767(pt)

Hughes Clarke, E.J., 2016, First wide-angle view of channelised turbidity currents links migrating cyclic steps to flow characteristics: Nature Communications, v. 7, p. 11896, doi:10.1038/ncomms11896.

Hughes Clarke, J.E., 2018. Multibeam Echosounders, in: Micallef, A., Krastel, S., Savini, A. (Eds.), Submarine Geomorphology, Springer Geology. Springer International Publishing, Cham, pp. 25–41. https://doi.org/10.1007/978-3-319-57852-1_3

Hughes Clarke, J.E., Brucker, S., Muggah, J., Hamilton, T., Cartwright, D., Church, I., Kuus, P., 2012. Temporal progression and spatial extent of mass wasting events on the Squamish prodelta slope. Presented at the Landslides and Engineered Slopes: Protecting Society through Improved Understanding - Proceedings of the 11th International and 2nd North American Symposium on Landslides and Engineered Slopes, 2012, pp. 1091–1096.

Hunt, J.E., Cassidy, M., Talling, P.J., 2018. Multi-stage volcanic island flank collapses with coeval explosive caldera-forming eruptions. Sci. Rep. 8, 1146. https://doi.org/10.1038/s41598-018-19285-2

Hunt, J.E., Jarvis, I., 2017. Prodigious submarine landslides during the inception and early growth of volcanic islands. Nat. Commun. 8, 2061. https://doi.org/10.1038/s41467-017-02100-3

Hunt, J.E., Talling, P.J., Clare, M.A., Jarvis, I., Wynn, R.B., 2014. Long-term (17 Ma) turbidite record of the timing and frequency of large flank collapses of the Canary Islands. Geochem. Geophys. Geosystems 15, 3322–3345. https://doi.org/10.1002/2014GC005232

Hunt, J.E., Tappin, D.R., Watt, S.F.L., Susilohadi, S., Novellino, A., Ebmeier, S.K., Cassidy, M., Engwell, S.L., Grilli, S.T., Hanif, M. and Priyanto, W.S., 2021. Submarine landslide megablocks show half of Anak Krakatau island failed on December 22nd, 2018. Nature communications, 12(1), p.2827.

Ikeda, S., Parker, G., Sawai, K., 1981. Bend theory of river meanders. Part 1. Linear development. J. Fluid Mech. 112, 363–377. https://doi.org/10.1017/S0022112081000451

Inman, D.L., Nordstrom, C.E., Flick, R.E., 1976. Currents in Submarine Canyons: An Air-Sea-Land Interaction. Annu. Rev. Fluid Mech. 8, 275–310. https://doi.org/10.1146/annurev.fl.08.010176.001423

Iverson, R.M., 1997. The physics of debris flows. Rev. Geophys. 35, 245–296. https://doi.org/10.1029/97RG00426

Janowski, L., Trzcinska, K., Tegowski, J., Kruss, A., Rucinska-Zjadacz, M., Pocwiardowski, P., 2018. Nearshore Benthic Habitat Mapping Based on Multi-Frequency, Multibeam Echosounder Data Using a Combined Object-Based Approach: A Case Study from the Rowy Site in the Southern Baltic Sea. Remote Sens. 10, 1983. https://doi.org/10.3390/rs10121983

Jobe, Z. R., Howes, N., Romans, B. W., & Covault, J. A. (2018). Volume and recurrence of submarine-fan-building turbidity currents. The Depositional Record, 4(2), 160-176. https://doi.org/10.1002/dep2.42

Jobe, Z.R., Howes, N.C., and Auchter, N.C., 2016, Comparing submarine and fluvial channel kinematics: Implications for stratigraphic architecture: Geology, v. 44, p. 931–934, doi:10.1130/G38158.1.

Jobe, Z.R., Howes, N.C., Straub, K.M., Cai, D., Deng, H., Laugier, F.J., Pettinga, L.A., Shumaker, L.E., 2020. Comparing Aggradation, Superelevation, and Avulsion Frequency of Submarine and Fluvial Channels. Front. Earth Sci. 8.

Jones, D.O.B., Kaiser, S., Sweetman, A.K., Smith, C.R., Menot, L., Vink, A., Trueblood, D., Greinert, J., Billett, D.S.M., Arbizu, P.M., Radziejewska, T., Singh, R., Ingole, B., Stratmann, T., Simon-Lledó, E., Durden, J.M., Clark, M.R., 2017. Biological responses to disturbance from simulated deep-sea polymetallic nodule mining. PLOS ONE 12, e0171750. https://doi.org/10.1371/journal.pone.0171750

Jorissen, E.L., de Leeuw, A., van Baak, C.G.C., Mandic, O., Stoica, M., Abels, H.A., Krijgsman, W., 2018. Sedimentary architecture and depositional controls of a Pliocene river-dominated delta in the semi-isolated Dacian Basin, Black Sea. Sediment. Geol. 368, 1–23. https://doi.org/10.1016/j.sedgeo.2018.03.001

Kameda, J., Yohei, H., 2021. Influence of biopolymers on the rheological properties of seafloor sediments and the runout behavior of submarine debris flows. Sci. Rep. 11, 1493. https://doi.org/10.1038/s41598-021-81186-8

Karstens, J., Preine, J., Carey, S., Bell, K.L.C., Nomikou, P., Hübscher, C., Lampridou, D., Urlaub, M., 2023. Formation of undulating seafloor bedforms during the Minoan eruption and their implications for eruption dynamics and slope stability at Santorini. Earth Planet. Sci. Lett. 616, 118215. https://doi.org/10.1016/j.epsl.2023.118215

Keevil, G.M., Peakall, J., Best, J.L., 2007. The influence of scale, slope and channel geometry on the flow dynamics of submarine channels. Mar. Pet. Geol., Sinuous Deep-Water Channels: Genesis, Geometry and Architecture 24, 487–503. https://doi.org/10.1016/j.marpetgeo.2007.01.009

Keevil, G.M., Peakall, J., Best, J.L., and Amos, K.J., 2006, Flow structure in sinuous submarine channels: Velocity and turbulence structure of an experimental submarine channel: Marine Geology, v. 229, p. 241–257, doi:10.1016/j.margeo.2006.03.010.

Khan, M.A., Basharat, M., Riaz, M.T., Sarfraz, Y., Farooq, M., Khan, A.Y., Pham, Q.B., Ahmed, K.S., Shahzad, A., 2021. An integrated geotechnical and geophysical investigation of a catastrophic landslide in the Northeast Himalayas of Pakistan. Geol. J. 56, 4760–4778. https://doi.org/10.1002/gj.4209

Khripounoff, A., Vangriesheim, A., Babonneau, N., Crassous, P., Dennielou, B., Savoye, B., 2003. Direct observation of intense turbidity current activity in the Zaire submarine valley at 4000 m water depth. Mar. Geol. 194, 151–158. https://doi.org/10.1016/S0025-3227(02)00677-1

Kim, W., Dai, A., Muto, T., Parker, G., 2009. Delta progradation driven by an advancing sediment source: Coupled theory and experiment describing the evolution of elongated deltas. Water Resour. Res. 45. https://doi.org/10.1029/2008WR007382

Klein, A., 2022. Tongan volcano erupts. New Sci. 253, 7. https://doi.org/10.1016/S0262-4079(22)00074-4

Kokelaar, P., Busby, C., 1992. Subaqueous Explosive Eruption and Welding of Pyroclastic Deposits. Science 257, 196–201. https://doi.org/10.1126/science.257.5067.196

Kokelaar, P., Raine, P., Branney, M.J., 2007. Incursion of a large-volume, spatter-bearing pyroclastic density current into a caldera lake: Pavey Ark ignimbrite, Scafell caldera, England. Bull. Volcanol. 70, 23–54. https://doi.org/10.1007/s00445-007-0118-5

Kolla, V., Bandyopadhyay, A., Gupta, P., Mukherjee, B., and Ramana, D.V., 2012, Morphology and Internal Structure of a Recent Upper Bengal Fan-Valley Complex, in Prather, B.E., Deptuck, M.E., Mohrig, D., Hoorn, B.V., and Wynn, R.B. eds., Application of the Principles of Seismic Geomorphology to Continental Slope and Base-of-Slope Systems: Case Studies from SeaFloor and Near-Sea Floor Analogues, SEPM Society for Sedimentary Geology, v. 99, p. 0, doi:10.2110/pec.12.99.0347.

Kostaschuk, R., McCann, S., 1989. Submarine Slope Stability of a Fjord Delta: Bella Coola, British Columbia. Géographie Phys. Quat. 43, 87–95. https://doi.org/10.7202/032756ar

Kostic, S., 2011. Modeling of submarine cyclic steps: Controls on their formation, migration, and architecture. Geosphere 7, 294–304. https://doi.org/10.1130/GES00601.1

Kostic, S., 2014. Upper flow regime bedforms on levees and continental slopes: Turbidity current flow dynamics in response to fine-grained sediment waves. Geosphere 10, 1094–1103. https://doi.org/10.1130/GES01015.1

Kramer, S.L., 1988. Triggering of liquefaction flow slides in coastal soil deposits. Eng. Geol. 26, 17–31. https://doi.org/10.1016/0013-7952(88)90004-X

Kremer, K., Hilbe, M., Simpson, G., Decrouy, L., Wildi, W., Girardclos, S., 2015. Reconstructing 4000 years of mass movement and tsunami history in a deep peri-Alpine lake (Lake Geneva, France-Switzerland). Sedimentology 62, 1305–1327. https://doi.org/10.1111/sed.12190

Kuenen, P.H. and Migliorini, C.I., 1950. Turbidity currents as a cause of graded bedding. The Journal of Geology, 58(2), pp.91-127.

Kurnio, H., Tuakia, M.Z., Aryanto, N.C.D., Pardiarto, B., Tampubolon, A., Kusnawan, Widi, B.N., Widodo, W., 2023. The characteristics of submarine landslide sediments in Eastern Indonesia with study case in Kai Archipelago Waters and Surrounding Area. IOP Conf. Ser. Earth Environ. Sci. 1163, 012013. https://doi.org/10.1088/1755-1315/1163/1/012013

Kvenvolden, K.A., 1993. Gas hydrates—geological perspective and global change. Rev. Geophys. 31, 173–187. https://doi.org/10.1029/93RG00268

Kvenvolden, K.A., 1999. Potential effects of gas hydrate on human welfare. Proc. Natl. Acad. Sci. 96, 3420–3426. https://doi.org/10.1073/pnas.96.7.3420

Laake, A.W., Sheneshen, M.S., Strobbia, C., Velasco, L., Cutts, A., 2011. Integration of surface/subsurface techniques reveals faults in Gulf of Suez oilfields. Pet. Geosci. 17, 165–179. https://doi.org/10.1144/1354-079310-014

Lai, S.Y.J., Amblas, D., Micallef, A., Gerber, T.P., Capart, H., 2022. Evolution of submarine canyon-fan systems in fault-controlled margins: Insights from physical experiments. Earth Surf. Dyn. Discuss. 1–26. https://doi.org/10.5194/esurf-2022-62

Lai, V.H., Tsai, V.C., Lamb, M.P., Ulizio, T.P., Beer, A.R., 2018. The Seismic Signature of Debris Flows: Flow Mechanics and Early Warning at Montecito, California. Geophys. Res. Lett. 45, 5528–5535. https://doi.org/10.1029/2018GL077683

Lamarche, G., Lurton, X., 2018. Recommendations for improved and coherent acquisition and processing of backscatter data from seafloor-mapping sonars. Mar. Geophys. Res. 39, 5–22. https://doi.org/10.1007/s11001-017-9315-6

Lamb, M.P., Parsons, J.D., Mullenbach, B.L., Finlayson, D.P., Orange, D.L., Nittrouer, C.A., 2008. Evidence for superelevation, channel incision, and formation of cyclic steps by turbidity currents in Eel Canyon, California. GSA Bull. 120, 463–475. https://doi.org/10.1130/B26184.1

Le Friant, A., Ishizuka, O., Boudon, G., Palmer, M.R., Talling, P.J., Villemant, B., Adachi, T., Aljahdali, M., Breitkreuz, C., Brunet, M., Caron, B., Coussens, M., Deplus, C., Endo, D., Feuillet, N., Fraas, A.J., Fujinawa, A., Hart, M.B., Hatfield, R.G., Hornbach, M., Jutzeler, M., Kataoka, K.S., Komorowski, J.-C., Lebas, E., Lafuerza, S., Maeno, F., Manga, M., Martínez-Colón, M., McCanta, M., Morgan, S., Saito, T., Slagle, A., Sparks, S., Stinton, A., Stroncik, N., Subramanyam, K.S.V., Tamura, Y., Trofimovs, J., Voight, B., Wall-Palmer, D., Wang, F., Watt, S.F.L., 2015. Submarine record of volcanic island construction and collapse in the Lesser Antilles arc: First scientific drilling of submarine volcanic island landslides by IODP Expedition 340. Geochem. Geophys. Geosystems 16, 420–442. https://doi.org/10.1002/2014GC005652

Leat, P.T., Tate, A.J., Tappin, D.R., Day, S.J., Owen, M.J., 2010. Growth and mass wasting of volcanic centers in the northern South Sandwich arc, South Atlantic, revealed by new multibeam mapping. Mar. Geol. 275, 110–126. https://doi.org/10.1016/j.margeo.2010.05.001

Lecours, V., Devillers, R., Schneider, D.C., Lucieer, V.L., Brown, C.J., Edinger, E.N., 2015. Spatial scale and geographic context in benthic habitat mapping: review and future directions. Mar. Ecol. Prog. Ser. 535, 259–284. https://doi.org/10.3354/meps11378

Lecours, V., Dolan, M.F.J., Micallef, A., Lucieer, V.L., 2016. A review of marine geomorphometry, the quantitative study of the seafloor. Hydrol. Earth Syst. Sci. 20, 3207–3244. https://doi.org/10.5194/hess-20-3207-2016

Lee, H., Ryan, H., Kayen, R.E., Haeussler, P.J., Dartnell, P. and Hampton, M.A., 2006. Varieties of submarine failure morphologies of seismically-induced landslides in Alaskan fjords. Norwegian Journal of Geology/Norsk Geologisk Forening, 86(3).

Lee, H.J., 2009. Timing of occurrence of large submarine landslides on the Atlantic Ocean margin. Mar. Geol., Tsunami hazard along the U.S. Atlantic coast 264, 53–64. https://doi.org/10.1016/j.margeo.2008.09.009

Lee, H.J., Syvitski, J.P.M., Parker, G., Orange, D., Locat, J., Hutton, E.W.H., Imran, J., 2002. Distinguishing sediment waves from slope failure deposits: field examples, including the 'Humboldt slide', and modelling results. Mar. Geol. 192, 79–104. https://doi.org/10.1016/S0025-3227(02)00550-9

Li, D.-Q., Xiao, T., Cao, Z.-J., Zhou, C.-B., Zhang, L.-M., 2016. Enhancement of random finite element method in reliability analysis and risk assessment of soil slopes using Subset Simulation. Landslides 13, 293–303. https://doi.org/10.1007/s10346-015-0569-2

Li, R., Lei, J., Kusche, J., Dang, T., Huang, F., Luan, X., Zhang, S.-R., Yan, M., Yang, Z., Liu, F., Dou, X., 2023. Large-Scale Disturbances in the Upper Thermosphere Induced by the 2022 Tonga Volcanic Eruption. Geophys. Res. Lett. 50, e2022GL102265. https://doi.org/10.1029/2022GL102265

Lintern, G., Blais-Stevens, A., Stacey, C., Shaw, J., Bobrowsky, P., Conway, K., Huntley, D., Mackillop, K., Overeem, I. and Scherwath, M., 2019. Providing multidisciplinary scientific

advice for coastal planning in Kitimat Arm, British Columbia. Geological Society, London, Special Publications, 477(1), pp.567-581.

Liu, J. T., Wang, Y., Yang, R. J., Hsu, R. T., Kao, S., Lin, H., ... & Kuo, F. H. (2012). Cyclone-induced hyperpycnal turbidity currents in a submarine canyon. Journal of Geophysical Research: Oceans, 117(C4). https://doi.org/10.1029/2011jc007630

Loget, N., Van Den Driessche, J., 2009. Wave train model for knickpoint migration. Geomorphology 106, 376–382. https://doi.org/10.1016/j.geomorph.2008.10.017Lotteri, A., Speake, J., Kennedy, V., Wallenstein, N., Coutinho, R., Chester, D., Duncan, A., Dibben, C., Ferreira, F., 2021. Changing hazard awareness over two decades: the case of Furnas, São Miguel (Azores). Geol. Soc. Lond. Spec. Publ. 519, SP519-2020–120. https://doi.org/10.1144/SP519-2020-120

Løvholt, F., Schulten, I., Mosher, D., Harbitz, C., Krastel, S., 2019. Modelling the 1929 Grand Banks slump and landslide tsunami. Geol. Soc. Lond. Spec. Publ. 477, 315–331. https://doi.org/10.1144/SP477.28

Łubczonek, J., Kazimierski, W., Zaniewicz, G., & Łącka, M. (2021). Methodology for combining data acquired by unmanned surface and aerial vehicles to create digital bathymetric models in shallow and ultra-shallow waters. Remote Sensing, 14(1), 105. https://doi.org/10.3390/rs14010105

Lynett, P., McCann, M., Zhou, Z., Renteria, W., Borrero, J., Greer, D., Fa'anunu, O., Bosserelle, C., Jaffe, B., La Selle, S., Ritchie, A., Snyder, A., Nasr, B., Bott, J., Graehl, N., Synolakis, C., Ebrahimi, B., Cinar, G.E., 2022. Diverse tsunamigenesis triggered by the Hunga Tonga-Hunga Ha'apai eruption. Nature 609, 728–733. https://doi.org/10.1038/s41586-022-05170-6

Maier, K.L., Fildani, A., McHargue, T.R., Paull, C.K., Graham, S.A., and Caress, D.W., 2012, Punctuated Deep-Water Channel Migration: High-Resolution Subsurface Data from the Lucia Chica Channel System, Offshore California, U.S.A: Journal of Sedimentary Research, v. 82, p. 1–8, doi:10.2110/jsr.2012.10.

Major, J.J., 1997. Depositional Processes in Large-Scale Debris-Flow Experiments. J. Geol. 105, 345–366. https://doi.org/10.1086/515930

Martínez-Doñate, A., Privat, A.M.-L.J., Hodgson, D.M., Jackson, C.A.-L., Kane, I.A., Spychala, Y.T., Duller, R.A., Stevenson, C., Keavney, E., Schwarz, E., Flint, S.S., 2021. Substrate Entrainment, Depositional Relief, and Sediment Capture: Impact of a Submarine Landslide on Flow Process and Sediment Supply. Front. Earth Sci. 9.

Maslin, M., Owen, M., Day, S., Long, D., 2004. Linking continental-slope failures and climate change: Testing the clathrate gun hypothesis. Geology 32, 53–56. https://doi.org/10.1130/G20114.1

Masson, D. g, Harbitz, C. b, Wynn, R. b, Pedersen, G., Løvholt, F., 2006. Submarine landslides: processes, triggers and hazard prediction. Philos. Trans. R. Soc. Math. Phys. Eng. Sci. 364, 2009–2039. https://doi.org/10.1098/rsta.2006.1810 43.

Mastbergen, D.R. and Van Den Berg, J.H., 2003. Breaching in fine sands and the generation of sustained turbidity currents in submarine canyons. Sedimentology, 50(4), pp.625-637.

McArthur, A.D., Crisóstomo-Figueroa, A., Wunderlich, A., Karvelas, A. and McCaffrey, W.D., 2022. Sedimentation on structurally complex slopes: Neogene to recent deep-water sedimentation patterns across the central Hikurangi subduction margin, New Zealand. Basin Research, 34(5), pp.1807-1837. 44.

McArthur, A.D., Tek, D.E., Poyatos-Moré, M., Colombera, L. and McCaffrey, W.D., 2024. Deep-ocean channel-wall collapse order of magnitude larger than any other documented. Communications Earth & Environment, 5(1), 143.

Metwalli, F.I., Yousif, M.S., Dally, N.H.E., Ata, A.S.A.E., 2019. Seismic Structural Analysis of the Alam-El Bueib Formation, Qasr Oil Field, North Western desert, Egypt. Edelweiss Appl. Sci. Technol. 3, 20–25. https://doi.org/10.33805/2576-8484.163

Micallef, A., Le Bas, T.P., Huvenne, V.A.I., Blondel, P., Hühnerbach, V., Deidun, A., 2012. A multi-method approach for benthic habitat mapping of shallow coastal areas with high-resolution multibeam data. Cont. Shelf Res. 39–40, 14–26. https://doi.org/10.1016/j.csr.2012.03.008 45.

Micallef, A., Mountjoy, J.J., Barnes, P.M., Canals, M. and Lastras, G., 2014. Geomorphic response of submarine canyons to tectonic activity: Insights from the Cook Strait canyon system, New Zealand. Geosphere, 10(5), pp.905-929.

Milliman, J.D., Farnsworth, K.L., 2011. River Discharge to the Coastal Ocean: A Global Synthesis. Cambridge University Press, Cambridge. https://doi.org/10.1017/CBO9780511781247Mishra, R., Pandey, D.K., Ramesh, P., Clift, P.D., 2016. Identification of new deep sea sinuous channels in the eastern Arabian Sea. SpringerPlus 5, 844. https://doi.org/10.1186/s40064-016-2497-6 38.46.

Miramontes, E., Eggenhuisen, J.T., Jacinto, R.S., Poneti, G., Pohl, F., Normandeau, A., Campbell, D.C. and Hernández-Molina, F.J., 2020. Channel-levee evolution in combined contour current–turbidity current flows from flume-tank experiments. Geology, 48(4), pp.353-357.

Mitchell, N.C., 2006, Morphologies of knickpoints in submarine canyons: GSA Bulletin, v. 118, p. 589–605, doi:10.1130/B25772.1. 39.49. 48.

Mitchell, N.C., 2014. Bedrock erosion by sedimentary flows in submarine canyons. Geosphere, 10(5), pp.892-904.

Mitchell, W.H., Whittaker, A.C., Mayall, M., Lonergan, L. and Pizzi, M., 2021. Quantifying the relationship between structural deformation and the morphology of submarine channels on the Niger Delta continental slope. Basin Research, 33(1), pp.186-209.

Moss, R.E., Seed, R.B., Kayen, R.E., Stewart, J.P., Der Kiureghian, A., Cetin, K.O., 2006. CPT-Based Probabilistic and Deterministic Assessment of In Situ Seismic Soil Liquefaction Potential. J. Geotech. Geoenvironmental Eng. 132, 1032–1051. https://doi.org/10.1061/(ASCE)1090-0241(2006)132:8(1032)

Mountjoy, J.J., Howarth, J.D., Orpin, A.R., Barnes, P.M., Bowden, D.A., Rowden, A.A., Schimel, A.C.G., Holden, C., Horgan, H.J., Nodder, S.D., Patton, J.R., Lamarche, G., Gerstenberger, M., Micallef, A., Pallentin, A., Kane, T., 2018. Earthquakes drive large-scale submarine canyon development and sediment supply to deep-ocean basins. Sci. Adv. 4, eaar3748. https://doi.org/10.1126/sciadv.aar3748

Mulder, T., 2011, Chapter 2 - Gravity Processes and Deposits on Continental Slope, Rise and Abyssal Plains, in HüNeke, H. and Mulder, T. eds., Developments in Sedimentology, Elsevier, Deep-Sea Sediments, v. 63, p. 25–148, doi:10.1016/B978-0-444-53000-4.00002-0.

Mycek, P., Gaurier, B., Germain, G., Pinon, G., Rivoalen, E., 2013. Numerical and experimental study of the interaction between two marine current turbines. Int. J. Mar. Energy 1, 70–83. https://doi.org/10.1016/j.ijome.2013.05.007

Nakanishi, M. and Hashimoto, J. (2011). A precise bathymetric map of the world's deepest seafloor, challenger deep in the mariana trench. Marine Geophysical Research, 32(4), 455-463. https://doi.org/10.1007/s11001-011-9134-0

Nemati, F., Leonard, L., Lintern, G., Brillon, C., Schaeffer, A., Thomson, R., 2023. Detection of Landslides and Tsunamis in Douglas Channel and Gardner Canal, British Columbia. Oceanography. https://doi.org/10.5670/oceanog.2023.s1.25

Nienhuis, J.H., Ashton, A.D., Edmonds, D.A., Hoitink, A.J.F., Kettner, A.J., Rowland, J.C. and Törnqvist, T.E., 2020. Global-scale human impact on delta morphology has led to net land area gain. Nature, 577(7791), pp.514-518.

Nienhuis, J.H., Ashton, A.D., Edmonds, D.A., Hoitink, A.J.F., Kettner, A.J., Rowland, J.C. and Törnqvist, T.E., 2020. Global-scale human impact on delta morphology has led to net land area gain. Nature, 577(7791), pp.514-518.

Normandeau, A., Campbell, D.C., Piper, D.J.W., Jenner, K.A., 2019. Are submarine landslides an underestimated hazard on the western North Atlantic passive margin? Geology 47, 848–852. https://doi.org/10.1130/G46201.1

Normandeau, A., Lajeunesse, P., Poiré, A.G., Francus, P., 2016. Morphological expression of bedforms formed by supercritical sediment density flows on four fjord-lake deltas of the south-eastern Canadian Shield (Eastern Canada). Sedimentology 63, 2106–2129. https://doi.org/10.1111/sed.12298

Norris, J.E., Stokes, A., Mickovski, S.B., Cammeraat, E., Van Beek, R., Nicoll, B.C., Achim, A. (Eds.), 2008. Slope Stability and Erosion Control: Ecotechnological Solutions. Springer Netherlands, Dordrecht. https://doi.org/10.1007/978-1-4020-6676-4

Pakoksung, K., Suppasri, A., Imamura, F., 2022. The near-field tsunami generated by the 15 January 2022 eruption of the Hunga Tonga-Hunga Ha'apai volcano and its impact on Tongatapu, Tonga. Sci. Rep. 12, 15187. https://doi.org/10.1038/s41598-022-19486-w

Palm, F.A., Peakall, J., Hodgson, D.M., Marsset, T., Silva Jacinto, R., Dennielou, B., Babonneau, N., and Wright, T.J., 2021, Width variation around submarine channel bends: Implications for sedimentation and channel evolution: Marine Geology, v. 437, p. 106504, doi:10.1016/j.margeo.2021.106504.

Pandolpho, B. (2023). Identification and differentiation of vertical movement through morphological changes and stratigraphic imprint: two distinct uplifting mechanisms in the upper calabrian accretionary wedge, western ionian sea. Basin Research, 36(1). https://doi.org/10.1111/bre.12819

Paris, R., 2015. Source mechanisms of volcanic tsunamis. Philos. Trans. R. Soc. Math. Phys. Eng. Sci. 373, 20140380. https://doi.org/10.1098/rsta.2014.0380

Paris, R., Switzer, A.D., Belousova, M., Belousov, A., Ontowirjo, B., Whelley, P.L., Ulvrova, M., 2014. Volcanic tsunami: a review of source mechanisms, past events and hazards in Southeast Asia (Indonesia, Philippines, Papua New Guinea). Nat. Hazards 70, 447–470. https://doi.org/10.1007/s11069-013-0822-8

Parsons, D.R., Peakall, J., Aksu, A.E., Flood, R.D., Hiscott, R.N., Beşiktepe, Ş., and Mouland, D., 2010, Gravity-driven flow in a submarine channel bend: Direct field evidence of helical flow reversal: Geology, v. 38, p. 1063–1066, doi:10.1130/G31121.1.

Parsons, J.D., Bush, J.W.M., Syvitski, J.P.M., 2001. Hyperpycnal plume formation from riverine outflows with small sediment concentrations. Sedimentology 48, 465–478. https://doi.org/10.1046/j.1365-3091.2001.00384.x

Paull, C.K., Caress, D.W., Lundsten, E., Gwiazda, R., Anderson, K., McGann, M., Conrad, J., Edwards, B., Sumner, E.J., 2013. Anatomy of the La Jolla Submarine Canyon system; offshore southern California. Mar. Geol. 335, 16–34. https://doi.org/10.1016/j.margeo.2012.10.003

Paull, C.K., Talling, P.J., Maier, K.L., Parsons, D., Xu, J., Caress, D.W., Gwiazda, R., Lundsten, E.M., Anderson, K., Barry, J.P., Chaffey, M., O'Reilly, T., Rosenberger, K.J., Gales, J.A., Kieft, B., McGann, M., Simmons, S.M., McCann, M., Sumner, E.J., Clare, M.A., Cartigny, M.J., 2018. Powerful turbidity currents driven by dense basal layers. Nat. Commun. 9, 4114. https://doi.org/10.1038/s41467-018-06254-6

Paull, C.K., Ussler III, W., Caress, D.W., Lundsten, E., Covault, J.A., Maier, K.L., Xu, J., Augenstein, S., 2010. Origins of large crescent-shaped bedforms within the axial channel of Monterey Canyon, offshore California. Geosphere 6, 755–774. https://doi.org/10.1130/GES00527.1

Peakall, J., Amos, K.J., Keevil, G.M., William Bradbury, P., and Gupta, S., 2007, Flow processes and sedimentation in submarine channel bends: Marine and Petroleum Geology, v. 24, p. 470–486, doi:10.1016/j.marpetgeo.2007.01.008.

Peakall, J., and Sumner, E.J., 2015, Submarine channel flow processes and deposits: A process-product perspective: Geomorphology, v. 244, p. 95–120, doi:10.1016/j.geomorph.2015.03.005.

Peakall, J., McCaffrey, B., and Kneller, B., 2000, A Process Model for the Evolution, Morphology, and Architecture of Sinuous Submarine Channels: Journal of Sedimentary Research, v. 70, p. 434–448, doi:10.1306/2DC4091C-0E47-11D7-8643000102C1865D. 57.

Peakall, J., Best, J., Baas, J.H., Hodgson, D.M., Clare, M.A., Talling, P.J., Dorrell, R.M. and Lee, D.R., 2020. An integrated process-based model of flutes and tool marks in deep-water environments: Implications for palaeohydraulics, the Bouma sequence and hybrid event beds. Sedimentology, 67(4), 1601-1666.

Piper, D.J., Cochonat, P. and Morrison, M.L., 1999. The sequence of events around the epicentre of the 1929 Grand Banks earthquake: initiation of debris flows and turbidity current inferred from sidescan sonar. Sedimentology, 46(1), pp.79-97.

Piper, D.J.W., Normark, W.R., 2009. Processes That Initiate Turbidity Currents and Their Influence on Turbidites: A Marine Geology Perspective. J. Sediment. Res. 79, 347–362. https://doi.org/10.2110/jsr.2009.046

Pohl, F., Eggenhuisen, J.T., Kane, I.A., Clare, M.A., 2020. Transport and Burial of Microplastics in Deep-Marine Sediments by Turbidity Currents. Environ. Sci. Technol. 54, 4180–4189. https://doi.org/10.1021/acs.est.9b07527

Poli, P., Shapiro, N.M., 2022. Rapid Characterization of Large Volcanic Eruptions: Measuring the Impulse of the Hunga Tonga Ha'apai Explosion From Teleseismic Waves. Geophys. Res. Lett. 49, e2022GL098123. https://doi.org/10.1029/2022GL098123

Pope, E.L., Jutzeler, M., Cartigny, M.J.B., Shreeve, J., Talling, P.J., Wright, I.C., Wysoczanski, R.J., 2018. Origin of spectacular fields of submarine sediment waves around volcanic islands. Earth Planet. Sci. Lett. 493, 12–24. https://doi.org/10.1016/j.epsl.2018.04.020

Pope, E.L., Cartigny, M., Clare, M., Talling, P. J., Lintern, G., Vellinga, A., ... & Vendettuoli, D. (2022). First source-to-sink monitoring shows dense head controls sediment flux and runout in turbidity currents. Science Advances, 8(20). https://doi.org/10.1126/sciadv.abj3220 47.58.

Pope, E.L., Heijnen, M.S., Talling, P.J., Jacinto, R.S., Gaillot, A., Baker, M.L., Hage, S., Hasenhündl, M., Heerema, C.J., McGhee, C. and Ruffell, S.C., 2022. Carbon and sediment fluxes inhibited in the submarine Congo Canyon by landslide-damming. Nature Geoscience, 15(10), pp.845-853.

Porębski, S. J. and Steel, R. J. (2006). Deltas and sea-level change. Journal of Sedimentary Research, 76(3), 390-403. https://doi.org/10.2110/jsr.2006.034

Porskamp, P., Schimel, A.C.G., Young, M., Rattray, A., Ladroit, Y., Ierodiaconou, D., 2022. Integrating multibeam echosounder water-column data into benthic habitat mapping. Limnol. Oceanogr. 67, 1701–1713. https://doi.org/10.1002/lno.12160

Postma, G., Kleverlaan, K., Cartigny, M.J.B., 2014. Recognition of cyclic steps in sandy and gravelly turbidite sequences, and consequences for the Bouma facies model. Sedimentology 61, 2268–2290. https://doi.org/10.1111/sed.12135

Prior, D.B., Bornhold, B.D., Wiseman, W.J., Lowe, D.R., 1987. Turbidity Current Activity in a British Columbia Fjord. Science 237, 1330–1333. https://doi.org/10.1126/science.237.4820.1330

Prior, D.B., Yang, Z.-S., Bornhold, B.D., Keller, G.H., Lu, N.Z., Wiseman, W.J., Wright, L.D., Zhang, J., 1986. Active slope failure, sediment collapse, and silt flows on the modern subaqueous Huanghe (Yellow River) delta. Geo-Mar. Lett. 6, 85–95. https://doi.org/10.1007/BF02281644

Proud, S.R., Prata, A.T., Schmauß, S., 2022. The January 2022 eruption of Hunga Tonga-Hunga Ha'apai volcano reached the mesosphere. Science 378, 554–557. https://doi.org/10.1126/science.abo4076

Puig, P., Canals, M., Company, J.B., Martín, J., Amblas, D., Lastras, G., Palanques, A., Calafat, A.M., 2012. Ploughing the deep sea floor. Nature 489, 286–289. https://doi.org/10.1038/nature11410

Puig, P., Palanques, A., Martín, J., 2014. Contemporary Sediment-Transport Processes in Submarine Canyons. Annu. Rev. Mar. Sci. 6, 53–77. https://doi.org/10.1146/annurev-marine-010213-135037

Purkis, S.J., Ward, S.N., Fitzpatrick, N.M., Garvin, J.B., Slayback, D., Cronin, S.J., Palaseanu-Lovejoy, M., Dempsey, A., 2023. The 2022 Hunga-Tonga megatsunami: Near-field simulation of a once-in-a-century event. Sci. Adv. 9, eadf5493. https://doi.org/10.1126/sciadv.adf5493

Rabouille, C. et al., 2019, Carbon and silica megasink in deep-sea sediments of the Congo terminal lobes: Quaternary Science Reviews, v. 222, p. 105854, doi:10.1016/j.quascirev.2019.07.036.

Ragno, N., Tambroni, N., Bolla Pittaluga, M., 2020. Effect of Small Tidal Fluctuations on the Stability and Equilibrium Configurations of Bifurcations. J. Geophys. Res. Earth Surf. 125, e2020JF005584. https://doi.org/10.1029/2020JF005584

Rahardjo, H., Lee, T.T., Leong, E.C., Rezaur, R.B., 2005. Response of a residual soil slope to rainfall. Can. Geotech. J. 42, 340–351. https://doi.org/10.1139/t04-101

Ren, P., 1992. Seafloor morphology and sedimentary processes in Knight Inlet, British Columbia . Master's thesis. University of Victoria (Canada).

Ren, P., Bornhold, B.D., and Prior, D.B., 1996, Seafloor morphology and sedimentary processes, Knight Inlet, British Columbia: Sedimentary Geology, v. 103, p. 201–228, doi:10.1016/0037-0738(95)00090-9.

Roland, E., Haeussler, P., Parsons, T., Hart, P., 2020. Submarine Landslide Kinematics Derived From High-Resolution Imaging in Port Valdez, Alaska. J. Geophys. Res. Solid Earth 125, e2019JB018007. https://doi.org/10.1029/2019JB018007

Rossi, V.M., Kim, W., Leva López, J., Edmonds, D., Geleynse, N., Olariu, C., Steel, R.J., Hiatt, M., Passalacqua, P., 2016. Impact of tidal currents on delta-channel deepening, stratigraphic architecture, and sediment bypass beyond the shoreline. Geology 44, 927–930. https://doi.org/10.1130/G38334.1

Royden, L., Taylor Perron, J., 2013. Solutions of the stream power equation and application to the evolution of river longitudinal profiles. J. Geophys. Res. Earth Surf. 118, 497–518. https://doi.org/10.1002/jgrf.20031

Salmanidou, D.M., Heidarzadeh, M., Guillas, S., 2019. Probabilistic Landslide-Generated Tsunamis in the Indus Canyon, NW Indian Ocean, Using Statistical Emulation. Pure Appl. Geophys. 176, 3099–3114. https://doi.org/10.1007/s00024-019-02187-3

Sassi, M.G., Hoitink, A.J.F., de Brye, B., Deleersnijder, E., 2012. Downstream hydraulic geometry of a tidally influenced river delta. J. Geophys. Res. Earth Surf. 117. https://doi.org/10.1029/2012JF002448

Sassi, M., Hoitink, A., Brye, B. d., Vermeulen, B., & Deleersnijder, É. (2011). Tidal impact on the division of river discharge over distributary channels in the mahakam delta. Ocean Dynamics, 61(12), 2211-2228. https://doi.org/10.1007/s10236-011-0473-9

Schofield, J.C., 1967. Notes on the geology of the Tongan Islands. N. Z. J. Geol. Geophys. 10, 1424–1428. https://doi.org/10.1080/00288306.1967.10423226

Schulten, I., Mosher, D.C., Piper, D.J.W., Krastel, S., 2019. A Massive Slump on the St. Pierre Slope, A New Perspective on the 1929 Grand Banks Submarine Landslide. J. Geophys. Res. Solid Earth 124, 7538–7561. https://doi.org/10.1029/2018JB017066

Schumm, S.A. (1963) Sinuosity of alluvial rivers on the Great Plains. GSA Bulletin, 74, 1089-1100.

Seabrook, S., Mackay, K., Watson, S.J., Clare, M.A., Hunt, J.E., Yeo, I.A., Lane, E.M., Clark, M.R., Wysoczanski, R., Rowden, A.A., Kula, T., Hoffmann, L.J., Armstrong, E., Williams, M.J.M., 2023. Volcaniclastic density currents explain widespread and diverse seafloor impacts of the 2022 Hunga Volcano eruption. Nat. Commun. 14, 7881. https://doi.org/10.1038/s41467-023-43607-2

Seminara, G., 2006. Meanders. J. Fluid Mech. 554, 271–297. https://doi.org/10.1017/S0022112006008925

Sequeiros, O.E., Bolla Pittaluga, M., Frascati, A., Pirmez, C., Masson, D.G., Weaver, P., Crosby, A.R., Lazzaro, G., Botter, G., and Rimmer, J.G., 2019, How typhoons trigger turbidity currents in submarine canyons: Scientific Reports, v. 9, p. 9220, doi:10.1038/s41598-019-45615-z.

Shor, A.N., Piper, D.J.W., Clarke, J.E.H., Mayer, L.A., 1990. Giant flute-like scour and other erosional features formed by the 1929 Grand Banks turbidity current. Sedimentology 37, 631–645. https://doi.org/10.1111/j.1365-3091.1990.tb00626.x

Shumaker, L.E., Jobe, Z.R., Johnstone, S.A., Pettinga, L.A., Cai, D., and Moody, J.D., 2018, Controls on submarine channel-modifying processes identified through morphometric scaling relationships: Geosphere, v. 14, p. 2171–2187, doi:10.1130/GES01674.1.

Silva, T.A., Girardclos, S., Stutenbecker, L., Bakker, M., Costa, A., Schlunegger, F., Lane, S.N., Molnar, P., and Loizeau, J.-L., 2019, The sediment budget and dynamics of a delta-canyon-lobe system over the Anthropocene timescale: The Rhone River delta, Lake Geneva (Switzerland/France): Sedimentology, v. 66, p. 838–858, doi:10.1111/sed.12519.

Silver, E., Day, S., Ward, S., Hoffmann, G., Llanes, P., Driscoll, N., Appelgate, B., Saunders, S., 2009. Volcano collapse and tsunami generation in the Bismarck Volcanic Arc, Papua New Guinea. J. Volcanol. Geotherm. Res. 186, 210–222. https://doi.org/10.1016/j.jvolgeores.2009.06.013

Simmons, S., Azpiroz-Zabala, M., Cartigny, M., Clare, M., Cooper, C., Parsons, D. R., ... & Talling, P. J. (2020). Novel acoustic method provides first detailed measurements of sediment concentration structure within submarine turbidity currents. Journal of Geophysical Research: Oceans, 125(5). https://doi.org/10.1029/2019jc015904

Skvortsov, A., Bornhold, B., 2007. Numerical simulation of the landslide-generated tsunami in Kitimat Arm, British Columbia, Canada, 27 April 1975. J. Geophys. Res. Earth Surf. 112. https://doi.org/10.1029/2006JF000499

Slootman, A. and Cartigny, M.J., 2020. Cyclic steps: review and aggradation-based classification. Earth-Science Reviews, 201, p.102949.

Smallhorn-West, P.F., Garvin, J.B., Slayback, D.A., DeCarlo, T.M., Gordon, S.E., Fitzgerald, S.H., Halafihi, T., Jones, G.P., Bridge, T.C.L., 2020. Coral reef annihilation, persistence and recovery at Earth's youngest volcanic island. Coral Reefs 39, 529–536. https://doi.org/10.1007/s00338-019-01868-8

Sovilla, B., Schaer, M., Kern, M., Bartelt, P., 2008. Impact pressures and flow regimes in dense snow avalanches observed at the Vallée de la Sionne test site. J. Geophys. Res. Earth Surf. 113. https://doi.org/10.1029/2006JF000688

Spinewine, B., Sequeiros, O.E., Garcia, M.H., Beaubouef, R.T., Sun, T., Savoye, B., and Parker, G., 2009, Experiments on Wedge-Shaped Deep Sea Sedimentary Deposits in Minibasins and/or on Channel Levees Emplaced by Turbidity Currents. Part II. Morphodynamic Evolution of the Wedge and of the Associated Bedforms: Journal of Sedimentary Research, v. 79, p. 608–628, doi:10.2110/jsr.2009.065.

Stagna, M.D., Maselli, V., van Vliet, A., 2023. Large-scale submarine landslide drives long-lasting regime shift in slope sediment deposition. Geology 51, 167–173. https://doi.org/10.1130/G50463.1

Stevenson, C.J., Feldens, P., Georgiopoulou, A., Schönke, M., Krastel, S., Piper, D.J.W., Lindhorst, K., Mosher, D., 2018. Reconstructing the sediment concentration of a giant submarine gravity flow. Nat. Commun. 9, 2616. https://doi.org/10.1038/s41467-018-05042-6

Stevenson, C.J., Jackson, C.A.-L., Hodgson, D.M., Hubbard, S.M., Eggenhuisen, J.T., 2015. Deep-Water Sediment Bypass. J. Sediment. Res. 85, 1058–1081. https://doi.org/10.2110/jsr.2015.63

Straub, K.M., Mohrig, D., McElroy, B., Buttles, J., Pirmez, C., 2008. Interactions between turbidity currents and topography in aggrading sinuous submarine channels: A laboratory study. GSA Bull. 120, 368–385. https://doi.org/10.1130/B25983.1

Stright, L., Jobe, Z., Fosdick, J.C., and Bernhardt, A., 2017, Modeling uncertainty in the three-dimensional structural deformation and stratigraphic evolution from outcrop data: Implications for submarine channel knickpoint recognition: Marine and Petroleum Geology, v. 86, p. 79–94, doi:10.1016/j.marpetgeo.2017.05.004.

Sultan, N., Cochonat, P., Canals, M., Cattaneo, A., Dennielou, B., Haflidason, H., Laberg, J.S., Long, D., Mienert, J., Trincardi, F., Urgeles, R., Vorren, T.O., Wilson, C., 2004. Triggering mechanisms of slope instability processes and sediment failures on continental margins: a geotechnical approach. Mar. Geol., COSTA - Continental Slope Stability 213, 291–321. https://doi.org/10.1016/j.margeo.2004.10.011

Sultan, N., Garziglia, S., Bompais, X., Woerther, P., Witt, C., Kopf, A. and Migeon, S., 2020. Transient groundwater flow through a coastal confined aquifer and its impact on nearshore submarine slope instability. Journal of Geophysical Research: Earth Surface, 125(9), p.e2020JF005654.

Summers, G., Lim, A., Wheeler, A.J., 2021. A Scalable, Supervised Classification of Seabed Sediment Waves Using an Object-Based Image Analysis Approach. Remote Sens. 13, 2317. https://doi.org/10.3390/rs13122317

Sumner, E.J., Paull, C.K., 2014. Swept away by a turbidity current in Mendocino submarine canyon, California. Geophys. Res. Lett. 41, 7611–7618. https://doi.org/10.1002/2014GL061863

Sumner, E.J., Peakall, J., Dorrell, R.M., Parsons, D.R., Darby, S.E., Wynn, R.B., McPhail, S.D., Perrett, J., Webb, A., and White, D., 2014, Driven around the bend: Spatial evolution and controls on the orientation of helical bend flow in a natural submarine gravity current: Journal of Geophysical Research: Oceans, v. 119, p. 898–913, doi:10.1002/2013JC009008.

Sun, W., Kuriakose, A.K., Li, G., Li, Yu, Zhao, X., Hu, L., Yang, S., Xie, H., Li, Yi, Ning, B., Liu, L., 2022. Unseasonal super ionospheric plasma bubble and scintillations seeded by the 2022 Tonga Volcano Eruption related perturbations. J. Space Weather Space Clim. 12, 25. https://doi.org/10.1051/swsc/2022024

Sylvester, Z., and Covault, J.A., 2016, Development of cutoff-related knickpoints during early evolution of submarine channels: Geology, v. 44, p. 835–838, doi:10.1130/G38397.1. 57.69.

Sylvester, Z., Pirmez, C., and Cantelli, A., 2011, A model of submarine channel-levee evolution based on channel trajectories: Implications for stratigraphic architecture: Marine and Petroleum Geology, v. 28, p. 716–727, doi:10.1016/j.marpetgeo.2010.05.012

Sylvester, Z., Durkin, P., and Covault, J.A., 2019, High curvatures drive river meandering: Geology, v. 47, p. 263–266, doi:10.1130/G45608.1. 59.71.

Sylvester, Z., Durkin, P.R., Hubbard, S.M. and Mohrig, D., 2021, Autogenic translation and counter point bar deposition in meandering rivers. Geological Society of America Bulletin, 133, 2439-2456

Sylvester, Z., Pirmez, C., and Cantelli, A., 2011, A model of submarine channel-levee evolution based on channel trajectories: Implications for stratigraphic architecture: Marine and Petroleum Geology, v. 28, p. 716–727, doi:10.1016/j.marpetgeo.2010.05.012

Symons, W.O., Sumner, E.J., Talling, P.J., Cartigny, M.J.B., Clare, M.A., 2016. Large-scale sediment waves and scours on the modern seafloor and their implications for the prevalence of supercritical flows. Mar. Geol. 371, 130–148. https://doi.org/10.1016/j.margeo.2015.11.009

Synolakis, C.E., Bardet, J.-P., Borrero, J.C., Davies, H.L., Okal, E.A., Silver, E.A., Sweet, S., Tappin, D.R., 2002. The slump origin of the 1998 Papua New Guinea Tsunami. Proc. R. Soc. Lond. Ser. Math. Phys. Eng. Sci. 458, 763–789. https://doi.org/10.1098/rspa.2001.0915

Syvitski, J.P.M., Farrow, G.E., 1983. Structures and processes in bayhead deltas: Knight and bute inlet, British Columbia. Sediment. Geol. 36, 217–244. https://doi.org/10.1016/0037-0738(83)90010-6

Syvitski, J.P.M., Saito, Y., 2007. Morphodynamics of deltas under the influence of humans. Glob. Planet. Change 57, 261–282. https://doi.org/10.1016/j.gloplacha.2006.12.001

Talling, P.J., Baker, M., Pope, E., Cula, C.A., Cartigny, M., Faria, R., Clare, M.A., Simmons, S., Jacinto, R.S., Heijnen, M., Hage, S., Heerema, C.J., Ruffell, S., McGee, C., Hasenhündl, M., Appriοual, R., Gaillot, A., Wallace, D., Griffiths, A., Tshimanga, R., Bola, G., Trigg, M., Robertson, R., Urlaub, M., Parsons, D., Nambala, L., Nunny, R., 2021. Novel sensor array helps to understand submarine cable faults off West Africa.

Talling, P.J., Baker, M.L., Pope, E.L., Ruffell, S.C., Jacinto, R.S., Heijnen, M.S., Hage, S., Simmons, S.M., Hasenhündl, M., Heerema, C.J., McGhee, C., Appriοual, R., Ferrant, A., Cartigny, M.J.B., Parsons, D.R., Clare, M.A., Tshimanga, R.M., Trigg, M.A., Cula, C.A., Faria, R., Gaillot, A., Bola, G., Wallance, D., Griffiths, A., Nunny, R., Urlaub, M., Peirce, C., Burnett, R., Neasham, J., Hilton, R.J., 2022. Longest sediment flows yet measured show how major rivers connect efficiently to deep sea. Nat. Commun. 13, 4193. https://doi.org/10.1038/s41467-022-31689-3

Talling, P.J., Cartigny, M.J., Pope, E., Baker, M., Clare, M.A., Heijnen, M., Hage, S., Parsons, D.R., Simmons, S.M., Paull, C.K. and Gwiazda, R., 2023. Detailed monitoring reveals the nature of submarine turbidity currents. Nature Reviews Earth & Environment, pp.1-17.

Talling, P.J., Masson, D.G., Sumner, E.J. and Malgesini,G., 2012. Subaqueous sediment density flows: Depositional processes and deposit types. Sedimentology, 59(7), pp.1937-2003.

Talling, P. J., Allin, J. R., Armitage, D. A., Arnott, R. W. C., Cartigny, M., Clare, M., ... & Xu, J. (2015). Key future directions for research on turbidity currents and their deposits. Journal of Sedimentary Research, 85(2), 153-169. https://doi.org/10.2110/jsr.2015.03

Talling, Peter.J., Paull, C.K., Piper, D.J.W., 2013. How are subaqueous sediment density flows triggered, what is their internal structure and how does it evolve? Direct observations from monitoring of active flows. Earth-Sci. Rev. 125, 244–287. https://doi.org/10.1016/j.earscirev.2013.07.005 62.74.

Talling, P. J., Hage, S., Baker, M. L., Bianchi, T. S., Hilton, R., & Maier, K. L. (2024), January 17). The Global Turbidity Current Pump and Its Implications for Organic Carbon Cycling. Annual Review of Marine Science, 16, 105-133. https://doi.org/10.1146/annurev-marine-032223-103626

Tang, H., Nsangue, B.T.N., Pandong, A.N., He, P., Liuxiong, X., Hu, F., 2022. Flume Tank Evaluation on the Effect of Liners on the Physical Performance of the Antarctic Krill Trawl. Front. Mar. Sci. 8.

Tappin, D.R., 2021. Submarine landslides and their tsunami hazard. Annual Review of Earth and Planetary Sciences, 49, pp.551-578.

Tek, D.E., McArthur, A.D., Poyatos-Moré, M., Colombera, L., Patacci, M., Craven, B., and McCaffrey, W.D., 2021, Relating seafloor geomorphology to subsurface architecture: How mass-transport deposits and knickpoint-zones build the stratigraphy of the deep-water Hikurangi Channel: Sedimentology, v. 68, p. 3141–3190, doi:10.1111/sed.12890.

Tek, D. E., McArthur, A. D., Poyatos-Moré, M., Colombera, L., Allen, C., Patacci, M., ... & McCaffrey, W. D. (2021). Controls on the architectural evolution of deep-water channel overbank sediment wave fields: insights from the hikurangi channel, offshore new zealand. New Zealand Journal of Geology and Geophysics, 65(1), 141-178. https://doi.org/10.1080/00288306.2021.1978509

Terzaghi, K., 1943. Theoretical Soil Mechanics. John Wiley and Sons, New York, NY.

Tessler, Z.D., Vörösmarty, C.J., Grossberg, M., Gladkova, I., Aizenman, H., Syvitski, J.P. and Foufoula-Georgiou, E., 2015. Profiling risk and sustainability in coastal deltas of the world. Science, 349(6248), pp.638-643.

Thal, J., Tivey, M., Yoerger, D.R., Bach, W., 2016. Subaqueous cryptodome eruption, hydrothermal activity and related seafloor morphologies on the andesitic North Su volcano. J. Volcanol. Geotherm. Res. 323, 80–96. https://doi.org/10.1016/j.jvolgeores.2016.04.041

Tian, D., Jiang, T., Wang, H., Zhang, D., and Meiburg, E., 2023, Flow dynamics and sedimentation at a turbidity channel confluence in the Yinggchai Basin, northwestern South China Sea. Geoenergy Science and Engineering, v. 227, 211927.

Trofimovs, J., Foster, C., Sparks, R.S.J., Loughlin, S., Le Friant, A., Deplus, C., Porritt, L., Christopher, T., Luckett, R., Talling, P.J. and Palmer, M.R., 2012. Submarine pyroclastic deposits formed during the 20th May 2006 dome collapse of the Soufriere Hills Volcano, Montserrat. Bulletin of Volcanology, 74, pp.391-405.

Turmel, D., Locat, J., Parker, G., 2015. Morphological evolution of a well-constrained, subaerial–subaqueous source to sink system: Wabush Lake. Sedimentology 62, 1636–1664. https://doi.org/10.1111/sed.12197

Urgeles, R., Camerlenghi, A., 2013. Submarine landslides of the Mediterranean Sea: Trigger mechanisms, dynamics, and frequency-magnitude distribution. J. Geophys. Res. Earth Surf. 118, 2600–2618. https://doi.org/10.1002/2013JF002720

Urlaub, M., Talling, P.J., Zervos, A., Masson, D., 2015. What causes large submarine landslides on low gradient (<2°) continental slopes with slow (~0.15 m/kyr) sediment accumulation? J. Geophys. Res. Solid Earth 120, 6722–6739. https://doi.org/10.1002/2015JB012347

Vaiomounga, S.J.C., M. Brenna, I.E.M. Smith, S.J. Barker, M. Tost, M. Ford, S. Tonga'onevai, T. Kula, R., 2017. New Volcanic Island Unveils Explosive Past [WWW Document]. Eos. URL http://eos.org/science-updates/new-volcanic-island-unveils-explosive-past (accessed 8.2.23).

Van Bergeijk, V., Warmink, J., Hulscher, S., 2022. The Effect Of Geometrical Transitions On The Wave Overtopping Load, in: Proceedings of the 39th IAHR World Congress. Presented at the Proceedings of the 39th IAHR World Congress From Snow to Sea, International Association for Hydro-Environment Engineering and Research (IAHR), pp. 4394–4402. https://doi.org/10.3850/IAHR-39WC252171192022428

Vanneste, M., Sultan, N., Garziglia, S., Forsberg, C.F., L'Heureux, J.-S., 2014. Seafloor instabilities and sediment deformation processes: The need for integrated, multi-disciplinary investigations. Mar. Geol., 50th Anniversary Special Issue 352, 183–214. https://doi.org/10.1016/j.margeo.2014.01.005

Vendettuoli, D., Clare, M.A., Hughes Clarke, J.E., Vellinga, A., Hizzet, J., Hage, S., Cartigny, M.J.B., Talling, P.J., Waltham, D., Hubbard, S.M., Stacey, C., Lintern, D.G., 2019. Daily bathymetric surveys document how stratigraphy is built and its extreme incompleteness

in submarine channels. Earth Planet. Sci. Lett. 515, 231–247. https://doi.org/10.1016/j.epsl.2019.03.033

Walter, T.R., Haghshenas Haghighi, M., Schneider, F.M., Coppola, D., Motagh, M., Saul, J., Babeyko, A., Dahm, T., Troll, V.R., Tilmann, F., Heimann, S., Valade, S., Triyono, R., Khomarudin, R., Kartadinata, N., Laiolo, M., Massimetti, F., Gaebler, P., 2019. Complex hazard cascade culminating in the Anak Krakatau sector collapse. Nat. Commun. 10, 4339. https://doi.org/10.1038/s41467-019-12284-5

Watt, S., Talling, P., Hunt, J., 2014. New Insights into the Emplacement Dynamics of Volcanic Island Landslides. Oceanography 27, 46–57. https://doi.org/10.5670/oceanog.2014.39

Wei, T., Peakall, J., Parsons, D.R., Chen, Z., Zhao, B., and Best, J., 2013, Three-dimensional gravity-current flow within a subaqueous bend: Spatial evolution and force balance variations: Sedimentology, v. 60, p. 1668–1680, doi:10.1111/sed.12052. 80.

Weihaupt, J.G., 1989, Disparities in the Forms of River Meanders and Oxbow Lakes (A Case Study). Water Resources Publications, Littleton, 186 pp.

Wells, M., Cossu, R., 2013. The possible role of Coriolis forces in structuring large-scale sinuous patterns of submarine channel–levee systems. Philos. Trans. R. Soc. Math. Phys. Eng. Sci. 371, 20120366. https://doi.org/10.1098/rsta.2012.0366

Wheeler, J., Brookfield, A., Gabrielse, H., Monger, J., Woodsworth, G., 1991. Terrane map of the Canadian Cordillera. Geol Surv Can Map 1713A, scale 1:2 000 000.

White, S.M., Crisp, J.A., Spera, F.J., 2006. Long-term volumetric eruption rates and magma budgets. Geochem. Geophys. Geosystems 7. https://doi.org/10.1029/2005GC001002Wolinsky, M.A., Pratson, L.F., 2007. Overpressure and slope stability in prograding clinoforms: Implications for marine morphodynamics. J. Geophys. Res. Earth Surf. 112. https://doi.org/10.1029/2007JF000770

Wilberg, P., Cacchione, D., Sternberg, R., & Wright, L. (1996). Linking sediment transport and stratigraphy on the continental shelf. Oceanography, 9(3), 153-157. https://doi.org/10.5670/oceanog.1996.02 68.81.

Winterwerp, J.C., van Kesteren, W.G.M., van Prooijen, B. and Jacobs, W., 2012, A conceptual framework for shear flow–induced erosion of soft cohesive sediment beds. J. Geophys. Res. [Oceans], 117, C10020.

Wolman, M.G., and Miller, J.P., 1960, Magnitude and frequency of forces in geomorphic processes. The Journal of Geology, 68(1), 54–74. https://doi.org/10.1086/626637

Wright, C.J., Hindley, N.P., Alexander, M.J., Barlow, M., Hoffmann, L., Mitchell, C.N., Prata, F., Bouillon, M., Carstens, J., Clerbaux, C., Osprey, S.M., Powell, N., Randall, C.E., Yue, J., 2022. Surface-to-space atmospheric waves from Hunga Tonga–Hunga Ha'apai eruption. Nature 609, 741–746. https://doi.org/10.1038/s41586-022-05012-5

Wright, I.C., Worthington, T.J., Gamble, J.A., 2006. New multibeam mapping and geochemistry of the 30°–35° S sector, and overview, of southern Kermadec arc volcanism. J. Volcanol. Geotherm. Res. 149, 263–296. https://doi.org/10.1016/j.jvolgeores.2005.03.021

Wynn, R.B., Cronin, B.T., Peakall, J., 2007. Sinuous deep-water channels: Genesis, geometry and architecture. Mar. Pet. Geol., Sinuous Deep-Water Channels: Genesis, Geometry and Architecture 24, 341–387. https://doi.org/10.1016/j.marpetgeo.2007.06.001

Xu, W., Xie, L., Bürgmann, R., Liu, X., & Wang, J. (2023). The 2022 eruption of wolf volcano, galápagos: the role of caldera ring-faults during magma transfer from insar deformation data. Geophysical Research Letters, 50(14). https://doi.org/10.1029/2023gl103704

Xue, Z., Oñate, E., Galindo-Torres, S. A., Bleyer, J., & Krabbenhøft, K. (2019). A unified lagrangian formulation for solid and fluid dynamics and its possibility for modelling submarine landslides and their consequences. Computer Methods in Applied Mechanics and Engineering, 343, 314-338. https://doi.org/10.1016/j.cma.2018.07.043

Zeng, J., Lowe, D.R., Prior, D.B., Wiseman Jr, W.J., and Bornhold, B.D., 1991, Flow properties of turbidity currents in Bute Inlet, British Columbia: Sedimentology, v. 38, p. 975–996, doi:10.1111/j.1365-3091.1991.tb00367.x.

Zhang, S., Li, H., Zhang, T., Pang, Y., Chen, Q., 2019. Numerical Simulation Study on the Effects of Course Keeping on the Roll Stability of Submarine Emergency Rising. Appl. Sci. 9, 3285. https://doi.org/10.3390/app9163285

Zhang, W., Puzrin, A.M., 2022. How Small Slip Surfaces Evolve Into Large Submarine Landslides—Insight From 3D Numerical Modeling. J. Geophys. Res. Earth Surf. 127, e2022JF006640. https://doi.org/10.1029/2022JF006640Zhong, G., Cartigny, M.J.B., Kuang, Z., Wang, L., 2015. Cyclic steps along the South Taiwan Shoal and West Penghu submarine canyons on the northeastern continental slope of the South China Sea. GSA Bull. 127, 804–824. https://doi.org/10.1130/B31003.1

Zhang, X., Lu, X., Xiao, M., 2015. Gas outburst with sediments because of tetrahydrofuran hydrate dissociation. Int. J. Numer. Anal. Methods Geomech. 39, 1884–1897. https://doi.org/10.1002/nag.2377

Zhang, X., Oñate, E., Torres, S.A.G., Bleyer, J., Krabbenhoft, K., 2019. A unified Lagrangian formulation for solid and fluid dynamics and its possibility for modelling submarine landslides and their consequences. Comput. Methods Appl. Mech. Eng. 343, 314–338. https://doi.org/10.1016/j.cma.2018.07.043

Zheng, H., Wang, N., Wu, J., 2017. Minimizing deep sea data collection delay with autonomous underwater vehicles. J. Parallel Distrib. Comput. 104, 99–113. https://doi.org/10.1016/j.jpdc.2017.01.006

Zoccarato, C., Minderhoud, P.S.J., Teatini, P., 2018. The role of sedimentation and natural compaction in a prograding delta: insights from the mega Mekong delta, Vietnam. Sci. Rep. 8, 11437. https://doi.org/10.1038/s41598-018-29734-7